UAB
Universitat Autònoma de Barcelona

Nanoplastic-induced endothelial dysfunction Physicochemical properties as key determinants of biological outcomes in human vascular cells

Joan Martín Pérez

ADVERTIMENT. L'accés als continguts d'aquesta tesi queda condicionat a l'acceptació de les condicions d'ús establertes per la següent llicència Creative Commons: https://creativecommons.org/licenses/?lang=ca

ADVERTENCIA. El acceso a los contenidos de esta tesis queda condicionado a la aceptación de las condiciones de uso establecidas por la siguiente licencia Creative Commons: https://creativecommons.org/licenses/?lang=es

WARNING. The access to the contents of this doctoral thesis it is limited to the acceptance of the use conditions set by the following Creative Commons license: https://creativecommons.org/licenses/?lang=en

UAB
Universitat Autònoma de Barcelona

Facultat de Biociències
Departament de Genètica i de Microbiologia
Grup de Mutagènesi

DOCTORAL DISSERTATION · 2026

Nanoplastic-induced endothelial *dysfunction*

Physicochemical properties as key determinants of biological outcomes in human vascular cells

Joan Martín Pérez

UAB
Universitat Autònoma de Barcelona

Facultat de Biociències
Departament de Genètica i de Microbiologia
Grup de Mutagènesi

DOCTORAL DISSERTATION · 2026

Nanoplastic-induced endothelial *dysfunction*

Physicochemical properties as key determinants of biological outcomes in human vascular cells

Dissertation submitted by

Joan Martín Pérez

To Universitat Autònoma de Barcelona in partial fulfillment of the requirements for the degree of Doctor of Philosophy, as per the Doctorate Program in Genetics. Under the supervision of Alba Hernández Bonilla and Alba García Rodríguez.

Alba Hernández Bonilla, PhD
DIRECTOR/TUTOR

Alba García Rodríguez, PhD
DIRECTOR

Joan Martín Pérez
PHD CANDIDATE

Agradecimientos

Hace cinco años, en plena pandemia mundial y tras un momento especialmente complicado a nivel personal y profesional, recibí un correo de Cristina S., quien había sido mi mentora durante el grado de Biología y el máster de Antropología Biológica. Aquel mensaje marcaría un punto de inflexión en mi vida: Cristina S. me ponía en contacto con Alba H., IP del Grupo de Mutagénesis de la Universidad Autónoma de Barcelona.

Tras un par de años alejado de la universidad, Alba H. me ofreció la posibilidad de realizar un doctorado en genética, centrado en un tema entonces completamente desconocido para mí: los micro y nanoplásticos, un campo sobre el que apenas existían un par de artículos científicos cuando Alba H. apostó por él, y del que hoy se publican miles. Pero lo más importante era que me ofrecía la oportunidad de volver a la UAB, mi segunda casa, y en ocasiones, incluso la primera. En octubre de 2021 inicié una nueva etapa en el grupo de Alba H. y Ricard M., dos grandes jefes y excelentes gestores de equipo. Mis primeros agradecimientos son para ellos tres: Cristina S., Alba H. y Ricard M., por abrirme la puerta a este doctorado.

Los comienzos nunca son fáciles, y mi personalidad tampoco ayuda demasiado. Algunos pensaron que era borde; otros quizá lo sigan pensando. A estas alturas, tampoco es algo que nos vaya a quitar el sueño. Pero siempre hay personas que te tienden la mano, y ahí aparece Aliro V. Nuestra relación ha tenido altos y bajos, como todo lo que vale la pena, pero nunca olvidaré su apoyo tanto a nivel personal como profesional. Como diría él, aquí tiene “un hermano de otra madre”. Me enseñó mis primeros experimentos, fue un gran maestro, intentó enseñarme a tratar con la gente (eso sigue en proceso... quizá la clave esté en terminar una frase antes) y me acompañó cuando más lo necesitaba. Gracias, Aliro. Seguiremos trabajando el acento chileno.

De esos primeros meses también quiero mencionar a Alireza T., con quien aprendí mucho sobre la cultura iraní y que, junto con Aliro V., fue de las primeras personas en acercarse a mí.

Más adelante empezó una nueva etapa con la incorporación de Alba G., quien pasó a ser mi directora de tesis junto con Alba H. Alba G. trabajó conmigo codo a codo en el laboratorio, guió mi progreso y, sobre todo, demostró una calidad humana enorme: vino a visitarme a casa tras mi lesión de rodilla y ayudó a formar un nuevo equipo de trabajo junto con Gooya B. Los tres nos apoyábamos mutuamente con un objetivo común.

Y aquí entra Gooya B., con quien probablemente he compartido más horas en el laboratorio. Una persona con una sensibilidad especial, que siempre quiere que todo el mundo esté bien y que lo da todo incluso cuando su propia situación es difícil. De ella aprendí muchas cosas, pero sobre todo su capacidad de superación ante las adversidades.

Después agradecer a Javier G., con quien quizá no compartí tantas horas de laboratorio, pero sí muchas en el despacho. Gracias por tus palomitas y por todas las conversaciones, especialmente las de fútbol junto con Massimo B. y Michelle M.

Y esto me lleva naturalmente a Michelle M. Si Aliro tuvo un papel clave al inicio, Michelle M. tomó el relevo cuando él se doctoró y volvió a Chile. Ha sido la mejor compañera de poyata que podría haber tenido: gracias a ella seguí aprendiendo nuevas técnicas día a día. Pero, sin duda, lo más importante ha sido la dimensión personal de nuestra relación. Cuando he tenido dudas en cualquier aspecto de mi vida, he acudido a ella, y siempre ha tenido una respuesta: a veces la que quería oír, otras una verdad incómoda. Esa transparencia, esa claridad y esa forma directa de decir las cosas son lo que hacen nuestra relación tan valiosa. Este párrafo podría extenderse mucho más, pero Michelle M. ya sabe lo agradecido que siempre le estaré y lo importante que ha sido para mí.

Quiero agradecer también a todas esas personas que dan personalidad a los espacios y que asocio inevitablemente a ellos. En el grupo de Mutagénesis, mi núcleo más cercano, gracias a Laura R., Gloria U. (que hace que Mutas sea Mutas, siempre la primera en llegar y en dejarlo todo a punto), Cristian V. por las incontables horas diseccionando larvas de Drosophila, Jéssica A. por mostrarme la importancia del ejercicio físico, Mohamed A. por tu ayuda y tu

sonrisa, Susana P., e Irene B. y Raquel E. por formar parte de ese núcleo tan especial. Gracias también al “socari”, Raquel y Miriam, por vuestra ayuda y las buenas conversaciones. Y al Servei de Microscopia, donde pasé incontables horas: un lugar donde la gente vale mucho más que los equipos, que ya es decir teniendo en cuenta el precio de estos. Gracias a Meritxell V., Martí dC., Mariana T., Cristina N., Helena, Paqui y al resto del equipo. En especial a Meritxell V. y Martí dC., con quienes compartí muchas más horas y de quienes guardo un recuerdo enorme.

Quiero mencionar también a un conjunto de estudiantes que despertaron en mí una vocación que quizá aún no había descubierto: la de enseñar, transmitir conocimiento y acompañar. No todos me recordarán con la misma estima, pero siempre intenté hacerlo lo mejor posible, y pido perdón si en algún momento no estuve a la altura. Gracias a Arnau R. y Laia P., mis primeros estudiantes de máster, que además coincidieron con mi lesión de rodilla; a Mireia C., mi primera estudiante de grado y pieza clave para mi segundo artículo; y a Marta B. de Sicilia, con quien pude compartir técnicas y aprender un poco de italiano. La mención más especial en este grupo es para Hannes RVG. Pasamos muchísimo tiempo juntos en el laboratorio: le enseñé todo lo que pude y aprendí aún más. Gracias por ser un amigo. Y aunque no fuese mi alumna, gracias a Claudia A., estudiante de máster, que participó activamente en mis últimos ensayos y, sobre todo, me ayudó a ver la vida desde otras perspectivas y a buscar nuevos caminos. Con ella todo fue “más y mejor”. También a Carles C., mi alumno de prácticas de Bioquímica y hoy un amigo. Y a Sofia C., estudiante de intercambio, de quien guardo un muy buen recuerdo.

Más allá del laboratorio y del ámbito académico, también quiero dar las gracias a quienes me han acompañado desde mucho antes: los amigos de toda la vida. Me gustaría mencionar especialmente a Sergi S., Júlia dM., Domingo M., Alberto L., Miguel H. y Marcus T.

Finalmente, gracias a mi familia, porque directa e indirectamente han contribuido a formar mi personalidad y los valores que intento llevar siempre por bandera. Al fin y al cabo, la familia es lo más importante y quienes siempre están ahí cuando más los necesitamos. Quizá no sea un nieto, sobrino, primo o hijo modelo; quizá no sea la persona más expresiva y a veces parezca que

estoy en otro mundo (probablemente lo esté), pero eso no cambia lo agradecido que estoy por todo lo que habéis hecho por mí desde el día en que nací. Y lo mucho que os quiero. Gracias a mis abuelos Juan M., Braulia R., Julia M. y Manolo P.; a mis tías-abuelas Amalia M. y Luisa R.; a mi tete Félix P., a mi tita Mari H. y a mi primo Oriol P. También al resto de la familia, aunque no quiera alargar mucho más esta lista. Pero, sobre todo, gracias a mis padres, Maria P. y Juan M.

Gracias. Espero haber estado a la altura de vuestras expectativas, y si no... seguiremos intentándolo, seguiremos mejorando.

The more I know, the more I realize I know nothing.

SOCRATES

Abstract

Global plastic production has risen exponentially, surpassing 400 million tons annually, driven by the versatility, durability, and low cost that have made these materials indispensable across all sectors of modern life. However, throughout their life cycle, from manufacturing and routine use to environmental weathering, plastics undergo continuous degradation and fragmentation. These processes, which include mechanical stress, UV-driven photooxidation, and microbial degradation, progressively generate microplastics (MPLs; 1 µm–5 mm) and nanoplastics (NPLs; <1 µm), collectively referred to as micro- and nanoplastics (MNPLs). These particles constitute a heterogeneous population that differs in polymer composition, size, morphology, and surface chemistry. MNPLs are now ubiquitous across environmental compartments, resulting in chronic human exposure primarily through ingestion and inhalation. Once internalized, these particles, particularly the nanoscale fraction, can traverse biological barriers such as the intestinal and pulmonary epithelia, reach systemic circulation, and accumulate in multiple organs. Their confirmed presence in human blood and vascular tissues positions the endothelium as a primary interface for direct particle contact. Although emerging evidence associates MNPL exposure with cardiovascular risk, the specific endothelial responses elicited by these particles and, critically, how their physicochemical properties shape the nature and magnitude of such responses remain poorly defined. This Thesis provides a systematic characterization of NPL-induced endothelial dysfunction in primary human umbilical vein endothelial cells (HUVECs) and identifies surface functionalization, nanoscale size, and environmental realism as key physicochemical determinants of biological outcomes.

A progressive material strategy was implemented across three studies, combining controlled polystyrene (PS) reference particles with environmentally relevant materials in a standardized HUVEC model under controlled acute exposure conditions. In the first study, PS nanoplastics (PS-NPLs) were used to evaluate the role of surface chemistry across three distinct functionalizations: pristine (PS-P-NPLs), carboxylated (PS-C-NPLs), and

aminated (PS-A-NPLs). PS-A-NPLs exhibited the highest toxicity, including reduced viability and sustained genotoxicity, despite presenting the lowest intracellular burden. The second study assessed the influence of nanoscale size using PS-C-NPLs of 30, 50, and 100 nm through integrated transcriptomic and functional analyses. RNA sequencing revealed a shared core transcriptomic program dominated by cholesterol homeostasis, epithelial-mesenchymal transition, inflammatory signaling, and DNA damage-related pathways. These transcriptomic signatures were corroborated by targeted functional assays, including Filipin III staining for intracellular cholesterol, comet assay for genotoxicity, wound-healing and tube-formation assays for endothelial repair capacity, and interleukin-6 (IL-6) quantification for inflammatory output. Beyond this shared core, size exerted a modulatory role: 30 nm PS-C-NPLs consistently diverged from the 50/100 nm PS-C-NPLs cluster, which displayed more similar transcriptomic and functional profiles throughout all analyses. The third study extended the material space to NPLs of increasing environmental realism: spherical and monodisperse PS-NPLs and polylactic acid NPLs (PLA-NPLs), irregular and slightly heterogeneous polytetrafluoroethylene NPLs (PTFE-NPLs), and real-life polyethylene terephthalate NPLs (PET-NPLs) from post-consumer water bottles, representing the highest morphological and colloidal complexity. Under standardized conditions, PS-NPLs and PLA-NPLs produced negligible functional alterations, whereas PTFE-NPLs impaired endothelial migration, and real-life PET-NPLs induced the broadest response, encompassing IL-6 secretion, intracellular cholesterol accumulation, and migration inhibition, despite being the least internalized.

Across all studies, NPLs predominantly induced a sublethal endothelial dysfunction phenotype characterized by disruption of cholesterol homeostasis, impaired endothelial repair capacity, transcriptomic reprogramming, modulation of inflammatory signaling, and oxidative and genotoxic stress, with minimal cytotoxicity. Importantly, higher particle internalization did not predict greater biological impact, challenging the widespread use of uptake as a proxy for hazard. Instead, surface chemistry, nanoscale size, and the morphological

and colloidal complexity associated with environmental realism emerged as the principal determinants of the endothelial response profile.

Overall, this work demonstrates that physicochemical properties are important drivers of NPL-induced endothelial dysfunction and establishes a mechanistic framework linking particle attributes to specific vascular outcomes relevant to cardiovascular hazard assessment.

KEYWORDS nanoplastics · endothelial dysfunction · HUVECs · physicochemical properties · vascular toxicology

Abbreviation List

−COOH: Carboxyl Group

$-NH_2$: Amino Group

DEGs: Differentially Expressed Genes

DHE: Dihydroethidium

EMT: Epithelial-To-Mesenchymal Transition

FPG: Formamidopyrimidine DNA Glycosylase

FSC: Forward Scatter

GSEA: Gene Set Enrichment Analysis

HUVECs: Human Umbilical Vein Endothelial Cells

MNPLs: Micro- and Nanoplastics

MPLs: Microplastics

Mt: Million Tons

NanoEL: Nanoparticle-Induced Endothelial Leakiness

NPLs: Nanoplastics

ORA: Over-Representation Analysis

PE: Polyethylene

PET: Polyethylene Terephthalate

PLA: Polylactic Acid

PP: Polypropylene

PS: Polystyrene

PS-A-NPLs: Aminated Polystyrene Nanoplastics

PS-C-NPLs: Carboxylated Polystyrene Nanoplastics

PS-P-NPLs: Pristine Polystyrene Nanoplastics

PTFE: Polytetrafluoroethylene

PU: Polyurethane

PVC: Polyvinyl Chloride

RNA-seq: RNA Sequencing

ROS: Reactive Oxygen Species

SSC: Side Scatter

TEM: Transmission Electron Microscopy

Index

1. Introduction 1

1.1. Global Context: The Plastic Age and its Environmental Consequences 3

1.1.1. Definition and Classification of Plastics 3

1.1.2. The Plastics Industry: Production, Applications, and Global Relevance 4

1.1.3. Plastic Pollution: Environmental Persistence and Global Health Concerns 5

1.2. Micro- and Nanoplastics (MNPLs): An Emerging Contaminant 7

1.2.1. Formation, Origin, and Definition of MNPLs 7

1.2.2. Intrinsic Physicochemical Properties of MNPLs 8

1.2.3. Environmental Occurrence of MNPLs: Presence in Abiotic and Biotic Systems 11

1.3. Human Exposure to MNPLs and Evidence of Body Burden 16

1.3.1. Major Exposure Routes and Estimated Levels 16

1.3.2. Translocation Across Biological Barriers and Evidence of Presence in Human Tissues and Fluids 18

1.4. Biological Impact of MNPLs on Human Health: State of the Art 21

1.4.1. Reported Effects in Animal Models (*in vivo*) 21

1.4.2. Observed Effects in Human Cellular Models (*in vitro/ex vivo*) ... 24

1.4.3. The Influence of Physicochemical Properties on the Bio-reactivity of MNPLs: Previous Evidence 27

1.4.3.1. Impact of Surface Chemistry and Functionalization 27

1.4.3.2. Impact of Particle Size 30

1.4.3.3. Impact of Environmental Realism 31

1.5. The Vascular Endothelium: A Critical Target for Circulating MNPLs ... 34

1.5.1. Cardiovascular Impact of MNPLs: Clinical Evidence and Systemic Pathophysiology 34

1.5.2. State of the Art on MNPL-Induced Endothelial Dysfunction 36
1.5.3. HUVECs as a Representative Model of the Human Endothelium 41
1.6. Knowledge Gaps and Rationale for This Thesis 43
2. Objectives 45
3. Results 49
3.1. Chapter 1 (Paper 1) 53
3.2. Chapter 2 (Paper 2) 67
3.3. Chapter 3 (Paper 3) 83
4. Discussion 103
4.1. Overview of Key Findings and Thesis Logic 105
4.2. Methodological Framework and Study Design 106
4.2.1. Primary HUVECs as a Physiologically Relevant Endothelial Model 106
4.2.2. The Rationale for Acute Exposure 107
4.2.3. Progressive Complexity Approach for NPL Material Selection 108
4.3. NPL-Induced Functional Impairment in Endothelial Cells 110
4.3.1. Viability and Cytotoxicity 110
4.3.2. Lipid Homeostasis and Metabolism 111
4.3.3. Endothelial Repair Capacity: Migration and Angiogenesis 113
4.4. Mechanisms Driving Endothelial Dysfunction 115
4.4.1. Cellular Uptake and Intracellular Trafficking Burden 115
4.4.2. Transcriptomic Alterations 118
4.4.3. Inflammatory Signaling 119
4.4.4. Oxidative Stress and Genotoxicity 121
4.5. Physicochemical Determinants of Endothelial Responses 123
4.5.1. Surface Functionalization 123
4.5.2. Size at the Nanoscale 124

4.5.3. Environmental Realism.....126
4.6. Limitations and Future Perspectives.....128
4.6.1. Advancing Toward Realistic Exposure Scenarios.....128
4.6.2. Advancing Toward Physiologically Relevant Vascular Models .129
5. Conclusions 131
6. References.....135

1

Introduction

1.1. Global Context: The Plastic Age and its Environmental Consequences

1.1.1. DEFINITION AND CLASSIFICATION OF PLASTICS

Plastics are a class of synthetic materials characterized by their versatility, which stems from desirable properties such as being lightweight, highly durable, flexible, and low-cost to produce (Pilapitiya & Ratnayake, 2024). According to the International Union of Pure and Applied Chemistry (IUPAC), a plastic is formally defined as a *"polymeric material that may contain other substances to improve performance and/or reduce costs"* (IUPAC, 2012). This definition highlights that plastics are not pure polymers but rather formulated systems comprising a polymer matrix and various additives, such as plasticizers, stabilizers, and flame retardants, that enhance their final properties (Hartmann et al., 2019). The specific polymer backbone, composed of repeating monomer units covalently bonded into macromolecular chains (IUPAC, 1996), together with these additives, determines the material's mechanical properties and, critically, its resistance to degradation, which is a key factor in the environmental persistence of conventional plastics (Hartmann et al., 2019).

From an industrial and environmental standpoint, plastics are primarily classified by the origin of their raw materials and by their thermal behavior. More than 98% of plastics are derived from fossil fuels, synthesized from non-renewable feedstocks such as petroleum, natural gas, and coal (Landrigan et al., 2025). This group includes major commodity polymers such as polyethylene (PE), polypropylene (PP), polystyrene (PS), polyethylene terephthalate (PET), and polyvinyl chloride (PVC), whose large-scale production is tightly linked to a linear "take–make–use–dispose" economic model that has driven unprecedented levels of waste accumulation (Landrigan et al., 2025). In contrast, bioplastics are derived from renewable feedstocks and currently represent less than 1% of global production (Plastics Europe, 2025). This category includes biodegradable polymers such as polylactic acid (PLA), which is particularly relevant to this Thesis given its growing use in packaging and food-contact applications (Hartmann et al., 2019).

Regarding thermal behavior, thermoplastics, which constitute approximately 80% of global output (Pilapitiya & Ratnayake, 2024), can be repeatedly melted and reshaped, making them, in principle, recyclable. In contrast, thermosets undergo irreversible cross-linking during curing, which limits their recyclability but provides high thermal and mechanical stability for specialized applications such as coatings and adhesives (Pilapitiya & Ratnayake, 2024).

1.1.2. THE PLASTICS INDUSTRY: PRODUCTION, APPLICATIONS, AND GLOBAL RELEVANCE

Since the development of the first synthetic plastics in the early twentieth century, plastic production has grown exponentially, from approximately 2 million tons (Mt) in 1950 (Geyer et al., 2017) to 430.9 Mt in 2024 (Plastics Europe, 2025). Current projections indicate that output may double within the next two decades, potentially reaching 1,200 Mt by 2060 (Landrigan et al., 2025). A small group of thermoplastics dominates this growth: PE, PP, PVC, PET, and PS together account for nearly 80% of total global output, with PE and PP alone representing approximately 45% of all plastics produced (Table 1). Among the principal end-use sectors, packaging is the largest single consumer, followed by building and construction, automotive, and electronics (Plastics Europe, 2025; Houssini et al., 2025).

Table 1: *Global plastic production by polymer type in 2024 and their main industrial applications. Data adapted from Plastics Europe (2025). [1]The value for PE is the sum of PE-HD/MD (12.1%) and PE-LD/LLD (13.9%). [2]The value for recycled plastics is the sum of mechanically (9.5%) and chemically (0.1%) recycled materials.*

Plastics	Production %	Main uses
Polyethylene (PE)	26.0%[1]	Packaging, containers, pipes
Polypropylene (PP)	19.0%	Packaging, automotive, textiles, appliances
Polyvinyl Chloride (PVC)	12.8%	Construction, medical, cables
Polystyrene (PS)	5.1%	Packaging, appliances, insulation
Polyurethane (PU)	5.3%	Foams, automotive
Polyethylene Terephthalate (PET)	6.2%	Bottles, food packaging, textiles
Secondary plastics (recycled)	9.6%[2]	Different uses
Bioplastics	0.6%	Different uses

Beyond material output, the plastics industry consumes approximately 4% of global oil and gas production as both feedstock and energy source (Pilapitiya & Ratnayake, 2024), and its global market exceeded USD 600 billion in 2022 (Grand View Research, 2024). This dual nature, as a cornerstone of modern economic development and a major consumer of non-renewable resources, captures the paradox of the Plastic Age: a material revolution that sustains contemporary life while simultaneously posing growing environmental and sustainability challenges.

1.1.3. PLASTIC POLLUTION: ENVIRONMENTAL PERSISTENCE AND GLOBAL HEALTH CONCERNS.

The massive scale of plastic production, combined with inadequate waste management, has created one of the most pressing environmental challenges of the modern era. It is estimated that less than 10% of all plastic ever produced has been recycled (Landrigan et al., 2025), while approximately 80% of the generated plastic waste has accumulated in landfills or the natural environment (Geyer et al., 2017). As a consequence, nearly 8 billion tonnes of plastic waste are currently dispersed across terrestrial and aquatic ecosystems worldwide (Landrigan et al., 2025).

At the heart of this crisis lies the remarkable persistence, mobility, and ubiquity of plastic debris. Owing to their chemical stability and resistance to biodegradation, most conventional polymers can persist in the environment for centuries (Rodrigues et al., 2022). This durability underpins their accumulation across all major environmental compartments. In marine and freshwater systems, an estimated 8 Mt of plastic enters the oceans each year, a figure projected to double by 2030 and potentially again by 2050, when the total mass of marine plastic could surpass that of fish (Hong, 2023; Matthews et al., 2021). Terrestrial environments act as even larger sinks, receiving between four and twenty-three times more plastic waste than the oceans, which can alter soil structure, permeability, and fertility (Yu & Flury, 2021). The atmosphere also plays a key role as a transport vector for plastic particles; airborne microplastics, often derived from synthetic textile fibers, are now detected in

both indoor and outdoor air, with indoor concentrations frequently exceeding those in outdoor air (Zhu et al., 2023).

The ecological consequences of this pervasive contamination were recognized as early as the 1960s and 1970s, with reports highlighting the physical impacts on wildlife, such as entanglement in nets and gastrointestinal obstruction in seabirds and marine mammals following ingestion (Landrigan et al., 2025). Beyond these direct physical hazards, plastic debris also poses chemical risks. Many plastics contain potentially harmful additives (e.g., bisphenol A, phthalates) that can leach into the environment (Yee et al., 2021; Facciolà et al., 2021), while the particle surfaces can adsorb persistent organic pollutants from surrounding waters, acting as vectors for toxic exposure upon ingestion (Bajt, 2021). Furthermore, the plastic particles themselves can induce biological stress, as demonstrated by studies showing impaired reproduction in oysters exposed to PS microplastics (Pilapitiya & Ratnayake, 2024).

Concerns regarding human health implications also have historical roots. As early as the 1970s, occupational exposure to vinyl chloride monomer in PVC manufacturing was linked to hepatic angiosarcoma (Landrigan et al., 2025). Today, the scope of concern has broadened significantly, as reflected in estimates that place the global health-related economic burden of plastic pollution at over USD 1.5 trillion annually (Landrigan et al., 2025). Recognizing the severity and complexity of the issue, the international community took a decisive step in 2022, when United Nations member states unanimously adopted a resolution to develop a legally binding global treaty addressing the entire life cycle of plastics (Lampitt et al., 2023). This global commitment underscores the urgent need to understand the risks posed by plastics, particularly those stemming from their fragmentation into micro- and nanoplastics, which have become a primary focus of current environmental health research.

1.2. Micro- and Nanoplastics (MNPLs): An Emerging Contaminant

1.2.1. FORMATION, ORIGIN, AND DEFINITION OF MNPLS

Throughout their entire life cycle, plastics are subjected to continuous mechanical stress and environmental weathering. These processes drive their gradual degradation and fragmentation into microplastics (MPLs) and nanoplastics (NPLs), collectively referred to as micro- and nanoplastics (MNPLs) (Yee et al., 2021; Shi et al., 2022). Notably, MNPL generation is not limited to poorly managed waste; even under ideal recycling, the routine use of plastic products inevitably generates microscopic plastic debris.

Although formal definitions remain under debate, size-based terminology for MNPLs is frequently applied inconsistently across the literature, with many authors using partially overlapping thresholds. MPLs are commonly described as solid polymer particles ranging from 1 µm to 5 mm (Da Costa Filho et al., 2021), whereas NPLs generally refer to particles below 1 µm (Rodrigues et al., 2022). However, risk-assessment frameworks often adopt more restrictive cut-offs. For instance, the European Food Safety Authority (EFSA) proposes operational definitions classifying MPLs as 0.1–5000 µm and NPLs as 1–100 nm (EFSA CONTAM Panel, 2016). Regardless of the specific threshold applied, the submicrometric fraction, particularly nanoscale particles, can exhibit distinct environmental mobility and biological reactivity, which may facilitate penetration into biological systems and translocation across physiological barriers (Jahedi & Jaafarzadeh Haghighi Fard, 2025).

Based on their origin, MNPLs are classified as primary or secondary. Primary MNPLs are intentionally manufactured at the micro- or nanoscale for industrial or commercial applications, such as exfoliating microbeads for cosmetics or pre-production pellets for industry (Jeong et al., 2024). These account for an estimated 15–30% of the total MNPLs present in the environment (Ali et al., 2024). The majority (70–80%) are secondary MNPLs, generated by fragmentation of larger plastic materials during product use and in environmental settings (Ali et al., 2024). Environmental weathering is governed by a complex interplay of physical, chemical, and biological mechanisms that

progressively reduce particle size and alter the material's physicochemical properties. These mechanisms include mechanical abrasion, UV-driven photooxidation, hydrolysis, and microbial degradation (Lehner et al., 2019). Weathering not only fragments plastics but also modifies their polymer structure, reducing molecular weight and introducing new functional groups (e.g., carboxyl and other oxygen-containing functional groups) (Rubio et al., 2019). These transformations affect the particles' surface charge, hydrophilicity, and capacity to adsorb environmental contaminants or biomolecules, thereby influencing their environmental fate and biological interactions (Rubio et al., 2019).

To investigate the effects of MNPLs, researchers employ two main strategies for generating test materials: bottom-up synthesis and top-down fragmentation. The bottom-up approach involves chemical synthesis from monomers, producing uniform, spherical, and monodisperse MNPLs with precise control over size, composition, and surface chemistry (El Hadri et al., 2020). These engineered MNPLs, often commercially available polystyrene nanoplastics (PS-NPLs), facilitate reproducibility and mechanistic studies under controlled conditions, though they poorly reflect the complexity of environmentally aged plastics (Pradel et al., 2023). In contrast, top-down approaches aim to reproduce the heterogeneity of secondary MNPLs by physically or photochemically degrading bulk plastics, using methods such as mechanical grinding, cryomilling, or UV/laser ablation (Crosset-Perrotin et al., 2025). These processes generate irregular, polydisperse fragments with roughened surfaces and altered surface chemistry, more closely resembling real-life environmental MNPLs (Sørensen et al., 2024). Consequently, combining both approaches is essential to balance experimental control with environmental relevance, enabling a more realistic assessment of MNPL behavior and toxicity.

1.2.2. INTRINSIC PHYSICOCHEMICAL PROPERTIES OF MNPLS

The physicochemical properties of MNPLs are complex factors that critically determine their environmental behavior, colloidal stability, and biological interactions (Pradel et al., 2023; Reynaud et al., 2021). As seen in Figure 1, four

major characteristics define these properties: material composition, size, shape, and surface chemistry.

MNPLs originate from a diverse range of plastic materials, each defined by its specific polymer composition and often incorporating various additives (Hartmann et al., 2019). While MNPLs are predominantly derived from synthetic organic polymers (primarily thermoplastics, reflecting global production trends), materials such as bioplastics also contribute significantly. This is particularly true, as their environmental behavior remains less well studied (Nik Mut et al., 2024). This Thesis specifically examines four key polymers: PS, a widely used homopolymer often employed as a model system in NPL research due to its commercial availability and tunable surface properties (Oliveira et al., 2020; El Hadri et al., 2020); PET, a common synthetic polymer extensively used in packaging (especially beverage bottles) and textiles, frequently found as secondary environmental fragments (Pivokonsky et al., 2018); polytetrafluoroethylene (PTFE), a highly hydrophobic and chemically resistant fluoropolymer known for its use in non-stick coatings (Cole et al., 2024); PLA, a prominent bio-based and potentially biodegradable aliphatic polyester derived from lactic acid, used in packaging and medical applications (Abdullayeva & Alizadeh, 2023).

Particle size is a fundamental property distinguishing MNPLs. Particularly at the nanoscale, the dramatically increased surface-area-to-volume ratio has significant physical consequences (Kik et al., 2020). This enhances surface reactivity and adsorption capacity for environmental contaminants (Ivleva, 2021). Furthermore, the nanometric dimensions ensure that Brownian motion, rather than sedimentation or buoyancy, governs transport in fluids (Gigault et al., 2021). Critically, this size range also increases bioavailability by potentially facilitating translocation across biological barriers (Yagublu et al., 2022).

The shape of MNPLs also varies significantly, often reflecting their origin. Common shapes include spheres or beads, typically associated with primary MNPLs intentionally manufactured via bottom-up synthesis (like commercial PS test materials), which are often monodisperse (El Hadri et al., 2020). In contrast, irregular fragments are characteristic of secondary MNPLs generated by environmental weathering or artificial top-down fragmentation (e.g., PET from

bottles). Irregular MNPLs usually exhibit high polydispersity and are frequently detected in environmental and biological samples (Jeong et al., 2024). Lastly, fibers or filaments, primarily resulting from the degradation of synthetic textiles, are reported to be the predominant MNPL morphology in atmospheric samples (Li et al., 2020c).

Surface chemistry dictates how MNPLs interact with their surroundings (Lundqvist et al., 2008). Intrinsic properties include the inherent hydrophobicity of polymers like PS and PTFE, and a slight negative surface charge (Kik et al., 2020; Lundqvist et al., 2008). However, acquired properties arise from environmental weathering (e.g., photooxidation, which introduces oxygen-containing functional groups and alters surface charge) or through intentional, engineered functionalization (e.g., adding carboxyl (-COOH) or amino ($-NH_2$) groups for model studies) (Yu & Flury, 2021). The resulting surface charge, measured as ζ-potential, is crucial for determining colloidal stability (aggregation vs. dispersion) in different media (Pradel et al., 2023). Importantly, upon entering biological fluids, surface characteristics drive the rapid formation of a protein corona; this layer of adsorbed biomolecules masks the original surface and presents a new biological identity that governs subsequent cellular interactions, stability, and fate (Rampado et al., 2020).

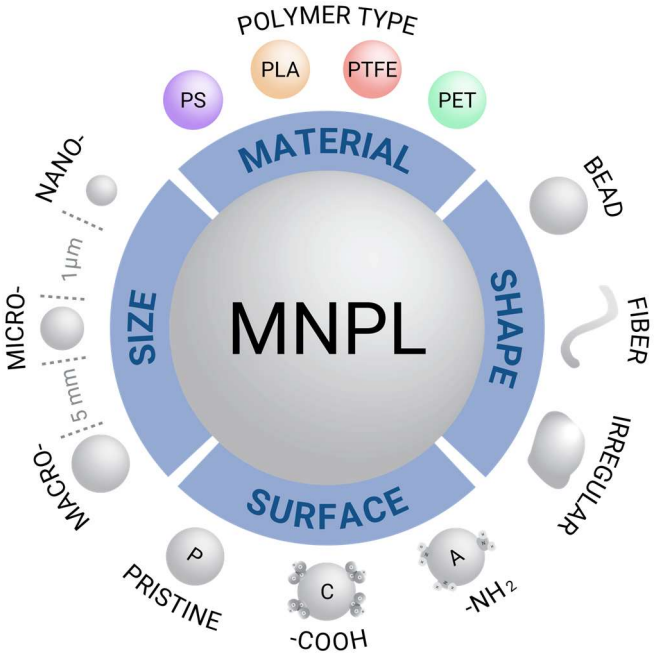


Figure 1: *Intrinsic physicochemical properties of MNPLs — material composition, size, shape, and surface chemistry — influence their interactions with biological systems. Adapted from Yagublu et al., 2022, and created with BioRender.com.*

Ultimately, the interplay of these key intrinsic properties (material composition, size, shape, and surface chemistry) along with acquired characteristics such as the protein corona, dictates the overall colloidal behavior and interactions of MNPLs within environmental and biological systems (Reynaud et al., 2021).

1.2.3. ENVIRONMENTAL OCCURRENCE OF MNPLS: PRESENCE IN ABIOTIC AND BIOTIC SYSTEMS

The widespread persistence of plastics in the environment, together with the minute size of MNPLs, has led to their distribution across all major environmental compartments: atmosphere, hydrosphere, lithosphere, and biosphere (Petersen & Hubbart, 2021). Numerous studies have reported measurable concentrations in these matrices, demonstrating the global scale and ubiquity of this contaminant (see Table 2 for abiotic compartments and Table 3 for biotic systems).

In the atmosphere, airborne MNPLs are transported over long distances and deposited globally (Allen et al., 2019). Atmospheric deposition can reach substantial magnitudes, with estimates indicating that between 3 and 10 tons of MNPLs settle annually over the Paris metropolitan area (Dris et al., 2016). Daily deposition rates reported worldwide further highlight this burden, ranging from 31–43 particles/m^2/day in Dongguan (China) (Cai et al., 2017) to 575–1,008 particles/m^2/day in London (UK) (Wright et al., 2020). Indoor air typically contains even higher concentrations (Alqahtani et al., 2023), with reported levels up to 14,000 particles/m^3 (Din et al., 2024), compared to a maximum of approximately 400 particles/m^3 in outdoor environments (Din et al., 2024), emphasizing the relevance of indoor exposure. The global dispersal capacity of airborne MNPLs is underscored by their detection in remote regions, including Arctic snow, polar ice, and Alpine glaciers (Materić et al., 2021; Materić et al., 2022b), confirming that atmospheric transport is a key vector for long-range distribution.

Within the hydrosphere, MNPLs are now recognized as pervasive contaminants in both marine and freshwater ecosystems (Jeong et al., 2024). Concentrations vary widely across matrices and sampling methodologies, reaching up to 42,213 particles/km^2 in the Northwestern Pacific Ocean (Pan et al., 2019) and

ranging from 0.02 to 2.19 particles/m^3 in freshwater bodies (Jeong et al., 2024). Furthermore, MNPLs have been quantified in water sources directly relevant to human activities, including drinking water supplies, which average around 700 particles/L (Yu et al., 2024), and bottled water, where levels can reach over 10,000 particles/L (Mason et al., 2018). Although most studies historically focused on MPLs, advances in analytical techniques have enabled the detection of NPLs in aquatic environments. For instance, PS-NPLs have been measured at 4.2 µg/L in the Dutch Wadden Sea (Materić et al., 2022a) and up to 0.73 µg/L in Chinese rivers (Li et al., 2022), confirming the environmental relevance of the nanoscale fraction considered in this Thesis.

The lithosphere acts as a major sink for MNPLs (Yu & Flury, 2021), primarily due to particle retention in soils and sediments. Agricultural soils accumulate high loads of these materials through repeated applications of sewage sludge, compost, and manure (Edo et al., 2020). Reported concentrations range from a global median of 1,167 particles/kg in soil surveys (Büks & Kaupenjohann, 2020) to 13,460 particles/kg in sewage sludge samples from China (Li et al., 2019). However, these values must be interpreted with caution, as the literature displays considerable variability in sampling methods, size thresholds, and reporting units, which currently limits cross-study comparability (Jeong et al., 2024).

The widespread contamination of abiotic environments inevitably leads to the uptake of MNPLs by living organisms, facilitating their incorporation into food webs across both aquatic and terrestrial ecosystems (Carbery et al., 2018). As summarized in Table 3, MNPLs have been consistently detected in aquatic invertebrates such as mussels (0.36 particles/g) (Van Cauwenberghe & Janssen, 2014) and shrimps (24 particles/g) (Nan et al., 2020), as well as in fishes, where average burdens of approximately 50 particles per individual have been reported (Alaraby et al., 2025a). Bioaccumulation extends to higher trophic levels, with MNPLs found in seabirds (Haave et al., 2021), penguins (Kim et al., 2023), and mammals, including otters (Haave et al., 2021). Notably, polymers relevant to this Thesis, particularly PET and PS, have been identified in the tissues of wild birds (Haave et al., 2021), confirming their ecological transfer. Terrestrial organisms are also affected. MNPLs have been detected in

soil invertebrates (Thrift et al., 2025), and PTFE MPLs have been reported on honeybee surfaces (Schiano et al., 2024), suggesting atmospheric deposition as an additional pathway. Even plants can internalize MNPLs, with significant accumulations of PET-NPLs and PS-MPLs observed in leaf tissues collected near pollution sources (Ishfaq et al., 2025), providing further evidence of entry into terrestrial food chains.

Overall, current evidence indicates that MNPLs are ubiquitous contaminants, present in all environmental compartments and across biological taxa. Their widespread distribution not only reflects the persistence and mobility of plastic-derived particles but also provides a foundation for understanding human exposure pathways, which are addressed in the following section.

Table 2: *Summary of reported MNPL concentrations and deposition rates in abiotic environmental compartments (atmosphere, hydrosphere, lithosphere), compiled from selected literature sources. The table highlights the diversity of reported units.*

Compartment	Location	Concentration	Particle fraction	Source
Atmosphere	Outdoor air (across studies)	0 – 393 particles/m^3	MPLs	Din et al., 2024
Atmosphere	Indoor air (across studies)	0.13 – 14,000 particles/m^3	MPLs	Din et al., 2024
Atmosphere	China	4.18 particles/m^3	MPLs	Liu et al., 2019a
Atmosphere	Iran	0.3–1.1 particles/m^3	MPLs	Abassi et al., 2019
Atmosphere	Paris agglomeration, France	3-10 tons/year	MPLs (fibers)	Dris et al., 2016
Atmosphere	Dongguan, China	31–43 particles/m^2/day	MPLs	Cai et al., 2017
Atmosphere	London, United Kingdom	575–1,008 particles/m^2/day	MPLs	Wright et al., 2020
Hydrosphere	Freshwater (across studies)	0.02–2.19 particles/m^3	MPLs	Jeong et al., 2024
Hydrosphere	Drinking water (supply chain average)	700 particles/L	MPLs	Yu et al., 2024
Hydrosphere	Bottled water	Over 10,000 particles/L	MPLs	Mason et al., 2018
Hydrosphere	Danube river	900 particles/L	MPLs	Moore et al., 2005
Hydrosphere	Municipal wastewater plants (across studies)	15.1–640 particles/L	MPLs	Kang et al., 2018
Hydrosphere	Littoral zones, Africa and Europe	$7.25x10^{-7}$ – 100 particles/L	MNPLs	Besseling et al., 2019
Hydrosphere	Northwestern Pacific Ocean	10,000 particles/km^2	MNPLs	Pan et al., 2019
Hydrosphere	Dutch Wadden Sea	4.2 µg/L	PS-NPLs (<200 nm)	Materić et al., 2022a
Hydrosphere	Liao and Dalio rivers, China	<0.07 – 0.73 µg/L	PS-NPLs	Li et al., 2022
Lithosphere	Global soil (across studies)	1,167 particles/kg	MPLs	Büks & Kaupenjohann, 2020
Lithosphere	Agricultural soil, China	320–12,560 particles/kg	MPLs	Chen et al., 2020a
Lithosphere	Agricultural soil, Shanghai	136.6 - 256.7 particles/kg	MPLs	Liu et al., 2019b
Lithosphere	Agricultural soil, Germany	0.34 particles/kg	MPLs	Piehl et al., 2018
Lithosphere	Sewage sludge, China	5,553-13,460 particles/kg	MPLs	Li et al., 2019

Table 3: *Summary of reported MNPLs detections in various organisms from aquatic and terrestrial ecosystems, focusing on field observations. The table illustrates bioaccumulation across different trophic levels. Data compiled from selected literature sources.*

Category	Species	Concentration	Particle fraction	Source
Aquatic - Invertebrate	Mussels, Norway	1.5 particles/ind.	MPLs	Bråte et al., 2018
Aquatic - Invertebrate	Mussels, Tunisia	2.6–12 particles/ind.	MPLs	Wakkaf et al., 2020
Aquatic - Invertebrate	Mussels, farmed, Germany	0.36 particles/g	MPLs	Van Cauwenberghe & Janssen, 2014
Aquatic - Invertebrate	Shrimp (*P. australiensis*)	24 ± 31 particles/g	MPLs	Nan et al., 2020
Aquatic - Fish	Fish (global avg)	51.0 ± 72.4 particles/ind.	MPLs	Alaraby et al., 2025
Aquatic - Fish	Fish, East China	0.3 – 5.3 particles/ind.	MPLs	Su et al., 2019
Aquatic - Fish	*Solea solea*, Adriatic Sea	1.64 – 1.73 particles/ind.	MPLs	Pellini et al., 2018
Terrestrial & Semi-Aquatic	Soil invertebrate taxa	2.24 particles/sample; 32.2 particles/g	MPLs	Thrift et al., 2025
Terrestrial & Semi-Aquatic	Honeybees, multiple locations	Detected on body surface	MPLs	Schiano et al., 2024
Terrestrial & Semi-Aquatic	Otter (*Lutra lutra*)	Stomach: 1.7 µg/g (PVC)	MPLs	Haave et al., 2021
Terrestrial & Semi-Aquatic	Common guillemot (*Uria aalge*)	Stomach: 1.7 µg/g (PVC); Liver: 1.0 µg/g (PET)	MPLs	Haave et al., 2021
Terrestrial & Semi-Aquatic	Sawbill duck (*Mergus serrator*)	Intestine: 1.0 µg/g (PVC); 1.2 µg/g (PS)	MPLs	Haave et al., 2021
Terrestrial & Semi-Aquatic	Gentoo penguin chicks (*Pygoscelis papua*)	27.00 ± 25.28 particles/ind.	MPLs	Kim et al., 2023
Plants / Photosynthetic	Plant leaves (pollution hotspots)	10,000 ng/g	PET-NPLs and PS-MPLs	Ishfaq et al., 2025

1.3. Human Exposure to MNPLs and Evidence of Body Burden

1.3.1. MAJOR EXPOSURE ROUTES AND ESTIMATED LEVELS

The ubiquitous presence of MNPLs across all major environmental compartments inevitably results in widespread human exposure to these emerging contaminants (Vethaak & Legler, 2021). However, it is important to acknowledge at the outset the considerable uncertainty in quantifying exposure levels. The lack of standardized methodologies for sampling, detection, and analysis of MNPLs in environmental and biological matrices hinders the generation of accurate, comparable data; therefore, the figures presented below should be interpreted with caution (Domenech & Marcos, 2021).

Humans are chronically exposed to MNPLs through several primary pathways, namely ingestion (oral exposure) and inhalation (respiratory exposure), with dermal contact and iatrogenic sources representing additional, albeit less significant, routes (Jahedi & Jaafarzadeh Haghighi Fard, 2025; Zhang et al., 2025) (Figure 2).

Ingestion is recognized as a major pathway of human exposure, primarily through the consumption of contaminated food and beverages (Jahedi & Jaafarzadeh Haghighi Fard, 2025). MNPLs have been detected in a wide range of dietary sources; for instance, concentrations reported for drinking water range from around 700 MP particles/L in tap water (Yu et al., 2024) to over 10,000 particles/L in bottled water (Mason et al., 2018). Contamination is also widespread in solid food items, including fruits and vegetables (e.g., 132,740 particles/g) (Oliveri Conti et al., 2020), seafood (e.g., 0.98 particles/g) (Domenech & Marcos, 2021), and terrestrial meats such as beef (0.19 particles/g) and lamb (0.11 particles/g) (Bahrani et al., 2024). Beyond intrinsic contamination, food preparation and packaging substantially contribute to the ingestion burden. PP infant feeding bottles can release as many as 16.2 million particles/L during formula preparation (Li et al., 2020a), plastic teabags can shed up to 800 million MNPLs per cup (Banaei et al., 2023), and disposable PS

takeaway containers have been shown to release up to 29 MNPL particles per container (Du et al., 2020).

Inhalation constitutes another major exposure pathway. The low density and small size of MNPLs, especially NPLs, favor their suspension in air and subsequent respiratory uptake (Alzaben et al., 2023). Airborne MNPLs originate from diverse sources, including fiber shedding from textiles, tire wear, construction materials, and waste incineration (Domenech & Marcos, 2021). Notably, indoor air concentrations often exceed outdoor levels by several orders of magnitude (Din et al., 2024), increasing the potential risk of chronic exposure in domestic and occupational environments.

Dermal contact represents a comparatively inefficient route of entry, particularly when the skin barrier remains intact (Revel et al., 2018). Exposure occurs mainly through personal care products containing microbeads (Hernandez et al., 2017) and through direct contact with synthetic fibers released from clothing (Domenech & Marcos, 2021). Finally, iatrogenic exposure involves the direct introduction of MNPLs into the body via medical devices or clinical procedures. Potential sources include plastics shed from syringes, intravenous bags, catheters, and implants, as well as airborne contaminants in surgical settings (Jahedi & Jaafarzadeh Haghighi Fard, 2025). Recent evidence even suggests that procedures such as cardiac surgery may represent a direct, barrier-bypassing route for MNPL entry into the bloodstream (Liu et al., 2024).

Several studies have attempted to estimate overall human exposure by integrating uptake values from ingestion and inhalation data. However, as expected, given the methodological inconsistencies, these estimates vary by several orders of magnitude. For instance, a systematic review estimated annual ingestion exposure at 2.93×10^{10} particles per person (Domenech & Marcos, 2021), a figure consistent with the high concentrations reported in some dietary items. Conversely, other commonly cited assessments combining ingestion and inhalation yield considerably lower estimates, typically between 74,000 and 121,000 particles per person per year (Yee et al., 2021). This wide discrepancy underscores the current lack of harmonization and the substantial uncertainty surrounding exposure quantification (Zhu & Wang, 2020).

Moreover, existing exposure estimates likely underrepresent the true burden, particularly concerning the nanoscale fraction (Zhang et al., 2023a). Current analytical methodologies face significant challenges in detecting and quantifying NPLs within complex environmental and biological matrices (Pradel et al., 2023). Because standard sampling and spectroscopic techniques often lack the nanometer-scale resolution required, most available data focus predominantly on MPLs (Gigault et al., 2021). This results in a scarcity of reliable quantitative measures of NPLs, leaving current exposure scenarios for this segment largely model-based rather than empirically validated (Rubio et al., 2019).

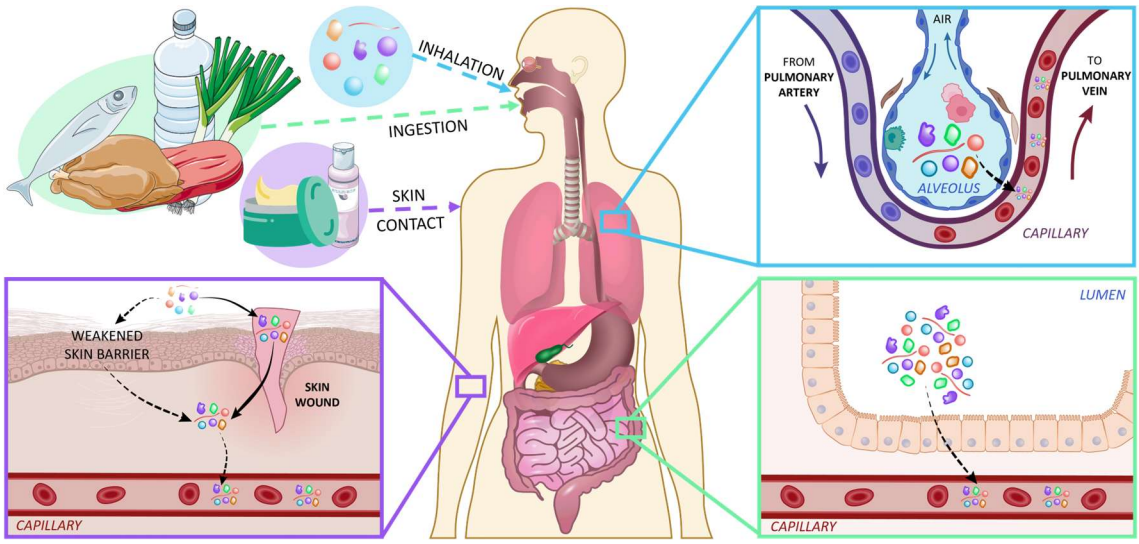


Figure 2: *Routes of human exposure to MNPLs and their translocation into the bloodstream. Ingestion, inhalation, and dermal contact represent the primary exposure pathways, with MNPLs crossing biological barriers, including the intestinal epithelium, alveolar membrane, and skin, to reach systemic circulation. Adapted from Yee et al., 2021.*

1.3.2. TRANSLOCATION ACROSS BIOLOGICAL BARRIERS AND EVIDENCE OF PRESENCE IN HUMAN TISSUES AND FLUIDS

Following the main exposure routes of ingestion and inhalation (Jahedi & Jaafarzadeh Haghighi Fard, 2025), MNPLs, particularly NPLs, can traverse epithelial barriers via translocation (Bai et al., 2024). This mechanism enables their entry into the internal environment, allowing access to systemic circulation and subsequent distribution to organs and tissues (Zhu et al., 2023).

Among the parameters influencing this process, particle size is the most critical. Translocation efficiency increases markedly as particle dimensions enter the nanoscale (Rubio et al., 2019), enhancing absorption and

biodistribution. This is attributed to NPLs exploiting active cellular uptake pathways that are inaccessible to larger particles (Sousa de Almeida et al., 2021). These include endocytic pathways, such as clathrin-mediated endocytosis, macropinocytosis, and transcytosis, which allow NPLs to cross tight junctions and reach internal compartments (Sousa de Almeida et al., 2021). Additionally, NPLs may facilitate their own passage via passive diffusion or by inducing membrane fluidization and disruption (Liu et al., 2021). In contrast, larger MPLs exhibit limited permeability, being largely restricted to phagocytic uptake by immune cells or alternative mechanisms such as persorption (migration of particles through epithelial gaps) (Rubio et al., 2019).

The capacity for MNPL translocation has been substantiated by multiple *in vitro* models. Intestinal co-cultures using Caco-2 and HT-29 cell lines have shown that MNPLs can traverse epithelial monolayers (Domenech et al., 2020), while Calu-3 pseudostratified epithelium maintained at the air–liquid interface (ALI) has demonstrated disruption of the bronchial barrier (García-Rodríguez et al., 2024).

This experimental evidence is supported by the detection of MNPLs in human biological samples, confirming a measurable internal “body burden”. MNPLs have been identified in several fluids, including blood, breast milk, urine, semen, sputum, amniotic fluid, cerebrospinal fluid, and saliva (Enyoh et al., 2023; Halfar et al., 2023; He et al., 2025; Pechcińska et al., 2025). Their presence in blood provides direct evidence of systemic distribution. A pivotal study detected MNPLs (≥ 700 nm) in the blood of 21 out of 22 healthy donors, with an average concentration of 1.6 µg/mL; PET, PS, and PE were the most prevalent polymers (detected in 50%, 36%, and 23% of donors, respectively) (Leslie et al., 2022).

Evidence of systemic distribution is further evident in secondary organs and tissues. MNPLs have been detected in the human placenta, where MPLs—including polyamide, PE, PP, PET, and PU—were found in 100% of the 18 placenta samples tested (Liu et al., 2023). This observation is supported by *ex vivo* placental perfusion models demonstrating that PS-NPLs up to 300 nm can cross the placental barrier (Grafmueller et al., 2015). Similarly, PET-MPLs have been identified in meconium, indicating prenatal exposure (Jahedi &

Jaafarzadeh Haghighi Fard, 2025). In the respiratory system, MNPLs were found in human lung tissue in more than half of the analyzed samples, with detected particles (1.60–5.56 µm) being of a size capable of reaching the deep bronchoalveolar regions (Amato-Lourenço et al., 2021). Accumulation has also been reported in hepatic and renal tissues; post-mortem analyses showed that total MNPL concentrations in the liver increased over time (2016 vs 2024), with comparable levels measured in the kidney (Nihart et al., 2025).

Remarkably, translocation across the blood–brain barrier (BBB) has been suggested by the detection of MNPLs in human brain tissue. Samples from the frontal cortex displayed higher MNPL concentrations (median approx. 4917 µg/g, 2024) than those observed in the liver or kidney, consisting mainly of NPL fragments between 100 and 200 nm. Greater accumulations were reported in the brains of individuals diagnosed with dementia, where MNPLs were localized along cerebrovascular walls (Nihart et al., 2025). Additional studies have identified MNPLs in the heart (Ali et al., 2024), spleen (Jahedi & Jaafarzadeh Haghighi Fard, 2025), testes, and endometrium (Prattichizzo et al., 2024), indicating extensive systemic dissemination.

Collectively, findings from mechanistic models and human biomonitoring converge on the conclusion that MNPLs, particularly at the nanoscale, can breach primary biological barriers, such as the intestinal and pulmonary epithelia, enter the systemic circulation, and accumulate in multiple organs. The confirmed presence of MNPLs in human tissues and biological fluids underscores the importance of evaluating the biological consequences of this internal exposure. This requires integrating evidence from controlled *in vivo* models that capture systemic responses with mechanistic insights from human cellular systems, which enable the dissection of molecular pathways in specific target tissues (Figure 3).

1.4. Biological Impact of MNPLs on Human Health: State of the Art

1.4.1. REPORTED EFFECTS IN ANIMAL MODELS *(IN VIVO)*

A wide range of animal models has been employed to investigate the biodistribution of MNPLs and the systemic consequences of their exposure. Mammalian models, primarily rodents such as mice and rats, are most frequently used owing to their genetic, biochemical, and physiological similarity to humans (O'Neill & Lawler, 2021). Aquatic organisms, including zebrafish (*Danio rerio*) and marine medaka (*Oryzias melastigma*), are widely applied in ecotoxicological research, providing insights into environmentally relevant exposure scenarios (Cormier et al., 2022). Invertebrate models such as *Drosophila melanogaster* and the nematode *Caenorhabditis elegans* offer powerful genetic systems for mechanistic studies (Irion & Nüsslein-Volhard, 2022). Across these models, MNPL accumulation has been consistently observed following controlled exposures. In rodents, MNPLs have been detected in metabolic and filtration organs (liver, kidney, spleen), as well as in reproductive tissues and the brain; transplacental transfer into fetal tissues has been documented following maternal exposure (Fournier et al., 2020). Similarly, aquatic models such as zebrafish show accumulation in the liver, gills, and gonads, in addition to the brain (Sarasamma et al., 2020), while in invertebrates like *D. melanogaster*, internalization has been confirmed in the gut, hemolymph, and reproductive organs (Alaraby et al., 2025b). Collectively, these findings demonstrate that MNPLs can cross biological barriers and distribute systemically, reinforcing experimental evidence of their detection in human tissues and biological fluids.

Beyond biodistribution, *in vivo* models have been instrumental in elucidating the systemic effects associated with MNPL exposure (Figure 3, central panel). The most consistent findings converge on oxidative stress and inflammation as central toxicological pathways (Mahmud et al., 2024). Excessive generation of reactive oxygen species (ROS) is widely recognized as a primary mechanism of MNPL-induced toxicity (Fan et al., 2022). For example, oral administration of PS-NPLs in mice elevates ROS levels, disrupts antioxidant defenses, and

induces oxidative damage (Fan et al., 2022). Similar effects have been reported in the brain tissue of zebrafish embryos (Sökmen et al., 2020) and in *D. melanogaster* larvae (Alaraby et al., 2023), indicating a conserved oxidative-stress response across taxa. In parallel, an inflammatory response frequently accompanies this oxidative imbalance. Experimental studies in mice show immune dysregulation after MNPL exposure, including elevated leukocyte and lymphocyte counts (Wang et al., 2023a), together with increased expression of pro-inflammatory mediators such as interleukin-1 (IL-1), interleukin-6 (IL-6), monocyte chemoattractant protein-1 (MCP-1), and transforming growth factor-beta (TGF-β) (Jeong et al., 2024; Wang et al., 2023a). Invertebrate models further support these findings, with transcriptomic analyses in *D. melanogaster* confirming the upregulation of genes involved in inflammation and immune activation (Alaraby et al., 2024a). Taken together, this oxidative–inflammatory cascade is considered a fundamental driver of the systemic dysfunctions and organ-specific toxicities discussed next.

In addition to oxidative and inflammatory responses, MNPL exposure has been implicated in disrupting several systemic processes, most notably metabolic homeostasis, as well as genotoxicity, neurotoxicity, and reprotoxicity. Metabolic alterations are among the most consistently reported outcomes (Ali et al., 2024). Oral exposure to PS-NPLs in mice induces abnormal hepatic lipid droplet accumulation, elevates triglyceride and cholesterol levels, and reduces ATP, consistent with impaired energy metabolism (Yu et al., 2024). Perturbations in glucose regulation, such as increased plasma glucose levels following chronic exposure, have also been reported (Fan et al., 2022). These metabolic effects are frequently associated with gut dysbiosis; studies in rodents and *D. melanogaster* show shifts in microbiota composition and diversity (Fan et al., 2022; Rocabert et al., 2025), accompanied by evidence of intestinal epithelial damage in zebrafish (Lei et al., 2018) and altered mucus secretion in mice (O'Neill & Lawler, 2021).

Genotoxicity is also emerging as a concern associated with MNPL exposure. Evidence across diverse organisms shows that MNPLs can induce DNA strand breaks, micronucleus formation, and abnormal sperm morphology (Tang, 2025; Alimba et al., 2025). Although direct interactions with nuclear DNA have been

hypothesized, current evidence more consistently supports an indirect mechanism mediated by ROS-driven oxidative damage to nucleic acids (Tang, 2025; Alimba et al., 2025). In rodents, PS-NPL exposure increases markers of oxidative DNA damage in gastrointestinal tissues (Ding et al., 2024a), whereas in *D. melanogaster*, real-life PET-titanium NPLs (PET-Ti-NPLs) induce dose-dependent DNA damage in hemocytes (Alaraby et al., 2024b). Germ-cell alterations, including increased sperm abnormalities and DNA damage, have also been reported in mice and rats (Xie et al., 2020; Amereh et al., 2020; Jin et al., 2021). Collectively, these findings indicate that genotoxicity is a relevant component of MNPL-induced systemic toxicity, largely mediated by oxidative mechanisms.

Neurotoxicity represents another critical endpoint. Multiple *in vivo* studies confirm that NPLs can cross the BBB and accumulate in neural tissue (Kik et al., 2020). This accumulation triggers oxidative stress in the brain. It is often accompanied by neurobehavioral impairments, including hypoactivity in fish (Sökmen et al., 2020) and anxiety-like behavior in rats (O'Neill & Lawler, 2021). In mice, PS-NPL exposure alters cerebral metabolic profiles and reduces acetylcholinesterase (AChE) activity, suggesting interference with neurotransmission (Ali et al., 2024).

Reproductive toxicity has also been widely documented in vertebrate and invertebrate models (Ali et al., 2024). In female mice, exposure to PS-MPLs has been linked to reduced ovarian size and follicle number, hormonal changes, lower pregnancy rates, and fewer embryos (Ali et al., 2024). In male rodents, prolonged PS-NPL exposure reduces circulating testosterone, luteinizing hormone (LH), and follicle-stimulating hormone (FSH), resulting in reduced sperm count, motility, and maturation, as well as increased DNA damage (O'Neill & Lawler, 2021). Comparable findings have been reported in *D. melanogaster*, where NPLs accumulate within the gonads, causing structural damage (e.g., ovarian atrophy) and reductions in fecundity and fertility (Alaraby et al., 2025b).

While these *in vivo* findings collectively demonstrate MNPLs' capacity to induce systemic toxicity, a fundamental limitation persists: the inherent challenge of extrapolating toxicological data from animal physiology to human

health (O'Neill & Lawler, 2021). Species-specific differences in metabolism, immune response, and protein interactions mean that animal data provide critical evidence of potential risk, but cannot fully predict human-specific cellular responses (O'Neill & Lawler, 2021). Consequently, to elucidate the molecular mechanisms underlying these adverse effects in a direct human context and to overcome this interspecies gap, human-based *in vitro* systems are an essential complementary approach, as explored in the following section.

1.4.2. OBSERVED EFFECTS IN HUMAN CELLULAR MODELS (*IN VITRO/EX VIVO*)

To clarify the molecular mechanisms of MNPL exposure in humans and reduce interspecies extrapolation uncertainties, a broad range of *in vitro* and *ex vivo* human models has been employed (Rubio et al., 2019). These systems encompass principal biological barriers such as intestinal Caco-2 and HT29-MTX (Banaei et al., 2024) and pulmonary Calu-3 or primary airway epithelia (HNEpCs) (García-Rodríguez et al., 2024; Annangi et al., 2023a), immune components such as THP-1 monocytes and primary peripheral blood mononuclear cells (PBMCs) (Vela et al., 2023; Ballesteros et al., 2020), and major target tissues including hepatic HUH-7 (Morataya-Reyes et al., 2025a), renal HK-2, and placental BeWo b30 cells (Dusza et al., 2023). Across these models, internalization is consistently observed and acts as the initiating event for downstream toxicity. Once inside the cell, MNPLs elicit responses at sublethal doses that align with core toxicological pathways and also reveal tissue-specific dysfunctions, including autophagic disturbance, metabolic imbalance, and loss of barrier function (Ali et al., 2024) (Figure 3, right panel).

Oxidative stress is the most common effect and typically manifests as increased intracellular ROS levels, which are associated with mitochondrial dysfunction, including loss of mitochondrial membrane potential (Siemiątkowska & Szczepanowska, 2025). The resulting redox imbalance weakens antioxidant defenses and promotes oxidative damage to lipids, proteins, and DNA in immune, epithelial, and hepatic models alike (Mahmud et al., 2024). In parallel, a pro-inflammatory program is frequently activated. Canonical signaling pathways, such as nuclear factor kappa-B (NF-κB) and the

NLR family pyrin domain containing 3 (NLRP3) inflammasome, contribute to cytokine maturation and release, including interleukin-1 beta (IL-1β), IL-6, interleukin-8 (IL-8), and tumor necrosis factor-alpha (TNF-α), and can bias macrophage polarization toward a pro-inflammatory M1 phenotype (Prattichizzo et al., 2024; Tavakolpournegari et al., 2024; Mahmud et al., 2024). The intensity of this inflammatory response varies with particle characteristics, underscoring the central role of physicochemical properties (Weber et al., 2022).

Direct cellular damage has also been documented. Genotoxicity has been reported across various cell models, including intestinal, hepatic, and lymphocyte cells, with documented effects ranging from single-strand breaks to cytogenetic alterations such as micronuclei, nucleoplasmic bridges, and chromosomal aberrations (Roursgaard et al., 2022; Sarma et al., 2022). Cytotoxicity is generally dose- and time-dependent, although the specific toxic threshold varies significantly based on cell type and particle characteristics. Consequently, many studies using concentrations below this variable threshold report minimal or no loss of cell viability. This highlights the importance of evaluating subtoxic functional endpoints, which can reveal significant cellular damage even when viability appears unaffected (Tavakolpournegari et al., 2024; Mahmud et al., 2024).

Specialized pathways are frequently perturbed in a tissue-dependent manner. Autophagy is a consistent target, often in connection with endoplasmic reticulum stress or attenuation of phosphoinositide 3-kinase/protein kinase B/mechanistic target of rapamycin (PI3K/Akt/mTOR) signaling (Wan et al., 2024; Annangi et al., 2023b; Mahmud et al., 2024). An increase in microtubule-associated protein light chain 3-II (LC3-II) is commonly observed. Depending on the model, this occurs with p62 (sequestosome-1) accumulation, indicative of blocked autophagic flux, or with p62 reduction, consistent with autophagy induction (Wan et al., 2024; Annangi et al., 2023a). Metabolic disruption is likewise prevalent. Lipid homeostasis is altered in macrophages and liver organoids, with lipid droplet accumulation, activation of lipogenic programs such as protein kinase R-like endoplasmic reticulum kinase/activating transcription factor 4 (PERK/ATF4), and reduced expression of cholesterol

efflux transporters, including ATP-binding cassette transporter A1 (ABCA1) and G1 (ABCG1) (Zhang et al., 2025; Yu et al., 2024). Glucose metabolism in hepatic cells is affected by interference with the PI3K/Akt pathway, whereas mitochondrial injury and reduced ATP levels indicate impaired energy production across models (Yu et al., 2020; Fan et al., 2022). Barrier integrity is compromised in intestinal and pulmonary epithelia models, as demonstrated by alterations in key functional and molecular markers. These effects include decreases in transepithelial electrical resistance (TEER), increases in barrier permeability, and disruption of tight junction proteins such as zonula occludens-1 (ZO-1). Notably, molecular disruption (ZO-1) has been observed even when functional resistance (TEER) was not significantly affected, indicating multiple pathways of damage (Brouwer et al., 2025; García-Rodríguez et al., 2024).

Longer exposures raise concerns about carcinogenic potential. Cell transformation assays and sensitive models indicate that MNPLs can act as non-genotoxic tumor promoters by facilitating the expansion of initiated cells (Domenech et al., 2024). Prolonged treatments to thirty weeks have been associated with a tumorigenic phenotype *in vitro*, including anchorage-independent growth, increased invasion, genomic instability, activation of epithelial-to-mesenchymal transition (EMT), and upregulation of oncogenes, with stronger effects under co-exposures with cigarette smoke condensate (Gutiérrez-García et al., 2025; Morataya-Reyes et al., 2025b).

Overall, human cellular models reveal a consistent pattern that spans oxidative stress, inflammation, genotoxicity, cytotoxicity, autophagic and metabolic dysregulation, and barrier failure across diverse systems. The magnitude and nature of these effects depend strongly on the cell type studied and, most importantly, on the MNPLs' intrinsic physicochemical properties. The following section examines how surface chemistry and functionalization, particle size, polymer type, and environmental realism together determine this bio-reactivity.

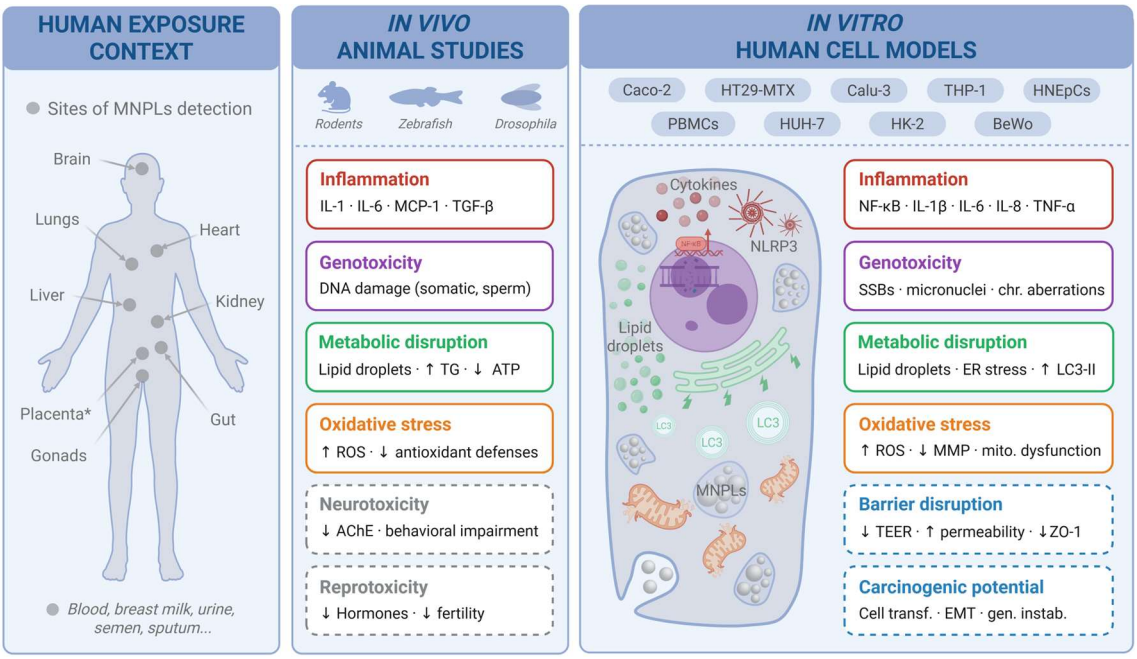


Figure 3: *Integrated overview of human exposure to MNPLs and associated biological effects. The left panel depicts MNPL detection sites in human tissues and fluids; the central and right panels summarize toxicological findings from in vivo and in vitro models, respectively. Shared mechanistic pathways are color-coded (red: inflammation; purple: genotoxicity; green: metabolic disruption; orange: oxidative stress). Dashed gray borders: effects exclusive to animal models (neurotoxicity, reprotoxicity); dashed blue borders: findings exclusive to cell culture systems (barrier disruption, carcinogenic potential). *Transplacental transfer to fetal tissues has been documented. Abbreviations: AChE, acetylcholinesterase; ATP, adenosine triphosphate; EMT, epithelial-to-mesenchymal transition; ER, endoplasmic reticulum; LC3-II, microtubule-associated protein light chain 3-II; MCP-1, monocyte chemoattractant protein-1; MMP, mitochondrial membrane potential; MNPLs, micro- and nanoplastics; NF-κB, nuclear factor kappa-B; NLRP3, NLR family pyrin domain containing 3; ROS, reactive oxygen species; SSBs, single-strand breaks; TEER, transepithelial electrical resistance; TG, triglycerides; TGF-β, transforming growth factor-beta; TNF-α, tumor necrosis factor-alpha; ZO-1, zonula occludens-1. Created with BioRender.com.*

1.4.3. THE INFLUENCE OF PHYSICOCHEMICAL PROPERTIES ON THE BIO-REACTIVITY OF MNPLS: PREVIOUS EVIDENCE

1.4.3.1. Impact of surface chemistry and functionalization

The intrinsic surface chemistry of MNPLs plays a central role in determining their biological interactions and toxicological behavior. Most studies addressing this aspect rely on three surface variants of PS-NPLs as model materials: pristine NPLs (PS-P-NPLs), which provide the baseline; carboxylated NPLs (PS-C-NPLs), which introduce anionic groups; and aminated NPLs (PS-A-NPLs; a category that also includes amidine-functionalized variants), which incorporate cationic amino groups. These functional groups strongly influence particle–cell interactions (Shi et al., 2022). Because cellular membranes are predominantly negatively charged, cationic amino groups facilitate strong, localized electrostatic interactions. Consequently, a general trend in the

literature is that PS-A-NPLs exhibit greater cellular association, internalization, and acute cytotoxicity than their PS-P-NPLs or PS-C-NPLs counterparts (Płuciennik et al., 2024).

High internalization efficiencies of PS-A-NPLs have been reported in several non-phagocytic models. For instance, PS-A-NPLs (20 and 120 nm) showed a 20-40-fold higher transport rate across rat alveolar epithelial cell monolayers than PS-C-NPLs (Yacobi et al., 2010). This trend was even more pronounced in Madin Darby canine kidney cell II (MDCK-II), where PS-A-NPLs demonstrated a 500-fold higher translocation rate compared to PS-C-NPLs across different particle sizes (Fazlollahi et al., 2011). Human models show comparable patterns: 50 nm PS-A-NPLs exhibit higher uptake than 50 nm PS-C-NPLs, which in turn exhibit higher uptake than 50 nm PS-P-NPLs, in gastric SNU-1 cells (Banerjee et al., 2021). Similarly, a comparable trend of increased internalization of PS-A-NPLs relative to PS-C-NPLs has been reported in respiratory cells such as A549 and BEAS-2B (Siemiątkowska & Szczepanowska, 2025). This pattern, however, is not universal. In professional phagocytes, such as macrophages, and in *ex vivo* human whole-blood models, PS-C-NPLs are internalized more efficiently (Martin et al., 2022; Arribas Arranz et al., 2024). A preference for PS-C-NPLs has also been reported in gastrointestinal co-cultures of Caco-2 and HT29-MTX cells (Banerjee & Shelver, 2021). This dual behavior demonstrates that internalization is not governed solely by simple electrostatic interactions but rather by distinct internalization mechanisms that depend on both the particle's specific physicochemical characteristics and, critically, the cell type in question (Banerjee & Shelver, 2021).

Despite the variability in uptake, acute cytotoxicity is consistently stronger for PS-A-NPLs across various nanoscale sizes in a wide range of human models, including respiratory, gastrointestinal, and immune cells, as well as in animal cell lines (Banerjee & Shelver, 2021; Płuciennik et al., 2024). These effects occur at concentrations at which their pristine or carboxylated counterparts typically exhibit no loss of viability. The prevailing explanation links this enhanced toxicity to direct membrane damage induced by the cationic groups. In TT1 alveolar epithelial cells, 50 nm PS-A-NPLs caused severe disruption of

the plasma membrane (Ruenraroengsak et al., 2012), whereas in lipid bilayer membranes, 20 nm PS-A-NPLs have been shown to induce deformation and pore formation (Li & Malmstadt, 2013). Other studies associate this toxicity with mitochondrial injury, rapid ATP depletion, and necrotic cell death (Banerjee & Shelver, 2021; Płuciennik et al., 2024).

Beyond cytotoxicity, sublethal endpoints such as oxidative stress, inflammation, and genotoxicity are widely reported. PS-A-NPLs usually elicit the strongest responses (Płuciennik et al., 2024). They induce substantial ROS production across different nanoscale sizes in hepatic, immune, and respiratory models (He et al., 2020; Banerjee & Shelver, 2021; Shi et al., 2022), often linked to mitochondrial dysfunction or ROS-driven autophagy (Płuciennik et al., 2024). Regarding the inflammatory response, 100 nm PS-A-NPLs activate the NLRP3 inflammasome in macrophages (Lunov et al., 2011) and promote high secretion of IL-6 and IL-8 in respiratory cells (Ruenraroengsak et al., 2012). However, PS-C-MNPLs also induce cytokine release in monocytes and macrophages (Banerjee & Shelver, 2021). Genotoxicity is likewise influenced by surface chemistry. 50 nm PS-A-NPLs increase DNA damage in Calu-3 cells, an effect linked to glutathione depletion (Paget et al., 2015), while in A549 cells, both 80 nm PS-A-NPLs and 80 nm PS-C-NPLs increase micronuclei formation more than 80 nm PS-P-NPLs (Shi et al., 2022).

Importantly, high internalization does not necessarily correlate with higher toxicity. Several studies report a disconnect between uptake and biological outcome. In HUH-7 cells, 50 nm PS-C-NPLs internalized efficiently but produced minimal oxidative or genotoxic effects (Morataya-Reyes et al., 2025a). Conversely, in *ex vivo* human blood, 50 nm PS-A-NPLs triggered a strong cytokine response despite markedly lower internalization than 50 nm PS-C-NPLs (Arribas Arranz et al., 2024).

The particle's biological environment further modulates these complex interactions. For PS-NPLs, surface chemistry governs how NPLs interact with components of biological fluids, promoting the formation of a protein corona that confers a new biological identity (Sabourian et al., 2020). This corona can either dampen or enhance cellular interactions. In some models, such as A549 cells, the formation of protein corona reduces cytotoxicity (Kihara et al., 2021),

whereas in others, the development of the corona increases uptake and toxicity (Sabourian et al., 2020; Płuciennik et al., 2024). Thus, although cationic surfaces are typically associated with acute membrane disruption, the broader spectrum of sublethal responses (including oxidative stress, inflammation, and genotoxicity) is shaped not only by intrinsic functionalization but also by the dynamic biological identity acquired upon exposure to complex media.

1.4.3.2. Impact of particle size

Particle size is widely considered the most critical physicochemical determinant defining the biological effects of MNPLs. NPLs (<1 µm) are generally regarded as significantly more hazardous than MPLs (1 µm–5 mm). This heightened bio-reactivity stems from their larger surface-to-volume ratio, which increases membrane interaction, intracellular transport, and surface reactivity (Gigault et al., 2021). Consistently, an inverse relationship between particle size and uptake efficiency has been reported across multiple human cell lines. In intestinal Caco-2 models, PLA-NPLs (250 nm) crossed the epithelial barrier more efficiently than 2000 nm PLA-MPLs (Paul et al., 2023). This trend persists strictly within the nanoscale: in gastric SNU-1 cells, PS-A-MNPLs followed a clear size-dependent pattern, with 50 nm PS-A-NPLs taken up to a greater extent than 100 nm PS-A-NPLs, which in turn surpassed 1000 nm PS-A-MPLs (Banerjee et al., 2021). Comparable inverse correlations have been reported in hematopoietic models, such as Raji-B and THP-1 cells, with PS-P-NPLs (50 nm > 200 nm > 500 nm) (Tavakolpournegari et al., 2023). The mechanistic basis for this behavior lies in the internalization pathways favored at each size range. The smallest NPLs may partially enter the cell by passive diffusion across the lipid bilayer (Gigault et al., 2021). NPLs below 200 nm typically engage clathrin-mediated endocytosis, an efficient constitutive pathway. Intermediate sizes (200–1000 nm) rely more heavily on caveolae-mediated endocytosis or macropinocytosis, which proceed at slower kinetics or require activation (Khan & Jia, 2023; Rejman et al., 2004). Larger MPLs (>1 µm) generally require phagocytosis, restricting their uptake into professional phagocytes and limiting entry into non-phagocytic cells (Alqahtani et al., 2023; Khan & Jia, 2023).

As a direct result of their enhanced uptake and surface activity, smaller NPLs trigger more pronounced toxicological responses than larger MNPLs. This size-dependent pattern is evident across cytotoxicity, oxidative stress, and genotoxicity. In murine macrophages, 80 nm PS-P-NPLs induced greater cell death than 3 µm PS-P-MPLs (Wang et al., 2023b). This inverse relationship holds strictly within the nanoscale as well. In human lung A549 cells, 25 nm PS-P-NPLs induced significant toxicity and apoptosis at low concentrations (25–30 µg/mL), whereas 70 nm PS-P-NPLs required concentrations an order of magnitude higher (160–300 µg/mL) to elicit comparable effects (Xu et al., 2019). Oxidative stress follows the same trend. In primary human nasal epithelial cells (HNEpCs), 50 nm PS-P-NPLs induced greater mitochondrial membrane potential loss than 500 nm PS-P-NPLs, accompanied by a higher trend in ROS production (Annangi et al., 2023a). This oxidative pressure translates into greater genotoxicity. In A549 cells, 80 nm PS-P-NPLs were markedly more genotoxic than 2 µm PS-P-MPLs (Shi et al., 2022), and in human PBMCs, 29 nm PS-P-NPLs produced stronger DNA damage than larger PS-P-NPLs (44 and 72 nm) (Malinowska et al., 2022), a trend also observed *in vivo* in *D. melanogaster* (Alaraby et al., 2022).

However, the inverse size–toxicity relationship is not universal, particularly in the context of inflammatory responses, where diverging results have emerged. In airway TT1 cells, 50 nm PS-A-NPLs stimulated significantly higher IL-8 and IL-6 release than 100 nm PS-A-NPLs (Ruenraroengsak et al., 2012), in line with the general trend. However, in macrophage-like models, 500 nm PS-C-NPLs and 1000 nm PS-C-MPLs enhanced IL-6 secretion, whereas the smaller 20 nm and 100 nm PS-C-NPLs did not produce a statistically significant increase (Prietl et al., 2014). These observations indicate that, unlike oxidative stress or genotoxicity, the inflammatory potential of MNPLs does not consistently follow a size-dependent trend; rather, it varies substantially across cellular contexts and experimental conditions.

1.4.3.3. Impact of environmental realism

Most nanotoxicological research has predominantly focused on pristine, spherical, and monodisperse PS-P-MNPLs. While these idealized model MNPLs offer strong experimental reproducibility, they do not accurately

represent the physicochemical complexity of secondary MNPLs formed in the environment (Villacorta et al., 2022). Unlike primary PS-P-NPLs, environmentally derived MNPLs are typically characterized by irregular morphologies, heterogeneous surface chemistries, and broad polydispersity (Gigault et al., 2021). This heterogeneity reflects both their intrinsic size distribution, arising from fragmentation, and their strong tendency to aggregate in biological media (Gigault et al., 2021; Morataya-Reyes et al., 2025a). As a result, relying exclusively on stable, monodisperse materials may lead to simplified toxicity profiles that are not fully representative of real-world exposure scenarios (Weber et al., 2022). Consequently, NPLs cannot be considered a single homogeneous group, and emerging research has begun to investigate the influence of environmental realism through test materials generated by top-down degradation or environmental aging procedures (Weber et al., 2022).

Regarding the specific contribution of particle morphology and heterogeneity, several studies indicate that irregular and polydisperse MNPLs elicit stronger toxicological responses than spherical, monodisperse counterparts. Weber et al. (2022) reported that irregular, polydisperse PS-NPLs induced higher IL-6 and TNF secretion in primary human monocytes and dendritic cells compared with spherical PS-P-NPLs. Rough or fractured surface structures also appear relevant; PE-MPLs with uneven surfaces produced higher cytotoxicity, pro-inflammatory cytokine release, and hemolysis across multiple cell types, whereas smooth PE-MPLs lacked significant cytotoxicity and only triggered immune and hemolytic responses at high concentrations (Choi et al., 2021). Mechanistically, these effects have been suggested to result from the larger relative surface area of irregular MNPLs, which provides more extensive cell-particle contact (Weber et al., 2022) and, in some cases, with sharp edges that can induce mechanical membrane damage (Choi et al., 2021).

Environmental realism also encompasses the physicochemical transformations induced by weathering processes. In natural settings, plastic debris is exposed to UV radiation, mechanical abrasion, oxidation, and microbial activity, all of which modify its surface properties relative to pristine laboratory materials (Płuciennik et al., 2024). These environmental processes can introduce

oxygen-containing functional groups, reduce particle size, and generate more irregular and porous surfaces (Yu & Flury, 2021; Shi et al., 2021). Consistently, several studies have shown that weathered MNPLs exhibit higher biological reactivity than untreated ones. UV-photodegraded PS-NPLs induced stronger cytotoxicity and ROS generation in A549 lung cells than PS-P-NPLs (Shi et al., 2021). Similar trends have been reported for other polymers; while pristine PET-MPLs already induced IL-1β secretion in human macrophages, combined UV and ultrasound weathering significantly amplified this effect (Washihira et al., 2024).

Given the growing evidence that physicochemical realism strongly influences biological responses, recent studies have explored the use of real-life MNPLs generated directly from consumer plastic products. Secondary PET-NPLs derived from water bottles have demonstrated significantly stronger effects than pristine standards. In human hepatic models, Morataya-Reyes et al. (2025a) showed that realistic PET-NPLs induced oxidative stress and genotoxicity, whereas PS-P-NPLs did not. In the Bhas 42 cell transformation assay, real-life PET-NPLs acted as tumor promoters, increasing the number of transformed foci (Domenech et al., 2024). This enhanced bioactivity has also been documented *in vivo*; secondary PET-NPLs induced oxidative stress in *D. melanogaster* (Alaraby et al., 2023), and recent proteomic analyses in murine macrophages revealed that real-life PET-NPLs modulate immune-related pathways and endoplasmic reticulum stress (Collin-Faure et al., 2025). Taken together, these findings indicate that environmental realism, including polymer type, irregular morphology, polydispersity, and weathering, plays a decisive role in shaping the biological effects of MNPLs. This underscores the importance of incorporating representative test materials into experimental designs to better reflect real-world exposure and enhance the relevance of health risk assessment.

1.5. The Vascular Endothelium: A Critical Target for Circulating MNPLs

Once MNPLs gain access to the systemic circulation, the vascular system becomes the first and most extensive biological interface they encounter (Prattichizzo et al., 2024). Circulating MNPLs remain in continuous contact with the blood compartment and, critically, with the vascular endothelium. This highly sensitive and metabolically active barrier governs vascular tone, inflammation, coagulation, and overall cardiovascular homeostasis (Cao et al., 2017). As a result, the cardiovascular system represents the primary systemic target for translocated MNPLs. Emerging clinical and experimental evidence indicates that their presence in blood and vascular tissues is not merely a marker of exposure but may contribute directly to vascular dysfunction and cardiometabolic disease (Prattichizzo et al., 2024). The following sections summarize the current state of knowledge regarding the cardiovascular impact of MNPLs, integrating clinical observations with mechanistic findings derived from *in vivo* and *in vitro* models.

1.5.1. CARDIOVASCULAR IMPACT OF MNPLS: CLINICAL EVIDENCE AND SYSTEMIC PATHOPHYSIOLOGY

As previously detailed in Section 1.3.2, the presence of MNPLs in human blood was first confirmed in 2022 by Leslie et al. (Leslie et al., 2022). Subsequent work expanded this evidence: in 2023, Yang et al. detected several MNPL polymers in cardiac tissues collected from patients undergoing heart surgery (Yang et al., 2023a), and additional studies identified MNPLs in human thrombi, supporting their ability to circulate systemically and accumulate within cardiovascular structures (Wu et al., 2023). The first direct clinical investigation linking MNPLs to cardiovascular risk was published in 2024 by Marfella et al. In this prospective, multicenter study involving 257 patients undergoing carotid endarterectomy, MNPLs were detected in the excised carotid plaque of 150 patients (58.4%) (Marfella et al., 2024). Their presence was associated with a markedly increased risk of major adverse cardiovascular events, with an adjusted Hazard Ratio of 4.53 for the composite endpoint of nonfatal myocardial infarction, nonfatal stroke, or death from any cause at 34 months of

follow-up (Marfella et al., 2024). Plaques containing MNPLs also exhibited significantly higher levels of inflammatory mediators, including interleukin-18 (IL-18), IL-1β, IL-6, and TNF-α (Marfella et al., 2024). Together, these findings provide the first clinical evidence that MNPL accumulation in vascular tissue is associated with enhanced local inflammation and a substantially higher risk of adverse cardiovascular outcomes.

The biological plausibility of these clinical observations is supported by extensive *in vivo* evidence describing a characteristic triad of cardiovascular alterations induced by MNPLs: cardiac structural damage, vascular endothelial dysfunction, and prothrombotic activity. Cardiac toxicity has been consistently documented in various animal models, where MNPL exposure induces cardiomyocyte apoptosis, inflammation, and myocardial fibrosis, frequently accompanied by elevated cardiac injury markers and involving signaling pathways such as Wnt/β-catenin or NLRP3–caspase-1 (Li et al., 2020d; Wei et al., 2021; Zhang et al., 2022). Additional studies report broader myocardial alterations, including impaired contractile function, ventricular dilation, myofilament disruption, and features of cardiac senescence (Zhang et al., 2023b; Wang et al., 2024). At the vascular level, MNPLs cause endothelial dysfunction, characterized by arterial wall thickening, inflammatory cell infiltration, disorganization of vascular layers, and, in some models, vascular calcification (Wang et al., 2023a; Yan et al., 2023). Evidence from zebrafish embryos further supports these findings, showing endothelial damage and hemodynamic alterations, including reduced cardiac output and blood flow velocity (Sun et al., 2021). Finally, MNPL exposure promotes a prothrombotic state. Experimental studies in zebrafish and rodents consistently describe accelerated thrombus formation, fibrin clot deposition, and enhanced platelet activation (Sun et al., 2021; Gao et al., 2021; Wang et al., 2023a), with some evidence indicating that MNPLs surface functionalization modulates these coagulation responses (Smyth et al., 2015; Kim et al., 2022). Collectively, this body of *in vivo* research provides mechanistic support for the cardiovascular alterations observed in humans and highlights the susceptibility of both cardiac and vascular tissues to MNPL exposure.

Beyond these organ-specific effects, MNPL exposure also contributes to systemic conditions known to promote cardiovascular disease. Experimental studies show that MNPLs entering the organism through the gut or lung stimulate systemic cytokine release and activate inflammatory pathways typically associated with vascular injury, including NF-κB- and NLRP3-dependent signaling (Zhu et al., 2023). In parallel, MNPLs disrupt hepatic lipid metabolism, leading to dyslipidemia, altered cholesterol handling, and conditions that favor foam cell formation, thereby promoting atherosclerosis (Zhang et al., 2025). Since MNPLs have been detected in human blood, the vascular endothelium is not only affected indirectly by this systemic environment but also constitutes a direct site of particle contact (Cao et al., 2017). Circulating MNPLs necessarily encounter the luminal surface of blood vessels, positioning the vascular endothelium as a primary interface for direct particle contact. While systemic inflammation and metabolic alterations clearly influence endothelial function, an increasing number of studies now focus on characterizing the intrinsic effects of MNPLs on endothelial cells themselves (Cao et al., 2017; Prattichizzo et al., 2024). This growing body of research underscores the need to isolate endothelial-specific responses and to determine how MNPLs interact with and potentially impair the integrity and homeostatic functions of the vascular barrier. Consequently, controlled endothelial models have become essential tools for dissecting the direct cellular and molecular processes through which MNPLs may contribute to cardiovascular pathology.

1.5.2. STATE OF THE ART ON MNPL-INDUCED ENDOTHELIAL DYSFUNCTION

The vascular endothelium, which lines the inner surface of blood vessels, functions as an active interface that interacts with circulating MNPLs. *In vitro* studies demonstrate that both intrinsic physicochemical properties of MNPLs and exposure parameters modulate this interaction. Among these, size and dose emerge as critical determinants. Lu et al. (2022) showed in Human Umbilical Vein Endothelial Cells (HUVECs) that uptake is highly size-selective, with 100 nm PS-P-NPLs being rapidly internalized in a time- and concentration-dependent manner. In contrast, larger 500 nm PS-P-NPLs remained

predominantly surface-bound at low and intermediate concentrations. This size-dependent restriction appears to extend across polymer types; Wang et al. (2025) similarly reported that 500 nm PP-NPLs predominantly adhered to the endothelial membrane with limited cytoplasmic distribution. van Boxel et al. (2025) further corroborated the size-dependent permeability by demonstrating that 50 nm PS-P-NPLs crossed endothelial layers significantly more efficiently than larger 200 nm PS-P-NPLs and 1 µm PS-P-MPLs. However, this apparent resistance to larger MNPLs can be overcome by increasing the concentration; Lee et al. (2021) reported that HUVECs successfully internalized PS-P-MPLs up to 1 µm at higher doses, although larger 5 µm PS-P-MPLs were not internalized at any concentration. Mechanistically, internalization is predominantly mediated by clathrin- and caveolae-dependent endocytosis (Cao et al., 2017). Collectively, these findings indicate that the endothelial uptake profile is not uniform but rather a complex outcome largely governed by the dimensional and dosage parameters of the exposure.

Upon interaction with the endothelium, MNPLs primarily act as chronic stressors rather than acute toxins at subcytotoxic doses, initiating cellular perturbations before compromising viability (Huo et al., 2024; Lu et al., 2023). Experimental evidence in endothelial models demonstrates that during short-term exposures (<24 h) and at environmentally relevant concentrations (<100 µg/mL), cytotoxicity is minimal or absent, effectively preserving the cell population for the development of sublethal functional defects (Wei et al., 2022; Wang et al., 2025). In contrast, cytotoxicity as defined by international standards (ISO 10993-5, viability below 70%, ISO, 2009) typically manifests under cumulative stress conditions, either through prolonged exposures (48–72 h) or at high concentrations exceeding 100 µg/mL (Lee et al., 2021; Wang et al., 2025). However, specific MNPL properties can markedly lower the cytotoxicity threshold. Regarding size, Lee et al. (2021) found that smaller PS-P-NPLs (500 nm) exerted significantly greater cytotoxicity than larger PS-P-MPLs (5 µm), a difference they attributed directly to greater intracellular accumulation of the smaller fraction. Beyond size, surface functionalization, particularly the introduction of a positive charge, acts as a potent toxicity amplifier. Fu et al. (2022) demonstrated that 50 nm PS-A-NPLs were highly

cytotoxic even at low doses of 10–15 µg/mL. In contrast, neutral (PS-P-NPLs) or anionic (PS-C-NPLs) particles of similar size and composition are comparatively well tolerated under equivalent exposure conditions.

Beyond loss of viability, subcytotoxic exposures induce sustained intracellular stress in endothelial cells. Across HUVECs and other endothelial models, MNPL exposure is consistently associated with oxidative imbalance and mitochondrial dysfunction. In HUVECs, 500 nm PS-P-NPLs and PP-NPLs induce a significant increase in intracellular ROS after 48 h, occurring at doses ≥1.5 µg/mL for PP-NPLs (Wang et al., 2025) and 25–100 µg/mL for PS-P-NPLs (Huo et al., 2024), with these changes coinciding with the activation of mitochondrial death signaling. Crucially, surface charge shapes the nature of oxidative and mitochondrial injury. Fu et al. (2022) demonstrated that 50 nm PS-A-NPLs triggered severe mitochondrial depolarization and ATP depletion at doses as low as 10–20 µg/mL, an effect that was significantly attenuated or absent in cells exposed to PS-P-NPLs of identical size. This disparity is consistent with a stronger association of cationic NPLs with negatively charged mitochondrial compartments, leading to more pronounced structural damage and severe cytotoxicity driven by direct physical disruption (Fu et al., 2022). In parallel, MNPLs interfere with autophagic homeostasis. Lu et al. (2022) reported that 100 nm PS-P-NPLs increased LC3-positive vesicles in HUVECs while causing p62 accumulation, consistent with an impaired autophagic flux. In contrast, larger 1 µm PS-P-MPLs at comparable mass concentrations did not measurably alter autophagy markers (Lu et al., 2023). Complementing these observations, Lee et al. (2021) showed that 500 nm PS-P-NPLs also activated autophagy in HUVECs and that pharmacological inhibition of this pathway partially rescues cell viability. This supports the view that, once dysregulated, autophagy is not merely an adaptive response but can actively contribute to the transition from sublethal stress to cell death.

Downstream of these intracellular perturbations, MNPLs compromise nuclear integrity and activate inflammatory signaling cascades in endothelial models. Lv et al. (2025) reported that 20–100 nm PS-P-NPLs accumulate in the perinuclear region of endothelial cells and, after 24 h of exposure, induce membrane protrusions and nuclear condensation, morphological features

consistent with apoptosis-related nuclear damage. Under more demanding exposure scenarios, this persistent intracellular stress can progress towards pyroptosis. Huo et al. (2024) showed that 500 nm PS-P-NPLs (25–200 µg/mL, 48 h) activate the NLRP3–caspase-1–gasdermin D (GSDMD) axis in HUVECs, with increased ROS production, lactate dehydrogenase (LDH) release, membrane permeabilization, and IL-1β/IL-18 secretion, consistent with canonical pyroptotic death. Likewise, Lv et al. (2025) demonstrated that co-exposure to PS-P-NPLs and the fluorosurfactant F-53B enhances NF-κB/NLRP3-mediated pyroptosis in endothelial cells, further strengthening the link between MNPL-induced intracellular stress and inflammatory forms of endothelial injury. Extending these observations, Wang et al. (2025) further demonstrated that PP-NPLs induced IL-6 and TNF-α expression and upregulated NLRP3 in HUVECs, reinforcing the link between MNPL exposure and inflammasome-related endothelial activation. In parallel, evidence across diverse endothelial models, including non-human systems, confirms that MNPLs promote a pro-adhesive phenotype. Vlacil et al. (2021) reported that 1 µm PS-C-MPLs upregulate intercellular adhesion molecule 1 (ICAM-1) and vascular cell adhesion molecule 1 (VCAM-1) in murine endothelial cells and enhance monocyte adhesion, and Lv et al. (2025) showed that 100 nm PS-P-NPLs, particularly in combination with F-53B, increase ICAM-1/VCAM-1 levels and activate NF-κB/NLRP3 signaling, thereby facilitating leukocyte recruitment. Collectively, these findings establish a coherent inflammatory program in which MNPL exposure drives cytokine release, inflammasome activation, and immune cell adhesion at the endothelial surface.

In addition to inflammatory activation, MNPLs profoundly compromise endothelial barrier integrity. A critical mechanistic insight is Nanoparticle-induced Endothelial Leakiness (NanoEL), described by Wei et al. (2022). Using HUVEC monolayers, they showed that PS-C-NPLs and polymethyl methacrylate (PMMA) NPLs (50–60 nm, 0.05–0.5 mg/mL, 1–6 h) trigger a dose- and time-dependent increase in fluorescein isothiocyanate (FITC)–dextran flux across the endothelial layer by inducing vascular endothelial cadherin (VE-cadherin) phosphorylation at Y658 and Y731, disrupting adherens junctions and reorganizing the actin cytoskeleton. This leakiness was Src-dependent and

could be blocked by PP1, but was insensitive to ROS scavengers or endocytosis inhibitors, indicating that a purely surface-level interaction with VE-cadherin is sufficient to compromise barrier function (Wei et al., 2022). Consistently, Wang et al. (2025) observed a significant downregulation of the tight junction protein ZO-1 at high doses of 500 nm PP-NPLs (≥210 µg/mL, 48 h), together with morphological signs of membrane damage, supporting a weakening of the endothelial gatekeeping function.

Beyond barrier disruption, MNPLs impair endothelial regenerative and angiogenic capacity. Wang et al. (2025) documented a marked inhibition of endothelial cell migration and wound closure following exposure to 500 nm PP-NPLs, with wound closure dropping from 90% in controls to 20–40% in treated cells, and transwell migration decreasing significantly at higher doses. Complementing these findings, Lee et al. (2021) found that 500 nm PS-P-NPLs significantly suppressed tube formation in HUVECs by 26–95% (between 20 and 100 µg/mL) after 6 h, without affecting viability at this time-point. This impairment was mechanistically linked to a reduced phosphorylation of key angiogenic kinases. Finally, using a relevant *ex vivo* model, Dhakal et al. (2023) showed that 22 nm PS-P-NPLs (0.1–10 µg/mL) induced premature senescence in porcine coronary artery endothelial cells through sodium-glucose cotransporter 2 (SGLT2) upregulation, increased senescence-associated β-galactosidase (SA-β-gal) activity, and p53/p21 activation, and impair endothelium-dependent vasorelaxation to bradykinin in arterial rings via reduced endothelial nitric oxide synthase (eNOS) expression and nitric oxide (NO) bioavailability. These effects were reversed by SGLT2 inhibition. Collectively, these defects (barrier leakage, inflammation, impaired repair, and metabolic senescence) establish a critical state of endothelial dysfunction that is consistent with an atheroprone endothelial phenotype, favoring lipid entry, immune cell retention, and loss of vascular tone (Figure 4).

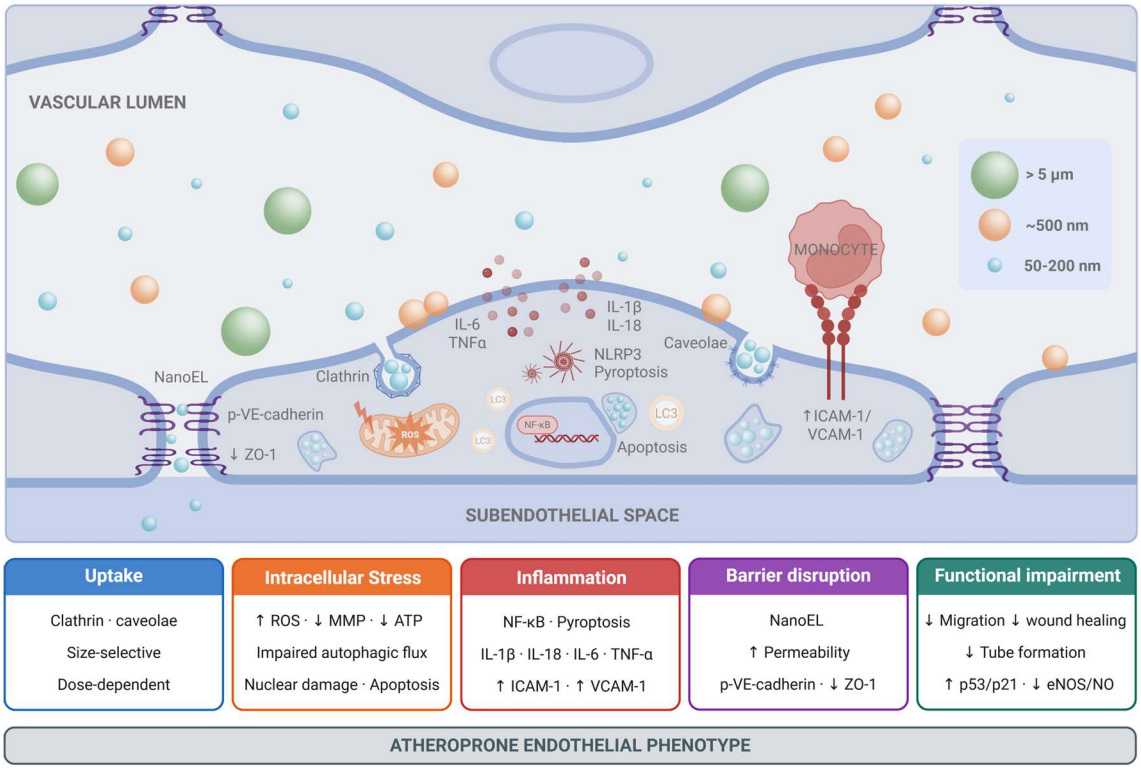


Figure 4: *Overview of MNPL-induced endothelial dysfunction based on in vitro evidence. The upper panel shows a cross-section of the vascular endothelium depicting size-dependent uptake (50–200 nm via clathrin/caveolae endocytosis; ~500 nm surface-bound; >5 µm not internalized), intracellular stress responses (mitochondrial ROS, autophagic flux impairment, nuclear damage), inflammatory signaling (NF-κB, NLRP3/caspase-1-mediated pyroptosis, IL-1β/IL-18 secretion, IL-6/TNF-α release, ICAM-1/VCAM-1 upregulation with monocyte adhesion), and junction disruption via Nanoparticle-induced Endothelial Leakiness (NanoEL; VE-cadherin phosphorylation, ↓ ZO-1). Elements represent co-occurring events, not a single causal cascade. The lower panel summarizes pathways and consequences converging on an atheroprone endothelial phenotype. Cytotoxicity is minimal at short-term exposures (<24 h, <100 µg/mL) but enhanced by smaller size and amino-functionalization (NH_2^+). Abbreviations: ATP, adenosine triphosphate; eNOS, endothelial nitric oxide synthase; ICAM-1, intercellular adhesion molecule 1; IL-1β, interleukin-1 beta; IL-6, interleukin-6; IL-18, interleukin-18; LC3-II, microtubule-associated protein light chain 3-II; MMP, mitochondrial membrane potential; NanoEL, Nanoparticle-induced Endothelial Leakiness; NF-κB, nuclear factor kappa-B; NLRP3, NLR family pyrin domain containing 3; NO, nitric oxide; ROS, reactive oxygen species; TNF-α, tumor necrosis factor-alpha; VCAM-1, vascular cell adhesion molecule 1; VE-cadherin, vascular endothelial cadherin; ZO-1, zonula occludens-1. Created with BioRender.com.*

1.5.3. HUVECS AS A REPRESENTATIVE MODEL OF THE HUMAN ENDOTHELIUM

Given that much of the mechanistic evidence described above relies on specific endothelial assays, establishing a robust experimental model is critical. HUVECs are among the most widely used *in vitro* models of the human vascular endothelium, the continuous monolayer that lines the inner surface of blood vessels. Isolated from the tunica intima of the human umbilical vein, these primary cells have become a reference system in vascular biology and nanotoxicology. Their adoption reflects a balance between biological fidelity

and practicality: umbilical veins are readily accessible, isolation protocols are well established, and commercial availability supports standardization and reproducibility across laboratories (Cao et al., 2017). Importantly, as primary human cells, HUVECs retain a stable endothelial phenotype and preserve key features of vascular homeostasis, including junctional architecture and vascular signaling machinery such as VE-cadherin and eNOS. This makes them well suited to study MNPL–endothelium interactions, including uptake processes mediated by clathrin- and caveolae-dependent endocytosis (Cao et al., 2017). In the context of MNPL toxicology, this model is particularly relevant because, once MNPLs cross primary barriers and reach the bloodstream, the vascular endothelium is the inevitable first point of contact (Lu et al., 2023; Wang et al., 2025).

Functionally, HUVEC monolayers provide endothelium-specific readouts that extend beyond classical cytotoxicity endpoints. When grown to confluence, HUVECs form a structured monolayer stabilized by VE-cadherin–based adherens junctions, enabling direct assessment of barrier integrity through paracellular permeability measurements. This is particularly relevant in MNPL research, as barrier disruption can occur in the absence of overt cell death (Wei et al., 2022). In parallel, HUVECs are extensively used to model regenerative competence. Their ability to organize into capillary-like networks during tube formation assays provides a sensitive functional readout for detecting sublethal effects of MNPL on endothelial remodeling and angiogenic competence (Lee et al., 2021).

Finally, HUVECs facilitate the mechanistic dissection of MNPL-induced injury at the molecular level. This includes resolving organelle-specific toxicity, such as alterations in mitochondrial dynamics and bioenergetics triggered by MNPLs (Fu et al., 2022; Wang et al., 2025), as well as identifying inflammatory programs, including NF-κB activation and NLRP3 inflammasome signaling (Huo et al., 2024; Lv et al., 2025). Together, this combination of human relevance, functional versatility, and mechanistic tractability consolidates HUVECs as a core model for vascular nanotoxicology. However, as with any *in vitro* system, interpretation must account for the fact that the microenvironment shapes endothelial responses; static HUVEC cultures do not fully recapitulate the

complex hemodynamic forces or the specialized heterogeneity of specific vascular beds found *in vivo* (Cao et al., 2017).

1.6. Knowledge Gaps and Rationale for This Thesis

The impact of MNPLs on human health is a rapidly expanding research area, and an increasing body of evidence supports the vascular endothelium as a relevant target tissue (Section 1.5.2), in line with the cardiovascular implications described above (Section 1.5.1). However, a comprehensive understanding of the cellular and functional mechanisms underlying MNPL-induced endothelial injury remains lacking. Current literature is characterized by substantial heterogeneity in experimental models, exposure conditions, and test materials, which limits cross-study comparability and prevents firm conclusions. As a result, two key knowledge gaps currently limit the precision of cardiovascular risk assessment.

First, there is a lack of integrated, framework-based characterization of MNPL-induced endothelial dysfunction in standardized primary human models. While individual effects have been reported, relatively few studies capture the toxicological cascade within a single, consistent experimental system. In HUVECs, functional readouts—such as viability, lipid homeostasis, migration, and angiogenesis—are rarely assessed alongside upstream mechanisms, including cellular uptake and intracellular trafficking burden, transcriptomic reprogramming, inflammatory signaling, and oxidative–genotoxic stress, under comparable exposure and characterization conditions. Establishing these mechanistic-to-functional links is a prerequisite for defining the hazard potential of MNPL exposure in the vascular endothelium.

Second, the extent to which intrinsic physicochemical properties of MNPLs modulate these endothelial responses remains poorly defined. Building on a standardized mechanistic and functional characterization, it becomes essential to determine how material attributes shape both the magnitude and the nature of endothelial dysfunction. However, few systematic, head-to-head studies in primary endothelium have dissected: (i) surface chemistry, clarifying how distinct functionalizations drive specific endothelial outcomes beyond general

cytotoxicity; (ii) subtle size effects within the nanoscale—particularly below 100 nm—on intracellular handling and downstream functional responses; and (iii) environmental realism, as most mechanistic evidence still relies on idealized spherical reference NPLs, leaving uncertainty as to whether these profiles predict the hazard of irregular, polydisperse, and colloidally complex secondary NPLs.

To address these limitations, this Thesis adopts a dual-material strategy. Controlled, idealized reference NPLs are used to isolate and systematically test single variables—such as surface functionalization and nanoscale size—under standardized conditions (bottom-up approach). In contrast, environmentally relevant real-life NPLs are incorporated to capture the heterogeneity of secondary MNPLs and evaluate whether mechanistic insights from reference standards translate to realistic exposure scenarios (top-down approach). By integrating these complementary materials in a standardized HUVEC framework, this work supports a mechanistic interpretation of endothelial dysfunction to inform cardiovascular hazard assessment.

2

Objectives

Based on the identified knowledge gaps, the **General Objective** of this Thesis is to characterize the interaction, toxicity, and functional impact of NPLs on the human vascular endothelium, and to determine how key physicochemical properties shape these biological responses.

To achieve this, the following **Specific Objectives** have been established:

Objective 1: To comprehensively characterize NPL–endothelium interactions and associated adverse effects in primary human endothelial cells (HUVECs), integrating mechanistic events with functional outcomes. Specifically, this objective includes:

1.1. To quantify cellular uptake and intracellular trafficking burden.

1.2. To characterize key mechanistic pathways involved in NPL-induced injury, including oxidative stress, inflammatory signaling, genotoxicity, and molecular alterations.

1.3. To assess endothelial functional impairments, focusing on cell viability, lipid homeostasis, migration, and angiogenesis.

Objective 2: To systematically determine how intrinsic physicochemical properties modulate the endothelial toxicity and dysfunction profile of NPLs. This objective is addressed through three sub-objectives:

2.1. To investigate how surface functionalization influences internalization dynamics and downstream toxicological and functional responses of PS-NPLs in HUVECs.

2.2. To determine how particle size within the nanoscale range modulates uptake mechanisms, molecular pathways, and functional outcomes induced by PS-NPLs in HUVECs.

2.3. To assess how the degree of environmental realism influences biological and functional responses in HUVECs by comparing idealized reference PS-NPLs with NPLs of increasing environmental complexity of comparable nominal size.

3

Results

The results of this Thesis have been organized into three studies that have already been published as three scientific papers in different peer-reviewed journals.

Each chapter is linked to a specific objective of the Thesis and ordered as follows:

3.1. Chapter 1 (Paper 1): Hazard assessment of nanoplastics is driven by their surface-functionalization. Effects in human-derived primary endothelial cells.

3.2. Chapter 2 (Paper 2): Transcriptomic and functional profiling of endothelial dysfunction induced by polystyrene nanoplastics.

3.3. Chapter 3 (Paper 3): Real-life nanoplastics induce endothelial dysfunction in primary human endothelial cells.

3.1. Chapter 1 (Paper 1)

Hazard assessment of nanoplastics is driven by their surface-functionalization. Effects in human-derived primary endothelial cells.

Science of The Total Environment, 934, 173236. (2024)

DOI: 10.1016/j.scitotenv.2024.173236

Impact Factor: 8.0 (2024)

Science of the Total Environment 934 (2024) 173236

Contents lists available at ScienceDirect

Science of the Total Environment

journal homepage: www.elsevier.com/locate/scitotenv

Hazard assessment of nanoplastics is driven by their surface-functionalization. Effects in human-derived primary endothelial cells

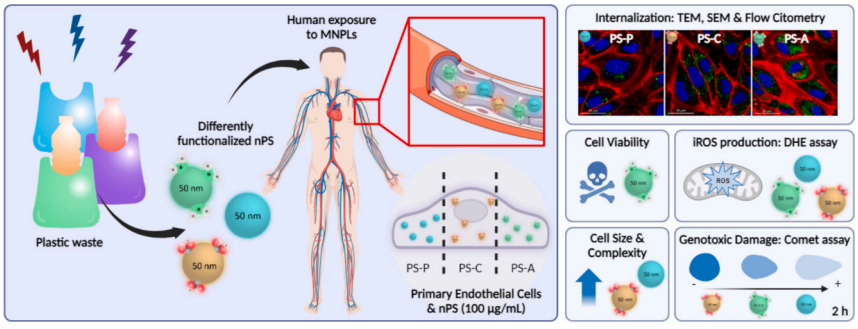
Joan Martín-Pérez [a], Aliro Villacorta [a,b], Gooya Banaei [a], Michelle Morataya-Reyes [a], Alireza Tavakolpournegari [a], Ricard Marcos [a,*], Alba Hernández [a,*], Alba García-Rodriguez [a,*]

[a] Group of Mutagenesis, Department of Genetics and Microbiology, Faculty of Biosciences, Universitat Autònoma de Barcelona, Cerdanyola del Vallès 08193, Spain
[b] Facultad de Recursos Naturales Renovables, Universidad Arturo Prat, Iquique, Chile

HIGHLIGHTS

- Polystyrene nanoplastics with different surface functionalizations were used.
- Primary human umbilical vein endothelial cells exposed at different times were used.
- Cell internalization dynamics were evaluated using different methodological approaches.
- Aminated shows a lower tendency to internalize than pristine and carboxylated forms.
- All forms triggered oxidative stress and genotoxicity responses.

GRAPHICAL ABSTRACT



ARTICLE INFO

Editor: Susanne Brander

Keywords:
HUVEC
Polystyrene nanoplastics
Functionalization
Internalization
Genotoxicity

ABSTRACT

During plastic waste degradation into micro/nanoplastics (MNPLs) their physicochemical characteristics including surface properties (charge, functionalization, biocorona, *etc.*) can change, potentially affecting their biological effects. This paper focuses on the surface functionalization of MNPLs to determine if it has a direct impact on the toxicokinetic and toxicodynamic interactions in human umbilical vein endothelial cells (HUVECs), at different exposure times. Pristine polystyrene nanoplastics (PS-NPLs), as well as their carboxylated (PS-C-NPLs) and aminated (PS-A-NPLs) forms, all around 50 nm, were used in a wide battery of toxicological assays. These assays encompassed evaluations on cell viability, cell internalization, induction of intracellular reactive oxygen species (iROS), and genotoxicity. The experiments were conducted at a concentration of 100 µg/mL, chosen to ensure a high internalization rate across all treatments while maintaining a sub-toxic concentration. Our results show that all PS-NPLs are internalized by HUVECs, but the internalization dynamic depends on the particle's functionalization. PS-NPLs and PS-C-NPLs internalization modify the morphology of the cell increasing its inner complexity/granularity. Regarding cell toxicity, only PS-A-NPLs reduced cell viability. Intracellular ROS was induced by the three different PS-NPLs but at different time points. Genotoxic damage was induced by the three PS-NPLs at short exposures (2 h), but not for PS-C-NPLs at 24 h. Overall, this study suggests that the

* Corresponding authors at: Group of Mutagenesis, Department of Genetics and Microbiology, Faculty of Biosciences, Universitat Autònoma de Barcelona, Campus of Bellaterra, 08193 Cerdanyola del Vallès, Spain.
E-mail addresses: ricard.marcos@uab.cat (R. Marcos), alba.hernandez@uab.cat (A. Hernández), alba.garcia.rodriguez@uab.cat (A. García-Rodriguez).

https://doi.org/10.1016/j.scitotenv.2024.173236
Received 4 January 2024; Received in revised form 14 April 2024; Accepted 12 May 2024
Available online 17 May 2024
0048-9697/© 2024 The Author(s). Published by Elsevier B.V. This is an open access article under the CC BY license (http://creativecommons.org/licenses/by/4.0/).

toxicological effects of PSNPLs on HUVEC cells are surface-dependent, highlighting the relevance of using human-derived primary cells as a target.

1. Introduction

Plastic waste has become a serious environmental problem due to the exponential production of plastic over the past few decades. In the last 60 years, plastic production has increased by >20-fold, resulting in an annual generation of approximately 400 million tons of plastic, with projections indicating a dramatic increase in the coming years (Bajt, 2021). Due to their characteristics, including low-cost production, high durability, and versatility, plastics are used for multiple purposes, such as packaging, cosmetics, building, and medical applications, among others (Domenech and Marcos, 2021). Regrettably, >80 % of these plastics are not adequately recycled and are being released into the natural environment, where they can persist for centuries due to their slow degradation rate (Kik et al., 2020; Lampitt et al., 2023). Exposure to environmental factors such as ultraviolet radiation, wave action, and various physicochemical and biological processes triggers the aging and fragmentation of plastics into smaller particles known as microplastics and even finer nanoplastics (Yee et al., 2021; Shi et al., 2022). These micro/nanoplastics (MNPLs) are contaminating all environmental compartments, including the hydrosphere, atmosphere, and biosphere (Pradel et al., 2023). During the weathering process, MNPLs undergo alterations in their surface properties, acquiring various functional groups such as amino or carboxyl, which in turn influence their properties, including net charge (Alimi et al., 2022).

Studies have highlighted the pathways through which environmental MNPLs can infiltrate the human body, encompassing inhalation, ingestion, and skin contact (Rubio et al., 2020a). Once inside the human body, owing to their minute size, MNPLs possess the potential to breach biological membranes, gaining access to the bloodstream (Yee et al., 2021). Notably, in the case of pulmonary exposure *via* inhalation, the lung's exceptionally thin tissue barrier, measuring <1 μm, facilitates the penetration of nanoscale particles into the capillary bloodstream (Lehner et al., 2019). The translocation of nanoplastics across the gastrointestinal tract through ingestion has been established in different model organisms, suggesting a comparable mechanism in human physiology. This phenomenon has been validated *in vitro* for polystyrene nanoparticles using both simple intestine cell monocultures and more complex human intestinal models including two/three different cell types (Lehner et al., 2019). Concerning dermal exposure, potential entry routes have been delineated, encompassing hair follicles, sweat gland exits, and compromised areas of the skin (Schneider et al., 2009). Substantiating the capacity of nanoplastics to traverse biological barriers and access the bloodstream, a groundbreaking biomonitoring study has revealed the presence of MNPLs (≥700 nm) in whole blood samples from 22 healthy volunteers (Leslie et al., 2022). Intriguingly, among the most prevalent plastics environmentally identified polystyrene, alongside polyethylene terephthalate and polyethylene have been reported (Jeong et al., 2024). The lumen of the human blood vessel is covered by a thin layer of endothelial cells (ECs). These cells are of particular interest in nanotoxicological studies as they function as the first contact for MNPLs entering the bloodstream. Additionally, ECs play a pivotal role in numerous processes, including the regulation of blood vessel tone and monocyte recruitment. Dysregulation of these processes has been implicated in the development of cardiovascular diseases, including atherosclerosis (Xue et al., 2023). Consequently, the study of the effects of nanoplastics on endothelial cells is of major concern nowadays mainly after the results showing that nanoplastics can induce vascular endothelial injury and coagulation dysfunction in mice (Wang et al., 2023), and the proposal of MNPLs as a potential cardiovascular risk factor (Zhu et al., 2023). Among endothelial cells, primary isolated human umbilical vein endothelial cells (HUVECs) are the most widely utilized in research, due to the accessibility of human umbilical veins and their ready availability from commercial sources (Cao et al., 2017).

Different studies have been conducted to investigate the effects of nanoplastics on HUVECs, commonly using nanopolystyrene particles as a model of nanoplastic. These studies have shown that PS-NPLs can induce cytotoxicity, intracellular reactive oxygen species (iROS) production, and autophagy, potentially affecting human health (Fu et al., 2022; Lu et al., 2022). Nevertheless, none of these studies have aimed to elucidate the implications of distinct surface properties of nanoplastics in HUVECs, nor explored the genotoxic potential of these particles. Thus, our study aimed to elucidate the potential biological effects of three distinct commercially available functionalized PS nanoparticles (pristine, carboxylated, and aminated) with a size of about 50 nm on HUVECs, at a concentration of 100 μg/mL and after acute time-points exposures (20 min, 2, 12, and 24 h). The internalization of the nanoparticles was evaluated with different analytical methods including flow cytometry, confocal microscopy, and transmission electronic microscopy. Specifically, changes in cellular morphology (size and inner complexity), cytotoxicity, intracellular ROS production, and genotoxicity were evaluated for the different functionalized PS nanoparticles. This study provides new insights into the potential effects of differently functionalized PS nanoplastics on primary human endothelial cells, offering valuable information for assessing the health risks associated with PS-NPLs on the cardiovascular system.

2. Materials and methods

2.1. Polystyrene nanoplastics characterization

Three differently functionalized (pristine, carboxylated, and aminated) 50 nm commercialized polystyrene (PS) nanoplastics were purchased, both fluorescent-labeled (FL) and non-labeled (NL), from different companies. Namely, PS-Pristine 50 nm non-labeled (PS-P 50 NL; PP-008-10; nominal size 0.05–0.1 μm) and PS-Pristine 50 nm fluorescent-labeled (PS-P 50 FL; FP-00552-2; nominal size 0.04–0.09 μm; ex./em.: 460/480 nm) from Spherotech Inc. (Lake Forest, IL, USA); PS-Carboxylated 50 nm non-labeled (PS-C 50 NL; 15913-10; mean diameter 0.05 μm) and PS-Carboxylated 50 nm fluorescent-labeled (PS-C 50 FL; 16661-10; mean diameter 0.05 μm; ex./em.: 441/486 nm) from Polysciences Inc. (Warrington, PA, USA); PS-Aminated 50 nm non-labeled (PS-A 50 NL; 228PS50-AM-1; mean diameter 0.05 μm; ex./em.: 498/517 nm) and PS-Aminated 50 nm fluorescent-labeled (PS-C 50 FL; 228PS50-AMFC-1; mean diameter 0.05 μm) from Nanocs Inc. (New York City, NY, USA). All used polystyrene nanoplastics were supplied dispersed in water.

For characterization purposes, polystyrene nanoplastic dispersions were diluted in Milli-Q water and/or Endothelial Cell Growth Medium 2 (Promocell; Heidelberg, Germany). First, for dry state description by transmission electron microscopy (TEM), polystyrene particle working solutions were prepared on Milli-Q water at a concentration of 200 μg/mL. A cooper grid with carbon coverture was clamped and immersed into the working solution, placed on a filter paper-covered Petri dish, and allowed to evaporate overnight. The particles on the grid were placed on a single axis holder and examined using a transmission electron microscopy system operated at 120 kV JEOL JEM 1400 instrument (JEOL Ltd., Tokyo, Japan). Images were acquired using an Orius SC200D sensor from Gatan (Ametek, Inc. Berwyn, PA, USA) and analyzed for particle size distribution by measuring the Martin diameter using the ImageJ software 1.8.0_172. To investigate the potential influence of the culture medium on the colloidal structures in the suspension of the different PS nanoparticles, the behavior was studied using a Zetasizer®

Ultra device from Malvern Panalytical (Cambridge, UK). To such end, working solutions were prepared for each particle at a final concentration of 100 μg/mL, this time not only on Milli-Q water but also on EGM-2 culture medium. For sizing, 1 mL of each suspension was placed on a DTS0012 cuvette and measured with a collection angle of 174.8 whereas for Z-potential a slightly small volume was placed on a DTS1070 cuvette both cuvettes purchased on the same mentioned company. In both cases, three independent measurements were carried out.

2.2. Cell line and culture conditions

Human Umbilical Vein Endothelial Cells (HUVEC) were utilized as representative of the human endothelial barrier of the blood vessels. The cells were kindly provided by our collaborator Dr. Alejandro Portela (Universitat Internacional de Catalunya, Spain) and purchased from Promocell (Heidelberg, Germany) under the name of HUVEC single-donor C-12200. These endothelial cells are primary cells isolated from the endothelium of the umbilical cord vein and are frequently used for physiological and pharmacological investigations. Cells were cultured with Endothelial Cell Growth Medium 2 (EGM-2; C-22011) from Promocell (Heidelberg, Germany) in manually thin-layer collagen-coated flasks until passage 6 was reached to perform the different experiments. Cells were cultured at 37 °C in a humidified atmosphere with 5 % CO_2, and the medium was changed every two days. To prepare the collagen coating, rat collagen I (tail tendon) from Corning Inc. (New York City, NY, USA) was diluted to the desired concentration in 20 mM acetic acid to cover the flasks or plates at 5 μg/cm^2. After 1 h of incubation, the collagen was rinsed twice with 1× PBS to remove the excess acid.

2.3. Polystyrene nanoplastics treatments

To assess the potential toxicological impact of the different polystyrene nanoplastics, cells were subjected to nanoplastics diluted in EGM-2 medium at a concentration of 100 μg/mL for different exposure times. Typically, a brief exposure time of 2 h and an extended exposure time of 24 h were utilized. To maintain a consistent cell density between treatments with different exposure times, cells were examined at the exact moment by adjusting the application time of treatment. Predominantly, cells were seeded at a cell density of 26,300 cells/cm^2 and allowed to grow for 48 h in thin-layer collagen-coated wells (5 μg/cm^2). Subsequently, the medium was replaced with the desired treatment.

2.4. Cell viability assay

The viability of the HUVECs after exposure to the different non-labeled PS nanoplastics was determined using the Coulter method with a Beckman Coulter Z1-D cell counter from Beckman Coulter Inc. (Pasadena, CA, USA). Briefly, cells at passage 6 were seeded in 24 thin-layer collagen-coated well plates at a density of 26,300 cells/cm^2. After incubation for 48 h, cells were exposed to 100 μg/mL of the different non-labeled PS nanoplastics (PS-P 50 NL, PS-C 50 NL, and PS-A 50 NL) for 20 min, 2, 12, and 24 h to assess cell toxicity. Non-treated cells were used as a negative control. Following exposure, the cells were washed twice with 1× PBS to remove the treatments and allow the trypsinization with 100 μL/well trypsin-EDTA 1 % for 5 min at 37 °C. Trypsin was then inactivated with 200 μL/well of 5 % FBS diluted in 1× PBS. The detached cells were diluted 1:100 in ISOTON diluent and counted with the Beckman Coulter Z1-D cell counter. The obtained percentage values represent an average of the number of cells counted on each treatment, relative to the average of the number of cells counted in the corresponding untreated control. The experiment was performed three times and technical duplicates were analyzed for each treatment.

2.5. Cellular uptake (FACS, fluorescent activated cell sorter) and cell complexity (flow cytometry)

The internalization of polystyrene nanoplastics by HUVECs was first assessed by FACS. To such end, the fluorescent-labeled versions of the nanoparticles (PS-P 50 FL, PS-C 50 FL, PS-A 50 FL) were utilized. Cells at passage 6 were seeded in 24 thin-layer collagen-coated well-plates at a density of 26,300 cells/cm^2 and after 48 h of incubation were exposed to 100 μg/mL of PS-P 50 FL, PS-C 50 FL, and PS-A 50 FL for 20 min, 2, 12, and 24 h. A negative control was also included. After exposure, cells were washed twice with 1× PBS to remove the treatments and allow the trypsinization of the cells with 100 μL/well trypsin-EDTA 1 % for 5 min at 37 °C. Trypsin was inactivated with 200 μL/well of 5 % FBS diluted in 1× PBS. The *Via*-Probe™ Red Nucleic Acid Stain (BD Biosciences; Franklin Lake, NJ, USA) was added to a final concentration of 1:200 to stain live cells. The fluorescence of the cells was determined by the CytoFLEX FACS from Beckman Coulter (Pasadena, CA, USA). Nanoplastics internalization was analyzed with an excitation/emission spectra of 488/525 nm and *Via*-Probe™ with an excitation/emission of 638/660 nm wavelength, respectively. From this approach, the absolute number of cells that internalized polystyrene was determined, as well as the increase in fluorescence intensity relative to the control. This means that two parameters were determined i) the percentage of cells that have internalized labeled PS-NPLs, and ii) the amount of internalized labeled PS-NPLs per cell. For the second parameter, the respective kinetics curves over time were generated following a lognormal Gaussian fit, and internalization velocities were determined for the entire time range (absolute velocity; 0–24 h) and segments corresponding to the 0–2 h and 2–24 h intervals. The segmentation point was set at 2 h, considering that this is the time-point when almost all cells in the culture had internalized the different polystyrene nanoplastics. The absolute internalization velocity (iv_{abs}), was determined as follows: $iv_{abs} = \sqrt{(\Delta x/\Delta t)^2 + (\Delta y/\Delta t)^2}$. Similarly, internalization ratios were calculated between each segment velocity and the absolute internalization velocity. This analytical approach provided a nuanced understanding of the kinetics of polystyrene nanoplastics internalization over the specified time intervals.

Alternatively, forward and side scattering measurements from the flow cytometry were used to determine changes in the size and complexity of the cells, relative to the negative control. A total number of 10,000 cells were scored for all the treatments, and the data was analyzed using the Cytexpert software from Beckman Coulter (Pasadena, CA, USA). The experiment was carried out three times and technical duplicates were analyzed in each condition.

2.6. Cellular uptake assessment by confocal microscopy

To corroborate the exact localization of the fluorescent-labeled polystyrene nanoplastics (PS-P 50 FL, PS-C 50 FL, and PS-A 50 FL), laser confocal microscopy was utilized. Cells at passage 6 were seeded onto individual thin-layer collagen-coated μ-Dish 35 mm from Ibidi GmbH (Gräfelfing, Germany) at a density of 26,300 cells/cm^2. After 48 h, cells were exposed to 100 μg/mL PS nanoplastics for 24 h, with a non-treated negative control included. The culture media was removed, cells were washed twice with PBS 1×, and fresh media containing Hoechst 33342 (1:500) (ThermoFisher Scientific; Waltham, MA, USA) and Cellmask™ Deep Red plasma (1:500) (ThermoFisher Scientific; Waltham, MA, USA) to stain the nuclei and cell membranes, respectively, was added. Several images of each sample were taken using a Leica TCS SP5 (Leica Microsystems GmbH; Mannheim, Germany). PS nanoplastics were observed within the cells at an emission wavelength of 488 nm, whereas nuclei and cell membranes were visible at emission wavelengths of 405 and 633 nm, respectively. For each sample, several fields were randomly selected, and the images were processed using the Fiji extension of ImageJ software and Imaris Microscopy Image Analysis Software v. 9.6 from Oxford Instruments (Abingdon, England).

2.7. Cellular uptake assessment by transmission electron microscopy (TEM)

To complement the results obtained with flow cytometry and confocal microscopy, transmission electron microscopy (TEM) was also utilized. TEM allowed us to pinpoint the exact location of nanoplastics within the cells and identify the cellular structures that could potentially enclose them. To such end, HUVECs at passage 6 were cultured in 75 cm^2 thin-layer collagen-coated flasks at a density of 15.555 cells/cm^2. After 48 h cells were exposed to 100 μg/mL of non-labeled PS nanoplastics for 24 h; negative control with non-treated cells was included. Following the exposure, cells were washed twice with 1× PBS to remove the treatments and allow the trypsinization of the cells with 5 mL/flask trypsin-EDTA 1 % for 5 min at 37 °C. Subsequently, trypsin was inactivated with 10 mL/flask 2 % FBS diluted in 1× PBS, and cells were centrifuged for 6 min at 150*g* in 15 mL falcons' flasks. Pellets were resuspended in 2.5 % (v/v) glutaraldehyde (EM grade, Merck; Darmstadt, Germany) and 2 % (w/v) paraformaldehyde (EMS; Hatfield, PA, USA) in 0.1 M cacodylate buffer (Sigma-Aldrich, Steinheim, Germany), pH 7.4. Cell suspensions were transferred to 1.5 mL Eppendorf tubes (Eppendorf; Hamburg, Germany) and pelleted by centrifugation for 6 min at 150*g*. Samples were processed employing conventional techniques, as previously described (Annangi et al., 2015). Briefly, samples were post-fixed with osmium trioxide, dehydrated in acetone, embedded in Eponate 12™ resin (Ted Pella Inc.; Redding, CA, USA), and finally polymerized at 60 °C and cut with an ultramicrotome. Ultrathin sections were placed in copper grids, contrasted with uranyl acetate and Reynolds lead citrate solutions, and observed using a JEOL 1400 TEM (JEOL LTD; Tokyo, Japan) equipped with an ES1000W Erlangshen CCD camera (GATAN Inc.; Pleasanton, CA, USA).

2.8. Production of intracellular reactive oxygen species (ROS)

To assess intracellular ROS production, the dihydroethidium (DHE) method was performed. Cells at passage 6 were seeded in 24 thin-layer collagen-coated well plates at a density of 26,300 cells/cm^2, and after 48 h of incubation were exposed to 100 μg/mL of the different non-labeled PS nanoplastics for 20 min, 2, 12, and 24 h. A negative control (untreated cells) and a positive control (100 μM antimycin-A, treated for 45 min at 37 °C) were also included. After exposure, cells were washed twice with 1× PBS to remove the treatments and allow the trypsinization with 100 μL/well trypsin-EDTA 1 % for 5 min at 37 °C. DHE was added to 5 % FBS diluted in 1× PBS (trypsin inactivator) and 200 μL were added per well at a final concentration of 10 μM DHE. Cells in the DHE solution were transferred to 1.5 mL Eppendorf tubes and incubated for 30 min at 37 °C, protected from the light. The *Via*-Probe™ Red Nucleic Acid Stain (BD Biosciences; Franklin Lake, NJ, USA) was added to a final concentration of 1:200 to stain live cells. The fluorescence of the cells was measured using CytoFLEX LX flow cytometry from Beckman Coulter (Pasadena, CA, USA). The DHE signal was analyzed with an excitation/emission spectra of 561/585 nm and *Via*-Probe™ with an excitation/emission of 638/660 nm, respectively. A total of 10,000 cells were scored for all the treatments and the Cytexpert software from Beckman Coulter (Pasadena, CA, USA) was used to analyze the data. The experiment was conducted six times, with technical duplicates analyzed in each condition.

2.9. Genotoxicity induction detected by the comet assay

This study evaluated the levels of genotoxic damage, specifically DNA breaks, in HUVECs using the single-cell gel electrophoresis (SCGE) alkaline comet assay using GelBond® film (GBF) (Lonza Bioscience; Basel, Switzerland) as a support. For the experiment, cells at passage 6 were seeded in thin-layer collagen-coated 12 well plates at a density of 26,300 cells/cm^2 and after 48 h of incubation were exposed to 100 μg/mL of the different non-labeled PS nanoplastics for either 2 or 24 h. The experiment included a negative control (non-treated cells) and a positive control, with methyl methanesulphonate (200 μM for 30 min at 37 °C Sigma-Aldrich; St. Louis, MO, USA). After exposure, cells were washed twice with 1× PBS, detached with trypsin-EDTA 1 %, and trypsin-inactivated with 5 % FBS diluted in 1× PBS. Cells were centrifuged for 6 min at 150*g* at 4 °C in a microcentrifuge and resuspended with cold PBS to a final concentration of 1 × 10^6 cells/mL. Cell suspensions were mixed 1:10 with 0.75 % low melting point agarose at 37 °C, and a drop of 7 μL from each sample was placed on GBFs in triplicates. GBFs were left overnight in lysis buffer at 4 °C, washed in electrophoresis buffer for 5 min, and incubated in electrophoresis buffer for 35 min at 4 °C to allow DNA unwinding. After the incubation time, electrophoresis was performed at 20 V/300 mA at 4 °C for 20 min. GBFs were washed twice with cold PBS for 5 min and once with water for 1 min. Cells were fixed in absolute ethanol for 1 h and air-dried overnight at room temperature with proper light protection. Cells were stained with 1:10000 SYBER™ Gold (Invitrogen; Waltham, MA, USA) in TE buffer for 20 min at room temperature in continuous agitation. GBFs were washed in distilled H_2O and air-dried for one day before being mounted and visualized using an Olympus BX50 epifluorescence microscope (Olympus; Tokyo, Japan) at 20 X magnification. The DNA damage was analyzed with the Komet 5.5 image software (Kinetic Imaging Ltd.; Liverpool, UK) as the percentage of DNA in the tail. One hundred randomly selected cells were analyzed per sample. Two different samples were studied for each condition in each one of the two replicate experiments performed.

2.10. Statistical analysis

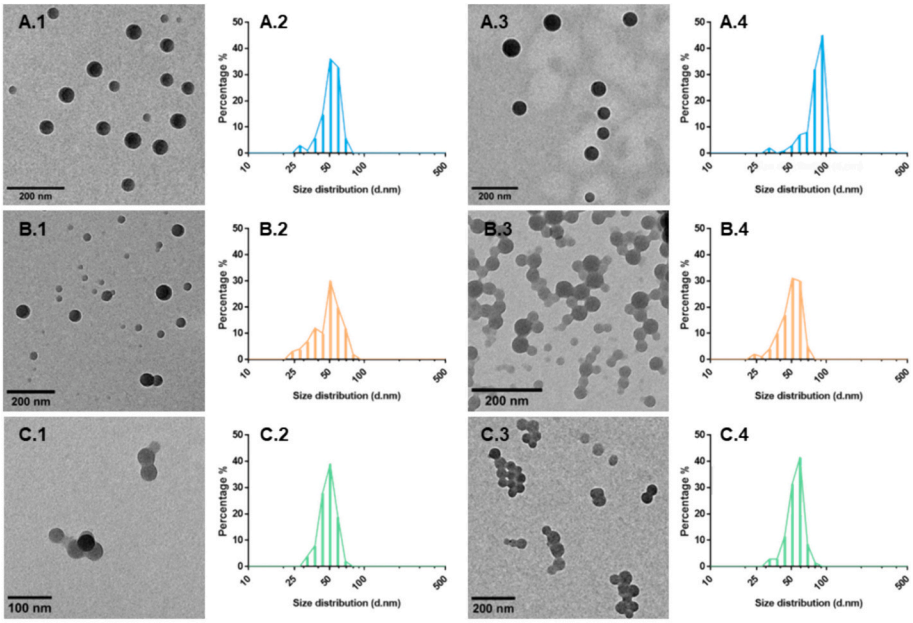
The data presented resulted from the average of different independent experiments (biological replicates), with the number of experiments stated in each section. Each experiment included at least two technical replicates for accuracy purposes. The data analyses were performed using GraphPad Prism 9 software (GraphPad Software Inc., CA, USA). The Shapiro-Wilk test was used as a normality test and the one-way ANOVA with Tukey's multiple comparison test for normal distributed data, or the Kruskal-Wallis test as a non-parametric test. Statistical significance was defined as $^{*}p \leq 0.05$, $^{**}p \leq 0.01$, and $^{***}p \leq 0.001$.

3. Results and discussion

3.1. Polystyrene nanoplastics characterization

The commercially obtained nanoplastics underwent further characterization through transmission electron microscopy (TEM) and dynamic light scattering (DLS) to determine key attributes including size, morphology, aggregation state, and surface charge when dispersed in both Milli-Q water and EGM-2 medium. As depicted in Fig. 1, TEM analysis revealed that, in line with the manufacturer's specifications, all particles were round-shaped with an approximate dry-state diameter of 50 nm. These size measurements exhibited some variability among particles, ranging from a minimum of 46.33 ± 11.18 nm (PS-P 50 FL) to a maximum of 76.45 ± 13.37 nm (PS-C 50 NL).

Upon investigating the hydrodynamic behavior of the nanoparticles in both Milli-Q water and EGM-2 medium, notable distinctions emerged. In general, Z-average sizes were larger in EGM-2 medium when compared to Milli-Q water. Furthermore, nanoparticles exhibited higher polydispersity indexes (PDI) in the EGM-2 medium, suggesting a tendency for particle aggregation when diluted in this culture medium containing various proteins. In terms of Z-potential, the obtained values exhibited fewer negative charges and showed fewer differences among the various functionalized nanoplastics when dispersed in media, compared to Milli-Q water. Similar differences in Z-potential and PDI values were obtained in a study comparing water and culture media dispersions with particles like we used (Paget et al., 2015). Such differences in Z-size average, polydispersity index, and Z-potential have



D	MiliQ				EGM-2		
	TEM	Z-Average	PDI	Z-Pot	Z-Average	PDI	Z-Pot
PS-P 50 FL	46.33 ± 11.18	58.50 ± 1.07	0.01	-44.40 ± 0.83	130.00 ± 5.27	0.28	-5.58 ± 1.21
PS-P 50 NL	46.65 ± 9.00	94.00 ± 0.86	0.03	-44.90 ± 0.49	117.00 ± 2.64	0.26	-8.74 ± 2.22
PS-C 50 FL	48.23 ± 7.99	64.70 ± 0.55	0.03	-40.30 ± 1.99	691.00 ± 33.50	0.75	-9.34 ± 1.38
PS-C 50 NL	76.45 ± 13.37	60.10 ± 0.30	0.04	-43.20 ± 0.78	131.00 ± 1.17	0.06	-8.21 ± 1.14
PS-A 50 FL	45.31 ± 6.56	176.00 ± 0.88	0.19	+2.06 ± 0.89	129.00 ± 1.54	0.01	-4.69 ± 1.21
PS-A 50 NL	50.26 ± 5.57	213.00 ± 28.30	0.42	-21.80 ± 1.11	176.00 ± 12.30	0.34	-4.61 ± 0.95

Fig. 1. Polystyrene nanoplastics characterization. (A–C) shows TEM characterization in Milli-Q water for the different nanoparticles: (A) PS-Pristine, (B) PS-Carboxylated, (C) PS-Aminated. (A1–C1) TEM images for fluorescently labeled (FL) nanoparticles. (A2–C2) show the corresponding frequency histograms of the fluorescently labeled nanoparticle size distribution measured from the TEM images. (A3–C3) TEM images for the corresponding non-labeled (NL) counterparts of the different nanoparticles. (A4–C4) Frequency histograms of the non-labeled particle size distribution measured from TEM images. (D) TEM and DLS data for the different particles in Milli-Q water and EGM-2 media; sizes in d. nm and Z-potential in mV.

also been documented by several authors (Liu et al., 2020; Rampado et al., 2020; Vela et al., 2023) when nanoparticles interact with proteins and develop the denominated protein corona (PC). This PC surrounding the nanoparticles is known to reduce Z-potential values, thereby diminishing electrostatic repulsion, and promoting undesirable nanoparticle aggregation (as reflected by the higher PDI values).

A closer examination of the particles dispersed in media revealed that Z-average sizes did not exhibit significant differences among the different functionalizations, except for the fluorescently labeled carboxylated polystyrene version. This discrepancy can be attributed to its relatively high PDI value (0.75), indicating substantial nanoparticle aggregation/agglomeration in the media. Variations in nanoparticle aggregation/agglomeration result from surface properties which play a crucial role in determining the protein corona (Lundqvist et al., 2008). Although some differences in Z-potential could be expected between the different functionalizations, it is worth noting that these differences, which were noticeable in Milli-Q water, tended to diminish in the culture medium. The aminated version of the nanoparticles displayed a slightly less negative Z-potential when compared to the carboxylated and pristine particles, aligning with previous observations (Paget et al., 2015). Nevertheless, based on the physicochemical characteristics of the particle surface and the findings of other researchers, more substantial Z-potential differences were expected among the different surface-functionalized polystyrenes (Banerjee et al., 2021). Lastly, negligible disparities were observed between the non-labeled nanoparticles and their fluorescently labeled counterparts, except for PS-C 50 FL, as previously mentioned.

3.2. Toxicity of the evaluated PS-NPLs

To compare the cytotoxic potential of the three differently functionalized polystyrene nanoparticles (pristine, carboxylated, and aminated), HUVECs were exposed to a concentration of 100 μg/mL in a time interval ranging from 20 min to 24 h. This concentration was chosen according to the lack of toxicity shown by PS-NPLs in previous studies using different cell lines (Annangi et al., 2023; Vela et al., 2023; Tavakolpournegari et al., 2023). As illustrated in Fig. 2, all particle types induced a significant reduction in cell viability, even at the shortest exposure time of 20 min, showing a special sensitivity of HUVECs to PS-NPLs. However, if we apply the criteria outlined in ISO 10993-5:2009 (E), which defines cytotoxicity as a reduction in cell viability exceeding 30 %, it can be concluded that only aminated polystyrene exhibited cytotoxicity towards HUVECs at 100 μg/mL, with a 37.95 % reduction in viability observed at the 12 h treatment. The most substantial reductions in viability for pristine and carboxylated PS nanoparticles reached 25.20 % at 24 h and 20.44 % at 12 h, respectively.

The cytotoxic potential of aminated PS was previously reported in HUVECs (Fu et al., 2022). In their study, the authors described concentration- and time-dependent cytotoxicity for aminated PS-treated cells after 12 and 24 h of exposure. In their research, cell survival rates fell below 30 % with a dose of 20 μg/mL, providing clear evidence of cytotoxic effects. The heightened cytotoxicity of aminated PS may stem from its increased positive charge, facilitating an enhanced interaction with negatively charged membranes. This interaction could potentially lead to membrane disruption and subsequent cellular damage, as hypothesized by Ruenraroengsak et al. (2012) and Fu et al.

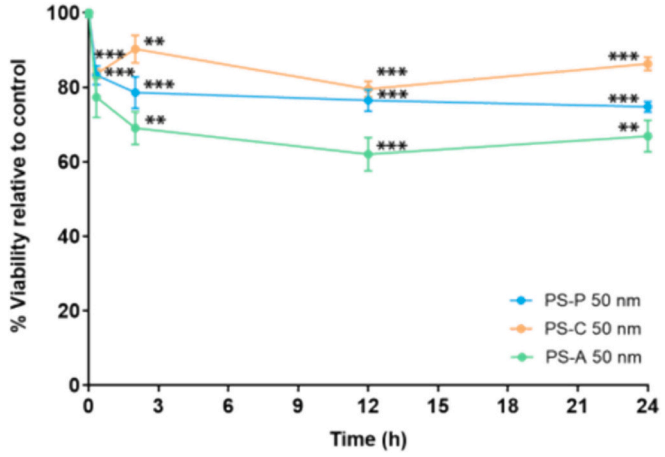


Fig. 2. Relative cell viability of HUVECS after exposure to the different PS nanoplastics at 100 μg/mL for 20 min, 2, 12, and 24 h exposure times. Data is represented as the percentage of living cells relative to the untreated control ± SEM. One-way ANOVA with Dunnett's post-test (normal distributed data) and Kruskal-Wallis's test (non-parametric test) were used for the statistical analysis. Statistical significance was indicated in the graph as $^{**}p < 0.01$ and $^{***}p < 0.001$.

(2022).

Differential cytotoxicity among pristine, carboxylated, and aminated PS was observed in other primary cells, including primary human alveolar type 2 epithelial cells and primary human alveolar macrophages (Ruenraroengsak and Tetley, 2015). This would indicate a special sensitivity of primary cells in comparison with established cell lines.

3.3. Assessing cell internalization of PSNPLs by different analytical methods

To correctly understand the toxicological profile of any MNPLs, it is essential to know their ability to internalize in the used cell line. In this study, cellular internalization of the PS nanoparticles was determined by different analytical methods, including flow cytometry, confocal microscopy, and transmission electron microscopy (TEM). This multimodal approach was followed since the different methods can complement each other, overcoming the individual limitations of each technique and providing a more robust result.

3.3.1. Cellular internalization by FACS

To investigate the internalization dynamics of the different PS nanoparticles FACS analyses were performed after treating the cells with the fluorescent-labeled counterparts of the particles at different time points (20 min, 2, 12, and 24 h). As depicted in Fig. 3A, HUVEC cells exhibited a rapid internalization dynamic for all types of nanoplastics. Our findings indicate that for both surface-modified carboxylated and aminated polystyrene nanoparticles the rate of positive cells internalizing nanoplastic was 95–100 % within just 20 min, while pristine nanoplastics required a slightly longer exposure time, with 40.94 % internalization at 20 min and 88.82 % at 2 h. Although some studies have reported data on the internalization of PS-C (Ho et al., 2018) and PS-A (Wei et al., 2022) in HUVECs, they used different methodological approaches, and no comparisons regarding the role of functionalization were established. Thus, our approach is a novelty in this type of cell. However, studies investigating the implications of surface functionalization on PS-NPLs internalization have been done on human hepatocellular carcinoma (HepG2) cells (He et al., 2020; Banerjee et al., 2022) showing a higher internalization of functionalized 50 nm PS-NPLs regarding the pristine version.

When analyzing the cell internalization kinetics (Fig. 3B), relying on absolute FITC fluorescence arbitrary values, we could infer that carboxylated PS exhibited the most substantial internalization by HUVECs after 24 h exposure (855.67 FITC folds related control). Following this, pristine PS was internalized to a lesser extent (96.69 FITC folds *vs* control at 24 h), while aminated PS demonstrated the lowest degree of internalization (41.48 FITC folds *vs* control at 24 h). It is important to notice that the differences in fluorescence can be misleading because they may arise due to variations in the fluorophores employed by the different companies in the production of the labeled nanoparticles. Therefore, we used a multi-parameter approach to minimize such uncertainty, incorporating TEM imaging analysis and flow cytometry size/complexity comparisons, as further discussed in detail in this manuscript. These complementary analyses reinforced and aligned with the trends observed in the FACS data, providing a more comprehensive understanding of nanoparticle internalization.

The internalization dynamics fitted to a lognormal Gaussian model in the three different treatment approaches (as can be observed in Supplementary Fig. S1). This modeling allowed us to establish differences in the internalization velocity of the different functionalized nanoplastics over time. At short-term treatments (0–2 h), aminated PS exhibited the fastest internalization velocity (5.13 folds *vs* its absolute *iv*), followed by carboxylated PS (3.43 folds when compared to its absolute *iv*) and, finally, the non-functionalized one (1.28 folds *vs* absolute *iv*). These trends, observed at short exposure times, seem to have an impact on the second part of the curve, regardless of the absolute quantity of internalized plastics. We can observe that after 2 h for pristine PS, the decrease in the velocity reaches up to 0.97 of the mean velocity, while it

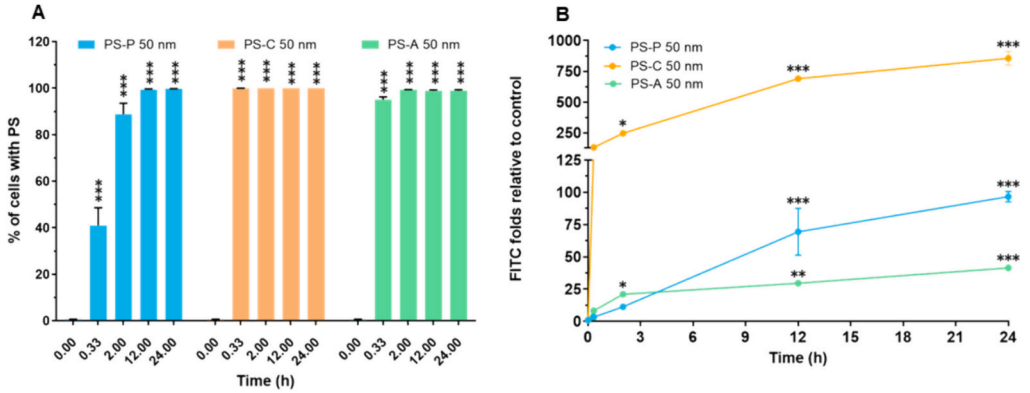


Fig. 3. (A) Quantification by FACS of the percentage of cells that have internalized the different PS nanoplastics at 100 μg/mL for 20 min, 2, 12, and 24 h exposure times. (B) Internalization kinetics (measured as FITC folds relative to control) of different PS nanoplastics at 100 μg/mL for 20 min, 2, 12, and 24 h exposure times in HUVEC. Data is represented as mean ± SEM. One-way ANOVA with Dunnett's post-test (normal distributed data) and Kruskal-Wallis's test (non-parametric test) were used for the statistical analysis. Statistical significance was indicated in the graph as $^{*}p < 0.05$, $^{**}p < 0.01$ and $^{***}p < 0.001$.

reaches 0.78 for carboxylated, and 0.70 for aminated. The faster uptake of aminated PS compared to carboxylated PS that we described at short-time periods (0–2 h) was also noted in a study involving human alveolar cells (Roshanzadeh et al., 2020). That may be attributed to the presence of positive substitution groups (—NH_2) on aminated particle surfaces, which can bind to the anionic headgroups of phospholipids or other negatively charged molecules on membrane proteins, facilitating the internalization, as larger electrostatic interactions tend to result in more effective cellular uptake (Roshanzadeh et al., 2020). Additionally, differences in internalization pathways could play a role, as particle charge is known to influence this process. For instance, anionic particles primarily undergo internalization through clathrin/caveolae-independent endocytosis, while cationic particles are often taken up *via* micropinocytosis (Foroozandeh and Aziz, 2018). However, studies aiming to elucidate the internalization pathways of nanoparticles in HUVECs have indicated that clathrin- and caveolae-based cellular uptake plays a significant role in the internalization of particles up to 180 nm in size (Ho et al., 2018). These findings underscore the complexity surrounding nanoparticle endocytosis mechanisms and emphasize the need for further research to clarify how nanoparticle surface functionalization affects the internalization pathways in HUVECs. It is important to note that our results, related to the absolute measurement of cellular uptake, agree with those reported in the literature.

3.3.2. Cellular internalization by confocal microscopy

By using confocal microscopy, we were able to visually ascertain the location of the nanoparticles inside the cells and distinguish if they were located within the cells or externally attached to the plasma membrane. The z-stacks images obtained *via* confocal microscopy (Fig. 4) demonstrate that after 24-h of treatment, the nanoparticles were distributed throughout the entire cytoplasm, rather than being affixed/adhered to the cell membrane. Additionally, some particles were observed close to the nucleus, suggesting potential interactions with this cellular compartment and/or its genetic material (Fig. 4A). In a general way, it is evident that after 24 h of exposure all treated cells have a big portion of the cytoplasm covered with the fluorescence emitted by nanoplastics (Fig. 4A–C), which is coherent with the previously described FACS data.

3.3.3. Cellular internalization by TEM

Transmission electron microscopy (TEM) was used to visualize and confirm the presence of unlabeled PS-NPLs nanoplastics in cell ultrastructure. The Fig. 5A–B illustrates the remarkable accumulation of nanoparticles in vesicles within HUVECs after 24 h exposure to the concentration of 100 μg/mL, both using pristine and carboxylated PS-NPLs. These findings are comparatively congruent with the distribution of the fluorescence observed in Fig. 4, where the amount of signal was rather concentrated on focused spots distributed over the cell structure (Fig. 4A–C). Therefore, it is relevant to note the different distribution of the functionalized nanoparticles inside the cells. First, and as depicted in Fig. 5A.1–2, pristine PS nanoparticles were found enclosed inside vesicles that can have up to 5 μm diameter, covering most of the cell cytoplasm. These vesicles exhibited well-defined membranes and an irregular pattern of electro-dense regions inside, which precluded the direct measurement or identification of individual nanoparticles. Additionally, smaller vesicles of approximately 1 μm diameter were also observed (see Supplementary Information, Fig. S2). Interestingly, these smaller vesicles were filled with round-shaped structures measuring 50–60 nm in diameter, consistent with the expected size of the used nanoplastics. Both types of vesicles, observed in the pristine treatments, were found in varying proportions among individual cells. Notably, the presence of these vesicles within the cytoplasm resulted in the reorganization of intracellular organelles and the nucleus, as described in Caco-2 cells (Cortés et al., 2019). Similar structures resembling the smaller vesicles (around 1 μm in diameter) were previously reported in HUVECs following treatment with 100 nm PS nanoplastics (Lu et al., 2022), as well as in other cells, such as Caco-2, after exposure to 50 nm

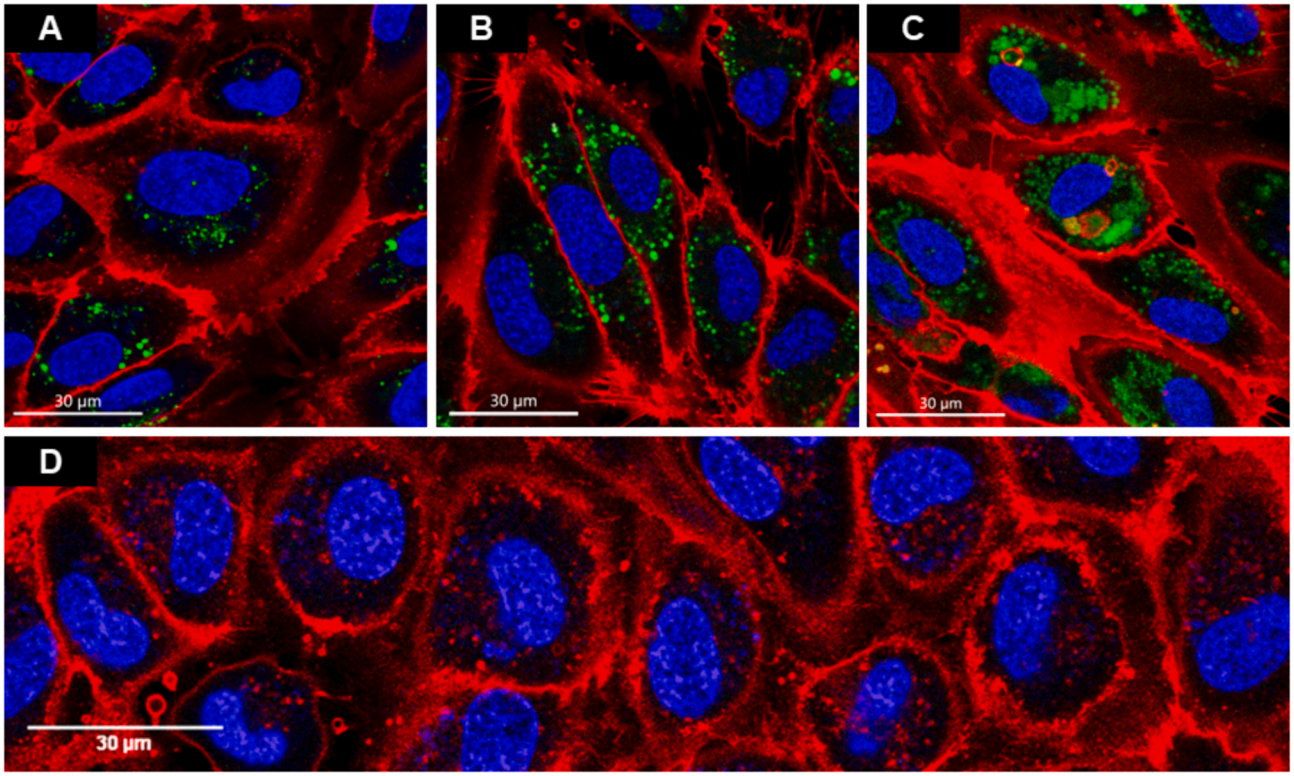


Fig. 4. Confocal images of polystyrene nanoplastics internalization by HUVECs exposed to 100 μg/mL for 24 h: (A) PS-Pristine, (B) PS-Carboxylated, (C) PS-Aminated, (D) Negative control. Different polystyrene nanoplastics (green), nuclei (blue), and cell membranes (red) were stained with Yellow-green core fluorophore, Hoechst 33342, and CellMask™, respectively.

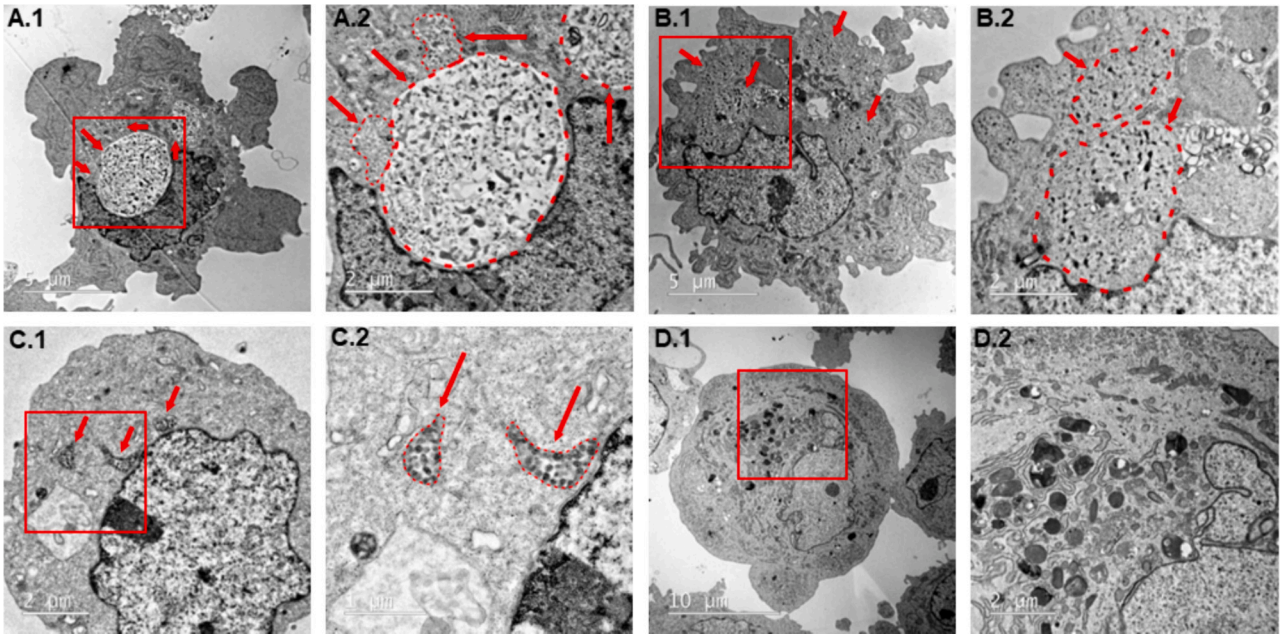


Fig. 5. TEM images of different PS nanoplastics at 100 μg/mL for 24 h exposure time in HUVECs. (A.1–A.2) Pristine PS treatment; vesicles up to 5 μm diameter can be found in the cytoplasm of the cells. Highlight the presence of different textures/patterns among the different vesicles. (B.1–B.2) In the cells treated with Carboxylated PS, 5 μm diameter vesicles can be observed with the presence of electrodense undefined structures inside. (C.1–C.2) Aminated PS treatment; 500–700 nm vesicles can be found filled with rounded shape structures of around 90 nm. (D.1–D.2) Shows the negative control with the absence of any vesicles that can suggest the presence of PS nanoplastics. Solid red squares indicate a zoom-in region; vesicles are pointed with red arrows and red dashed lines highlight its margins in all the pictures.

PS (Domenech et al., 2021). In cells treated with carboxylated polystyrene (Fig. 5B.1–2), vesicles exhibited similar characteristics, such as well-defined membranes, diameters of up to 5 μm, and an irregular electron-dense inner pattern, were also observed. The reorganization of the organelles and nucleus inside the cell was also present due to the size of the vesicles that covered a major part of the cytoplasm. Conversely, in the case of PS-aminated treatment, the number of vesicles was dramatically reduced, but in all cases, vesicles containing electron-dense dots measuring around 90 nm in diameter were found (Fig. 5C1–2). These vesicles were smaller than those beforehand described treatments, and the sizes were usually on the submicrometric scale, ranging predominantly from 500 to 700 nm in diameter, displaying irregularity in shapes as a common characteristic. PS-NPLs were detected confined within these structures which look like those previously described as autophagosomes following treatment with 100 nm pristine PS-NPLs (Lu et al., 2022). Additionally, non-canonical multilamellar bodies were found with a higher prevalence in these aminated PS-treated cells (Fig. S3). The only mention in the literature, resembling the structures we observed is a recently described putative phosphate-sensing organelle in *Drosophila melanogaster* midgut cells (Xu et al., 2023). Importantly, none of the structures described above were found in any of the negative controls (Fig. 5D1–2), after analyzing a substantial number of cells, indicating that the formation of these vesicles was caused by the treatments.

Collectively, our findings, supported by flow cytometry data, confocal microscopy imaging, and TEM images, consistently demonstrate a rapid and substantial internalization of PS nanoparticles by HUVECs under our experimental conditions for both pristine and carboxylated treatments. The limited number of vesicles observed in TEM images after aminated PS treatment is in line with the flow cytometry and confocal data. For the last technique, we can easily see differential intensities with more concentrated photons in the case of PS and PS-C and widely dispersed for PS-A, which can correlate with the presence/absence of vesicles. This could be attributed to the fact that once the aminated nanoparticles were inside the cell, these dispersed individually throughout the cytoplasm instead of being encapsulated within vesicles. It is important to note that the low atomic number of polymers in that nanoplastic could cause them to weakly scatter electrons that may result in a poor TEM contrast to observe individual nanoparticles (Sawyer et al., 2008). Something similar could happen if each vesicle is loaded with a few particles. Another additional explanation could relate to the different internalization pathways, resulting in the formation of various vesicle/structure types within cells, which may vary in their TEM visibility due to their inherent properties.

3.4. Size and inner complexity as assessed by flow cytometry

Flow cytometry forward scattered light (FSC) provides basic morphological information, such as relative cell size. Additionally, light scattered at a 90° angle to the incident beam (SSC) arises from refracted and reflected light and serves as an indicator of the internal cell granularity/complexity within the cell cytoplasm (Jaroszeski and Radcliff, 1999). Based on this principle, known as Mie scattering, forward- and side-scattered light offered valuable data regarding alterations in cell size and inner complexity resulting from the applied treatments.

In our study, statistically significant changes in cell size were found in treatments lasting for 12 and 24 h with both pristine and carboxylated PS-NPLs, displaying a time-dependent pattern (Fig. 6A). The increase in cell size was more pronounced at 24 h for carboxylated PS-NPLs (30 % increase relative to the negative control) compared to pristine forms (20 % increase relative to the negative control). No significant alterations in cell size were observed after treatment with aminated PS at any of the evaluated time points. Concerning cell complexity, a parameter previously utilized in our research group to detect cellular uptake of different nanomaterials (Vila et al., 2017; Villacorta et al., 2022), a pattern like for cell size was noted (Fig. 6B). This parameter exhibited its most substantial increase at 24 h of exposure with carboxylated PS-NPLs (56 % increase compared to the negative control). Treatment with aminated nanoparticles also resulted in a slight, yet statistically significant, increase in cell complexity at 24 h (20 % increase compared to the negative control). Similar increases in cell complexity were described in HUVECs following 3 h treatments with 80 nm AuNPs, although no

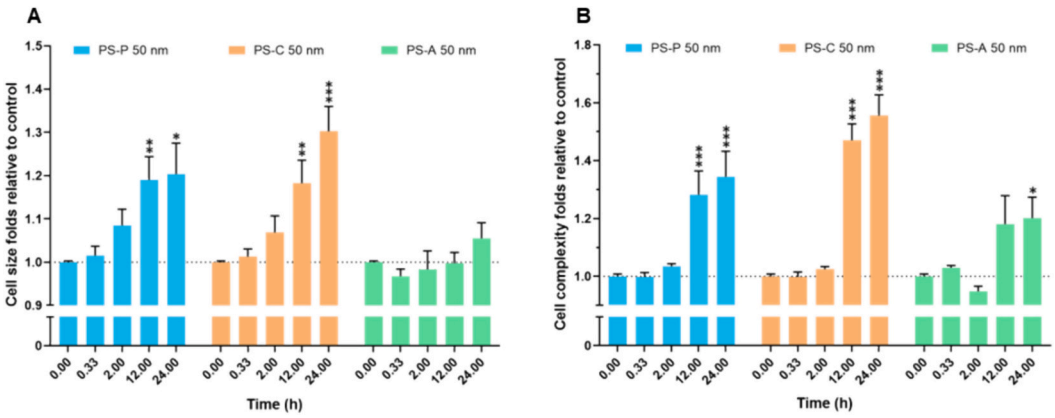


Fig. 6. Relative increment in cell size (A) and cell complexity (B) at exposure to different PS -NPLs at 100 μg/mL for 20 min, 2, 12, and 24 h, respectively. Data is represented as mean ± SEM. One-way ANOVA with Dunnett's post-test (normal distributed data) and Kruskal-Wallis's test (non-parametric test) were used for the statistical analysis. Statistical significance was indicated in the graph as $*p < 0.05$, $**p < 0.01$ and $***p < 0.001$.

changes in cell size were determined between exposed and unexposed cells (Klingberg et al., 2015). In human alveolar A549 cells, modest increases in both size and complexity were observed when exposed to carboxylated and aminated PS-NPLs (20 and 200 nm) (Kihara et al., 2021).

The obtained results suggest that pristine and carboxylated nanoparticles induce time-dependent changes in cell size and inner complexity, with carboxylated treatment exhibiting a more pronounced effect, which is coherent with the other approaches used on this study. Conversely, aminated PS treatment led to only slight increases in cell complexity at 24 h of treatment, which correlated with the limited number of vesicles observed in the TEM images. The absence or limited changes in cell size and complexity following PS-A treatment, in conjunction with the TEM and FACS results, highlight potential differences in internalization and particle disposition within the cells for aminated nanoparticles compared to pristine and carboxylated. This underscores the role of nanoparticle surface properties in cellular uptake and the potential subsequent effects. Further research should be carried out to explore the impact of size increases induced by pristine and carboxylated PS nanoplastics in three-dimensional models like tissue engineering blood vessels (Son et al., 2021).

3.5. Intracellular ROS production

Once demonstrated the role of functionalization in the internalization ability of PS-NPLs, their potential effects on cell functionality should be known. Among the different hazards associated with nanoparticle exposures, the induction of intracellular reactive oxygen species (iROS) stands out (Yu et al., 2020). Thus, iROS increases have been widely reported in different *in vivo* and *in vitro* studies after exposures to MNPLs. These investigations have been performed in different aquatic organisms, such as zebrafish (Sökmen et al., 2020) and *Drosophila* (Alaraby et al., 2023), and in cell lines including hematopoietic human cell lines (Rubio et al., 2020b; Vela et al., 2023), and notably, HUVECs. The studies of iROS imbalance in HUVECs are of major concern, as excessive ROS production in endothelial cells has been linked to cellular apoptosis and inflammatory mechanisms that play a pivotal role in atherosclerosis development, the leading cause of coronary heart disease (Li et al., 2017). Notably, a study performed in HUVECs described how ROS production triggered by amorphous SiO_2 nanoparticles played a central role in the assembly of the NLRP3 inflammasome and upregulation of HMGB1, subsequently activating MyD88 and NF-κB signaling pathways, leading to cellular inflammation (Liu et al., 2021).

In our study, we pursued to understand the influence of the time exposure, ranging from 20 min to 24 h in the levels of iROS. Investigating both short and long treatment times is crucial when studying iROS since the production and maintenance of these species within the cell is a dynamic process. Focusing solely on short periods may underestimate iROS production, as it does not provide sufficient time for enhanced production by the treatment; however, studying only longer durations may underestimate its induction due to the elimination of iROS by cellular protective mechanisms.

As depicted in Fig. 7, all three different treatments led to a significant increase in intracellular ROS production in all studied time points. While the differences between the time points were minimal, the smallest increases were consistently observed at the 12 h time point, with the most substantial increases occurring at 2 and 24 h time points, compared to negative controls. The heightened production of iROS in HUVECs following nanopolystyrene treatment was expected, as it was previously reported in studies such as after 30 nm carboxylated PS-NPLs exposure (Wei et al., 2022) and after 50 nm pristine and aminated PS-NPLs (Fu et al., 2022).

Interestingly, among the different functionalization of PS-NPLs, the lowest increases in iROS were consistently associated with the pristine treatment (*e.g.*, 21 % increase *vs* negative control at 24 h), while both carboxylated and aminated treatments exhibited very similar and higher values (*e.g.*, 30 % increase *vs* negative control at 24 h). This surface-dependent effect revealed in our study diverged from those findings

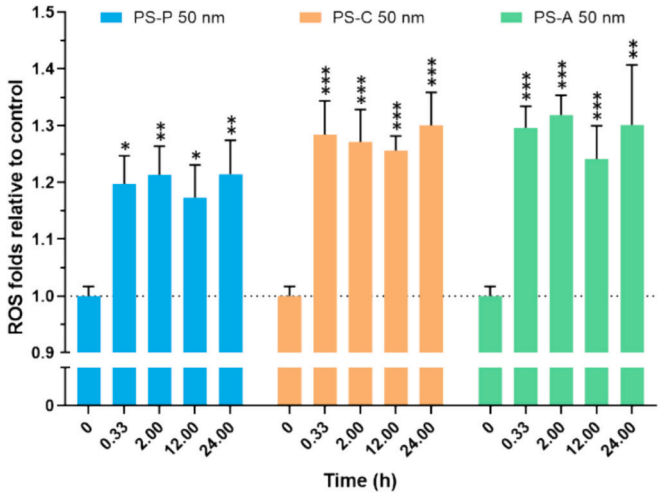


Fig. 7. Relative iROS production in HUVEC treated with different PS nanoplastics at 100 μg/mL for 20 min, 2, 12, and 24 h, as detected with DHE assay. Data is represented as mean ± SEM. One-way ANOVA with Dunnett's post-test was used for the statistical analysis. Statistical significance was indicated in the graph as $*p < 0.05$, $**p < 0.01$, and $***p < 0.001$.

reporting similar results for both 50 nm pristine and aminated nanoparticles (Fu et al., 2022). However, a major iROS production after aminated treatment, compared to pristine, was reported in human alveolar type II A549 cells (Halimu et al., 2022).

The enhanced iROS production following the aminated treatment could be explained by its stronger ability to interact with mitochondria, one of the main producers of intracellular ROS (Tirichen et al., 2021). Indeed, a major dysregulation of mitochondrial dynamics, replication, and function-related gene expression was observed after aminated treatment when compared to pristine PS-NPLs (Fu et al., 2022). As for the carboxylated nanoparticle, its capacity to increase ROS production could be explained by its major internalization compared to the pristine particle, as indicated by the major observed increases in cell size and complexity previously described.

3.6. Genotoxicity detection by the comet assay

Confocal microscopy and TEM images revealed a close spatial relationship between the nanoparticle vesicles and the nucleus of the cells, especially for the pristine and carboxylated PS-NPLs treatments. This interaction of the vesicles with the nucleus, which even reshaped the nuclear morphology, together with the increment of iROS, raised our concerns about the potential genotoxic effects of the evaluated PS-NPLs. In general, scarce studies have been undertaken to date to evaluate the genotoxic potential of such particles in human cells, with no prior studies recorded for HUVECs. Thus, considering the importance of genotoxicity as a surrogate biomarker of carcinogenesis (Shi et al., 2022), the alkaline comet assay was conducted to examine the induction of genotoxic damage by the differently functionalized polystyrene nanoplastics. The comet assay detects mainly DNA strand breaks, and it has been described as a reliable tool for detecting the genotoxic potential of metal-oxide nanoparticles (García-Rodríguez et al., 2019). Our results show that all PS-NPLs induce significant increases in DNA damage, after short exposures lasting for 2 h when the percentage of DNA in the tail is used as a biomarker (Fig. 8A). At these exposure times, pristine polystyrene induced the highest level of genotoxicity (57 % higher than the negative control), followed by aminated PS (39 % higher than the negative control). Carboxylated PS nanoparticles exhibited the lowest genotoxic effect, with a 24 % increase regarding the negative control.

To better understand the effects measured by the comet assay, a set of representative figures of the different treatments is presented in Fig. S4.

When exposures were extended to 24 h (Fig. 8B), the genotoxic effects appeared to diminish for both the pristine (28 % DNA in the tail *vs* control) and carboxylated forms (8 % DNA in the tail *vs* control), while remaining consistent for the aminated nanoparticle treatment. In this case, the aminated treatment reached the highest percentage of DNA in the tail when compared to the other treatments (39 % increase *vs* negative control). This general reduction in genotoxicity over time could be attributed to the concurrent repair of DNA lesions within the cells, as DNA repair mechanisms work to correct damage caused by genotoxic agents (Roursgaard et al., 2022).

It is noteworthy to compare these results with other studies utilizing the comet assay, which have reported little to no genotoxic effects of 50 nm PS nanoparticles in human cell lines, such as intestinal cells or white blood cells (Ballesteros et al., 2020; Domenech et al., 2020). Contrary, genotoxic effects for pristine, carboxylated, and aminated 80 nm PS-NPLs were reported in A549 cells at exposures lasting for 24 h but using the micronucleus assay instead of the comet assay (Shi et al., 2022). In such a study, the highest genotoxic effects were observed with aminated nanoparticles, followed by carboxylated, and pristine nanoparticles. The differences in genotoxicity reported in our study may be attributed to the differences in nanoparticle surface properties, although the cell type used can explain the differences with other studies. Nevertheless, our results are of high relevance since they have been obtained with human-derived primary cells, which are known to provide more physiologically relevant results than other immortalized and cancerous cell lines (Richter et al., 2021).

4. Conclusions

The human umbilical vein endothelial cells (HUVEC) utilized in this study are a good cell model for determining the kinetic cell uptake of PS-NPLs. These cells, as representative of the human endothelial barrier of the blood vessels, are primary cells isolated from the endothelium of the umbilical cord vein, which highlights the value of the obtained results. This model has confirmed that the functionalization of the PS-NPLs surface modulates their ability to internalize, pristine showing the slowest internalization. Moreover, it must be emphasized that even considering the lesser overall internalization, the main biological effects were found when cells were treated with aminated substituted nano polystyrene. This can give a different mindset related to what could or may be considered an effective dose more than a concentration-related treatment. The slow uptake of aminated polymers is associated with the relative increment in size and complexity of the cells exposed to the aminated type. Interestingly, all together show us that a slow

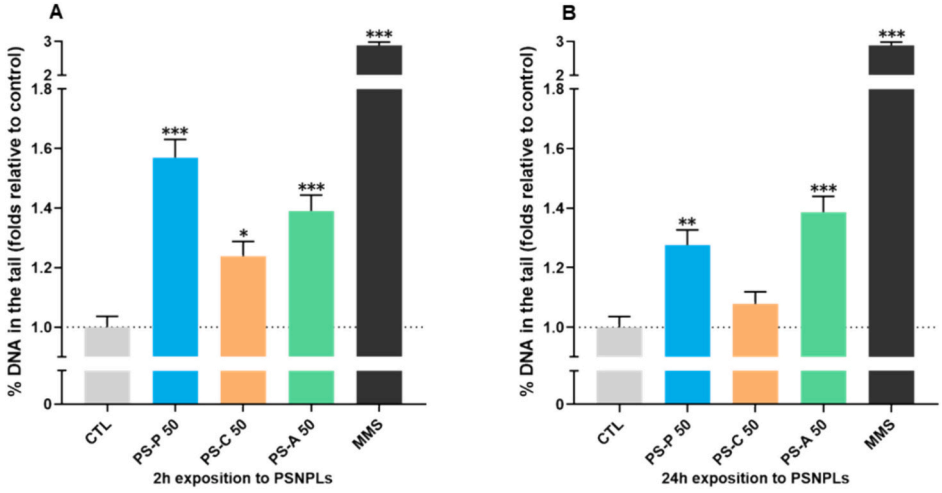


Fig. 8. Genotoxic damage detection in HUVEC by using the comet assay after exposures lasting for 2 h (A) and 24 h (B) to different PS-NPLs at 100 μg/mL. The concentration of 200 μM MMS was used as a positive control. Data is represented as mean ± SEM. The Kruskal-Wallis's test was used for statistical analysis. Statistical significance was indicated in the graph as $*p < 0.05$, $**p < 0.01$, and $***p < 0.001$.

internalization kinetics does not affect the ability of the aminated PS-NPLs to induce damage in the exposed cells, as determined by the ability to increase the intracellular ROS levels as well as their genotoxic potential, measured by the ability to induce DNA breaks. These effects of the surface characteristics should be considered when new true-to-life MNPLs, resulting from the degradation of plastic goods, are evaluated. Thus, determinations of the surface characteristics should be included in studies aiming to determine the hazardous effects of MNPLs.

Given that endothelial cells (such as HUVECs) constitute the main component of the human endothelial barrier within blood vessels, further investigation is warranted to comprehend the effects of variously functionalized and sized polystyrene (PS) nanoparticles (and MNPLs in general) on the endothelial barrier integrity. Notably, a phenomenon known as nanoparticle-induced endothelial leakiness (NanoEL) has already been documented for gold nanoparticles ranging from 10 to 30 nm (Setyawati et al., 2017), which must be explored using NPLs.

CRediT authorship contribution statement

Joan Martín-Pérez: Formal analysis, Investigation, Methodology, Writing – original draft. **Aliro Villacorta:** Investigation, Methodology. **Gooya Banaei:** Investigation, Methodology. **Michelle Morataya-Reyes:** Investigation, Methodology. **Alireza Tavakolpournegari:** Investigation, Methodology. **Ricard Marcos:** Conceptualization, Writing – review & editing. **Alba Hernández:** Writing – review & editing. **Alba García-Rodriguez:** Conceptualization, Writing – original draft, Writing – review & editing.

Declaration of competing interest

The authors declare that they have no known competing financial interests or personal relationships that could have appeared to influence the work reported in this paper.

Data availability

Data will be made available on request.

Acknowledgments

JM, MMR, and AT hold Ph.D. fellowships from the Generalitat de Catalunya. AV was supported by a Ph.D. fellowship from the National Agency for Research and Development (ANID), CONICYT PFCHA/DOCTORADO BECAS CHILE/2020-72210237. AGR received funding from the postdoctoral fellowship program Beatriu de Pinós (AGAUR, Goverment of Catalonia and Horizon 2020). AH was granted an ICREA ACADEMIA award.

The PlasticHeal project has received funding from the European Union's Horizon 2020 research and innovation programme under grant agreement No 965196. This study was supported by the Spanish Ministry of Science and Innovation (PID2020-116789RB-C43) and the Generalitat de Catalunya (2021-SGR-00731).

Appendix A. Supplementary data

Supplementary data to this article can be found online at https://doi.org/10.1016/j.scitotenv.2024.173236.

References

Alaraby, M., Villacorta, A., Abass, D., Hernández, A., Marcos, R., 2023. The hazardous impact of true-to-life PET nanoplastics in *Drosophila*. Sci. Total Environ. 863, 160954 https://doi.org/10.1016/j.scitotenv.2022.160954.

Alimi, O.S., Claveau-Mallet, D., Kurusu, R.S., Lapointe, M., Bayen, S., Tufenkji, N., 2022. Weathering pathways and protocols for environmentally relevant microplastics and nanoplastics: what are we missing? J. Hazard. Mater. 423 (Pt A), 126955 https://doi.org/10.1016/j.jhazmat.2021.126955.

Annangi, B., Bach, J., Vales, G., Rubio, L., Marcos, R., Hernández, A., 2015. Long-term exposures to low doses of cobalt nanoparticles induce cell transformation enhanced by oxidative damage. Nanotoxicology 9 (2), 138–147. https://doi.org/10.3109/17435390.2014.900582.

Annangi, B., Villacorta, A., López-Mesas, M., Fuentes-Cebrian, V., Marcos, R., Hernández, A., 2023. Hazard assessment of polystyrene nanoplastics in primary human nasal epithelial cells, focusing on the autophagic effects. Biomolecules 13 (2), 220. https://doi.org/10.3390/biom13020220.

Bajt, O., 2021. From plastics to microplastics and organisms. FEBS Open Bio 11 (4), 954–966. https://doi.org/10.1002/2211-5463.13120.

Ballesteros, S., Domenech, J., Barguilla, I., Cortés, C., Marcos, R., Hernández, A., 2020. Genotoxic and immunomodulatory effects in human white blood cells after *ex vivo* exposure to polystyrene nanoplastics. Environ. Sci. Nano 7, 3431–3446. https://doi.org/10.1039/D0EN00748J.

Banerjee, A., Billey, L.O., Shelver, W.L., 2021. Uptake and toxicity of polystyrene micro/nanoplastics in gastric cells: effects of particle size and surface functionalization. PLoS One 16 (12), e0260803. https://doi.org/10.1371/journal.pone.0260803.

Banerjee, A., Billey, L.O., McGarvey, A.M., Shelver, W.L., 2022. Effects of polystyrene micro/nanoplastics on liver cells based on particle size, surface functionalization, concentration, and exposure period. Sci. Total Environ. 836, 155621 https://doi.org/10.1016/j.scitotenv.2022.155621.

Cao, Y., Gong, Y., Liu, L., Zhou, Y., Fang, X., Zhang, C., Li, Y., Li, J., 2017. The use of human umbilical vein endothelial cells (HUVECs) as an *in vitro* model to assess the toxicity of nanoparticles to endothelium: a review. J. Appl. Toxicol. 37 (12), 1359–1369. https://doi.org/10.1002/jat.3470.

Cortés, C., Domenech, J., Salazar, M., Pastor, S., Marcos, R., Hernández, A., 2019. Nanoplastics as a potential environmental health factor: effects of polystyrene nanoparticles on human intestinal epithelial Caco-2 cells. Environ. Sci. Nano 7 (1), 272–285. https://doi.org/10.1039/C9EN00523D.

Domenech, J., Marcos, R., 2021. Pathways of human exposure to microplastics, and estimation of the total burden. Curr. Opin. Food Sci. 39, 144–151. https://doi.org/10.1016/j.cofs.2021.01.004.

Domenech, J., Hernández, A., Rubio, L., Marcos, R., Cortés, C., 2020. Interactions of polystyrene nanoplastics with *in vitro* models of the human intestinal barrier. Arch. Toxicol. 94 (9), 2997–3012. https://doi.org/10.1007/s00204-020-02805-3.

Domenech, J., de Britto, M., Velázquez, A., Pastor, S., Hernández, A., Marcos, R., Cortés, C., 2021. Long-term effects of polystyrene nanoplastics in human intestinal Caco-2 cells. Biomolecules 11 (10), 1442. https://doi.org/10.3390/biom11101442.

Foroozandeh, P., Aziz, A.A., 2018. Insight into cellular uptake and intracellular trafficking of nanoparticles. Nanoscale Res. Lett. 13 (1), 339. https://doi.org/10.1186/s11671-018-2728-6.

Fu, Y., Fan, M., Xu, L., Wang, H., Hu, Q., Jin, Y., 2022. Amino-functionalized polystyrene nano-plastics induce mitochondria damage in human umbilical vein endothelial cells. Toxics 10 (5), 215. https://doi.org/10.3390/toxics10050215.

García-Rodríguez, A., Rubio, L., Vila, L., Xamena, N., Velázquez, A., Marcos, R., Hernández, A., 2019. The comet assay as a tool to detect the genotoxic potential of nanomaterials. Nanomaterials (Basel) 10, 1385. https://doi.org/10.3390/nano9101385.

Halimu, G., Zhang, Q., Liu, L., Zhang, Z., Wang, X., Gu, W., Zhang, B., Dai, Y., Zhang, H., Zhang, C., Xu, M., 2022. Toxic effects of nanoplastics with different sizes and surface charges on epithelial-to-mesenchymal transition in A549 cells and the potential toxicological mechanism. J. Hazard. Mater. 430, 128485 https://doi.org/10.1016/j.jhazmat.2022.128485.

He, Y., Li, J., Chen, J., Miao, X., Li, G., He, Q., Xu, H., Li, H., Wei, Y., 2020. Cytotoxic effects of polystyrene nanoplastics with different surface functionalization on human HepG2 cells. Sci. Total Environ. 723, 138180 https://doi.org/10.1016/j.scitotenv.2020.138180.

Ho, Y.T., Kamm, R.D., Kah, J.C.Y., 2018. Influence of protein corona and caveolae-mediated endocytosis on nanoparticle uptake and transcytosis. Nanoscale 10 (26), 12386–12397. https://doi.org/10.1039/c8nr02393j.

Jaroszeski, M.J., Radcliff, G., 1999. Fundamentals of flow cytometry. Mol. Biotechnol. 11 (1), 37–53. https://doi.org/10.1007/BF02789175.

Jeong, J., Im, J., Choi, J., 2024. Integrating aggregate exposure pathway and adverse outcome pathway for micro/nanoplastics: a review on exposure, toxicokinetics, and toxicity studies. Ecotoxicol. Environ. Saf. 272, 116022 https://doi.org/10.1016/j.ecoenv.2024.116022.

Kihara, S., Ashenden, A., Kaur, M., Glasson, J., Ghosh, S., van der Heijden, N., Brooks, A. E.S., Mata, J.P., Holt, S., Domigan, L.J., Köper, I., McGillivray, D.J., 2021. Cellular interactions with polystyrene nanoplastics-the role of particle size and protein corona. Biointerphases 16 (4), 041001. https://doi.org/10.1116/6.0001124.

Kik, K., Bukowska, B., Sicińska, P., 2020. Polystyrene nanoparticles: sources, occurrence in the environment, distribution in tissues, accumulation, and toxicity to various organisms. Environ. Pollut. 262, 114297 https://doi.org/10.1016/j.envpol.2020.114297.

Klingberg, H., Oddershede, L.B., Loeschner, K., Larsen, E.H., Loft, S., Møller, P., 2015. Uptake of gold nanoparticles in primary human endothelial cells. Toxicol. Res. 4 (3), 655–666. https://doi.org/10.1039/C4TX00061G.

Lampitt, R.S., Fletcher, S., Cole, M., Kloker, A., Krause, S., O'Hara, F., Ryde, P., Saha, M., Voronkova, A., Whyle, A., 2023. Stakeholder alliances are essential to reduce the scourge of plastic pollution. Nat. Commun. 14 (1), 2849. https://doi.org/10.1038/s41467-023-38613-3.

Lehner, R., Weder, C., Petri-Fink, A., Rothen-Rutishauser, B., 2019. Emergence of nanoplastic in the environment and possible impact on human health. Environ. Sci. Technol. 53 (4), 1748–1765. https://doi.org/10.1021/acs.est.8b05512.

Leslie, H.A., van Velzen, M.J.M., Brandsma, S.H., Vethaak, A.D., Garcia-Vallejo, J.J., Lamoree, M.H., 2022. Discovery and quantification of plastic particle pollution in

human blood. Environ. Int. 163, 107199 https://doi.org/10.1016/j.envint.2022.107199.
Li, T., Song, X., Zhang, J., Zhao, L., Shi, Y., Li, Z., Liu, J., Liu, N., Yan, Y., Xiao, Y., Tian, X., Sun, W., Guan, Y., Liu, B., 2017. Protection of human umbilical vein endothelial cells against oxidative stress by MicroRNA-210. Oxidative Med. Cell. Longev. 17, 3565613 https://doi.org/10.1155/2017/3565613.
Liu, S., Wu, X., Gu, W., Yu, J., Wu, B., 2020. Influence of the digestive process on intestinal toxicity of polystyrene microplastics as determined by *in vitro* Caco-2 models. Chemosphere 256, 127204. https://doi.org/10.1016/j.chemosphere.2020.127204.
Liu, X., Lu, B., Fu, J., Zhu, X., Song, E., Song, Y., 2021. Amorphous silica nanoparticles induce inflammation via activation of NLRP3 inflammasome and HMGB1/TLR4/MYD88/NF-kb signaling pathway in HUVEC cells. J. Hazard. Mater. 404 (Pt B), 124050 https://doi.org/10.1016/j.jhazmat.2020.124050.
Lu, Y.Y., Li, H., Ren, H., Zhang, X., Huang, F., Zhang, D., Huang, Q., Zhang, X., 2022. Size-dependent effects of polystyrene nanoplastics on autophagy response in human umbilical vein endothelial cells. J. Hazard. Mater. 421, 126770 https://doi.org/10.1016/j.jhazmat.2021.126770.
Lundqvist, M., Stigler, J., Elia, G., Lynch, I., Cedervall, T., Dawson, K.A., 2008. Nanoparticle size and surface properties determine the protein corona with possible implications for biological impacts. Proc. Natl. Acad. Sci. USA 105 (38), 14265–14270. https://doi.org/10.1073/pnas.0805135105.
Paget, V., Dekali, S., Kortulewski, T., Grall, R., Gamez, C., Blazy, K., Aguerre-Chariol, O., Chevillard, S., Braun, A., Rat, P., Lacroix, G., 2015. Specific uptake and genotoxicity induced by polystyrene nanobeads with distinct surface chemistry on human lung epithelial cells and macrophages. PLoS One 10 (4), e0123297. https://doi.org/10.1371/journal.pone.0123297.
Pradel, A., Catrouillet, C., Gigault, J., 2023. The environmental fate of nanoplastics: what we know and what we need to know about aggregation. NanoImpact 29, 100453. https://doi.org/10.1016/j.impact.2023.100453.
Rampado, R., Crotti, S., Caliceti, P., Pucciarelli, S., Agostini, M., 2020. Recent advances in understanding the protein corona of nanoparticles and in the formulation of "stealthy" nanomaterials. Front. Bioeng. Biotechnol. 8, 166. https://doi.org/10.3389/fbioe.2020.00166.
Richter, M., Piwocka, O., Musielak, M., Piotrowski, I., Suchorska, W.M., Trzeciak, T., 2021. From donor to the lab: a fascinating journey of primary cell lines. Front. Cell Develop. Biol. 9, 711381 https://doi.org/10.3389/fcell.2021.711381.
Roshanzadeh, A., Park, S., Ganjbakhsh, S.E., Park, J., Lee, D.H., Lee, S., Kim, E.S., 2020. Surface charge-dependent cytotoxicity of plastic nanoparticles in alveolar cells under cyclic stretches. Nano Lett. 20 (10), 7168–7176. https://doi.org/10.1021/acs.nanolett.0c02463.
Roursgaard, M., Hezareh Rothmann, M., Schulte, J., Karadimou, I., Marinelli, E., Møller, P., 2022. Genotoxicity of particles from grinded plastic items in Caco-2 and HepG2 cells. Front. Public Health 10, 906430. https://doi.org/10.3389/fpubh.2022.906430.
Rubio, L., Marcos, R., Hernández, A., 2020a. Potential adverse health effects of ingested micro- and nanoplastics on humans. Lessons learned from *in vivo* and *in vitro* mammalian models. J. Toxicol. Environ. Health. Part B 23 (2), 51–68. https://doi.org/10.1080/10937404.2019.1700598.
Rubio, L., Barguilla, I., Domenech, J., Marcos, R., Hernández, A., 2020b. Biological effects, including oxidative stress and genotoxic damage, of polystyrene nanoparticles in different human hematopoietic cell lines. J. Hazard. Mater. 398, 122900 https://doi.org/10.1016/j.jhazmat.2020.122900.
Ruenraroengsak, P., Tetley, T.D., 2015. Differential bioreactivity of neutral, cationic, and anionic polystyrene nanoparticles with cells from the human alveolar compartment: robust response of alveolar type 1 epithelial cells. Part. Fibre Toxicol. 12, 19. https://doi.org/10.1186/s12989-015-0091-7.
Ruenraroengsak, P., Novak, P., Berhanu, D., Thorley, A.J., Valsami-Jones, E., Gorelik, J., Korchev, Y.E., Tetley, T.D., 2012. Respiratory epithelial cytotoxicity and membrane damage (holes) caused by amine-modified nanoparticles. Nanotoxicology 6 (1), 94–108. https://doi.org/10.3109/17435390.2011.558643.
Sawyer, L., Grubb, D.T., Meyers, G.F., 2008. Polymer Microscopy. Springer Science and Business Medium, New York. https://doi.org/10.1007/978-0-387-72628-1.
Schneider, M., Stracke, F., Hansen, S., Schaefer, U.F., 2009. Nanoparticles and their interactions with the dermal barrier. Dermato-endocrinology 1 (4), 197–206. https://doi.org/10.4161/derm.1.4.9501.
Setyawati, M.I., Tay, C.Y., Bay, B.H., Leong, D.T., 2017. Gold nanoparticles-induced endothelial leakiness depends on particle size and endothelial cell origin. ACS Nano 11 (5), 5020–5030. https://doi.org/10.1021/acsnano.7b01744.
Shi, X., Wang, X., Huang, R., Tang, C., Hu, C., Ning, P., Wang, F., 2022. Cytotoxicity and genotoxicity of polystyrene micro- and nanoplastics with different size and surface modification in A549 cells. Int. J. Nanomedicine 17, 4509–4523. https://doi.org/10.2147/IJN.S381776.
Sökmen, T.Ö., Sulukan, E., Türkoğlu, M., Baran, A., Özkaraca, M., Ceyhun, S.B., 2020. Polystyrene nanoplastics (20 nm) are able to bioaccumulate and cause oxidative DNA damages in the brain tissue of zebrafish embryos (*Danio rerio*). Neurotoxicology 77, 51–59. https://doi.org/10.1016/j.neuro.2019.12.010.
Son, J., Hong, S.J., Lim, J.W., Jeong, W., Jeong, J.H., Kang, H.W., 2021. Engineering tissue-specific, multiscale microvasculature with a capillary network for prevascularized tissue. Small Methods 5 (10), e2100632. https://doi.org/10.1002/smtd.202100632.
Tavakolpournegari, A., Annangi, B., Villacorta, A., Banaei, G., Martin, J., Pastor, S., Marcos, R., Hernández, A., 2023. Hazard assessment of different-sized polystyrene nanoplastics in hematopoietic human cell lines. Chemosphere 325, 138360. https://doi.org/10.1016/j.chemosphere.2023.138360.
Tirichen, H., Yaigoub, H., Xu, W., Wu, C., Li, R., Li, Y., 2021. Mitochondrial reactive oxygen species and their contribution in chronic kidney disease progression through oxidative stress. Front. Physiol. 12, 627837 https://doi.org/10.3389/fphys.2021.627837.
Vela, L., Villacorta, A., Venus, T., Estrela-Lopis, I., Pastor, S., García-Rodriguez, A., Rubio, L., Marcos, R., Hernández, A., 2023. The potential effects of *in vitro* digestion on the physicochemical and biological characteristics of polystyrene nanoplastics. Environ. Pollut. 329, 121656 https://doi.org/10.1016/j.envpol.2023.121656.
Vila, L., Rubio, L., Annangi, B., García-Rodríguez, A., Marcos, R., Hernández, A., 2017. Frozen dispersions of nanomaterials are a useful operational procedure in nanotoxicology. Nanotoxicology 11 (1), 31–40. https://doi.org/10.1080/17435390.2016.1262918.
Villacorta, A., Rubio, L., Alaraby, M., López-Mesas, M., Fuentes-Cebrian, V., Moriones, O. H., Marcos, R., Hernández, A., 2022. A new source of representative secondary PET nanoplastics. Obtention, characterization, and hazard evaluation. J. Hazard. Mater. 439, 129593 https://doi.org/10.1016/j.jhazmat.2022.129593.
Wang, X., Jia, Z., Zhou, X., Su, L., Wang, M., Wang, T., Zhang, H., 2023. Nanoplastic-induced vascular endothelial injury and coagulation dysfunction in mice. Sci. Total Environ. 865, 161271 https://doi.org/10.1016/j.scitotenv.2022.161271.
Wei, W., Li, Y., Lee, M., Andrikopoulos, N., Lin, S., Chen, C., Leong, D.T., Ding, F., Song, Y., Ke, P.C., 2022. Anionic nanoplastic exposure induces endothelial leakiness. Nat. Commun. 13 (1), 4757. https://doi.org/10.1038/s41467-022-32532-5.
Xu, C., Xu, J., Tang, H.W., Ericsson, M., Weng, J.H., DiRusso, J., Hu, Y., Ma, W., Asara, J. M., Perrimon, N., 2023. A phosphate-sensing organelle regulates phosphate and tissue homeostasis. Nature 617 (7962), 798–806. https://doi.org/10.1038/s41586-023-06039-y.
Xue, J., Zhang, Z., Sun, Y., Jin, D., Guo, L., Li, X., Zhao, D., Feng, X., Qi, W., Zhu, H., 2023. Research progress and molecular mechanisms of endothelial cells inflammation in vascular-related diseases. J. Inflamm. Res. 16, 3593–3617. https://doi.org/10.2147/JIR.S418166.
Yee, M.S., Hii, L.W., Looi, C.K., Lim, W.M., Wong, S.F., Kok, Y.Y., Tan, B.K., Wong, C.Y., Leong, C.O., 2021. Impact of microplastics and nanoplastics on human health. Nanomaterials (Basel) 11 (2), 496. https://doi.org/10.3390/nano11020496.
Yu, Z., Li, Q., Wang, J., Yu, Y., Wang, Y., Zhou, Q., Li, P., 2020. Reactive oxygen species-related nanoparticle toxicity in the biomedical field. Nanoscale Res. Lett. 15 (1), 115. https://doi.org/10.1186/s11671-020-03344-7.
Zhu, X., Wang, C., Duan, X., Liang, B., Genbo, Xu E., Huang, Z., 2023. Micro- and nanoplastics: a new cardiovascular risk factor? Environ. Int. 171, 107662 https://doi.org/10.1016/j.envint.2022.107662.

3.2. Chapter 2 (Paper 2)

Transcriptomic and functional profiling of endothelial dysfunction induced by polystyrene nanoplastics.

Frontiers in Toxicology, 8. (2026)

DOI: 10.3389/ftox.2026.1812922

Impact Factor: 4.6 (2024)

frontiers in Toxicology

TYPE Original Research
PUBLISHED 17 April 2026
DOI 10.3389/ftox.2026.1812922

Check for updates

OPEN ACCESS

EDITED BY
Rute Isabel Cesário,
University of Lisbon, Portugal

REVIEWED BY
Momoko Ishii,
Ramboll Group A/S, United States
Oksana Shevchuk,
I. Horbachevsky Ternopil National Medical University, Ukraine

*CORRESPONDENCE
Alba Hernández,
alba.hernandez@uab.cat
Alba García-Rodríguez,
alba.garcia.rodriguez@uab.cat

RECEIVED 17 February 2026
REVISED 11 March 2026
ACCEPTED 27 March 2026
PUBLISHED 17 April 2026

CITATION
Martín-Pérez J, Villacorta A, Gutiérrez-García J, Egea R, Morataya-Reyes M, Cassú-Casadevall M, Barguilla I, Marcos R, Hernández A and García-Rodríguez A (2026) Transcriptomic and functional profiling of endothelial dysfunction induced by polystyrene nanoplastics.
Front. Toxicol. 8:1812922.
doi: 10.3389/ftox.2026.1812922

COPYRIGHT
© 2026 Martín-Pérez, Villacorta, Gutiérrez-García, Egea, Morataya-Reyes, Cassú-Casadevall, Barguilla, Marcos, Hernández and García-Rodríguez. This is an open-access article distributed under the terms of the Creative Commons Attribution License (CC BY). The use, distribution or reproduction in other forums is permitted, provided the original author(s) and the copyright owner(s) are credited and that the original publication in this journal is cited, in accordance with accepted academic practice. No use, distribution or reproduction is permitted which does not comply with these terms.

Transcriptomic and functional profiling of endothelial dysfunction induced by polystyrene nanoplastics

Joan Martín-Pérez[1], Aliro Villacorta[1,2], Javier Gutiérrez-García[1], Raquel Egea[1], Michelle Morataya-Reyes[1], Mireia Cassú-Casadevall[1], Irene Barguilla[1], Ricard Marcos[1], Alba Hernández[1]* and Alba García-Rodríguez[1]*

[1]Group of Mutagenesis, Department of Genetics and Microbiology, Faculty of Biosciences, Universitat Autònoma de Barcelona, Barcelona, Spain, [2]Facultad de Recursos Naturales Renovables, Universidad Arturo Prat, Iquique, Chile

Background: The presence of micro- and nanoplastics (MNPLs) in human blood raises concerns about their vascular impact and their potential contribution to cardiovascular diseases. Endothelial cells are a primary target of circulating MNPLs; however, the molecular and functional consequences of this exposure remain largely undefined.
Methods: In this study, we exposed primary human umbilical vein endothelial cells (HUVECs) to carboxylated polystyrene nanoplastics (PS-NPLs; 30, 50, and 100 nm) and integrated RNA sequencing with targeted functional assays.
Results: Transcriptomics revealed a robust response characterized by coordinated dysregulation of cholesterol homeostasis, genotoxic stress and DNA repair, inflammatory signaling, and endothelial plasticity (endothelial-to-mesenchymal transition). Guided by these signatures, functional assays confirmed increased intracellular cholesterol, DNA damage, remodelling of migratory capacity and angiogenic behaviour, and reduced IL-6 secretion.
Discussion: Overall, the concordance between transcriptomic programs and functional endpoints supports a mechanistic framework in which PS-NPL exposure rewires endothelial metabolic and stress-response networks, with downstream consequences for key vascular functions. Differences across the nanoscale range modulated the magnitude and temporal profile of specific endpoints, but the shared molecular core response predominated across treatments.

KEYWORDS
functional effects, genotoxicity, HUVEC, internalization, polystyrene nanoplastics, transcriptomics

1 Introduction

Plastics are synthetic polymers predominantly composed of carbon–carbon (C–C) backbones. While a subset of biodegradable plastics is derived from natural feedstocks such as cellulose or cornstarch, the vast majority is derived from fossil resources (Rodrigues et al., 2022). Global plastic production has increased exponentially, from 2 million tons in 1950 to 359 million tons in 2018 (Shen et al., 2020). This expansion is driven by plastics' unique combination of durability, chemical resistance, low water

permeability, light weight, and cost-effectiveness, which has made them indispensable across packaging, consumer goods, medical devices, and construction (Oliveira et al., 2020; Domenech and Marcos, 2021). However, large-scale production, widespread use, and inadequate recycling have led to environmental accumulation (Hong, 2023). Their persistence to degradation allows plastics to accumulate in air, water, soil, and biota (Shen et al., 2020). Environmental processes such as fragmentation and photo-oxidation break plastics into smaller particles, generating secondary microplastics (<1 mm) and nanoplastics (<1 μm) (MNPLs). Moreover, MNPLs are deliberately produced for applications in cosmetics, drug delivery, and 3D printing inks (Facciolà et al., 2021; Rodrigues et al., 2022).

Beyond environmental pollution, MNPLs pose emerging human health risks owing to their ability to enter the body primarily via ingestion and inhalation (Rubio et al., 2020; O'Neill and Lawler, 2021). Their nanoscale dimensions enable them to traverse biological barriers, such as the gastrointestinal and respiratory epithelia (Lehner et al., 2019; Domenech et al., 2020), reach the systemic circulation, and accumulate in diverse tissues (Rajendran and Chandrasekaran, 2023). Indeed, MNPLs have been detected in human tissues/organs, including the placenta, lungs, liver, breast milk, and blood (Ali et al., 2024). In human blood, plastic particles ≥700 nm at concentrations averaging 1.6 μg/mL were reported with polystyrene (PS) among the most abundant polymers (Leslie et al., 2022). In blood vessels, MNPLs may interact with vascular endothelial cells, potentially contributing to cardiovascular disease (CVD). In line with this, Marfella et al. (2024) demonstrated that the presence of MNPL in carotid plaques increased the risk of myocardial infarction and stroke, providing a possible mechanistic link between exposure and CVD. Understanding the toxicity of nanoplastics (NPLs) in endothelial cells is therefore crucial for evaluating their cardiovascular impact. Among available models, human umbilical vein endothelial cells (HUVECs) are widely used owing to their primary human origin and their ability to recapitulate key features of the vascular endothelium (Cao et al., 2017). Prior studies have demonstrated that HUVECs efficiently internalize NPLs, eliciting responses such as cytotoxicity, oxidative stress, and autophagy (Cao et al., 2017; Martín-Pérez et al., 2024). However, most evidence remains fragmented across individual endpoints, and omics-level signatures are rarely connected to specialized endothelial functions. To address this gap, we combined transcriptomic profiling (RNA-seq; DEG, ORA, and GSEA) with functional assays that capture core features of endothelial dysfunction, including cholesterol accumulation (Filipin III staining), genome integrity (comet assay), migration (wound-healing assay), angiogenic behaviour (tube formation assay), and inflammatory signaling (IL-6 ELISA). We included three PS-NPL sizes (30, 50, and 100 nm) to assess whether the molecular programs and functional consequences identified are robust across the nanoscale range. This integrated approach provides mechanistic insight into how PS-NPLs modulate primary human endothelial cells and strengthens the biological interpretation of transcriptomic findings beyond their use as a screening layer for hazard identification.

2 Materials and methods

2.1 Sources of NPLs

Fluorescently labeled (FL) PS-C-NPLs of 30 nm (L5155; nominal size: 0.02–0.04 μm) were obtained from Sigma-Aldrich (Steinheim, Germany). For the 50 nm NPLs, both fluorescently labeled (16661-10; mean diameter: 0.05 μm) and non-labeled (NL) (15913-10; mean diameter: 0.05 μm) PS-C-NPLs were purchased from Polysciences Inc. (Warrington, PA, USA). Similarly, for the 100 nm NPLs, fluorescently labeled (16662-10; mean diameter: 0.10 μm) and non-labeled (16688-15; mean diameter: 0.10 μm) PS-C-NPLs were obtained from the same supplier.

2.2 PS-C-NPLs characterization

Characterization of the PS-C-NPLs was performed by diluting the dispersions in Milli-Q water and/or Endothelial Cell Growth Medium 2 (EGM-2; Promocell; Heidelberg, Germany). For dry-state transmission electron microscopy (TEM) analysis, PS-C-NPLs were prepared at a concentration of 200 μg/mL in Milli-Q water. Copper grids with a carbon coating were immersed in the working solutions, dried overnight, and imaged using a JEOL JEM 1400 TEM (JEOL Ltd., Tokyo, Japan) at 120 kV. Martin diameters of 100 individual NPLs were measured in ImageJ v1.8.0_172 to determine size distributions. For colloidal behaviour, PS-C-NPLs (100 μg/mL) were suspended in both Milli-Q water and EGM-2. Particle size and Z-potential were measured using a Zetasizer® Ultra (Malvern Panalytical, Cambridge, UK) with appropriate cuvettes. Each sample was analysed in triplicate.

2.3 Cell line and culture conditions

Human umbilical vein endothelial cells (HUVECs, single donor; C-12200) were obtained from Promocell (Heidelberg, Germany). Derived from the endothelial lining of umbilical cord veins, HUVECs are widely recognized as a representative primary model of the human endothelium for physiological and toxicological studies. Cells were cultured in EGM-2 medium (C-22011, Promocell) in collagen-coated flasks prepared with rat tail collagen I (Corning Inc., New York, NY, USA) at 5 μg/cm^2. Cultures were maintained at 37 °C in a humidified 5% CO_2 atmosphere with medium changes every other day, and experiments were performed with cells up to passage 6.

2.4 PS-C-NPL treatments

Cells were exposed to PS-C-NPLs diluted in EGM-2 at 100 μg/mL for 24 h, unless specified otherwise. To ensure comparable cell density, treatments with different durations were applied in a staggered manner and analyzed simultaneously. Cells were typically seeded at 26,300 cells/cm^2 in collagen I-coated wells (5 μg/cm^2) and cultured for 48 h before the medium was replaced with the corresponding treatment. Untreated cells served as negative controls.

2.5 Cytotoxicity of PS-C-NPLs

Cytotoxicity of PS-C-NPLs in HUVECs was assessed using the Coulter principle with a Beckman Coulter Z1-D cell counter (Beckman Coulter Inc., Pasadena, CA, USA). Cells were exposed to PS-C-NPLs (30, 50, and 100 nm) at 50, 100, and 200 μg/mL for 24 h. Viability was calculated as the mean cell count in each treatment relative to the untreated control, expressed as a percentage. Experiments were performed in triplicate with technical duplicates analyzed for each condition.

2.6 RNA isolation and sequencing

After 24 h exposure to 100 μg/mL PS-C-NPLs (30, 50, and 100 nm), RNA was isolated using the TRI Reagent® protocol (Merck, Darmstadt, Germany). Lysates were processed with chloroform extraction and 2-propanol precipitation, and RNA pellets were washed with 75% ethanol before resuspension in RNase-free water. RNA concentration and purity were determined with a NanoDrop® spectrophotometer (Thermo Fisher Scientific, Waltham, MA, USA). Samples were submitted to Macrogen (Seoul, South Korea) for RNA sequencing (RNA-seq). Experiments were performed with technical quadruplicates for each treatment and triplicates for the negative control.

2.7 Bioinformatic analysis for transcriptomic data

Statistical analyses were performed in R version 4.3.2 (R Core Team, 2023) using RStudio (Posit Team, 2023). Raw FASTQ files were quality filtered with Rfastp (Wang and Carroll, 2024) to remove adapters, trim low-quality bases, and discard reads shorter than 20 bp. Filtered reads were mapped to the human genome GRCh38 (GENCODE) and counted with Rsubread (Liao et al., 2019; Carlson, 2023). Lowly expressed genes were removed with the filterByExpr function from edgeR, and normalization factors were calculated with calcNormFactors (Law et al., 2016; Chen et al., 2024). Surrogate variable analysis (sva; Leek et al., 2023) was applied to account for technical variation, and differential expression was performed with limma-voom (Law et al., 2014; Ritchie et al., 2015). Differentially expressed genes (DEGs) were obtained by contrasting treated samples with the negative control. Functional enrichment was assessed using clusterProfiler (Wu et al., 2021; Dolgalev, 2022) by both over-representation analysis (ORA) and gene set enrichment analysis (GSEA), with GO Cellular Component and MSigDB hallmark (H) collections as references. Parameters were left as default, except for the maximum gene set size in GO GSEA, which was set to 800. ORA further analyzed unique and shared DEGs across treatments with the MSigDB hallmark collection. Data visualization was performed with ggplot2, eulerr, and ComplexHeatmap (Wickham, 2016; Gu, 2022; Larsson, 2024).

2.8 Cellular uptake by flow cytometry

The internalization of PS-C-NPLs by HUVECs was evaluated by flow cytometry. Cells were treated with 100 μg/mL of FL PS-C-NPLs (30, 50, and 100 nm) for 20 min, 2 h, 12 h, and 24 h. Viable cells were stained with Via-Probe™ Red Nucleic Acid Stain (1:200; BD Biosciences, Franklin Lake, NJ, USA). Fluorescence was measured using a CytoFLEX flow cytometer (Beckman Coulter, Pasadena, CA, USA) with excitation/emission wavelengths of 488/525 nm for FL PS-C-NPLs and 638/660 nm for Via-Probe™. Two parameters were quantified: (i) the percentage of cells internalizing PS-C-NPLs and (ii) the relative amount internalized per cell. For each condition, 10,000 cells were analyzed using Cytexpert software (Beckman Coulter, Pasadena, CA, USA). Experiments were performed in triplicate, and technical duplicates were analyzed for each replicate.

2.9 Cellular uptake assessment by confocal microscopy

Laser confocal microscopy was used to confirm the localization of FL PS-C-NPLs (30, 50, and 100 nm) within HUVECs. After exposure, the media were removed, and cells were incubated with Hoechst 33342 (1:500) and CellMask™ Deep Red (1:500) (ThermoFisher Scientific, Waltham, MA, USA) to stain nuclei and membranes, respectively. Images were acquired with a Leica TCS SP5 confocal microscope (Leica Microsystems GmbH, Mannheim, Germany). FL PS-C-NPLs were detected inside the cells at 488 nm, nuclei at 405 nm, and membranes at 633 nm. Several random fields were imaged per sample, and images were processed using ImageJ v1.8.0_172.

2.10 Cellular uptake assessment by TEM

TEM was used to complement flow cytometry and confocal microscopy by providing high-resolution localization of PS-C-NPLs and identifying associated subcellular structures. After 24 h of exposure to PS-C-NPLs (30, 50, and 100 nm), cells were collected, centrifuged, and fixed in 2.5% (v/v) glutaraldehyde (Merck, Darmstadt, Germany) and 2% (w/v) paraformaldehyde (EMS, Hatfield, PA, USA) in 0.1 M cacodylate buffer (pH 7.4; Sigma-Aldrich, Steinheim, Germany). Samples were processed following standard TEM protocols (Annangi et al., 2015). Cells were post-fixed with osmium tetroxide, dehydrated through a graded acetone series, and embedded in Eponate 12™ resin (Ted Pella Inc., Redding, CA, USA), polymerized at 60 °C. Ultrathin sections were stained with uranyl acetate and Reynolds lead citrate and examined with a JEOL JEM 1400 TEM (JEOL Ltd., Tokyo, Japan) equipped with an ES1000W Erlangshen CCD camera (GATAN Inc., Pleasanton, CA, USA).

2.11 Genotoxicity by the comet assay

The genotoxic potential of PS-C-NPLs (30, 50, and 100 nm) in HUVECs was evaluated by the comet assay to detect DNA strand breaks (Collins et al., 2023). Cells were exposed to PS-C-NPLs for 2 and 24 h, with methyl methanesulfonate (MMS; 200 μM, 30 min at 37 °C; Sigma-Aldrich, St. Louis, MO, USA) as the positive control. After exposure, cells were centrifuged (150 g, 6 min, 4 °C), resuspended in PBS (1×10^6 cells/mL), and mixed with 0.75% low-melting agarose (1:10). Drops of 7 μL were placed on Gelbond® film (Lonza Bioscience, Basel, Switzerland) in triplicate. Following overnight lysis at 4 °C, DNA was unwound in electrophoresis buffer (35 min, 4 °C) and electrophoresed (20 V, 300 mA, 20 min, 4 °C). Films were washed, fixed in ethanol for 1 h, and air-dried overnight.

Samples were stained with SYBR™ Gold (20 min, 1:10,000; Invitrogen, Waltham, MA, USA) and visualized using an Olympus BX50 epifluorescence microscope (Olympus, Tokyo, Japan) at ×20 magnification. DNA damage was quantified as % tail DNA using Komet 5.5 software (Kinetic Imaging Ltd., Liverpool, UK), with 100 cells per sample analyzed. Each experimental condition was assessed using two samples per replicate, and the entire experiment was performed in duplicate.

2.12 Cholesterol detection via Filipin III staining

HUVECs were seeded in µ-Plate 24 Well black plates (ibidi, Gräfelfing, Germany), and intracellular cholesterol was assessed by Filipin III staining. After 24 h exposure to PS-C-NPLs (30, 50, and 100 nm), cells were fixed with an optimized two-step protocol to preserve morphology. Cells were pre-fixed with a 1:1 mixture of EGM-2 and 4% paraformaldehyde (PFA) at 37 °C for 10 min, followed by 4% PFA at room temperature for 10 min. After PBS washes, aldehyde groups were quenched with 1.5 mg/mL glycine in PBS. Filipin III (SAE0087, Sigma-Aldrich, Steinheim, Germany) was diluted in PBS containing 10% FBS to 0.05 mg/mL and applied for 2 h at room temperature in the dark. Images were acquired using a Zeiss LSM 980 confocal microscope (Carl Zeiss Microscopy GmbH, Jena, Germany) at ×20 magnification (excitation 353 nm, emission 465 nm), with five images per well. Fluorescence intensity was quantified in 400 cells (20 per image) using ImageJ (v1.8.0_172) with manual ROIs, across two biological replicates with two technical replicates each. Raw Integrated Density values were normalized to cell area.

2.13 Wound healing assay

To evaluate the effects of PS-C-NPLs (30, 50, and 100 nm) on HUVEC migration, a wound-healing assay was performed using Culture-Inserts 2 Well (Ibidi GmbH, Gräfelfing, Germany) according to the manufacturer's protocol. Inserts were placed in collagen-coated wells, and 21,000 cells were seeded in each compartment with EGM-2 medium containing 100 µg/mL PS-C-NPLs. After 24 h of incubation, the inserts were removed, the wells were washed, and fresh medium at the same NPL concentration was added. Images were captured at 0 h with a Zeiss Axio Observer A1 inverted microscope (Carl Zeiss Microscopy GmbH, Jena, Germany) using a ×10 objective, and additional image were acquired every 2h for up to 8 h. Wound closure was quantified with ImageJ (v.8.0_172) using the "Wound Healing Size Tool" plug-in (Surez-Arnedo et al., 2020), applying the formula $Wound\ closure\ \% = \left(\frac{A_{t=0} - A_{t=\Delta t}}{A_{t=0}}\right) x100\%$, where $A_{t=0}$ is the initial wound area and $A_{t=\Delta t}$ the area at each time point. Experiments were repeated three times with technical triplicates per condition.

2.14 Tube formation assay

An angiogenesis assay was performed to assess the effects of PS-C-NPLs (30, 50, and 100 nm) on HUVEC tube formation. After 48 h incubation, passage 5 cells were treated for 24 h with 100 µg/mL PS-C-NPLs. Then, 10,000 cells were seeded into µ-Slide 15 Well 3D plates (Ibidi GmbH, Gräfelfing, Germany) pre-coated with Corning® Matrigel® Matrix (Corning, NY, USA) in medium containing the same concentration of PS-C-NPLs. Positive controls were treated with PTPase inhibitor/Suramin (Abcam, Cambridge, UK) at 10–20 µM. After 14 h of incubation, cells were washed, and tube formation was evaluated using a Zeiss LSM 980 confocal microscope (Carl Zeiss, Jena, Germany) in brightfield mode. For each well, 12 stitched Z-stack images were acquired at ×10 magnification with extended depth of focus. Quantitative parameters, including covered area, total tube length, and branching points, were analyzed with the WimTube image analysis service (Wimasis Image Analysis, Onimagin Technologies SCX, Córdoba, Spain). The experiment was repeated three times with technical quadruplicates per condition.

2.15 IL-6 ELISA (enzyme-linked immunosorbent assay)

IL-6 levels were quantified by ELISA in culture supernatants collected after 24 h of treatment with PS-C-NPLs (30, 50, and 100 nm). Supernatants were processed using ELISA kits (KHC0061, Invitrogen; Waltham, MA, USA) according to the manufacturer's instructions. Absorbance was measured at 450 nm, and standard curves were generated with a 4-parameter logistic fit. IL-6 concentrations were calculated for each treatment. Experiments were performed three times with technical triplicates per condition.

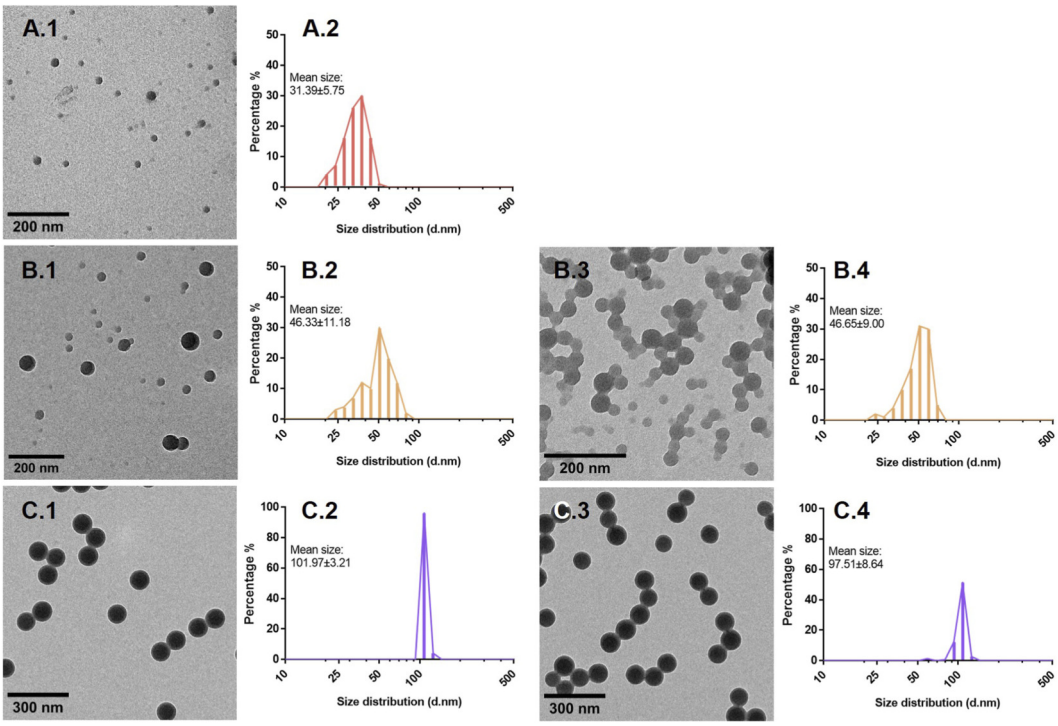
2.16 Statistical analysis for *in vitro* assays

Data analysis was conducted with GraphPad Prism 9 (GraphPad Software Inc., CA, USA). Normality was assessed with the Shapiro–Wilk test. For normally distributed data, one-way ANOVA was performed, followed by Dunnett's test to compare each treatment with the control (CTL vs. PS-C 30 nm, CTL vs. PS-C 50 nm, CTL vs. PS-C 100 nm) and Tukey's test to compare treatments with each other (PS-C 30 nm vs. PS-C 50 nm, PS-C 30 nm vs. PS-C 100 nm, PS-C 50 nm vs. PS-C 100 nm). For non-parametric data, the Kruskal–Wallis test followed by Dunn's test was used. Statistical significance was defined as $^{*}p \leq 0.05$, $^{**}p \leq 0.01$, and $^{***}p \leq 0.001$. Data is presented in figures as mean ± standard error of the mean (SEM).

3 Results and discussion

3.1 Physicochemical characterization of PS-C-NPLs

PS-C-NPLs of 30, 50, and 100 nm were selected to span a representative nanoscale range and to test the robustness of endothelial responses across particle sizes. TEM imaging confirmed that all three sizes maintained a spherical morphology in Milli-Q water, with diameters consistent with manufacturer specifications (Figures 1A–C). Hydrodynamic size measurements in Milli-Q water (Figure 1D) were close to nominal values for all NPLs. In EGM-2, PS-C 30 and 100 nm maintained Z-average sizes comparable to those in Milli-Q water. In contrast, PS-C 50 nm showed a pronounced size increase (650–690 nm) with high PDI



D

	MiliQ				EGM-2		
	TEM	Z-Average	PDI	Z-Pot	Z-Average	PDI	Z-Pot
PS-C 30 FL	31.39 ± 5.75	33.60 ± 0.28	0.08	-32.50 ± 0.79	39.90 ± 0.33	0.28	-10.10 ± 4.72
PS-C 50 FL	46.33 ± 11.18	64.70 ± 0.55	0.03	-40.30 ± 1.99	691.00 ± 33.50	0.75	-9.34 ± 1.38
PS-C 50 NL	46.65 ± 9.00	60.10 ± 0.30	0.04	-43.20 ± 0.78	656.00 ± 133.00	0.80	-9.66 ± 2.79
PS-C 100 FL	101.97 ± 3.21	120.00 ± 1.07	0.03	-52.30 ± 0.71	129.00 ± 0.87	0.05	-9.96 ± 0.08
PS-C 100 NL	97.51 ± 8.64	111.00 ± 1.16	0.01	-48.20 ± 0.87	131.00 ± 1.17	0.06	-8.21 ± 1.14

FIGURE 1
Physicochemical characterization of PS-C-NPLs. Panels **(A)** correspond to PS-C-NPLs of 30 nm, panels **(B)** to PS-C-NPLs of 50 nm, and panels **(C)** to PS-C-NPLs of 100 nm. Panels **(A.1–C.1)** show TEM images of fluorescently labeled NPLs, with panels **(A.2–C.2)** displaying the corresponding size distribution histograms. Panels **(B.3,C.3)** present TEM images of non-labeled NPLs, with panels **(B.4,C.4)** showing the respective histograms. Panel **(D)** summarizes TEM-derived Martin's diameter (nm), hydrodynamic diameter (d.nm), and ζ-potential (mV) values obtained by TEM and DLS in Milli-Q water and EGM-2.

(polydispersity indices) (0.75–0.80), indicating aggregation of both FL and NL counterparts. Importantly, DLS number-based distributions rather than intensity-based demonstrated that the predominant fraction of PS-C 50 nm in EGM-2 remained near 50 nm (Supplementary Figures S1B.1,B.2), and submicrometric fraction analysis confirmed that >99% of particles were below 200 nm in both cases. Thus, the elevated Z-average reflected a minor fraction of aggregates dominating the scattering signal. Surface charge analysis (Figure 1D) showed modest differences in Milli-Q water (−32.5 to −52.3 mV), but in EGM-2 all PS-C-NPLs displayed comparable ζ-potentials (−8.2 to −10.1 mV), consistent with previous observations (Santos et al., 2011; Paget et al., 2015; Banerjee et al., 2021). These values reflect partial charge screening by serum proteins forming a protein corona, thereby reducing surface charge differences among particles (da Silva et al., 2019). Overall, the characterization supports that the three PS-C-NPL preparations behave as expected under exposure conditions and provides a consistent basis for comparing molecular and functional responses across the nanoscale range under similar surface electrostatics.

3.2 Viability assessment of HUVECs exposed to PS-C-NPLs

Assessment of HUVEC viability after 24 h exposure to PS-C-NPLs (50–200 μg/mL) showed no significant cytotoxicity across particle sizes, with only a slight, non-significant reduction at 200 μg/mL (Supplementary Figure S2). These findings, consistent with previous reports in HUVECs (Martín-Pérez et al., 2024), indicate good acute tolerability and confirm that downstream alterations are not attributable to loss of viability. Accordingly, 100 μg/mL was selected as a sublethal concentration for subsequent assays, ensuring adequate exposure while preserving cellular integrity. This concentration is consistent with standard practice in *in vitro*

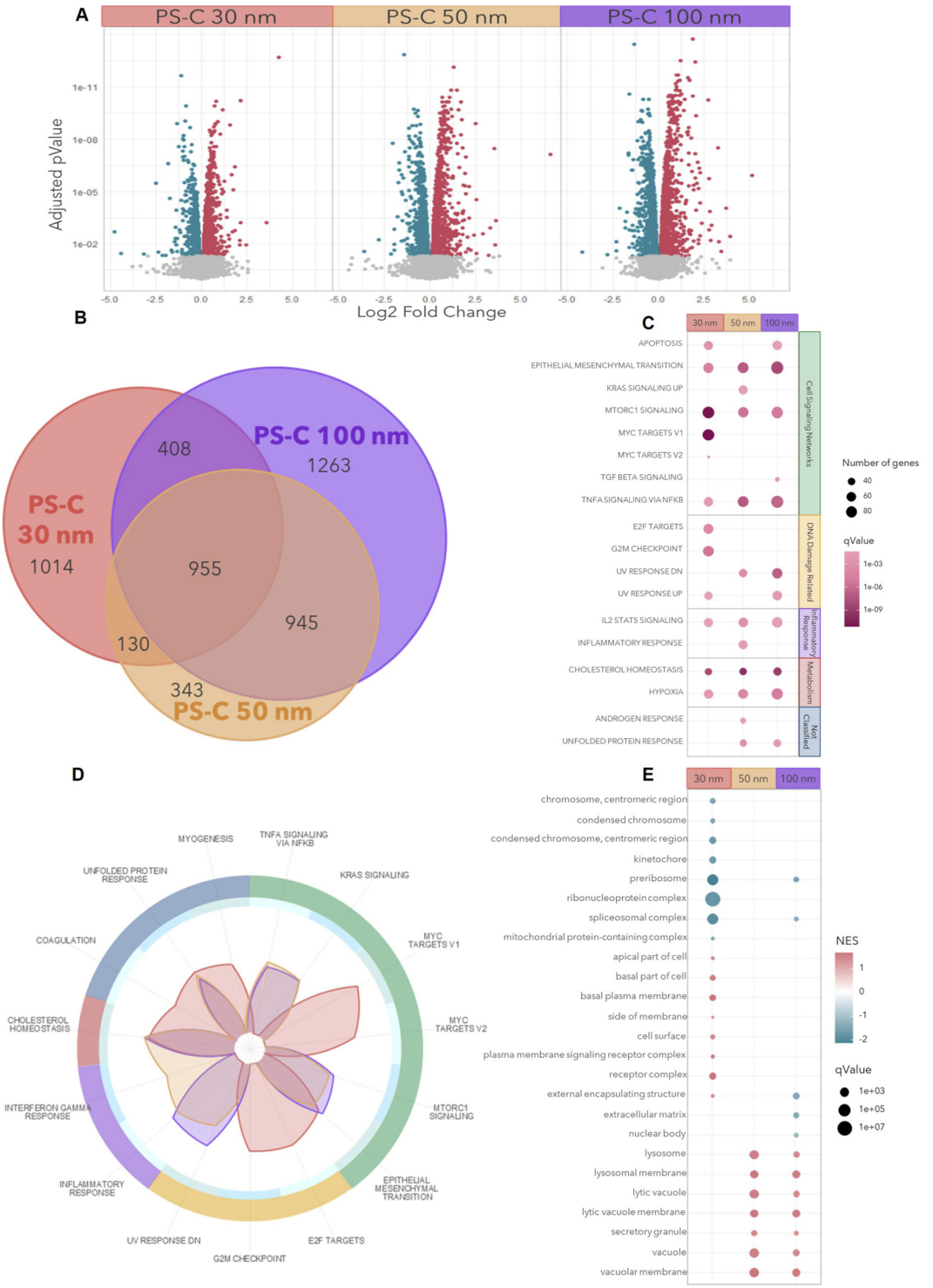


FIGURE 2
RNA-seq bioinformatic analyses of HUVECs exposed to PS-C-NPLs. **(A)** Volcano plots show gene-expression changes for each treatment, with upregulated genes shown in red and downregulated genes in blue. **(B)** Venn diagram illustrates the overlap and unique sets of DEGs across the different particle sizes. **(C)** Over-representation analysis (ORA, hallmark collection) identifies enriched pathways grouped into signaling, DNA damage, inflammation, metabolism, and unclassified categories. **(D)** Gene set enrichment analysis (GSEA, hallmark collection) is represented as radar plots of absolute NES values, highlighting enrichment patterns across treatments. **(E)** GSEA of Gene Ontology cellular components. PS-C 30 nm in red, PS-C 50 nm in orange, and PS-C 100 nm in purple.

nanotoxicology for hazard identification (Martín-Pérez et al., 2024; Lu et al., 2022; Lee et al., 2021; Brouwer et al., 2025). Furthermore, it is particularly justified given that current analytical methods cannot yet reliably quantify the nanometric fraction in biological matrices, leaving baseline circulating levels largely unknown. Moreover, local nanoplastic concentrations at the endothelial surface may be substantially higher than average blood levels due to tissue-level bioaccumulation, especially within areas of plaque formation (Marfella et al., 2024).

3.3 Transcriptomic profiling of HUVECs under PS-C-NPL exposure

RNA-seq analysis revealed that all PS-C-NPL treatments induced extensive transcriptional alterations in HUVECs (Figure 2A). PS-C 100 nm triggered the largest number of DEGs (3,571), followed by PS-C 30 nm (2,507) and PS-C 50 nm (2,373). Despite these differences in magnitude, 955 DEGs were shared across all treatments, delineating a core transcriptomic response to PS-C-NPL exposure (Figure 2B). Overlap analysis indicated condition-specific components, with more unique DEGs in PS-C 30 nm and greater overlap between PS-C 50 and 100 nm.

Functional enrichment analyses highlighted a dominant shared response and additional treatment-associated signatures. ORA of hallmark gene sets (Figure 2C; MSigDB) revealed a consistent core across all treatments, with "Cholesterol homeostasis" and "Epithelial–mesenchymal transition" as the most significantly enriched pathways, together with "IL-2 STAT5 signaling," "mTORC1 signaling," "TNFα signaling via NF-κB," and "Hypoxia." These findings define a shared axis of metabolic, inflammatory, and signaling-related alterations across the nanoscale range. Beyond this core, some enrichment patterns differed between conditions: PS-C 30 nm showed stronger enrichment of genome integrity–related programs coupled to cell-cycle control (e.g., "MYC targets," "E2F targets," "G2M checkpoint"), PS-C 50 nm was more closely associated with inflammatory signatures ("Inflammatory response"), and PS-C 50/100 nm showed enrichment of genome integrity–linked stress programs consistent with DNA damage and repair engagement (e.g., "UV response DN"). In addition, "UV response UP" was enriched in PS-C 30 and 100 nm, further supporting shared DNA damage–response/repair-associated transcriptional engagement across these conditions. GSEA corroborated these results, consistently recovering the core responses "Cholesterol homeostasis" and "Epithelial–mesenchymal transition," while also capturing modest condition-associated shifts in enrichment patterns (Figure 2D).

Finally, GSEA on cellular components (GO) revealed treatment-associated differences in the subcellular structures implicated (Figure 2E). PS-C 30 nm showed relatively stronger enrichment for DNA and cell division complexes ("chromosome, centromeric region," "condensed chromosome," "kinetochore"), RNA transcription and protein synthesis machinery ("preribosome," "ribonucleoprotein complex," "spliceosomal complex"), and membrane-related structures ("apical part of cell," "basal part of cell," "basal plasma membrane," "cell surface," "external encapsulating structure"). In contrast, PS-C 50 and 100 nm were more prominently associated with vacuolar and lysosomal structures ("lysosome," "lytic vacuole," "secretory granule," "vacuolar membrane"). Such patterns may be consistent with differences in intracellular distribution and processing pathways, thereby providing a rationale for subsequent flow cytometry, confocal microscopy, and TEM analyses of particle uptake and ultrastructural localization.

Together, these transcriptomic results provide a pathway-level map of endothelial responses to PS-C-NPL exposure. A robust core program emerged across treatments, centered on cholesterol metabolism, endothelial plasticity (EMT), inflammatory signaling, and stress-response networks, with genome integrity control emerging as a prominent additional axis across the dataset. Importantly, the convergence between ORA and GSEA allowed us to use the bioinformatic readouts as a hypothesis-generating and mechanistic layer to guide targeted phenotyping. We therefore examined NPL internalization and intracellular distribution (flow cytometry, confocal microscopy, and TEM), then assessed genome integrity (comet assay), cholesterol accumulation (Filipin III staining), endothelial migration (wound-healing assay), angiogenic behaviour (tube formation assay), and inflammatory signaling (IL-6 secretion).

3.4 Internalization and intracellular distribution of PS-C-NPLs in HUVECs

Flow cytometry showed that HUVECs rapidly internalized fluorescent PS-C-NPLs across all conditions, with near-complete uptake within the first 20 min (Figure 3B). This uniform internalization at the population level provides a robust basis to connect molecular perturbations with downstream functional phenotypes. While overall uptake efficiency was comparable, kinetic and imaging readouts indicated differences in intracellular handling across the nanoscale range (Figures 3A–C). Confocal microscopy revealed widespread cytoplasmic accumulation, and TEM provided ultrastructural evidence of vesicular sequestration. PS-C 30 nm showed fewer vesicles and a more diffuse fluorescence pattern, suggestive of a larger fraction of dispersed particles. In contrast, PS-C 50 and 100 nm were predominantly associated with abundant vesicular compartments, consistent with an endolysosomal processing route. Supporting this interpretation, endolysosomal involvement in the processing of PS-NPLs in this size range (≥50 nm) has been previously reported: in rat basophilic leukaemia (RBL-2H3) cells, PS-NPLs of 50 and 500 nm accumulated within lysosomes (Liu et al., 2021). Importantly, these cellular phenotypes aligned with the bioinformatic signatures. GO cellular component GSEA highlighted plasma membrane/cell-surface–associated structures in PS-C 30 nm and vacuolar/lysosomal compartments in PS-C 50 and 100 nm. Overall, this subcellular enrichment pattern, together with imaging readouts, suggests differential internalization routes and subsequent intracellular handling across conditions. These trafficking features provide a mechanistic basis for interpreting RNA-seq programs and contextualizing downstream functional outcomes, including cholesterol dysregulation.

3.5 Genotoxicity of PS-C-NPLs by the comet assay

The comet assay revealed genotoxic effects of PS-C-NPLs in HUVECs across multiple time points (Figure 4). After 2 h

10.3389/ftox.2026.1812922

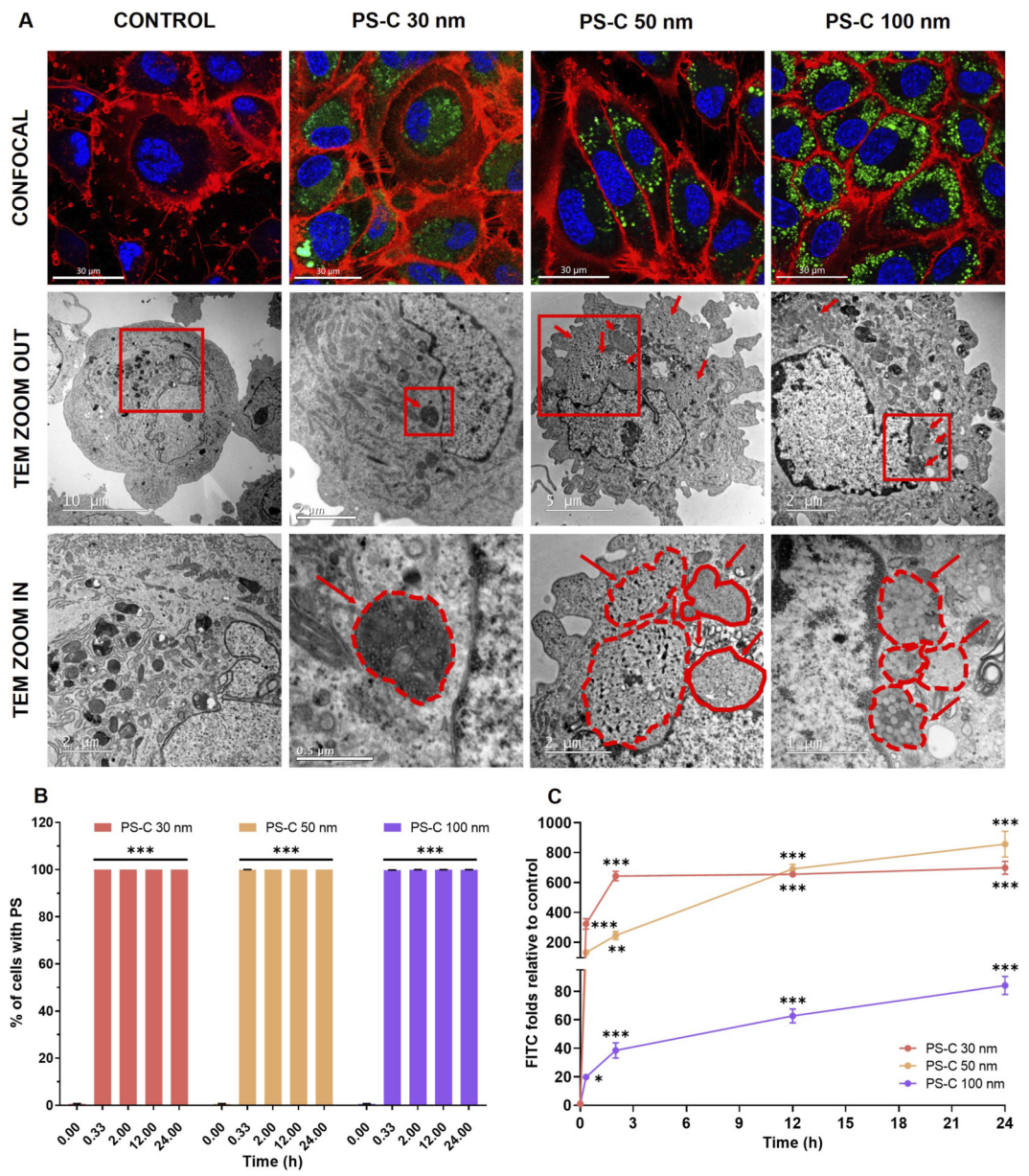


FIGURE 3
Internalization of PS-C-NPLs in HUVECs exposed to 100 μg/mL for 24 h. **(A)** Confocal microscopy shows labelled PS-C-NPLs (green), nuclei stained with Hoechst 33342 (blue), and cell membranes with CellMask™ (red). TEM images display vesicular structures containing PS-C-NPLs (red arrows), with magnified regions indicated by solid red squares and vesicle boundaries outlined by red dashed or continuous lines. **(B)** Flow cytometry quantification of the percentage of HUVECs internalizing PS-C-NPLs of 30, 50, and 100 nm. **(C)** Uptake kinetics represented as FITC fluorescence fold change vs. untreated controls at 20 min, 2 h, 12 h, and 24 h. Data are expressed as mean ± SEM. Statistical analysis was performed with one-way ANOVA with Dunnett's post-test (parametric data). $*p \leq 0.05$, $**p \leq 0.01$, $***p \leq 0.001$.

(Figure 4A), PS-C 100 nm significantly increased DNA strand breaks (40% above control), and PS-C 50 nm showed a similar trend (24% above control). At 24 h (Figure 4B), DNA damage was significantly increased only in the PS-C 30 nm condition (55% above control), indicating distinct temporal profiles across treatments. These data, together with the transcriptomic signatures previously described, suggest that PS-C-NPL exposure can elicit early DNA lesions and/or delayed genotoxic stress, with damage persistence reflecting the balance between lesion formation and activation of repair and cell-cycle control pathways.

The temporal profiles observed here are consistent with differential engagement of DNA repair and cell-cycle control responses. The early, transient increases observed for PS-C at 50/100 nm are consistent with activation of repair systems that resolve initial lesions (Roursgaard et al., 2022). In line with this interpretation, ORA and GSEA identified deregulation of UV response/DNA repair-related pathways for PS-C 50 and 100 nm ("UV response DN"), and ORA also detected "UV response UP" enrichment for PS-C 100 nm, suggesting a stronger induction of repair-associated transcriptional programs under this condition. In

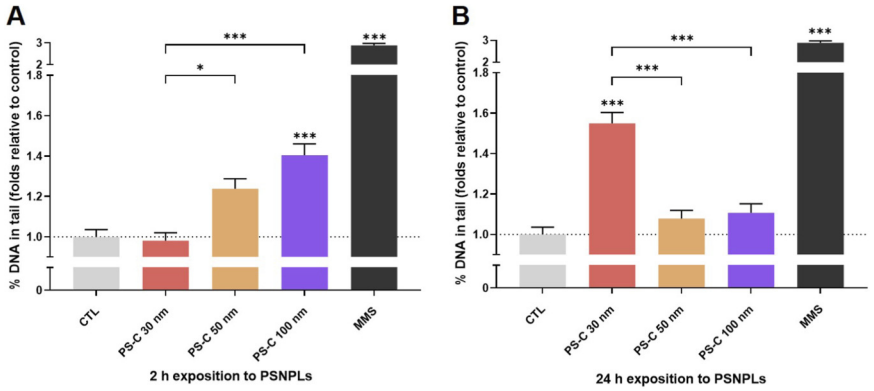


FIGURE 4
Genotoxic damage in HUVECs was assessed using the comet assay following 2-h **(A)** and 24-h **(B)** exposures to PS-C-NPLs at 100 μg/mL. MMS at 200 μM served as the positive control. Data are presented as mean ± SEM. Statistical analyses were performed using Kruskal–Wallis with Dunn's post-test (non-parametric data). Statistical significance is denoted as $*p \leq 0.05$, $**p \leq 0.01$, and $***p \leq 0.001$.

contrast, PS-C 30 nm showed less prominent enrichment of these repair-related signatures, while preferentially enriching cell-cycle and chromosome-associated pathways (E2F targets, G2M checkpoint; e.g., condensed chromosome, kinetochore). Together, these data support a mechanistic model in which PS-NPL exposure perturbs genome integrity and, depending on intracellular processing, can shift the response toward either repair-driven resolution or sustained stress coupled to cell-cycle dysregulation.

3.6 Intracellular cholesterol levels in HUVECs exposed to PS-C-NPLs by Filipin III staining

Filipin III staining revealed increased intracellular cholesterol accumulation in HUVECs treated with PS-C-NPLs compared to controls (Figures 5A,B). Quantification of 400 individual cells confirmed significant increases across treatments. The magnitude of accumulation differed between conditions (9% for PS-C 30 nm and 27%–28% for PS-C 50/100 nm). However, the directionality was consistent, supporting cholesterol dysregulation as a central functional phenotype of PS-NPL exposure. This observation was directly supported by transcriptomic data, in which cholesterol homeostasis emerged as one of the most significantly enriched hallmarks across conditions.

Animal studies in mice have previously shown that PS-NPLs of different sizes (80 and 200 nm) can disrupt lipid metabolism, increasing hepatic triglyceride and cholesterol accumulation (Fan et al., 2022; Yu et al., 2024), but effects on human cellular models have not yet been examined. Our results extend this knowledge, demonstrating that PS-C-NPLs induce intracellular cholesterol accumulation in HUVECs. This core response was corroborated by transcriptomic analyses, where ORA and GSEA identified cholesterol homeostasis as one of the most significantly dysregulated pathways across treatments. Interestingly, more than half of the genes within this pathway (Supplementary Figure S3A) were significantly altered, displaying a consistent upregulation pattern. Among the altered genes, *SREBF2* and its downstream effectors (*MVD*, *LDLR*, *HMGCR*) were upregulated (data not shown), suggesting that activation of cholesterol biosynthesis contributes to the observed accumulation (Fisher et al., 2021).

Additionally, qualitative analysis of Filipin III images also revealed differences in cholesterol localization. In control cells, cholesterol displayed a perinuclear distribution, reflecting synthesis in the endoplasmic reticulum (Lyu et al., 2017). In contrast, PS-C-treated cells exhibited cytoplasmic vesicular accumulation, particularly evident in the 50 and 100 nm groups. Similar accumulation patterns have been reported in HUVECs when cholesterol trafficking is blocked by inhibitors such as cepharanthine, resulting in late endolysosomal retention (Lyu et al., 2017). Supporting this, our cellular component GSEA identified lysosomal alterations in PS-C at 50 and 100 nm, corresponding to the treatments with the largest increases in cholesterol. Together, these findings indicate that PS-C-NPL internalization may interfere with lysosomal function, disrupting cholesterol trafficking and promoting intracellular accumulation.

Intracellular cholesterol accumulation in the endothelium is associated with endothelial dysfunction and early atherogenic events (Hassan et al., 2006; Baumer et al., 2017; Higashi, 2023). Reported consequences include cholesterol crystal formation, TNF-α–mediated apoptosis, cellular senescence, enhanced ROS production, and impaired vasodilation (Hassan et al., 2006; Baumer et al., 2017; Fisher et al., 2021; Ye et al., 2023; Ziegler et al., 2024). Importantly, alterations in cholesterol trafficking also influence membrane fluidity, intracellular transport, signaling, migration, and angiogenic capacity (Lyu et al., 2017). Based on the pronounced cytoplasmic accumulation observed here, we next assessed endothelial migration and angiogenesis, two key specialized functions of endothelial cells (Lee et al., 2021).

3.7 Migration of HUVECs exposed to PS-C-NPLs by wound healing assay

The wound healing assay showed that PS-C-NPL exposure remodelled HUVEC migratory behaviour (Figures 5C,D). At 8 h, PS-C 30 nm modestly increased wound closure (70.8% vs. 60.2% in controls), whereas PS-C 100 nm impaired migration (44.5%

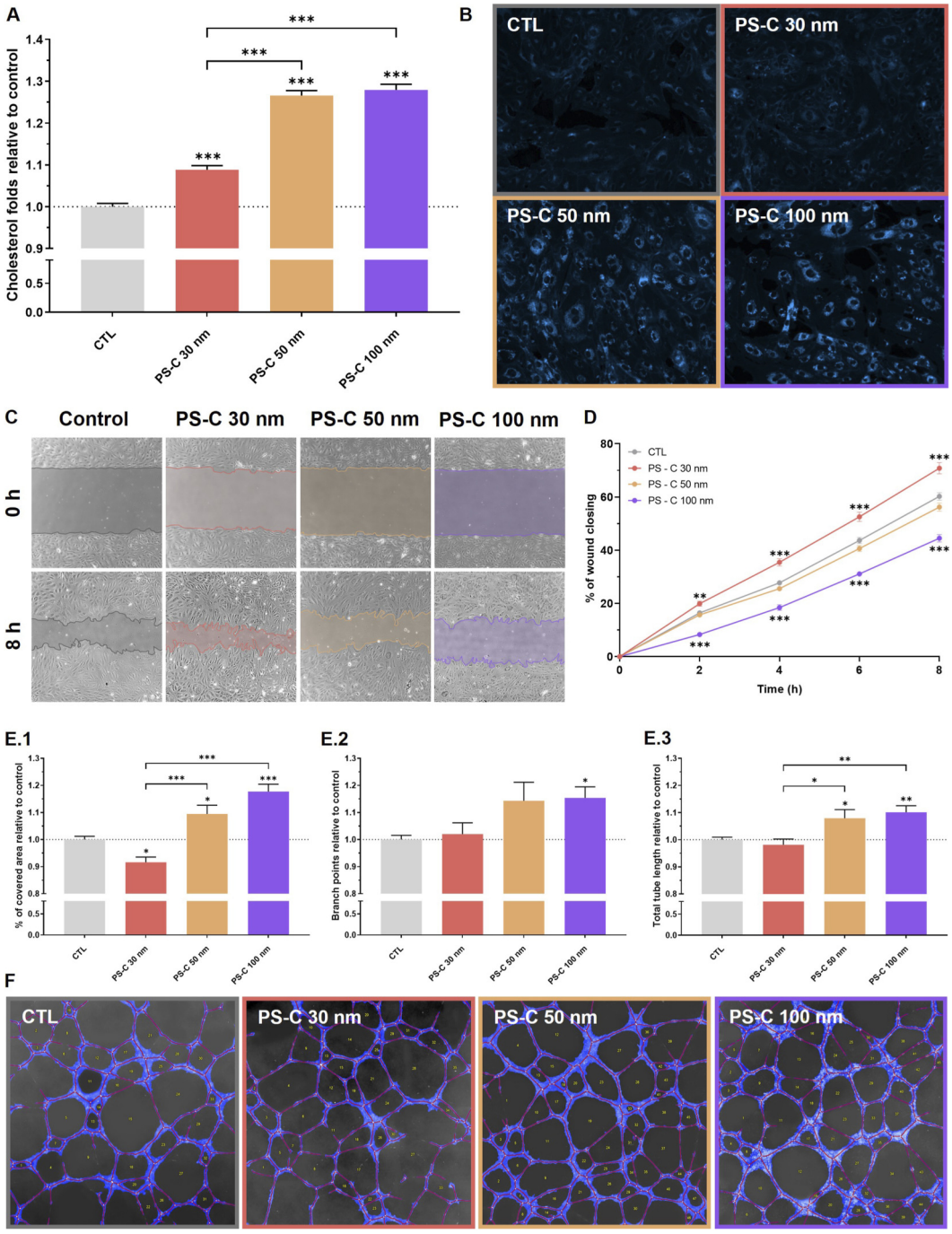


FIGURE 5
Effects of PS-C-NPLs on intracellular cholesterol, wound healing, and angiogenesis in HUVECs exposed to 100 μg/mL for 24 h. **(A,B)** Intracellular cholesterol: **(A)** Quantification of intracellular cholesterol levels after treatment with PS-C-NPLs. **(B)** Representative fluorescence microscopy images showing cholesterol staining with Filipin III in blue. **(C,D)** Wound healing assay: **(C)** Representative images showing wound closure at 0 and 8 h after treatment with PS-C-NPLs. **(D)** Quantification of wound closure dynamics (% of closure) over 8 h, measured at 2-h intervals. **(E,F)** Angiogenesis assay: **(E.1–3)** Quantitative analysis of angiogenesis potential, including **(E.1)** % of covered area relative to control, **(E.2)** number of branch points relative to control, and **(E.3)** total tube length relative to control. **(F)** Representative images of angiogenesis assays for each condition. Tubes are labelled in red, the covered area is highlighted in blue, and the number of loops is annotated within each loop, as analysed using Wimasis. Data are presented as mean ± SEM. Statistical analysis was performed using one-way ANOVA with Dunnett's or Tukey's post-tests for normally distributed data, and Kruskal–Wallis with Dunn's post-test for non-parametric data. Statistical significance is indicated as $*p \leq 0.05$, $**p \leq 0.01$, and $***p \leq 0.001$.

closure). PS-C 50 nm produced an intermediate effect that did not reach significance. These results indicate that nanoscale PS-NPL exposure can shift endothelial motility in different directions depending on the overall cellular response context.

Most studies have reported that MNPL exposure impairs cell migration across diverse models, including HUVECs, bronchial and alveolar epithelial cells, and trophoblasts, with PS-MNPLs (30–1,000 nm) reducing migratory capacity (Lee et al., 2021; Hu

et al., 2022; Wan et al., 2024; Lv et al., 2024). Moreover, abnormal cholesterol accumulation has been linked to reduced HUVEC migration (Lyu et al., 2017), consistent with our finding that PS-C at 100 nm induced the largest cholesterol increase and impaired migration. Nevertheless, enhanced migration has also been described in HUVECs following MNPL exposure. Traversa et al. (2024) reported that polyethylene MNPLs of 200 and 9,900 nm significantly increased migration, indicating that the stimulatory effect observed here for PS-C 30 nm is not unprecedented and may represent an alternative response of endothelial cells to NPL exposure.

Our transcriptomic data further corroborates these functional outcomes. Consistent with Traversa et al. (2024), who observed alterations of the EMT pathway in HUVECs after polyethylene exposure, our ORA and GSEA likewise identified EMT as significantly dysregulated across PS-C treatments. Activation of EMT-related transcriptomic programs is associated with increased motility and reduced adhesion (Chen et al., 2017), consistent with the wound-healing phenotypes observed here. However, it should be noted that these EMT signatures are based on pathway-level enrichment and have not been confirmed by gain or loss of canonical EMT protein markers (e.g., E-cadherin, N-cadherin, vimentin). The association between transcriptomic EMT enrichment and functional outcomes should therefore be considered correlative rather than evidence of a complete endothelial-to-mesenchymal transition. Interestingly, the heatmap of EMT-related genes (Supplementary Figure S3C) showed the strongest alterations in PS-C 100 nm, which displayed more dysregulated genes compared to PS-C 30 and 50 nm.

Migration is a critical endothelial function involved in vascular repair and homeostasis, and its disruption could contribute to early atherosclerotic events (Li et al., 2020). The migration phenotypes observed here are consistent with cholesterol-trafficking alterations that can impact adhesion and cytoskeletal dynamics, supporting PS-NPL–driven remodelling of endothelial motility.

3.8 Angiogenesis of HUVECs exposed to PS-C-NPLs by tube formation assay

In the tube formation assay, PS-C-NPL exposure altered vascular network formation (Figures 5E,F). PS-C 100 nm increased covered area, branch points, and total tube length relative to the control, and PS-C 50 nm produced a similar but generally smaller enhancement. In contrast, PS-C 30 nm reduced the covered area with limited effects on other parameters. These outcomes indicate that PS-NPL exposure can remodel angiogenic behaviour, consistent with the broad transcriptional reprogramming observed by RNA-seq.

Angiogenesis is a multifactorial process that depends not only on migration but also on proliferation, differentiation, extracellular matrix remodeling, and coordinated signaling (Flournoy et al., 2022). Accordingly, changes in migration and tube formation are not necessarily coupled. In our study, angiogenesis phenotypes were supported by transcriptomic alterations in EMT- and angiogenesis-related gene sets (Supplementary Figures S3B,C), reinforcing the notion that PS-NPL exposure can rewire endothelial programs that control vascular remodelling. Further mechanistic work will be required to identify the proximal drivers, but the multilayer concordance presented here provides a functional interpretation of the molecular signatures.

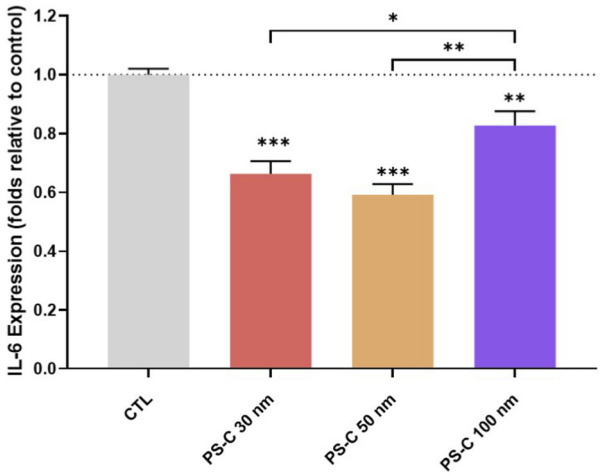


FIGURE 6
IL-6 expression in HUVECs exposed to PS-C-NPLs (100 μg/mL, 24 h). IL-6 levels were quantified after treatment and are shown as mean ± SEM. Statistical analysis was carried out using one-way ANOVA with Dunnett's and Tukey's post-test (parametric data). *$p \leq 0.05$, **$p \leq 0.01$, ***$p \leq 0.001$.

3.9 Evaluation of IL-6 expression in HUVECs after PS-C-NPL exposure

IL-6 secretion was significantly reduced in HUVECs following exposure to PS-C-NPLs (Figure 6). The decrease was most pronounced under PS-C 50 nm (41% reduction), followed by PS-C 30 nm (34%) and PS-C 100 nm (17%). Although the magnitude differed, the consistent downregulation of IL-6 indicates an immunomodulatory effect of PS-NPL exposure in this endothelial model. This functional phenotype was consistent with the transcriptomic signatures: ORA revealed dysregulation of IL2–STAT5 signaling across treatments, and GSEA supported enrichment for inflammatory response programs in PS-C at 50/100 nm. Together, these results support that PS-NPL exposure reshapes inflammatory signaling at the pathway level, with downstream consequences for cytokine output.

Beyond immunomodulation, several complementary mechanisms may contribute to the observed reduction in IL-6. Given the extensive vesicular accumulation and endolysosomal alterations observed in our study, particularly for PS-C 50 and 100 nm, the cellular secretory machinery may be physically or functionally impaired, thereby retaining IL-6 intracellularly. Additionally, protein corona formation on nanoplastics could sequester secreted IL-6, reducing its detection by ELISA. This is supported by recent evidence showing that microplastics efficiently adsorb functional proteins within their biocorona, impairing their biological availability (Brouwer et al., 2025). The observed reduction may therefore reflect both transcriptional reprogramming and physical sequestration of the cytokine.

Additionally, significant IL-6 dysregulation across all treatments provides mechanistic support for the observed alterations in HUVEC migration and angiogenesis, in line with extensive evidence linking IL-6 to endothelial motility and angiogenic regulation. IL-6 enhances inflammatory cell migration by promoting cell adhesion and inducing chemokine production (Suzuki et al., 2010). Furthermore, it plays a pivotal role in angiogenesis by regulating the expression of angiopoietins and VEGF, key mediators of blood vessel formation (Kayakabe et al., 2012). Beyond migration and angiogenesis, IL-6 modulates fundamental cellular functions in HUVECs, including proliferation and inflammation, thereby contributing to endothelial dysfunction. Specifically, IL-6 has been associated with the regulation of chemokines, such as MCP-1 and IL-8, and with the expression of adhesion molecules, such as ICAM-1 (Kang and Kishimoto, 2021). These factors facilitate monocyte infiltration and migration, marking a critical early step in the initiation and pathogenesis of atherosclerosis (Ohta et al., 2020). IL-6 has been linked to atherosclerosis pathogenesis through its ability to increase endothelial lipase expression via the p38 MAPK and NF-κB signaling pathways (Yue et al., 2016). Consistent with this role, our transcriptomic analyses identified enrichment of the WikiPathways "Fluid Shear Stress and Atherosclerosis" and "Lipid and Atherosclerosis" pathways (data not shown). This molecular evidence parallels recent clinical findings from Marfella et al. (2024), who demonstrated that the presence of MNPLs in human carotid plaques was associated with a significantly increased risk of cardiovascular events, including myocardial infarction, stroke, and all-cause mortality.

4 Conclusion

This study provides a comprehensive evaluation of the endothelial effects of carboxylated polystyrene nanoplastics (PS-C-NPLs) in primary HUVECs, using an integrated design that couples transcriptomics with phenotypic endpoints. By combining RNA-seq bioinformatics (DEG, ORA, and GSEA) with particle-uptake imaging and functional assays, we move beyond descriptive screening to link pathway-level alterations with measurable changes in endothelial homeostasis.

Across treatments, HUVECs rapidly internalized PS-C-NPLs and exhibited extensive intracellular accumulation. Transcriptomic analyses revealed a dominant core program characterized by dysregulation of cholesterol homeostasis, inflammatory and stress signaling, endothelial plasticity (EMT), and genome integrity pathways. Guided by these molecular signatures, functional assays confirmed intracellular cholesterol accumulation, DNA damage, changes in migratory capacity and angiogenic behaviour, and reduced IL-6 secretion. The concordance between RNA-seq-derived pathways and functional readouts supports a mechanistic framework in which PS-NPL exposure rewires endothelial metabolic and stress-response networks with downstream consequences for vascular function.

These findings highlight the potential for PS-NPL exposure to contribute to endothelial dysfunction, a key early event in vascular pathology. More broadly, the study demonstrates the value of bioinformatics as a mechanistic layer: transcriptomic programs were not merely catalogued but used to guide, interpret, and contextualize functional outcomes. While nanoscale differences modulated specific response features, the shared molecular core response provides a coherent basis for understanding PS-NPL-driven endothelial disruption and for prioritizing mechanistically anchored endpoints in future hazard assessment.

To extend this work, future studies should prioritize dose–response characterization at lower, environmentally realistic concentrations to establish quantitative thresholds for the molecular and functional endpoints identified here. Additional priorities include exploring other polymers such as polyethylene terephthalate or polylactic acid and employing more advanced experimental models, including endothelial barriers or tissue-engineered vessels. Such efforts may help refine our understanding of nanoplastic toxicity and its cardiovascular implications.

Data availability statement

The original contributions presented in the study are publicly available. This data can be found at Gene Expression Omnibus with the accession number GSE324731.

Ethics statement

Ethical approval was not required for the studies on humans in accordance with the local legislation and institutional requirements because only commercially available established cell lines were used.

Author contributions

JM-P: Writing – original draft, Investigation. AV: Methodology, Writing – review and editing, Investigation. JG-G: Investigation, Writing – review and editing, Methodology. RE: Writing – review and editing, Formal Analysis, Methodology. MM-R: Investigation, Writing – review and editing. MC-C: Writing – review and editing, Investigation. IB: Investigation, Supervision, Writing – review and editing. RM: Supervision, Conceptualization, Writing – review and editing. AH: Conceptualization, Supervision, Writing – review and editing, Resources. AG-R: Writing – review and editing, Conceptualization, Supervision.

Funding

The author(s) declared that financial support was received for this work and/or its publication. JM-P, MM-R, and JG-G hold Ph.D. fellowships from the Generalitat de Catalunya and UAB. AV was supported by a Ph.D. fellowship from the National Agency for Research and Development (ANID), CONICYT PFCHA/DOCTORADO BECAS CHILE/2020 -72210237. AG-R (Academic record 2020 BP 00177) and IB (Academic record 2023-BP-00212) were granted with a Beatriu de Pinós Postdoctoral Program from the Secretariat of Universities and Research of the Department of Business and Knowledge of the Government of Catalunya. AH is supported by the ICREA ACADEMIA Programme. The PlasticHeal project has received

funding from the European Union's Horizon 2020 research and innovation programme under grant agreement No 965196. This study was supported by the Spanish Ministry of Science and Innovation (PID2020-116789RB-C43) and the Generalitat de Catalunya (2021-SGR-00731).

Conflict of interest

The author(s) declared that this work was conducted in the absence of any commercial or financial relationships that could be construed as a potential conflict of interest.

Generative AI statement

The author(s) declared that generative AI was not used in the creation of this manuscript.

Any alternative text (alt text) provided alongside figures in this article has been generated by Frontiers with the support of artificial intelligence and reasonable efforts have been made to ensure accuracy, including review by the authors wherever possible. If you identify any issues, please contact us.

Publisher's note

All claims expressed in this article are solely those of the authors and do not necessarily represent those of their affiliated organizations, or those of the publisher, the editors and the reviewers. Any product that may be evaluated in this article, or claim that may be made by its manufacturer, is not guaranteed or endorsed by the publisher.

Supplementary material

The Supplementary Material for this article can be found online at: https://www.frontiersin.org/articles/10.3389/ftox.2026.1812922/full#supplementary-material

References

Ali, N., Katsouli, J., Marczylo, E. L., Gant, T. W., Wright, S., and Bernardino de la Serna, J. (2024). The potential impacts of micro- and nano-plastics on various organ systems in humans. *eBioMed* 99, 104901. doi:10.1016/j.ebiom.2023.104901

Annangi, B., Bach, J., Vales, G., Rubio, L., Marcos, R., and Hernández, A. (2015). Long-term exposures to low doses of cobalt nanoparticles induce cell transformation enhanced by oxidative damage. *Nanotoxicology* 9 (2), 138–147. doi:10.3109/17435390.2014.900582

Banerjee, A., Billey, L., and Shelver, W. (2021). Uptake and toxicity of polystyrene micro/nanoplastics in gastric cells: effects of particle size and surface functionalization. *PLoS One* 16 (12), e0260803. doi:10.1371/journal.pone.0260803

Baumer, Y., Mccurdy, S., Weatherby, T., Mehta, N., Halbherr, S., Halbherr, P., et al. (2017). Hyperlipidemia-induced cholesterol crystal production by endothelial cells promotes atherogenesis. *Nat. Comm.* 8 (1), 1129. doi:10.1038/s41467-017-01186-z

Brouwer, H., Busch, M., Yang, S., Venus, T., Aalderink, G., Ferrer Crespo, J. F., et al. (2025). Toxicity of true-to-life microplastics to human iPSC-derived intestinal epithelia correlates to their protein corona composition. *J. Hazard Mater* 495, 138908. doi:10.1016/j.jhazmat.2025.138908

Cao, Y., Gong, Y., Liu, L., Zhou, Y., Fang, X., Zhang, C., et al. (2017). The use of human umbilical vein endothelial cells (HUVECs) as an *in vitro* model to assess the toxicity of nanoparticles to endothelium: a review. *J. Appl. Toxicol.* 37 (12), 1359–1369. doi:10.1002/jat.3470

Carlson, M. (2023). org.Hs.eg.db: genome wide annotation for human (R package version 3.18.0). Available online at: https://CRAN.R-project.org/package=org.Hs.eg.db (Accessed February 12, 2026).

Chen, T., You, Y., Jiang, H., and Wang, Z. (2017). Epithelial–mesenchymal transition (EMT): a biological process in the development, stem cell differentiation, and tumorigenesis. *J. Cell Physiol.* 232, 3261–3272. doi:10.1002/jcp.25797

Chen, Y., Chen, L., Lun, A. T. L., Baldoni, P., and Smyth, G. K. (2024). edgeR 4.0: powerful differential analysis of sequencing data with expanded functionality and improved support for small counts and larger datasets. *bioRxiv*. doi:10.1101/2024.01.21.576131

Collins, A., Møller, P., Gajski, G., Vodenková, S., Abdulwahed, A., Anderson, D., et al. (2023). Measuring DNA modifications with the comet assay: a compendium of protocols. *Nat. Protoc.* 18 (3), 929–989. doi:10.1038/s41596-022-00754-y

da Silva, J., Jesus, S., Bernardi, N., Colaço, M., and Borges, O. (2019). Poly(D,L-lactic acid) nanoparticle size reduction increases its immunotoxicity. *Front. Bioeng. Biotechnol.* 7, 137. doi:10.3389/FBIOE.2019.00137

Dolgalev, I. (2022). Msigdbr: msigdb gene sets for multiple organisms in a tidy data format (R package version 7.5.1). Available online at: https://CRAN.R-project.org/package=msigdbr (Accessed February 12, 2026).

Domenech, J., and Marcos, R. (2021). Pathways of human exposure to microplastics, and estimation of the total burden. *Curr. Opin. Food Sci.* 39, 144–151. doi:10.1016/j.cofs.2021.01.004

Domenech, J., Hernández, A., Rubio, L., Marcos, R., and Cortés, C. (2020). Interactions of polystyrene nanoplastics with *in vitro* models of the human intestinal barrier. *Arch. Toxicol.* 94, 2997–3012. doi:10.1007/s00204-020-02805-3

Facciolà, A., Visalli, G., Ciarello, M., and Di Pietro, A. (2021). Newly emerging airborne pollutants: current knowledge of health impact of micro and nanoplastics. *Int. J. Environ. Res. Publ. Health* 18 (6), 2997. doi:10.3390/ijerph18062997

Fan, X., Wei, X., Hu, H., Zhang, B., Yang, D., Du, H., et al. (2022). Effects of oral administration of polystyrene nanoplastics on plasma glucose metabolism in mice. *Chemosphere* 288 (Pt3), 132607. doi:10.1016/j.chemosphere.2021.132607

Fisher, A., Srole, D., Palaskas, N., Meriwether, D., Reddy, S., Ganz, T., et al. (2021). Iron loading induces cholesterol synthesis and sensitizes endothelial cells to TNFα-mediated apoptosis. *J. Biol. Chem.* 297 (4), 101156. doi:10.1016/j.jbc.2021.101156

Flournoy, J., Ashkanani, S., and Chen, Y. (2022). Mechanical regulation of signal transduction in angiogenesis. *Front. Cell Dev. Biol.* 10, 933474. doi:10.3389/fcell.2022.933474

Gu, Z. (2022). Complex heatmap visualization. *iMeta* 1 (1), 43. doi:10.1002/imt2.43

Hassan, H., Denis, M., Krimbou, L., Marcil, M., and Genest, J. (2006). Cellular cholesterol homeostasis in vascular endothelial cells. *Can. J. Cardiol.* 22 (Suppl. B), 35B–40B. doi:10.1016/S0828-282X(06)70985-0

Higashi, Y. (2023). Endothelial function in dyslipidemia: roles of LDL-cholesterol, HDL-cholesterol and triglycerides. *Cells* 12 (9), 1293. doi:10.3390/cells12091293

Hong, Y. (2023). Study on the maximum level of disposable plastic product waste. *Sustainability* 15 (12), 9360. doi:10.3390/su15129360

Hu, J., Zhu, Y., Zhang, J., Xu, Y., Wu, J., Zeng, W., et al. (2022). The potential toxicity of polystyrene nanoplastics to human trophoblasts *in vitro*. *Environ. Pollut.* 311, 119924. doi:10.1016/j.envpol.2022.119924

Kang, S., and Kishimoto, T. (2021). Interplay between interleukin-6 signaling and the vascular endothelium in cytokine storms. *Exp. Mol. Med.* 53, 1116–1123. doi:10.1038/s12276-021-00649-0

Kayakabe, K., Kuroiwa, T., Sakurai, N., Ikeuchi, H., Kadiombo, A., Sakairi, T., et al. (2012). Interleukin-6 promotes destabilized angiogenesis by modulating angiopoietin expression in rheumatoid arthritis. *Rheumatology* 51 (9), 1571–1579. doi:10.1093/rheumatology/kes093

Larsson, J. (2024). Eulerr: area-Proportional Euler and venn diagrams with ellipses (R package version 7.0.2). Available online at: https://CRAN.R-project.org/package=eulerr (Accessed February 12, 2026).

Law, C. W., Chen, Y., Shi, W., and Smyth, G. K. (2014). Voom: precision weights unlock linear model analysis tools for RNA-seq read counts. *Genome Biol.* 15 (2), R29. doi:10.1186/gb-2014-15-2-r29

Law, C. W., Alhamdoosh, M., Su, S., Dong, X., Tian, L., Smyth, G. K., et al. (2016). RNA-seq analysis is easy as 1-2-3 with limma, Glimma and edgeR. *F1000Research* 5, 1408. ISCB Comm J-1408. doi:10.12688/f1000research.9005.3

Lee, H., Amarakoon, D., Wei, C., Choi, K., Smolensky, D., and Lee, S. (2021). Adverse effect of polystyrene microplastics (PS-MPs) on tube formation and viability of human umbilical vein endothelial cells. *Food Chem. Toxicol.* 154, 112356. doi:10.1016/j.fct.2021.112356

Leek, J. T., Johnson, W. E., Parker, H. S., Fertig, E. J., Jaffe, A. E., Zhang, Y., et al. (2023). *Sva: surrogate Variable Analysis (R package version 3.50.0)*. doi:10.18129/B9.bioc.sva

Lehner, R., Weder, C., Petri-Fink, A., and Rothen-Rutishauser, B. (2019). Emergence of nanoplastic in the environment and possible impact on human health. *Environ. Sci. Technol.* 53 (4), 1748–1765. doi:10.1021/acs.est.8b05512

Leslie, H. A., van Velzen, M. J. M., Brandsma, S. H., Vethaak, A. D., Garcia-Vallejo, J. J., and Lamoree, M. H. (2022). Discovery and quantification of plastic particle pollution in human blood. *Environ. Int.* 163, 107199. doi:10.1016/j.envint.2022.107199

Li, H., Liu, S., Hu, Y., Zhao, B., Sun, Y., and Xu, D. (2020). Endosulfan promotes cell migration *via* PTP4A3-mediated signaling pathways in HUVECs. *Ecotoxicol. Environ. Saft* 192, 110267. doi:10.1016/j.ecoenv.2020.110267

Liao, Y., Smyth, G. K., and Shi, W. (2019). The R package Rsubread is easier, faster, cheaper, and better for alignment and quantification of RNA sequencing reads. *Nucleic Acids Res.* 47 (8), e47. doi:10.1093/nar/gkz114

Liu, L., Xu, K., Zhang, B., Ye, Y., Zhang, Q., and Jiang, W. (2021). Cellular internalization and release of polystyrene microplastics and nanoplastics. *Sci. Total Environ.* 779, 146523. doi:10.1016/J.SCITOTENV.2021.146523

Lu, Y. Y., Li, H., Ren, H., Zhang, X., Huang, F., Zhang, D., et al. (2022). Size-dependent effects of polystyrene nanoplastics on autophagy response in human umbilical vein endothelial cells. *J. Hazard Mater* 421, 126770. doi:10.1016/j.jhazmat.2021.126770

Lv, J., He, Q., Yan, Z., Xie, Y., Wu, Y., Li, A., et al. (2024). Inhibitory impact of prenatal exposure to nano-polystyrene particles on the MAP2K6/p38 MAPK axis inducing embryonic developmental abnormalities in mice. *Toxics* 12 (5), 370. doi:10.3390/toxics12050370

Lyu, J., Yang, E., Head, S., Ai, N., Zhang, B., Wu, C., et al. (2017). Pharmacological blockade of cholesterol trafficking by cepharanthine in endothelial cells suppresses angiogenesis and tumor growth. *Cancer Lett.* 409, 91–103. doi:10.1016/j.canlet.2017.09.009

Marfella, R., Prattichizzo, F., Sardu, C., Fulgenzi, G., Graciotti, L., Spadoni, T., et al. (2024). Microplastics and nanoplastics in atheromas and cardiovascular events. *N. Engl. J. Med.* 390 (10), 900–910. doi:10.1056/nejmoa2309822

Martín-Pérez, J., Villacorta, A., Banaei, G., Morataya-Reyes, M., Tavakolpournegari, A., Marcos, R., et al. (2024). Hazard assessment of nanoplastics is driven by their surface-functionalization. Effects in human-derived primary endothelial cells. *Sci. Total Environ.* 934, 173236. doi:10.1016/j.scitotenv.2024.173236

O'Neill, S., and Lawler, J. (2021). Knowledge gaps on micro and nanoplastics and human health: a critical review. *Case Stud. Chem. Environ. Eng.* 3, 10091. doi:10.1016/J.CSCEE.2021.100091

Ohta, M., Kihara, T., Toriuchi, K., Aoki, H., Iwaki, S., Kakita, H., et al. (2020). IL-6 promotes cell adhesion in human endothelial cells *via* microRNA-126-3p suppression. *Exp. Cell Res.* 393 (2), 112094. doi:10.1016/j.yexcr.2020.112094

Oliveira, J., Belchior, A., Da Silva, V., Rotter, A., Petrovski, Ž., Almeida, P., et al. (2020). Marine environmental plastic pollution: mitigation by microorganism degradation and recycling valorization. *Front. Mar. Sci.* 7, 567126. doi:10.3389/fmars.2020.567126

Paget, V., Dekali, S., Kortulewski, T., Grall, R., Gamez, C., Blazy, K., et al. (2015). Specific uptake and genotoxicity induced by polystyrene nanobeads with distinct surface chemistry on human lung epithelial cells and macrophages. *PLoS One* 10 (4), e0123297. doi:10.1371/journal.pone.0123297

Posit Team (2023). *RStudio: integrated development environment for R. Posit software*. PBC. Available online at: https://www.posit.co/ (Accessed February 12, 2026).

R Core Team (2023). *R: a language and environment for statistical computing*. R Foundation for Statistical Computing. Available online at: https://www.r-project.org/ (Accessed February 12, 2026).

Rajendran, D., and Chandrasekaran, N. (2023). Journey of micronanoplastics with blood components. *RSC Adv.* 13 (45), 31435–31459. doi:10.1039/d3ra05620a

Ritchie, M. E., Phipson, B., Wu, D., Hu, Y., Law, C. W., Shi, W., et al. (2015). Limma powers differential expression analyses for RNA-sequencing and microarray studies. *Nucleic Acids Res.* 43 (7), e47. doi:10.1093/nar/gkv007

Rodrigues, A., De Jesus, G., Waked, D., Gomes, G., Silva, T., Yariwake, V., et al. (2022). Scientific evidence about the risks of micro and nanoplastics (MNPLs) to human health and their exposure routes through the environment. *Toxics* 10 (6), 308. doi:10.3390/toxics10060308

Roursgaard, M., Rothmann, M., Schulte, J., Karadimou, I., Marinelli, E., and Møller, P. (2022). Genotoxicity of particles from grinded plastic items in Caco-2 and HepG2 cells. *Front. Publ. Health* 10, 906430. doi:10.3389/fpubh.2022.906430

Rubio, L., Marcos, R., and Hernández, A. (2020). Potential adverse health effects of ingested micro- and nanoplastics on humans. Lessons learned from *in vivo* and *in vitro* mammalian models. *J. Toxicol. Environ. Health Pb.* 23 (2), 51–68. doi:10.1080/10937404.2019.1700598

Santos, D., Varela, J., Lynch, I., Salvati, A., and Dawson, K. (2011). Effects of transport inhibitors on the cellular uptake of carboxylated polystyrene nanoparticles in different cell lines. *PLoS One* 6 (9), e24438. doi:10.1371/journal.pone.0024438

Shen, M., Huang, W., Chen, M., Song, B., Zeng, G., and Zhang, Y. (2020). (Micro)plastic crisis: Un-ignorable contribution to global greenhouse gas emissions and climate change. *J. Clean. Prod.* 254, 120138. doi:10.1016/j.jclepro.2020.120138

Suarez-Arnedo, A., Torres Figueroa, F., Clavijo, C., Arbeláez, P., Cruz, J. C., and Muñoz-Camargo, C. (2020). An image J plugin for the high throughput image analysis of *in vitro* scratch wound healing assays. *PLOS One* 15 (7), e0232565. doi:10.1371/journal.pone.0232565

Suzuki, M., Hashizume, M., Yoshida, H., and Mihara, M. (2010). Anti-inflammatory mechanism of tocilizumab, a humanized anti-IL-6R antibody: effect on the expression of chemokine and adhesion molecule. *Rheumatol. Int.* 30, 309–315. doi:10.1007/s00296-009-0953-0

Traversa, A., Mari, E., Pontecorvi, P., Gerini, G., Romano, E., Megiorni, F., et al. (2024). Polyethylene micro/nanoplastics exposure induces epithelial–mesenchymal transition in human bronchial and alveolar epithelial cells. *Int. J. Mol. Sci.* 25 (18), 10168. doi:10.3390/ijms251810168

Wan, S., Wang, X., Chen, W., Xu, Z., Zhao, J., Huang, W., et al. (2024). Polystyrene nanoplastics activate autophagy and suppress trophoblast cell migration/invasion and migrasome formation to induce miscarriage. *ACS Nano* 18 (4), 3733–3751. doi:10.1021/acsnano.3c11734

Wang, W., and Carroll, T. (2024). Rfastp: an ultra-fast and all-in-one fastq preprocessor (quality control, adapter, low quality, and polyX trimming) and UMI sequence parsing (Version 1.14.0) [R package]. Available online at: https://CRAN.R-project.org/package=Rfastp (Accessed February 12, 2026).

Wickham, H. (2016). *ggplot2: elegant graphics for data analysis*. New York: Springer-Verlag.

Wu, T., Hu, E., Xu, S., Chen, M., Guo, P., Dai, Z., et al. (2021). clusterProfiler 4.0: a universal enrichment tool for interpreting omics data. *Innovation* 2 (3), 100141. doi:10.1016/j.xinn.2021.100141

Ye, H., Liu, Q., Wang, Y., Zhen, X., and Yan, N. (2023). The effect of cholesterol efflux on endothelial dysfunction caused by oxidative stress. *Int. J. Mol. Sci.* 24 (6), 5939. doi:10.3390/ijms24065939

Yu, Z., Fan, X., Zhao, X., He, T., Li, X., Du, H., et al. (2024). Polystyrene nanoplastics induce lipid metabolism disorder by activating the PERK-ATF4 signaling pathway in mice. *ACS Appl. Mater Interf.* 16 (27), 34524–34537. doi:10.1021/acsami.4c04416

Yue, X., Wu, M., Jiang, H., Hao, J., Zhao, Q., Zhu, Q., et al. (2016). Endothelial lipase is upregulated by interleukin-6 partly *via* the p38 MAPK and p65 NF-κB signaling pathways. *Mol. Med. Rep.* 14, 1979–1985. doi:10.3892/mmr.2016.5457

Ziegler, D., Czarnecka-Herok, J., Vernier, M., Scholtes, C., Camprubi, C., Huna, A., et al. (2024). Cholesterol biosynthetic pathway induces cellular senescence through ERRα. *NPJ Aging.* 10 (1), 5. doi:10.1038/s41514-023-00128-y

3.3. Chapter 3 (Paper 3)

Real-life nanoplastics induce endothelial dysfunction in primary human endothelial cells.

Archives of Toxicology. (2026)

DOI: 10.1007/s00204-026-04417-9

Impact Factor: 6.9 (2024)

Archives of Toxicology
https://doi.org/10.1007/s00204-026-04417-9

NANOTOXICOLOGY

Real-life nanoplastics induce endothelial dysfunction in primary human endothelial cells

Joan Martín-Pérez[1] · Michelle Morataya-Reyes[1] · Aliro Villacorta[1,2] · Claudia Anguita-Solé[1] · Juan Francisco Ferrer[3] · Irene Barguilla[1] · Mohamed Alaraby[1,4] · Ricard Marcos[1] · Alba Hernández[1] · Alba García-Rodríguez[1]

Received: 5 December 2025 / Accepted: 9 April 2026
© The Author(s) 2026

Abstract

Understanding how nanoplastics (NPLs) exposure affects vascular endothelium is essential for determining their potential cardiovascular risk. To this end, four different NPLs of similar nominal sizes (about 200 nm), but different environmental relevance, have been used. They are: (i) spherical and monodisperse pristine polystyrene (PS), (ii) biodegradable polylactic acid (PLA), (iii) moderately irregular and polydisperse polytetrafluoroethylene (PTFE), and (iv) highly irregular and polydisperse polyethylene terephthalate (PET) derived from post-consumer bottles. To determine their hazardous risk, primary human umbilical vein endothelial cells (HUVECs) were used as a physiologically relevant model of the vascular endothelium. Results show that all NPLs were internalized by HUVECs, although uptake efficiency and intracellular distribution varied among polymers. None of the NPLs induced cytotoxicity or DNA damage at 25 µg/mL for 24 h. However, PTFE- and PET-NPLs elicited functional alterations consistent with endothelial dysfunction. PET-NPLs triggered IL-6 secretion and intracellular cholesterol accumulation, while both PTFE- and PET-NPLs significantly impaired cell migration, reducing wound closure. These findings reveal a clear gradient of biological impact, with irregular NPLs inducing stronger endothelial stress responses. By linking morphological realism to vascular inflammation, cholesterol dysregulation, and impaired migration, this study underscores the relevance of environmentally realistic NPLs into human health risk assessment frameworks.

Keywords Polystyrene · Polylactic acid · Polytetrafluoroethylene · Polyethylene terephthalate · Primary human umbilical vein endothelial cells

Introduction

Plastics are synthetic organic polymers primarily derived from petroleum or other hydrocarbon sources, with some biodegradable variants produced from renewable resources such as cellulose or cornstarch (Nayanathara Thathsarani Pilapitiya and Ratnayake 2024). Their durability, lightweight, cost-effectiveness, and excellent barrier properties have driven their widespread use across numerous sectors, including the food industry (Ncube et al. 2021). In this context, plastics are employed in applications ranging from beverage bottles and packaging films to non-stick cookware and biodegradable tableware. During use, these materials can degrade through various physicochemical processes, such as mechanical abrasion, thermal stress, or prolonged contact with food and beverages, resulting in the environment release of microplastics (<1 mm) and nanoplastics

✉ Alba Hernández
alba.hernandez@uab.cat

✉ Alba García-Rodríguez
alba.garcia.rodriguez@uab.cat

1 Group of Mutagenesis, Department of Genetics and Microbiology, Faculty of Biosciences, Universitat Autònoma de Barcelona, Campus of Bellaterra, 08193 Cerdanyola del Vallès, Barcelona, Spain

2 Facultad de Recursos Naturales Renovables, Universidad Arturo Prat, Iquique, Chile

3 Plastics Technology Center, AIMPLAS, Valencia Parc Tecnològic, 46980 Paterna, Spain

4 Zoology Department, Faculty of Science, Sohag University, Sohag 82524, Egypt

Published online: 05 May 2026

(< 1 µm), collectively referred to as micro- and nanoplastics (MNPLs).

In the environment, MNPLs enter the food web (Hussain et al. 2023), as documented for several polymer types, including polystyrene (PS) from disposable food containers and packaging, polylactic acid (PLA) from biodegradable packaging and teabags (Banaei et al. 2023), polytetrafluoroethylene (PTFE) from non-stick cookware (Cole et al. 2024), and polyethylene terephthalate (PET) from water bottles (Hussain et al. 2023). Once in the food chain, MNPLs can enter the human body primarily through ingestion, cross the intestinal barrier, and distribute to various tissues via systemic circulation (Rajendran and Chandrasekaran 2023). This is particularly relevant for nanoplastics, whose nanometric size allows for more efficient uptake and translocation across biological barriers, facilitating their biodistribution (Jahedi and Jaafarzadeh Haghighi Fard 2025). The ability of different MNPLs (such as those composed of PS, PLA, PTFE, and PET) to traverse biological barriers, including the intestinal barrier, has been demonstrated in several experimental models, suggesting their potential to reach the bloodstream (Alaraby et al. 2024; Landrigan et al. 2025). Despite the technical challenges associated with detecting MNPLs in complex biological matrices such as blood, Leslie et al. (2022) successfully identified PS- and PET-based MNPLs in human blood samples, providing direct evidence of systemic exposure. Once in circulation, MNPLs can interact with endothelial cells (ECs), which form the inner lining of blood vessels. ECs are key regulators of vascular homeostasis, controlling permeability, inflammatory signaling, and angiogenesis, and their dysfunction is strongly associated with the development of cardiovascular diseases (Xue et al. 2023). Several studies have reported associations between the presence of MNPLs in humans and adverse cardiovascular outcomes, suggesting a potential link between MNPL exposure and cardiovascular disease risk (Zhang et al. 2025; Prattichizzo et al. 2024). In this context, the interaction between MNPLs and endothelial cells may represent a key event underlying the development of such adverse cardiovascular effects.

In in vitro studies, human umbilical vein endothelial cells (HUVECs) are widely used as a physiologically relevant model, as they are primary human ECs derived from the umbilical vein and closely reproduce the structural and functional characteristics of the vascular endothelium (Cao et al. 2017). Studies using HUVECs have shown that PS-NPLs can induce a wide range of adverse effects, often modulated by particle charge and size. Reported impacts include reduced cell viability, increased production of reactive oxygen species (ROS), mitochondrial dysfunction, impaired autophagy, and activation of inflammatory pathways (Fu et al. 2022; Lu et al. 2022; Ahamed and Javed Akhtar 2024; Martín-Pérez et al. 2024).

Unfortunately, most research on the vascular effects of NPLs has focused on commercially available PS-NPL, mainly due to the limited availability of MNPL test materials (Drzewinska and Belz 2024). These pristine PS-NPL, are spherical, monodisperse, and chemically uniform, which facilitate experimental reproducibility; nevertheless, they fail to capture the diversity of morphologies, colloidal behaviors and surface chemistries present in the environmental MNPLs (Ma et al. 2024). Consequently, establishing links between MNPL exposure, endothelial responses, and downstream cardiovascular effects remains difficult without studies employing test materials that more closely mimic those found in real-life scenarios. To address this gap, the present study compares the biological effects of four different NPLs test materials (PS-NPLs, PLA-NPLs, PTFE-NPLs, and PET-NPLs) of approximately similar size (about 200 nm) to minimize size-related variability. Thus, PS-NPLs and PLA-NPLs present regular and spherical shapes; PTFE-NPLs exhibit moderate irregularity; and PET-NPLs were produced in-house from post-consumer water bottles, generating irregular, polydisperse particles that better resemble environmentally weathered plastics (Villacorta et al. 2022). With such four NPL types, internalization kinetics and multiple biological effects (including cytotoxicity and apoptosis, genotoxicity, inflammation, intracellular cholesterol accumulation, and cell migration) was investigated and comparatively assessed under standardized exposure conditions in HUVECs. By combining both commercially available and environmentally realistic NPLs within a controlled experimental framework, and using a low concentration, this work provides new insights into how polymer chemistry, particle morphology, and colloidal behavior influence endothelial cell responses, thereby contributing to a better understanding of the potential cardiovascular risks associated with NPL exposure.

Materials and methods

Sources and labeling of the selected NPLs

NPLs of around 200 nm were obtained from different sources. Polystyrene nanoplastics (PS-NPLs; PP-015-10, nominal size 0.19 µm) were purchased as an aqueous suspension from Spherotech Inc. (Lake Forest, IL, USA). Polylactic acid nanoplastics (PLA-NPLs; PRO20-0103-80) were produced by AIMPLAS (Valencia, Spain) in the frame of the EU project PlasticHeal, following the protocol previously described (Alaraby et al. 2024). Polytetrafluoroethylene nanoplastics (PTFE-NPLs; 430935-5G, nominal size

1 µm) in powder form were purchased from Sigma-Aldrich (St. Louis, MO, USA) and dispersed in Milli-Q water. Polyethylene terephthalate nanoplastics (PET-NPLs) were prepared in-house from commercial water bottles (Villacorta et al. 2022). Briefly, PET fragments from commercial water bottles were mechanically sanded using a diamond rotary burr to avoid metal contamination. The resulting debris was sieved (<0.20 mm) and chemically dispersed in trifluoroacetic acid (TFA) at 50 °C under continuous stirring. After centrifugation, the pellet was resuspended in 0.5% sodium dodecyl sulfate (SDS) and subjected to ultrasonication. Following 1 h of sedimentation to remove larger particles, the upper fraction was collected, extensively washed (Milli-Q water and ethanol) to eliminate SDS residues, and resuspended in Milli-Q water. Finally, the suspension was sonicated, aliquoted, snap-frozen in liquid nitrogen, and stored at -80 °C. All NPLs were dispersed using the NanoGenotox protocol (Jensen et al. 2009). For internalization assays, NPLs were fluorescently labeled with iDye Poly Pink textile dye (Villacorta et al. 2024). Labeling was performed by incubating 1 mL of each NPL suspension (5 mg/mL) with 0.01 g of dye at 70 °C for 2 h. The mixture was diluted with 9 mL of Milli-Q water, and excess dye was removed by repeated centrifugation (Amicon® Ultra-15 Ultracel®-100 K, Merck KGaA, Darmstadt, Germany) at 3500 rcf for 15 min, performed at least ten times. The retained fraction (80–160 µL) was recovered, diluted to 1 mL with Milli-Q water, aliquoted, and stored at 4 °C protected from light until use.

NPLs characterization

For dry-state morphology, NPL suspensions in Milli-Q water (200 µg/mL) were deposited onto carbon-coated copper grids, air-dried overnight, and imaged with a JEOL JEM-1400 transmission electron microscopy (TEM) operated at 120 kV (JEOL Ltd., Tokyo, Japan). Micrographs were acquired using an Orius SC200D camera (Gatan, Ametek Inc., Berwyn, PA, USA), and Martin diameters of 100 individual NPLs were measured in ImageJ v1.8.0_172 to determine size distributions. For colloidal characterization, hydrodynamic size (dynamic light scattering, DLS) and surface charge (ζ-potential, electrophoretic light scattering) were measured with a Zetasizer® Ultra (Malvern Panalytical, Cambridge, UK). Suspensions (100 µg/mL) were prepared in both Milli-Q water and Endothelial Cell Growth Medium-2 (EGM-2; PromoCell, Heidelberg, Germany). All measurements were conducted in triplicate.

Cell line and culture conditions

Primary HUVEC (single donor, C-12200; PromoCell, Heidelberg, Germany) were used as a model of the human vascular endothelium. Cells were maintained in EGM-2 (C-22011; PromoCell, Heidelberg, Germany) in flasks coated with rat tail collagen I (5 µg/cm²; Corning, NY, USA) at 37 °C in a humidified 5% CO_2 atmosphere, with medium replaced every other day. Collagen coating was prepared by diluting collagen I in 20 mM acetic acid, incubating flasks for 1 h, and rinsing twice with PBS. Experiments were performed with cells up to passage 5.

NPLs exposure

Cells were exposed to NPL suspensions prepared in EGM-2 medium at 25 µg/mL for 24 h, unless stated otherwise. Untreated cells cultured under the same conditions served as negative controls. Typically, cells were seeded at 26,300 cells/cm² in collagen I–coated wells (5 µg/cm²), grown for 48 h, and then the medium was replaced with the treatment for 24 h.

NPLs internalization

Internalization of the different NPLs by HUVECs was assessed using flow cytometry, confocal microscopy, and TEM, providing complementary quantitative, qualitative, and ultrastructural information. Untreated cells were included as negative controls.

Flow cytometry

Cells were exposed for 24 h to fluorescently labeled NPLs at 12.5, 25, or 50 µg/mL. After exposure, cells were washed twice with PBS, detached, and analyzed on a CytoFLEX cytometer (Beckman Coulter, Pasadena, CA, USA) using 561 nm excitation and 585/42 BP emission. A total of 10,000 events were collected per condition and analyzed with CytExpert software. Two parameters were quantified: (i) the percentage of cells positive for internalization and (ii) the mean fluorescence intensity per cell, reflecting the amount of internalized NPLs at each concentration. Side scatter (SSC) was also recorded to evaluate changes in cell complexity. Experiments were performed in triplicate, with technical duplicates for each condition.

Confocal microscopy

For intracellular localization, HUVECs were seeded on collagen I–coated µ-Dish 35 mm plates (Ibidi GmbH, Gräfelfing, Germany), cultured for 48 h, and then exposed for 24 h

to fluorescently labeled NPLs at 25 µg/mL. After exposure, cells were washed twice with PBS and incubated with fresh medium containing Hoechst 33,342 (1:500; nuclei) and CellMask™ Deep Red (1:500; plasma membrane) (Thermo Fisher Scientific). Imaging was performed on an LSM 980 Airyscan 2 equipped with a Plan-Apochromat 63× objective (Carl Zeiss Microscopy GmbH, Jena, Germany). Excitation/emission settings were 348/455 nm for nuclei, 659/676 nm for plasma membrane, and 577/603 nm for iDye Poly Pink-labeled NPLs. Several random fields were imaged per condition. Image processing was performed using Fiji/ImageJ (Schindelin et al. 2012).

Transmission electron microscopy (TEM)

For ultrastructural confirmation, HUVECs were seeded in collagen I-coated T25 flasks, cultured for 48 h, and then exposed for 24 h to 25 µg/mL of non-labeled NPLs. After treatment, cells were washed with PBS, detached, and fixed in 2.5% glutaraldehyde and 2% paraformaldehyde in 0.1 M cacodylate buffer (pH 7.4). Samples were post-fixed with osmium tetroxide, dehydrated in graded acetone, embedded in Eponate 12™ resin (Ted Pella Inc., Redding, CA, USA), and polymerized at 60 °C. Ultrathin sections were obtained with an ultramicrotome, mounted on copper grids, contrasted with uranyl acetate and Reynolds lead citrate, and examined with a JEOL 1400 TEM (JEOL Ltd., Tokyo, Japan) equipped with an ES1000W Erlangshen CCD camera (Gatan Inc., Pleasanton, CA, USA). Several random fields were imaged. TEM processing steps followed conventional protocols as described (Annangi et al. 2015).

Cell viability and apoptosis

Cell viability and apoptosis were assessed after NPLs treatment using the Dead Cell Apoptosis Kit with Annexin V Alexa Fluor 488 and Propidium Iodide (Thermo Fisher Scientific, Waltham, MA, USA) according to the manufacturer's instructions. To avoid loss of detached apoptotic or dead cells, the culture supernatant was collected and combined with the trypsinized fraction before staining. After labeling, cells were analyzed by flow cytometry (CytoFLEX, Beckman Coulter, Pasadena, CA, USA) using 488 nm excitation with fluorescence emission collected at 525/40 BP and 690/50 BP. Gating was applied to distinguish live, apoptotic, and necrotic populations, and results were normalized to 100%. Camptothecin (5 µM, 24 h) was included as a positive control. Experiments were performed in triplicate, with technical duplicates for each condition.

DNA damage induction

DNA damage levels were assessed using the comet assay with and without formamidopyrimidine DNA glycosylase (FPG) (Collins et al. 2023). The assay without FPG quantified DNA single-strand breaks (basal damage), whereas the FPG-modified assay measured the total DNA damage, including both single-strand breaks and oxidized DNA bases. After corresponding treatments, cells were washed with PBS, trypsinized, centrifuged (300 rcf, 8 min, 4 °C), and resuspended in cold PBS at 1×10^6 cells/mL. A 1:10 dilution in 0.75% low-melting agarose (37 °C) was prepared, and 7 µL aliquots were placed on Gelbond® films (GBF, Lonza Bioscience, Basel, Switzerland). Cells were lysed for 2 h at 4 °C (2.5 M NaCl, 0.1 M EDTA, 0.01 M Tris, 0.2 M NaOH, 1% Triton X-100, 1% N-lauroylsarcosine, 10% DMSO; pH 10), rinsed twice in enzyme buffer (0.04 M HEPES, 0.1 M KCl, 0.5 mM EDTA, 0.2 mg/mL; pH 8), and incubated for 50 min in the same buffer. A second incubation with or without activated FPG was carried out at 37 °C for 30 min. After washing in electrophoresis buffer (0.3 M NaOH, 1 mM EDTA; pH 13.4), DNA was allowed to unwind for 25 min before electrophoresis (20 V, 300 mA, 20 min). GBFs were rinsed in PBS, fixed in ethanol, and stained with SYBR Gold (1:2500 in TE buffer: 10 mM Tris Base, 1 mM EDTA; pH 8). Comets were visualized with an Olympus BX50 microscope (20×), and the percentage of DNA in the tail was quantified using Komet 5.5 software (Kinetic Imaging Ltd, Liverpool, UK). Two independent biological experiments were conducted, each with two technical replicates, and 100 cells were scored per replicate. Methyl methanesulfonate (MMS, 200 µM, 40 min) was used as a positive control for single-strand breaks, and potassium bromate ($KBrO_3$, 5 mM, 40 min) as a positive control for total DNA damage in the FPG-modified assay.

IL-6 secretion levels

IL-6 levels in culture supernatants were measured after 24 h exposure to NPLs using the commercial IL-6 ELISA kit (KHC0061, Invitrogen; Waltham, MA, USA) according to the manufacturer's instructions. Absorbance was read at 450 nm, and concentrations were calculated from standard curves generated by a four-parameter logistic model. Three independent experiments were performed, each with technical duplicates per condition.

Intracellular cholesterol levels

HUVECs were seeded in µ-Plate 24 Well black plates (ibidi, Gräfelfing, Germany), and cholesterol levels were evaluated by Filipin III staining after 24 h exposure to NPLs. Briefly,

cells were fixed with a two-step protocol: pre-fixation in a 1:1 mix of EGM-2 and 4% paraformaldehyde (PFA) for 10 min at 37 °C, followed by 4% PFA for 10 min at room temperature. After PBS washes, residual aldehydes were quenched with 1.5 mg/mL glycine in PBS. Filipin III (SAE0087, Sigma-Aldrich, Steinheim, Germany) was prepared in PBS supplemented with 10% FBS and applied at a final concentration of 0.05 mg/mL for 2 h at room temperature in the dark. Images were acquired with a Zeiss LSM 980 Airyscan 2 confocal microscope (Carl Zeiss Microscopy GmbH, Jena, Germany) using a 20× objective (excitation 353 nm, emission 465 nm). For image analysis, 100 independent cells (manual Regions of Interest) were quantified per technical replicate, resulting in a total of 600 cells across three biological experiments with two technical replicates each. Fluorescence was analyzed as the mean intensity of each ROI.

Cell migration potential

Cell migration was assessed with a wound-healing assay using Culture-Inserts 2 Well (Ibidi GmbH, Gräfelfing, Germany). Inserts were placed in collagen-coated wells, and 21,000 cells were seeded in each compartment in EGM-2 medium containing 25 µg/mL of NPLs. After 24 h (37 °C, 5% CO_2), inserts were removed, wells washed, and fresh medium with the same NPL concentration added. Images were acquired at 0 h and every 2 h up to 8 h with a Zeiss Axio Observer A1 inverted microscope (10× objective; Carl Zeiss Microscopy GmbH, Jena, Germany). Wound closure was analyzed in ImageJ (v1.8.0_172) with the "Wound Healing Size Tool" plug-in (Suarez-Arnedo et al. 2020). Two parameters were calculated: (i) front velocity, expressed in µm/h, as $(A_0 - A_t)/(2 \cdot L \cdot \Delta t)$, and (ii) percentage of wound closure, as $(A_0 - A_t)/A_0 \times 100$. Here A_0 and A_t are wound areas at 0 h and time t, L is wound length, and Δt the elapsed time. Four independent experiments were performed, each with technical triplicates.

Statistical analysis

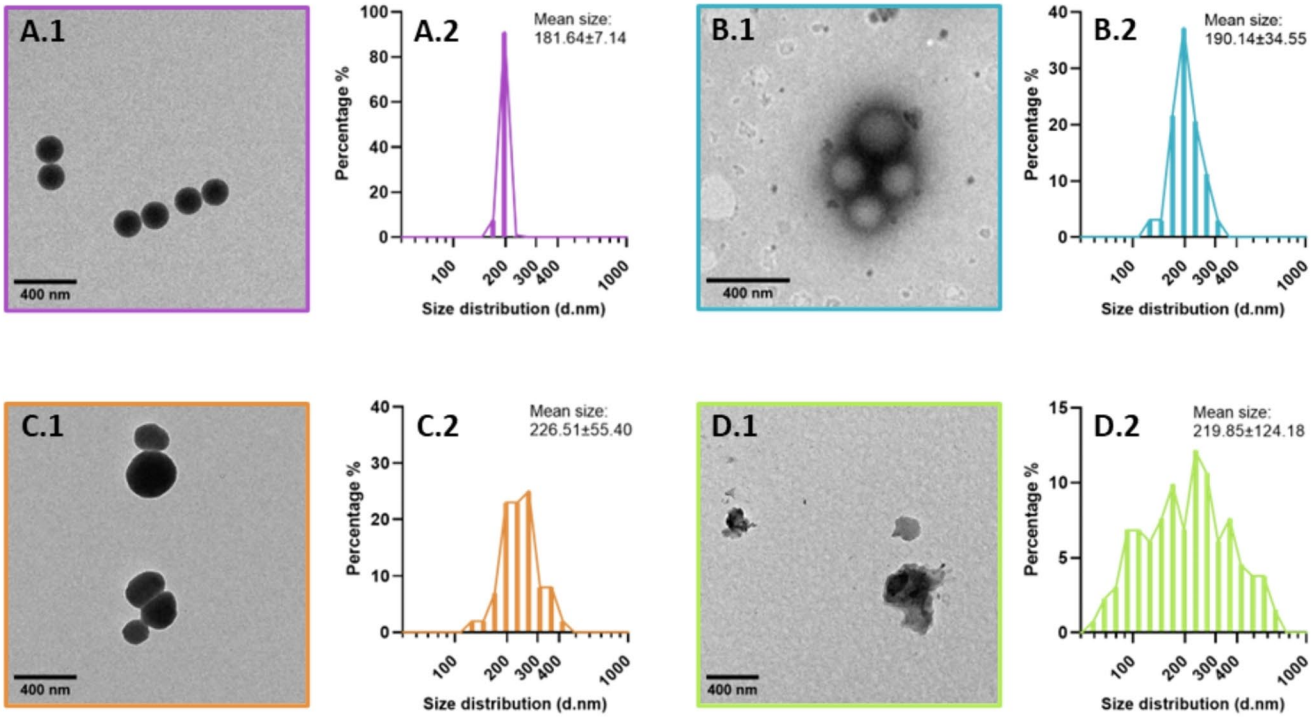
Data analysis was performed with GraphPad Prism 9 (GraphPad Software Inc., CA, USA). Normality was assessed using the Kolmogorov-Smirnov test. For normally distributed data, one-way ANOVA was followed by: Dunnett's test (comparisons of each NPL vs. the negative control, excluding the positive control), Tukey's test (pairwise comparisons among NPLs, excluding both the negative and positive control), and Dunnett's test for the comparison of the positive control vs. the negative control (including all groups). For non-parametric data, the Kruskal-Wallis test with Dunn's post hoc test was applied following the same criteria. Statistical significance was defined as $*p \leq 0.05$, $**p \leq 0.01$, and $***p \leq 0.001$. Results are expressed as mean ± SEM.

Results and discussion

NPLs characterization

TEM confirmed that all NPL types displayed mean diameters around 200 nm (Figs. 1A.2–D.2, E). This suggests that the biological effects observed in subsequent assays are likely influenced primarily by the intrinsic properties of each polymer and to differences in morphology and colloidal behavior, rather than by major size discrepancies between individual NPLs. Controlling for particle size is important, as it is a key factor affecting NPL-cell interactions and biological responses (Lu et al. 2022). In terms of morphology (Figs. 1A.1–D.1), PS-NPLs and PLA-NPLs presented uniform, spherical shapes, whereas PTFE-NPLs appeared spherical but slightly irregular. PET-NPLs displayed the most heterogeneous and irregular morphologies, consistent with Villacorta et al. (2022) observations. This gradation, from idealized synthetic spheres to irregular, "real-life" fragments, provides a model system spanning from controlled laboratory particles to those more representative of environmental NPLs (El Hadri et al. 2020). The same pattern was reflected in size distributions, PS-NPLs showed the narrowest range (164.9–200.7 nm; SD 7.1 nm), PLA-NPLs and PTFE-NPLs were broader (171.6–353.2 nm and 118.3–387.2 nm, respectively), and PET-NPLs displayed by far the widest dispersion (56.9–587.8 nm; SD 124.2 nm).

DLS measurements further characterized the NPLs in suspension (Fig. 1E). Hydrodynamic diameters in Milli-Q water were consistently larger than TEM sizes, as expected for hydrated particles (Wilson and Prud'homme 2021). Polydispersity indexes (PDI) values increased in EGM-2 compared to Milli-Q water across all polymers, consistent with biomolecule adsorption (protein corona formation) and subsequent particle aggregation in biological media (da Silva et al. 2019; Ferreira et al. 2022). PS-NPLs and PLA-NPLs maintained low PDI values (<0.3), reflecting higher colloidal stability, whereas PTFE-NPLs and particularly PET-NPLs showed markedly higher values. The strong aggregation tendency of PET-NPLs was evident in its large hydrodynamic diameter (946.7 nm in EGM-2) and high PDI (0.70 in EGM-2), underscoring its resemblance to environmentally derived NPLs. ζ-potential values were negative in Milli-Q water (–18.5 to −35.5 mV), reflecting stable dispersions, but shifted towards neutrality in EGM-2 (–1.6 to −10.7 mV) for all NPLs. PLA-NPLs showed the strongest shift, reaching near-neutral values (–1.55 mV) in EGM-2,



E	MiliQ				EGM-2		
	TEM	Z-Average	PDI	Z-Pot	Z-Average	PDI	Z-Pot
PS	181.64 ± 7.14	194.80 ± 3.45	0.02	-35.50 ± 0.35	225.10 ± 4.48	0.07	-9.14 ± 0.66
PLA	190.14 ± 34.55	230.50 ± 6.65	0.14	-22.60 ± 0.74	214.40 ± 2.85	0.23	-1.55 ± 0.26
PTFE	226.51 ± 55.40	321.40 ± 22.77	0.39	-25.00 ± 0.95	202.50 ± 50.45	0.67	-10.80 ± 1.17
PET	219.85 ± 124.18	857.80 ± 226.80	0.61	-18.50 ± 0.93	946.70 ± 217.80	0.70	-10.70 ± 0.95

Fig. 1 Characterization of NPLs. (A–D) TEM characterization in Milli-Q water for **A** PS, **B** PLA, **C** PTFE, and **D** PET. (**A.1**–**D.1**) Representative TEM images and (**A.2**–**D.2**) corresponding size distribution histograms obtained from TEM measurements. (**E**) Summary of TEM particle diameters, hydrodynamic diameters (DLS), and ζ-potential values of the NPLs in Milli-Q water and in EGM-2 medium. Sizes are expressed in nm (diameter) and ζ-potential in mV (mean ± SD)

consistent with previous reports of PLA-NPLs charge neutralization in culture media (da Silva et al. 2019). The other polymers stabilized around −10 mV in EGM-2, consistent with values reported for NPLs such as PS-NPLs dispersed in cell culture media (Martín-Pérez et al. 2024). This general reduction in surface charge is explained by protein adsorption on the NPL surface, which masks the original charge, reduces electrostatic repulsion, and facilitates aggregation in culture environments (da Silva et al. 2019); however, although these medium-dependent shifts are consistent with protein corona formation in biological media, we did not directly visualize or profile the corona after cellular internalization in this study.

Overall, TEM and DLS analyses indicate that while PS-NPLs and PLA-NPLs behave as relatively stable, uniform model systems, PTFE-NPLs shows limited stability, and PET-NPLs display strong aggregation and heterogeneity, making it the closest proxy for environmentally derived NPLs. Taken together, this panel provides a controlled gradation of environmental relevance, from idealized spherical reference particles (PS) to more heterogeneous and colloidally unstable materials (PTFE), real-life PLA spherical shaped resulting from the in-house degradation of PLA pellets, and ultimately to real-life, polydisperse PET fragments derived from PET water bottles.

NPLs internalization

The uptake of the different NPLs was assessed using flow cytometry, confocal fluorescence microscopy, and TEM. Flow cytometry was performed at 12.5, 25, and 50 µg/mL to evaluate internalization across a concentration range. This

approach identified polymer-dependent uptake patterns and guided the selection of optimal concentration for subsequent assays, ensuring substantial internalization while avoiding cellular overload and maintaining relatively lower concentrations compared to our previous studies. Choosing a concentration that preserves differential uptake among polymers is particularly valuable, as it enables comparison of their internalization patterns and how differences in uptake correlate with subsequent biological responses. Finally, at 25 µg/mL, confocal microscopy was applied to corroborate the intracellular distribution of NPLs, while TEM was used to provide ultrastructural insight into their localization.

NPLs internalization by flow cytometry

Flow cytometry after 24 h of exposure revealed generally high levels of NPL internalization across all polymers in HUVECs (Fig. 2A). This robust uptake underscores the

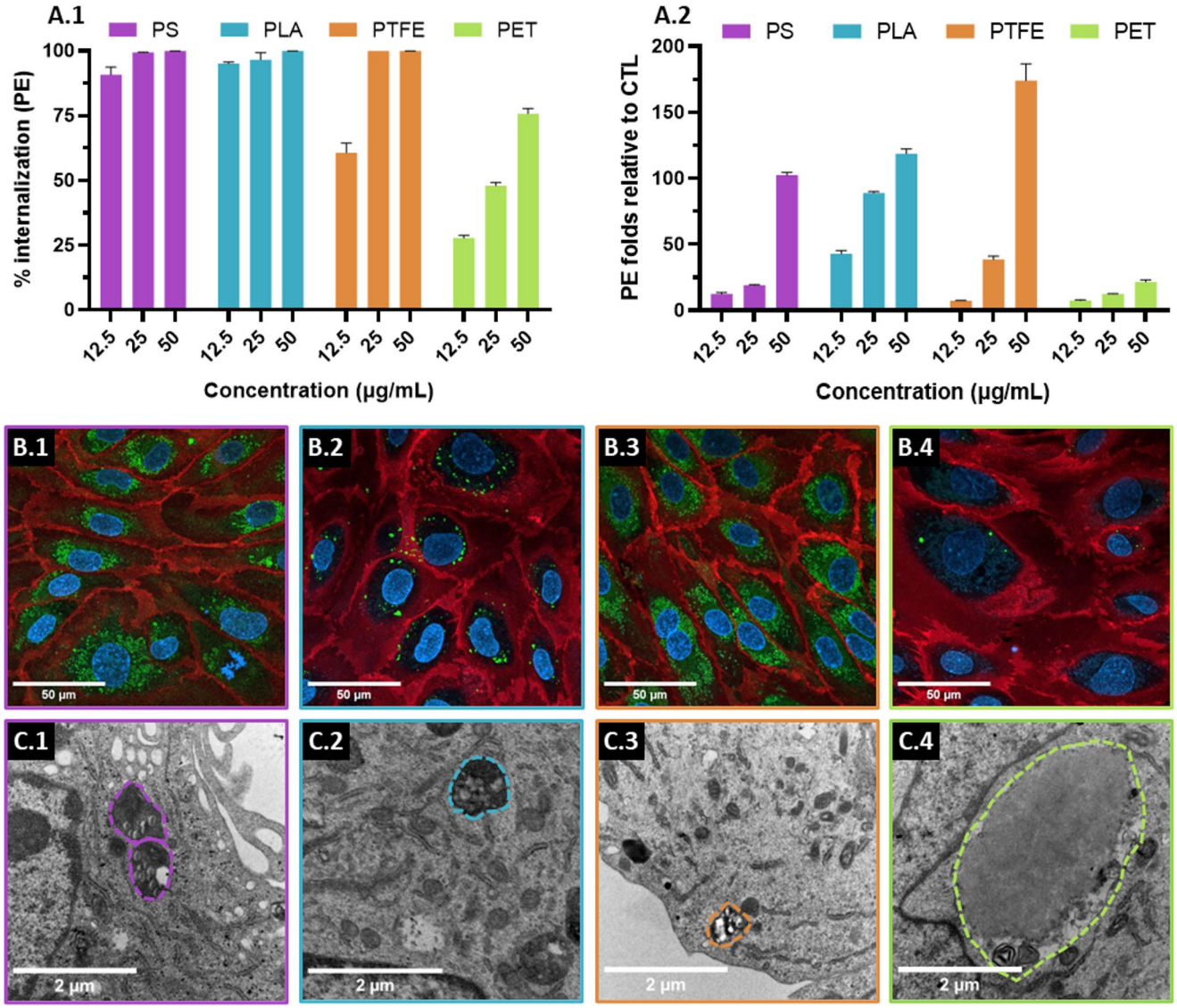


Fig. 2 Internalization of NPLs. (**A.1**–**A.2**) Flow cytometry analysis of NPL uptake at 12.5, 25, and 50 µg/mL for 24 h: (**A.1**) percentage of NPL-positive cells and (**A.2**) mean fluorescence intensity of internalized NPLs. (**B.1**–**B.4**) Representative confocal images showing NPL uptake at 25 µg/mL for 24 h. NPLs are shown in green, nuclei in blue, and cell membrane in red. Panels correspond to (**B.1**) PS- NPLs, (**B.2**) PLA-NPLs, (**B.3**) PTFE-NPLs, and (**B.4**) PET-NPLs. (**C.1**–**C.4**) Representative TEM images of HUVECs exposed to 25 µg/mL of NPLs for 24 h. NPL-containing vesicles are highlighted with dotted lines. PS (**C.1**) formed numerous vesicles of 700–800 nm in diameter containing individual NPLs abundantly distributed throughout the cytoplasm. PLA (**C.2**) displayed less abundant vesicles of 800 nm containing clearly visible nanoparticles (zoom-in at Sup. Fig. 2 A.1–A.2), together with occasional larger vesicles up to 2 µm in diameter with granular content (Sup. Fig. 2 A.3). PTFE-NPLs (**C.3**) accumulated in numerous vesicles of 700–800 nm, each containing clearly individualized nanoparticles. PET-NPLs (**C.4**) induced scarce but very large vesicles, up to 4 µm in diameter, with diffuse and homogeneous electrodense internal content lacking discernible NPLs. Negative controls for confocal and TEM shown in Sup. Fig. 3

suitability of HUVECs as a sensitive model for NPLs hazard assessment studies, in agreement with previous reports using nanomaterials (Cao et al. 2017). Compared to other cell types commonly used in nanotoxicology, such as Raji-B, THP-1, or TK6, which typically show < 10% of positive cells for 200 nm PS-NPLs even at 100 µg/mL (Tavakolpournegari et al. 2023), HUVECs demonstrated near-complete internalization at considerably lower exposure levels (12.5–50 µg/mL). This strong endocytic capacity has been documented in HUVECs for other nanomaterials, including silica nanoparticles, titanium dioxide, carbon nanotubes, and PS-NPLs (Blechinger et al. 2013; Gholinejad et al. 2019; Zhao et al. 2019; Martín-Pérez et al. 2024). To our knowledge, however, this is the first study to quantify the uptake of PLA-NPLs, PTFE-NPLs, and PET-NPLs in this endothelial cell model.

Despite the generally high internalization, uptake efficiency differed between polymers. PS-NPLs and PLA-NPLs showed nearly identical profiles, with approximately 100% of positive cells across all tested concentrations. PTFE-NPLs showed intermediate uptake at 12.5 µg/mL (60.7%) but reached complete internalization at 25 and 50 µg/mL, aligning with PS-NPLs and PLA-NPLs at these concentrations. In contrast, PET-NPLs consistently exhibited the lowest uptake, with only 27.8% of positive cells at 12.5 µg/mL, 48.1% at 25 µg/mL, and 75.8% at 50 µg/mL. Thus, while PS-NPLs, PLA-NPLs, and PTFE-NPLs converge toward near-complete internalization from 25 µg/mL onwards, PET-NPLs remain clearly less internalized. The reduced uptake of PET-NPLs is likely related to their colloidal instability. Dynamic light scattering of PET-NPLs suspensions in EGM-2 revealed the highest polydispersity index (0.70) and largest hydrodynamic size (946 ± 217.80 nm), indicating extensive aggregation. Since clathrin- and caveolin-mediated endocytosis generally accommodate nanoparticles up to 200 nm (Voigt et al. 2014; Sabourian et al. 2020), aggregates approaching or exceeding 500 nm are more dependent on macropinocytosis or phagocytosis, which are comparatively slower and less efficient internalization routes (Kuhn et al. 2014). In addition, polymer-specific surface chemistry and the resulting protein corona could modulate receptor interactions and influence uptake efficiency (Sousa De et al. 2021; Cao et al. 2022).

Mean fluorescence intensity (MFI; folds relative to control, Fig. 2B) supported these internalization patterns by reflecting intracellular accumulation. All polymer NPLs showed a clear dose-dependent increase, yet PET-NPLs consistently produced the lowest signal, with differences versus other polymers widening at higher concentrations. PTFE-NPLs exhibited lower MFI than PS-NPLs and PLA-NPLs at 12.5 µg/mL, but equaled or exceeded their levels at 25 and 50 µg/mL. The strong agreement between uptake percentages and MFI reinforces the conclusion that PET-NPLs are the least efficiently internalized polymer, while PS-NPLs, PLA-NPLs, and PTFE-NPLs are readily taken up. Based on these results, 25 µg/mL was selected as the working concentration for subsequent experiments. This concentration ensures robust uptake across polymers without causing cellular overload and remains within environmentally relevant ranges.

NPLs internalization by confocal microscopy

Z-stack confocal imaging confirmed that the fluorescent signal corresponded to NPLs internalized within the cytoplasm rather than adhered to the plasma membrane, in line with previous reports using this approach (Morataya-Reyes et al. 2025a, b a). After 24 h of exposure at 25 µg/mL, most treatments produced a broad cytoplasmic distribution of NPL-associated fluorescence (Fig. 2B and supplementary Fig. S3), consistent with the quantitative flow cytometry data. In PS-NPLs-treated cells (Fig. 2B.1), fluorescence was homogeneously distributed throughout the cytoplasm of all cells, consistent with the complete proportion of NPL-positive HUVECs detected by flow cytometry. PLA-NPLs-treated cells (Fig. 2B.2) also showed 100% positivity, although with a less uniform and abundant cytoplasmic distribution. PTFE-NPLs-treated cells (Fig. 2B.3) resembled PS-NPLs, with fluorescence widely distributed across the cytoplasm of all cells. By contrast, PET-NPLs-treated cells (Fig. 2B.4) displayed a restricted uptake, with fluorescence confined to discrete punctate regions in only about half of the cell population, in line with the approximately 50% internalization measured by flow cytometry. Taken together, these fluorescence patterns demonstrate that both the magnitude of uptake and the subcellular distribution of NPLs depend strongly on the polymer type, emphasizing the importance of these differences when assessing NPL-cell interactions and their potential biological consequences.

NPLs internalization by TEM

TEM corroborated the confocal observations and provided ultrastructural insights into the vesicular compartments containing NPLs (Fig. 2C, and supplementary Fig. S3).

In PS-NPLs-treated cells (Fig. 2C.1), numerous 700–800 nm vesicles containing individualized electron-dense nanoparticles were widely dispersed throughout the cytoplasm, consistent with lysosomal or autophagosomal compartments previously reported for PS-NPLs in RBL-2H3 cells and HUVECs (Liu et al. 2021; Lu et al. 2022 a). The presence of NPLs in these compartments agrees with receptor-mediated endocytosis via clathrin or caveolin (Liu et al. 2021). The high vesicular abundance matched the increase

in complexity detected by flow cytometry side-scattering (SSC) (Supplementary Fig. S1). Compared to PS, PLA-NPLs exposure (Fig. 2C.2) produced fewer vesicles of similar size together with occasional larger vesicles (up to 2 µm) with granular content, suggesting partial involvement of macropinocytosis or phagocytosis-like uptake. Their less negative ζ-potential (−1.55 mV vs. −10 mV for other polymers) supports the formation of a distinct protein corona that may alter receptor interactions and promote alternative entry routes (Cao et al. 2017; Sousa De et al. 2021). PTFE-NPLs (Fig. 2C.3) showed a pattern like PS, with 700–800 nm vesicles containing clearly visible nanoparticles, yet their number was lower than in PS-treated cells. This morphology remains compatible with efficient clathrin- or caveolin-mediated endocytosis but indicates a slightly reduced extent of vesicular formation compared to PS. In contrast, PET-NPLs were in much larger, but scarce, vesicles (up to 4 µm in diameter), consistent with macropinosomes or phagosome-like structures formed through macropinocytosis or phagocytosis-like uptake in non-professional phagocytes such as HUVECs. This is in line with the hydrodynamic size measured by DLS for PET-NPLs in EGM-2, around 900 nm, which revealed extensive aggregation and supports uptake through these pathways. Since both macropinocytosis and phagocytic pathways eventually converge into the lysosomal route, the vesicles observed here may represent phagolysosomes. Such a mechanism agrees with the macropinocytosis-mediated internalization described by Liu et al. (2021) for 500 nm PS-NPLs and with the typical size ranges reported for phagocytosis in the literature (Sousa De et al. 2021). Although endocytic routes dominate, passive translocation across the plasma membrane cannot be ruled out for any of the tested materials, as hydrophobic and van der Waals interactions may allow limited diffusion of small NPLs (Liu et al. 2021). The low electron density of polymers, however, limits direct visualization of individualized NPLs in the cytoplasm by TEM (Sawyer et al. 2008). Overall, TEM confirms that polymer chemistry and colloidal behavior govern both the efficiency and pathway of NPL internalization in HUVECs.

Cytotoxicity and genotoxicity

Cytotoxicity and apoptosis

The Annexin V/PI assay demonstrated that none of the NPL exposures compromised HUVEC viability at 25 µg/mL after 24 h (Fig. 3A). In all NPL-treated groups, more than 80% of cells remained viable, with necrotic fractions consistently below 15% and apoptotic fractions below 5%, values comparable to the negative control. These findings indicate that, under the tested conditions, NPLs of different polymer types do not trigger acute cytotoxicity or apoptosis in primary endothelial cells. In contrast, the apoptotic inducer camptothecin (5 µM, 24 h) produced the expected marked decrease in cell viability (<25%) together with a pronounced increase in both necrotic (>58%) and apoptotic (>17%) populations, thereby validating the sensitivity of the assay (Morris and Geller 1996). These results are consistent with previous studies reporting a lack of acute cytotoxicity

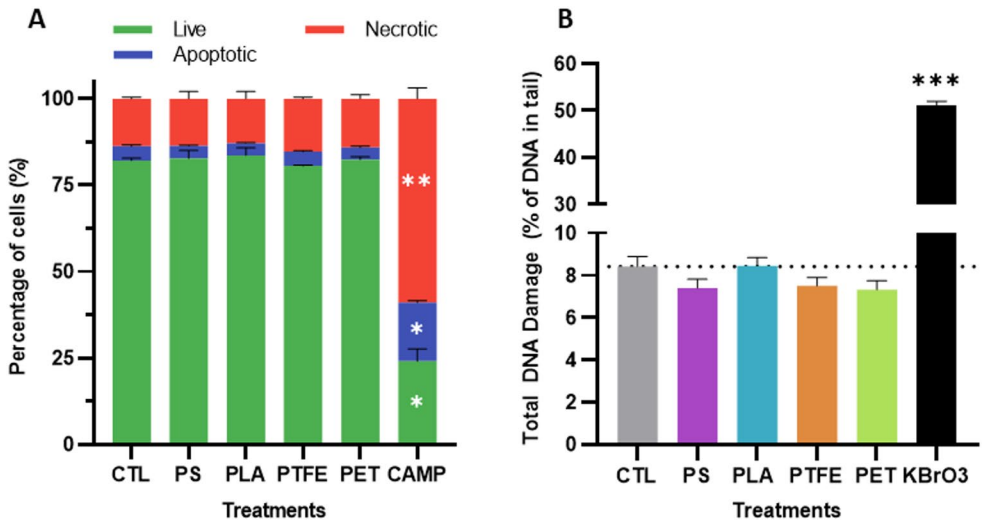


Fig. 3 Cytotoxic and genotoxic effects of NPLs in HUVECs. **A** Apoptosis was assessed after 24 h exposure to NPLs (25 µg/mL) using Annexin V/PI staining and flow cytometry. Bars represent the percentage of viable (green), apoptotic (blue), and necrotic (red) cells. Camptothecin (5 µM, 24 h) was used as a positive control. **B** Total DNA damage was evaluated by the FPG-modified comet assay, expressed as the percentage of DNA in the tail. Data are expressed relative to the negative control (CTL, set to 1). $KBrO_3$ (5 mM, 40 min) served as positive control. Data are shown as mean ± SEM from ≥2 independent experiments. Statistical analysis was performed using the Kruskal–Wallis test with Dunn's multiple comparisons. Significant differences were observed only between the positive controls and the negative control; no significant differences were detected for NPLs vs. control or among NPLs. *$p \leq 0.05$, **$p \leq 0.01$, ***$p \leq 0.001$

for PS-NPLs, PLA-NPLs, PTFE-NPLs, and PET-NPLs when tested at environmentally relevant concentrations across different cell types (Annangi et al. 2023; Banaei et al. 2023; Martín-Pérez et al. 2024; Abass et al. 2025).

The absence of cytotoxicity at the selected 25 µg/mL for 24 h validates this exposure condition as an appropriate experimental window to investigate more subtle environmentally meaningful endpoints, including genotoxicity, inflammatory signaling, metabolic disruption, and alterations in endothelial functionality, without confounding effects derived from cell death.

Genotoxicity

Although genotoxic effects of PS-NPLs have been reported in several human cell models, including HUVECs, Raji-B, and TK-6 cells (Rubio et al. 2020; Martín-Pérez et al. 2024), systematic evaluations encompassing other NPL types remain scarce. To date, no studies have examined the genotoxic potential of PLA-, PTFE-, or PET-NPLs in endothelial cells, and only limited evidence exists in other human cell systems. To address this gap, the comet assay was employed to assess whether the tested NPLs induce DNA strand breaks or oxidative DNA lesions. This assay has been widely validated as a reliable method for evaluating the genotoxicity of NPLs (García-Rodríguez et al. 2019).

In our study, application of the comet assay, both in its standard alkaline version and in the FPG-modified form to reveal oxidized bases, showed no increase in DNA damage levels in HUVECs exposed to 25 µg/mL of the different NPLs for 24 h (Fig. 3B and supplementary Fig. S4). Across all polymer treatments, values were about 6–8% DNA in tail, comparable to the negative control, with no significant differences observed. In contrast, the positive controls, potassium bromate ($KBrO_3$) for the FPG assay and methyl methanesulfonate (MMS) for the alkaline assay, produced the expected marked increases, confirming the assay sensitivity. Thus, under the tested conditions, 200 nm NPLs did not induce detectable single strand breaks or oxidative DNA lesions in primary endothelial cells. These results expand the scarce evidence on NPL-induced genotoxicity in endothelial cells and suggest that, under environmentally relevant conditions, these NPLs do not inherently compromise DNA integrity. Nonetheless, interpretation must remain cautious, as genotoxic responses to NPLs appear highly dependent on experimental context. For example, strand breaks have been detected with smaller PS NPLs in HUVECs (Martín-Pérez et al. 2024). PLA-NPLs-induced genotoxicity has been observed only at higher doses and longer exposures (García-Rodríguez et al. 2024; Morataya-Reyes et al. 2025b), while PTFE-NPLs effects were observed from 50 to 200 µg/mL in Caco-2 and HT29-MTX cells (Abass et al. 2025). For PET-NPLs, findings remain contradictory, with no effects reported in THP-1 cells up to 50 µg/mL for 3 h (Villacorta et al. 2022) but clear dose-dependent damage in A549 cells across starting from just 2 µg/mL (Alzaben et al. 2023). Taking together, this variability highlights that polymer chemistry, particle size, exposure dose, and cell type jointly shape the genotoxic potential of NPLs, and that absence of damage in one setting cannot be generalized across systems.

Inflammation – IL-6 ELISA

Regarding the inflammatory response in HUVECs, IL-6 secretion was quantified in cell culture supernatants after 24 h exposure to NPLs (25 µg/mL). Exposure to PET-NPLs led to a significant increase in IL-6 secretion, reaching 1.93-fold relative to the control ($p \leq 0.001$). This effect was also significantly higher compared with all other polymer types tested ($p \leq 0.01$). In contrast, PS-NPLs, PLA-NPLs, and PTFE-NPLs did not induce significant changes in IL-6 levels compared with the control, indicating that the pro-inflammatory response was specific to real-life PET-NPLs under the tested conditions.

The absence of IL-6 induction after exposure to PS-NPLs, PLA-NPLs, and PTFE-NPLs is in line with several previous studies. For PS-NPLs, Weber et al. (2022) reported no increase in IL-6 when using monodisperse spherical particles of 50–310 nm in monocytes and dendritic cells, while Arribas Arranz et al. (2024) similarly observed no IL-6 response in whole blood at 100 µg/mL. In the case of PLA-NPLs, our results are consistent with da Silva et al. (2019), who found no pro-inflammatory activation in macrophages exposed to PLA-NPLs of comparable size across a wide dose range (0.5–100 µg/mL). For PTFE-NPLs, Abass et al. (2025) reported no induction of IL-8 secretion in an intestinal barrier model after 24 h exposure, further supporting the notion that PTFE-NPLs do not trigger acute pro-inflammatory signaling, at least through major cytokine and chemokine mediators. Together, these findings suggest that spherical, monodisperse polymers such as PS-NPLs, PLA-NPLs, and PTFE-NPLs generally exhibit limited pro-inflammatory activity under acute exposure conditions.

The enhanced IL-6 secretion triggered by real-life PET-NPLs is consistent with Weber et al. (2022) results, who reported that real-life, irregular, and polydisperse NPLs, including PS-NPLs and PVC-NPLs, induced IL-6 expression in monocytes and dendritic cells, whereas monodisperse spherical NPLs did not show such effects. These results suggest that particle morphology and colloidal behavior, rather than polymer identity alone, may play important roles in modulating inflammatory potential of NPLs.

The induction of IL-6 by PET-NPLs in HUVECs is biologically relevant because IL-6 is a central mediator of

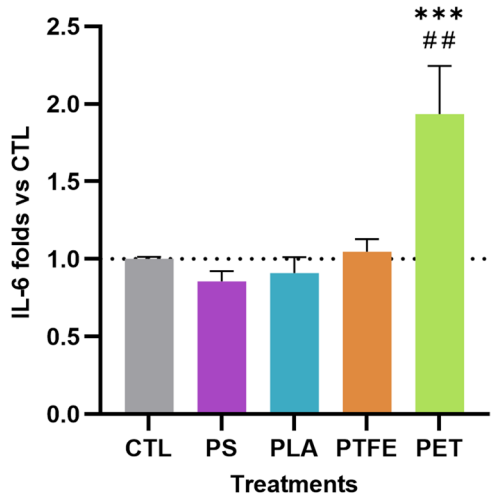


Fig. 4 IL-6 secretion in HUVECs exposed to NPLs. IL-6 levels in culture supernatants were quantified by ELISA after 24 h exposure to NPLs (25 µg/mL). Bars represent fold change relative to the negative control (CTL, set to 1). Data are shown as mean ± SEM from ≥3 independent experiments. Statistical analysis was performed using one-way ANOVA followed by Dunnett's test (comparisons vs. control) and Tukey's test (pairwise comparisons among NPLs). ***$p \leq 0.001$ vs. control; $^{\#\#}p \leq 0.01$ PET vs. different NPLs

vascular inflammation and endothelial dysfunction (Kang et al. 2020). In endothelial cells, IL-6 signaling promotes inflammatory cell adhesion (Suzuki et al. 2010), disrupts endothelial barrier integrity increasing permeability and favoring vascular leakage (Kang et al. 2020), and induces a pro-thrombotic phenotype (Cimmino et al. 2022), collectively contributing to endothelial dysfunction and atherosclerosis development (Zegeye et al. 2023) (Fig. 4).

Cholesterol detection

Filipin III staining was applied to visualize unesterified cholesterol within the cytoplasm of HUVECs. Fluorescence microscopy images (Figs. 5B.1–B.5) revealed clear differences across treatments, with PET-NPLs-treated cells (Fig. 5B.5) displaying visibly stronger fluorescence than control and the other polymers (Figs. 5B.1–B.4). Quantification of Filipin III intensity in approximately 600 individual cells confirmed these observations (Fig. 5A). After 24 h at 25 µg/mL, only PET-NPLs significantly increased intracellular cholesterol, reaching 1.22-fold compared with the negative control ($p \leq 0.01$). PTFE-NPLs showed a modest but non-significant increase of 1.09-fold, whereas PS-NPLs and PLA-NPLs remained comparable to control. Pairwise comparisons indicated that PET-NPLs differed significantly only from PLA-NPLs ($p \leq 0.05$).

PET-NPLs exposure also altered the spatial distribution of cholesterol. While control, PS-NPLs, PLA-NPLs, and PTFE-NPLs showed predominantly perinuclear fluorescence consistent with synthesis in the endoplasmic reticulum (Lyu et al. 2017), PET-NPLs resulted in a more dispersed

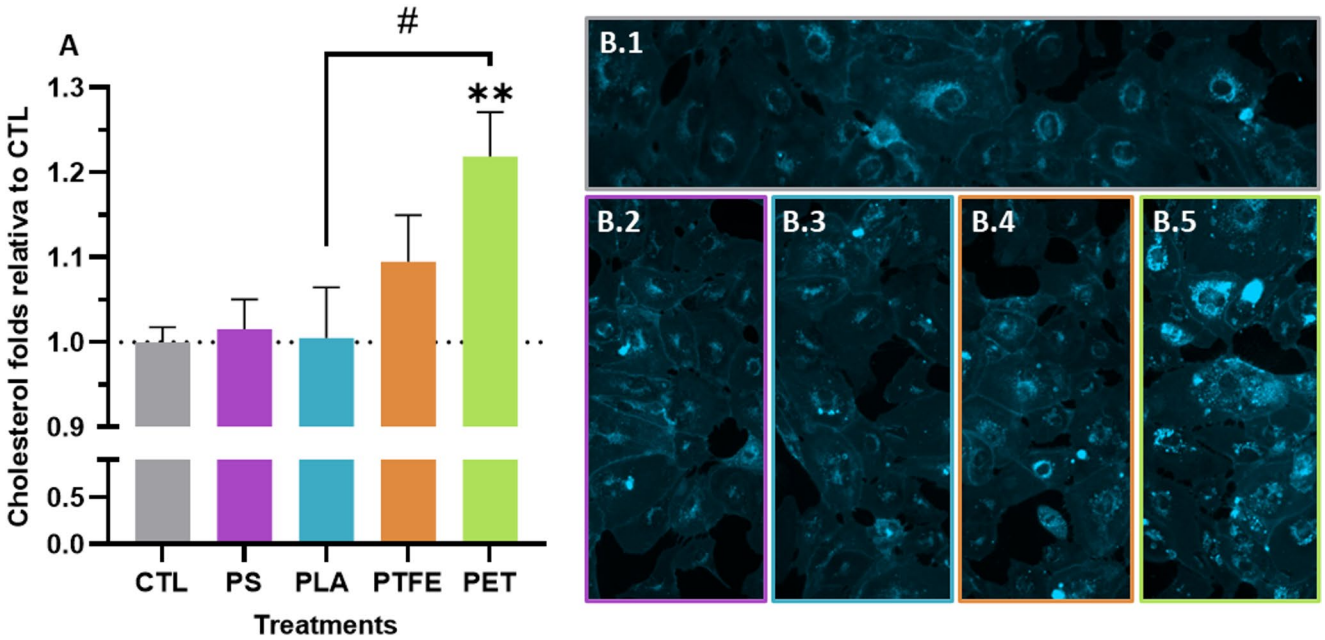


Fig. 5 Cholesterol levels in HUVECs after NPLs exposure. **A** Cholesterol levels were quantified by Filipin III staining after 24 h exposure to NPLs (25 µg/mL). Bars represent fold change relative to the negative control (CTL, set to 1). Data are shown as mean ± SEM from ≥3 independent experiments. Statistical analysis was performed using one-way ANOVA followed by Dunnett's test (comparisons vs. control) and Tukey's test (pairwise comparisons among NPLs). **$p \leq 0.01$ vs. control; $^{\#}p \leq 0.05$ PET-NPLs vs. PLA-NPLs. (B) Representative confocal images of Filipin III staining (cyan) in HUVECs exposed to **B.1** CTL, **B.2** PS-NPLs, **B.3** PLA-NPLs, **B.4** PTFE-NPLs, and **B.5** PET-NPLs. Images were acquired with a 20× objective

cytoplasmic signal with punctate structures compatible with vesicular accumulation. Increased intracellular cholesterol has previously been reported in HUVECs exposed to PS-NPLs of smaller sizes up to 100 nm at higher concentrations of 100 µg/mL (Martín-Pérez et al. 2025). However, PS-NPLs did not induce significant changes in the present study, which may reflect the lower exposure concentration of 25 µg/mL or the larger particle size of 200 nm, since greater size is generally associated with reduced cellular reactivity (Płuciennik et al. 2024).

To our knowledge, the effects of NPLs beyond PS-NPLs on cholesterol metabolism have not yet been investigated. This study therefore provides the first evaluation of PLA-NPLs, PTFE-NPLs, and PET-NPLs on endothelial intracellular cholesterol. Only real-life PET-NPLs induced significant accumulation, likely due to physicochemical properties that favor the formation of unusually large vesicles up to 4 µm. Their persistence in the cytoplasm may impair vesicular trafficking pathways responsible for cholesterol export and redistribution, a process previously associated with elevated intracellular cholesterol levels (Litvinov et al. 2018; Martello et al. 2020). Interestingly, the cholesterol increase observed in PET-treated cells is also consistent with the pro-inflammatory response described above, as intermediates of cholesterol biosynthesis can promote IL-6 induction (Omoigui 2007).

Cholesterol accumulation is linked to endothelial dysfunction (Ziegler et al. 2024), whereas altered cholesterol trafficking affects membrane fluidity and cellular migration capacity (Lyu et al. 2017). In this context, we evaluated migration as a key component of endothelial function.

Migration assay

The wound healing assay revealed polymer-specific effects on endothelial migration (Fig. 6). Closing velocity measurements (Fig. 6A) demonstrated that PS-NPLs and PLA-NPLs did not significantly alter HUVEC migration at any time point, whereas both PTFE-NPLs and PET-NPLs markedly impaired closure kinetics. PET-NPLs consistently induced the strongest inhibition, with migration velocity reduced by approximately 25% relative to the control at 8 h. The reduction was already significant from 2 h onwards and persisted throughout the assay. PTFE-NPLs produced a more moderate effect, leading to about a 15% decrease in closing velocity at 8 h, though this reduction was also significant and evident from the 2 h time-point. Pairwise analyses confirmed that PET-NPLs differed significantly from PS-NPLs and PLA-NPLs from 4 h onwards, and from PTFE-NPLs at 6–8 h. In addition, PTFE-NPLs differed significantly from PS-NPLs and PLA-NPLs starting at 4 h, except for the comparison with PLA-NPLs at 8 h, where no significant difference was detected (Supplementary Table S1). Representative phase-contrast images at 8 h illustrate the impaired wound closure in both PET-NPLs and PTFE-NPLs -treated cells compared with the efficient closure observed in control, PS-NPLs, and PLA-NPLs (Fig. 6B). These findings were reinforced by the complementary metric of wound closing percentage (Supplementary Fig. S5). The consistency across both readouts underscores the robustness of the observed impairment. Our results with PTFE-NPLs and PET-NPLs are in line with most of the existing research showing that MNPL exposure reduces cell migration under a variety of conditions. In vitro studies have consistently reported decreased migration in both HUVECs and human trophoblasts after exposure to PS-NPLs ranging from 30 to 500 nm (Lee et al. 2021; Hu et al. 2022; Lv et al. 2024; Wan et al. 2024). Comparable effects have also been demonstrated in vivo, where exposure of the freshwater leech *Hirudo verbana* to polypropylene MNPLs (100 nm–5 µm) delayed wound repair (Bon et al. 2025).

The inhibitory effects of PTFE-NPLs and PET-NPLs on migration may be linked to alterations in intracellular cholesterol levels, since elevated cholesterol in HUVECs has been associated with reduced migratory capacity (Lyu et al. 2017). This interpretation is consistent with our observations, with PET-NPLs inducing the highest intracellular cholesterol accumulation together with the most pronounced reduction in migration. Endothelial migration is essential for vascular repair, angiogenesis, and barrier integrity. Impairment of this process, as observed here for PTFE-NPLs and particularly PET-NPLs, can compromise angiogenesis and delay vascular repair, thereby aggravating pathological conditions such as atherosclerosis (Zhang et al. 2020). Taken together, our findings indicate that migration is a sensitive and functionally relevant endpoint for NPL toxicity in endothelial cells, with real-life polymers exerting the strongest inhibitory effects.

Conclusions

This study provides a systematic comparison of NPLs of increasing environmental relevance, ranging from model spherical PS to irregular, polydisperse PET derived from post-consumer bottles, and their effects on primary human endothelial cells. By standardizing particle size and exposure conditions, we were able to assess how increasing environmental significance, defined by particle morphology, size heterogeneity, and colloidal behavior, influences endothelial responses. All NPLs were efficiently internalized by HUVECs, although their intracellular distribution varied, suggesting the involvement of distinct uptake pathways depending on their physicochemical characteristics.

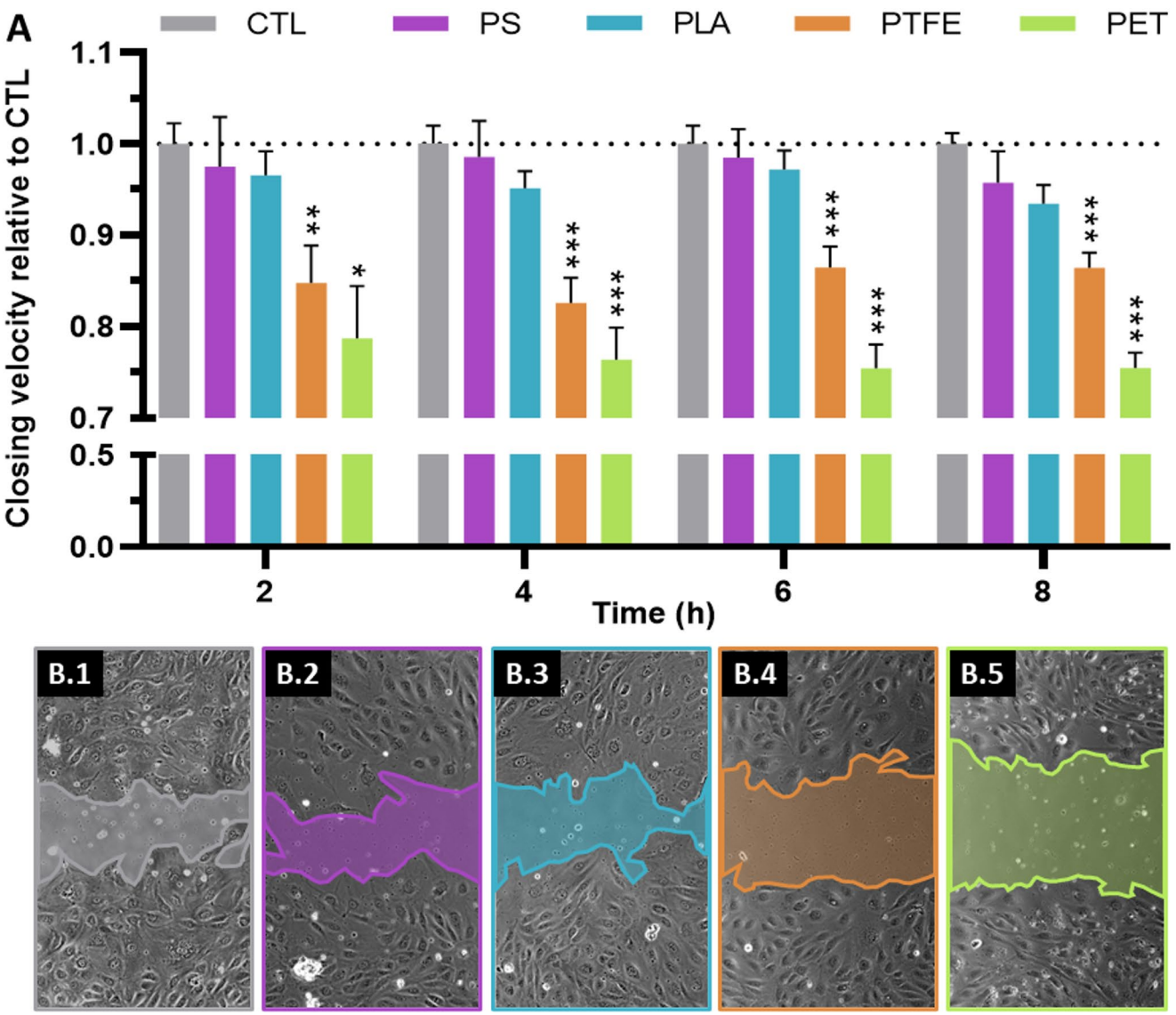


Fig. 6 Effect of NPLs on HUVEC migration. **A** Closing velocity of HUVECs exposed for 24 h to NPLs (25 µg/mL) during wound healing assay, expressed as fold change relative to the negative control (CTL, set to 1). Data correspond to 2, 4, 6, and 8 h after scratch. Bars represent mean ± SEM from ≥4 independent experiments. Statistical analysis was performed by one-way ANOVA followed by Dunnett's test (vs. control) and Tukey's test (among NPLs). *$p \leq 0.05$, **$p \leq 0.01$, ***$p \leq 0.001$. Complete results of pairwise comparisons for each time point are provided in Supplementary Table 1. **B** Representative phase-contrast images of wound areas at 8 h after scratch: **B.1** CTL, **B.2** PS-NPLs, **B.3** PLA-NPLs, **B.4** PTFE-NPLs, and **B.5** PET-NPLs. Colored lines delineate the wound edges used for quantification

None of the NPLs induced cytotoxicity or genotoxicity after 24 h of exposure at 25 µg/mL. However, functional assays revealed clear differences related to NPL properties. Spherical and monodisperse PS- and PLA-NPLs produced negligible alterations, whereas irregular, heterogeneous, and polydisperse PTFE- and PET-NPLs triggered functionally relevant signs of endothelial stress. Specifically, PET-NPLs promoted IL-6 secretion and intracellular cholesterol accumulation, while both PTFE- and PET-NPLs significantly reduced cell migration, compromising the wound-healing capacity of endothelial monolayers. The observed gradient of biological responses supports the notion that particle shape, heterogeneity, and colloidal behavior are key determinants of NPL bioactivity. Altogether, our findings establish a potential link between real-life NPLs and early vascular impairment through inflammation, cholesterol dysregulation, and migration inhibition. They also emphasize the limitations of relying exclusively on idealized, monodisperse NPLs for hazard assessment. Incorporating environmentally realistic NPLs into toxicological testing is essential to predict genuine human health risks and to design regulatory frameworks that capture the true complexity of plastic pollution. To extend this work, future studies should include NPLs with a broader diversity of shapes, such as

fibers or fragments, and employ more advanced experimental systems, particularly endothelial barriers and microfluidic tissue-engineered vascular models to better reproduce physiological conditions. Beyond these controlled in vitro settings, addressing more complex atherosclerosis-related outcomes that are outside the scope of short-term static HUVEC monocultures (e.g., plaque formation and stenosis-related processes), will ultimately require in vivo studies and human biomonitoring approaches to capture systemic, long-term and flow-dependent mechanisms. Such approaches may refine our understanding of NPL-induced vascular dysfunction and its potential cardiovascular implications.

Supplementary Information The online version contains supplementary material available at https://doi.org/10.1007/s00204-026-04417-9.

Acknowledgements JMP, and MMR hold Ph.D. fellowships from the Generalitat de Catalunya and UAB. AV was supported by a Ph.D. fellowship from the National Agency for Research and Development (ANID), CONICYT PFCHA / DOCTORADO BECAS CHILE / 2020 -72210237. AGR (Academic record 2020 BP 00177), MA (Academic record 2022 BP 00026), and IB (Academic record 2023-BP-00212) were granted with a Beatriu de Pinós Postdoctoral Program from the Secretariat of Universities and Research of the Department of Business and Knowledge of the Government of Catalunya. AH is supported by the ICREA ACADEMIA Programme.

Author contribution RM, AH, and AGR planned the experiments. JMP wrote the first manuscript. JMP, MMR, AV, CAS, IB, and MA carried out the experimental part. JMP, and MMR analyzed the data, carried out the statistical analysis, and prepared tables/figures. JFF provide PLA samples. MMR, RM, and AH wrote the final manuscript. All authors read and agree with the final version.

Funding Open Access Funding provided by Universitat Autonoma de Barcelona. This study has received funding from the European Union's Horizon 2020 research and innovation programme under grant agreement No 965196. This work was partially supported by the Spanish Ministry of Science and Innovation (PID2020-116789RB-C43) and the Generalitat de Catalunya (2021-SGR-00731).

Declarations

Conflict of interest The authors declare that they have no known competing financial interests or personal relationships that could have appeared to influence the work reported in this paper.

Open Access This article is licensed under a Creative Commons Attribution 4.0 International License, which permits use, sharing, adaptation, distribution and reproduction in any medium or format, as long as you give appropriate credit to the original author(s) and the source, provide a link to the Creative Commons licence, and indicate if changes were made. The images or other third party material in this article are included in the article's Creative Commons licence, unless indicated otherwise in a credit line to the material. If material is not included in the article's Creative Commons licence and your intended use is not permitted by statutory regulation or exceeds the permitted use, you will need to obtain permission directly from the copyright holder. To view a copy of this licence, visit http://creativecommons.org/licenses/by/4.0/.

References

Abass D, Alaraby M, Elkady EF, Morataya-Reyes M, Banaei G, Martín-Pérez J, Rubio L, Barguilla I, Marcos R, Hernández A, García-Rodríguez A (2025) Polytetrafluoroethylene (PTFE, Teflon) micro/nanoplastics induce oxidative stress, mitochondrial damage, and genotoxicity in human intestinal cells. J Hazard Mater 499:140255. https://doi.org/10.1016/j.jhazmat.2025.140255

Ahamed M, Javed Akhtar M (2024) Cytotoxic effect of polystyrene nanoplastics in human umbilical vein endothelial cells (HUVECs) and normal rat kidney cells (NRK52E). J King Saud Univ Sci 36(11):103505. https://doi.org/10.1016/J.JKSUS.2024.103505

Alaraby M, Abass D, Farre M, Hernández A, Marcos R (2024) Are bioplastics safe? Hazardous effects of polylactic acid (PLA) nanoplastics in *Drosophila*. Sci Total Environ 919:170592. https://doi.org/10.1016/J.SCITOTENV.2024.170592

Alzaben M, Burve R, Loeschner K, Møller P, Roursgaard M (2023) Nanoplastics from ground polyethylene terephthalate food containers: genotoxicity in human lung epithelial A549 cells. Mut Res/Gen Toxicol Environ Mutagen 892:503705. https://doi.org/10.1016/J.MRGENTOX.2023.503705

Annangi B, Bach J, Vales G, Rubio L, Marcos R, Hernández A (2015) Long-term exposures to low doses of cobalt nanoparticles induce cell transformation enhanced by oxidative damage. Nanotoxicology 9(2):138–147. https://doi.org/10.3109/17435390.2014.900582

Annangi B, Villacorta A, Vela L, Tavakolpournegari A, Marcos R, Hernández A (2023) Effects of true-to-life PET nanoplastics using primary human nasal epithelial cells. Environ Toxicol Pharmacol 100:104140. https://doi.org/10.1016/J.ETAP.2023.104140

Arribas Arranz J, Villacorta A, Rubio L, García-Rodríguez A, Sánchez G, Llorca M, Farre M, Ferrer JF, Marcos R, Hernández A (2024) Kinetics and toxicity of nanoplastics in *ex vivo* exposed human whole blood as a model to understand their impact on human health. Sci Total Environ 948:174725. https://doi.org/10.1016/J.SCITOTENV.2024.174725

Banaei G, García-Rodríguez A, Tavakolpournegari A, Martín-Pérez J, Villacorta A, Marcos R, Hernández A (2023) The release of polylactic acid nanoplastics (PLA-NPLs) from commercial teabags. Obtention, characterization, and hazard effects of real-life PLA-NPLs. J Hazard Mater 458:131899. https://doi.org/10.1016/J.JHAZMAT.2023.131899

Blechinger J, Bauer AT, Torrano AA, Gorzelanny C, Bräuchle C, Schneider SW (2013) Uptake kinetics and nanotoxicity of silica nanoparticles are cell type dependent. Small 9(23):3970–3980. https://doi.org/10.1002/SMLL.201301004

Bon C, Maretti A, Pulze L, Paris N, Santoro O, Pragliola S, Izzo L, Baranzini N, Grimaldi A (2025) The exposure to polypropylene micro- and nanoplastics impairs wound healing and tissue regeneration in the leech *Hirudo verbana*. Microplastics 4(3):56. https://doi.org/10.3390/MICROPLASTICS4030056

Cao Y, Gong Y, Liu L, Zhou Y, Fang X, Zhang C, Li Y, Li J (2017) The use of human umbilical vein endothelial cells (HUVECs) as an *in vitro* model to assess the toxicity of nanoparticles to endothelium: a review. J Appl Toxicol 37(12):1359–1369. https://doi.org/10.1002/JAT.3470

Cao J, Yang Q, Jiang J, Dalu T, Kadushkin A, Singh J, Fakhrullin R, Wang F, Cai X, Li R (2022) Coronas of micro/nano plastics: a key determinant in their risk assessments. Part Fibre Toxicol 19(1):1–25. https://doi.org/10.1186/S12989-022-00492-9

Cimmino G, Conte S, Morello M, Pellegrino G, Marra L, Morello A, Nicoletti G, De Rosa G, Golino P, Cirillo P (2022) Vitamin D inhibits IL-6 pro-atherothrombotic effects in human endothelial cells: a potential mechanism for protection against COVID-19

infection? J Cardiovasc Dev Dis 9(1):27. https://doi.org/10.3390/JCDD9010027

Cole M, Gomiero A, Jaén-Gil A, Haave M, Lusher A (2024) Microplastic and PTFE contamination of food from cookware. Sci Total Environ 929:172577. https://doi.org/10.1016/J.SCITOTENV.2024.172577

Collins A, Møller P, Gajski G, Vodenková S, Abdulwahed A, Anderson D, Bankoglu EE, Bonassi S, Boutet-Robinet E, Brunborg G et al (2023) Measuring DNA modifications with the comet assay: a compendium of protocols. Nat Protoc 18(3):929–989. https://doi.org/10.1038/s41596-022-00754-y

da Silva J, Jesus S, Bernardi N, Colaço M, Borges O (2019) Poly(D, L-lactic acid) nanoparticle size reduction increases its immunotoxicity. Front Bioeng Biotechnol 7:137. https://doi.org/10.3389/FBIOE.2019.00137

De Sousa M, Susnik E, Drasler B, Taladriz-Blanco P, Petri-Fink A, Rothen-Rutishauser B (2021) Understanding nanoparticle endocytosis to improve targeting strategies in nanomedicine. Chem Soc Rev 50(9):5397–5434. https://doi.org/10.1039/d0cs01127d

Drzewinska K, Belz S (2024) Stakeholder survey on microplastics materials needs. Publications Office of the European Union. https://data.europa.eu/doi/10.2760/18013

El Hadri H, Gigault J, Maxit B, Grassl B, Reynaud S (2020) Nanoplastic from mechanically degraded primary and secondary microplastics for environmental assessments. NanoImpact 17:100206. https://doi.org/10.1016/j.impact.2019.100206

Ferreira LF, Picco AS, Galdino FE, Albuquerque LJC, Berret JF, Cardoso MB (2022) Nanoparticle-protein interaction: demystifying the correlation between protein corona and aggregation phenomena. ACS Appl Mater Interfaces 14(25):28559–28569. https://doi.org/10.1021/acsami.2C05362

Fu Y, Fan M, Xu L, Wang H, Hu Q, Jin Y (2022) Amino-functionalized polystyrene nano-plastics induce mitochondria damage in human umbilical vein endothelial cells. Toxics 10(5):215. https://doi.org/10.3390/toxics10050215

García-Rodríguez A, Rubio L, Vila L, Xamena N, Velázquez A, Marcos R, Hernández A (2019) The comet assay as a tool to detect the genotoxic potential of nanomaterials. Nanomaterials 9(10):1385. https://doi.org/10.3390/nano9101385

García-Rodríguez A, Gutiérrez J, Villacorta A, Arribas Arranz J, Romero-Andrada I, Lacoma A, Marcos R, Hernández A, Rubio L (2024) Polylactic acid nanoplastics (PLA-NPLs) induce adverse effects on an *in vitro* model of the human lung epithelium: The Calu-3 air-liquid interface (ALI) barrier. J Hazard Mater 475:134900.

Gholinejad Z, Khadem Ansari MH, Rasmi Y (2019) Titanium dioxide nanoparticles induce endothelial cell apoptosis via cell membrane oxidative damage and p38, PI3K/Akt, NF-κB signaling pathways modulation. J Trace Elem Med Biol 54:27–35. https://doi.org/10.1016/j.jtemb.2019.03.008

Hu J, Zhu Y, Zhang J, Xu Y, Wu J, Zeng W, Lin Y, Liu X (2022) The potential toxicity of polystyrene nanoplastics to human trophoblasts *in vitro*. Environ Pollut 311:119924. https://doi.org/10.1016/j.envpol.2022.119924

Hussain KA, Romanova S, Okur I, Zhang D, Kuebler J, Huang X, Wang B, Fernandez-Ballester L, Lu Y, Schubert M, Li Y (2023) Assessing the release of microplastics and nanoplastics from plastic containers and reusable food pouches: implications for human health. Environ Sci Technol 57(26):9782–9792. https://doi.org/10.1021/acs.est.3C01942

Jahedi F, Jaafarzadeh Haghighi Fard N (2025) Micro- and nanoplastic toxicity in humans: Exposure pathways, cellular effects, and mitigation strategies. Toxicol Rep 14:102043. https://doi.org/10.1016/j.toxrep.2025.102043

Jensen KA, Kembouche Y, Christiansen E, Jacobsen NR, Wallin H, Guiot C, Spalla O, Witschger O (2009) WP4: Physicochemical characterisation of manufactured nanomaterials (MNs) and exposure media (EMs). Deliverable 3: Final protocol for producing suitable MN exposure media. NRCWE. https://www.nanogenotox.eu

Kang S, Tanaka T, Inoue H, Ono C, Hashimoto S, Kioi Y, Matsumoto H, Matsuura H, Matsubara T, Shimizu K, Ogura H, Matsuura Y, Kishimoto T (2020) IL-6 trans-signaling induces plasminogen activator inhibitor-1 from vascular endothelial cells in cytokine release syndrome. Proc Nat Acad Sci USA 117(36):22351–22356. https://doi.org/10.1073/pnas.2010229117

Kuhn DA, Vanhecke D, Michen B, Blank F, Gehr P, Petri-Fink A, Rothen-Rutishauser B (2014) Different endocytotic uptake mechanisms for nanoparticles in epithelial cells and macrophages. Beilstein J Nanotechnol 5(1):1625–1636. https://doi.org/10.3762/bjnano.5.174

Landrigan PJ, Dunlop S, Treskova M, Raps H, Symeonides C, Muncke J, Spring M, Stegeman J, Almroth BC, Chiles TC et al (2025) The Lancet Countdown on health and plastics. Lancet 406(10507):1044–1062. https://doi.org/10.1016/S0140-6736(25)01447-3

Lee HS, Amarakoon D, Wei CI, Choi KY, Smolensky D, Lee SH (2021) Adverse effect of polystyrene microplastics (PS-MPs) on tube formation and viability of human umbilical vein endothelial cells. Food Chem Toxicol 154:112356. https://doi.org/10.1016/j.fct.2021.112356

Leslie HA, van Velzen MJM, Brandsma SH, Vethaak AD, Garcia-Vallejo JJ, Lamoree MH (2022) Discovery and quantification of plastic particle pollution in human blood. Environ Int 163:107199. https://doi.org/10.1016/j.envint.2022.107199

Litvinov DY, Savushkin EV, Dergunov AD (2018) Intracellular and plasma membrane events in cholesterol transport and homeostasis. J Lipids 2018:1–22. https://doi.org/10.1155/2018/3965054

Liu L, Xu K, Zhang B, Ye Y, Zhang Q, Jiang W (2021) Cellular internalization and release of polystyrene microplastics and nanoplastics. Sci Total Environ 779:146523. https://doi.org/10.1016/j.scitotenv.2021.146523

Lu YY, Li H, Ren H, Zhang X, Huang F, Zhang D, Huang Q, Zhang X (2022) Size-dependent effects of polystyrene nanoplastics on autophagy response in human umbilical vein endothelial cells. J Hazard Mater 421:126770. https://doi.org/10.1016/j.jhazmat.2021.126770

Lv J, He Q, Yan Z, Xie Y, Wu Y, Li A, Zhang Y, Li J, Huang Z (2024) Inhibitory impact of prenatal exposure to nano-polystyrene particles on the MAP2K6/p38 MAPK axis inducing embryonic developmental abnormalities in mice. Toxics 12(5):370. https://doi.org/10.3390/toxics12050370

Lyu J, Yang EJ, Head SA, Ai N, Zhang B, Wu C, Li RJ, Liu Y, Yang C, Dang Y, Kwon HJ, Ge W, Liu JO, Shim JS (2017) Pharmacological blockade of cholesterol trafficking by cepharanthine in endothelial cells suppresses angiogenesis and tumor growth. Cancer Lett 409:91–103. https://doi.org/10.1016/j.canlet.2017.09.009

Ma L, Wu Z, Lu Z, Yan L, Dong X, Dai Z, Sun R, Hong P, Zhou C, Li C (2024) Differences in toxicity induced by the various polymer types of nanoplastics on HepG2 cells. Sci Total Environ 918:170664. https://doi.org/10.1016/j.scitotenv.2024.170664

Martello A, Platt FM, Eden ER (2020) Staying in touch with the endocytic network: the importance of contacts for cholesterol transport. Traffic 21(5):354–363. https://doi.org/10.1111/TRA.12726

Martín-Pérez J, Villacorta A, Banaei G, Morataya-Reyes M, Tavakolpournegari A, Marcos R, Hernández A, García-Rodriguez A (2024) Hazard assessment of nanoplastics is driven by their surface-functionalization. Effects in human-derived primary endothelial cells. Sci Total Environ 934:173236. https://doi.org/10.1016/j.scitotenv.2024.173236

Martín-Pérez J, Villacorta A, Gutiérrez J, Egea R, Morataya-Reyes M, Cassú-Casadevall M, Marcos R, Hernández A, García-Rodríguez

A (2025) Size-dependent effects of polystyrene nanoplastics on human primary endothelial cell function. Span J Environ Mutagen Genomics 29(1):31. https://ojs.diffundit.com/index.php/sema/issue/view/95/12 Conference abstract

Morataya-Reyes M, Villacorta A, Gutiérrez-García J, Egea R, Martín-Pérez J, Barguilla I, Marcos R, Hernández A (2025a) The long-term in vitro co-exposure of polyethylene terephthalate (PET) nanoplastics and cigarette smoke condensate exacerbates the induction of carcinogenic traits. J Hazard Mater 493:138359. https://doi.org/10.1016/j.jhazmat.2025.138359

Morataya-Reyes M, Villacorta A, Arranz JA, Martín-Pérez J, Ferrer JF, Pastor S, Egea R, Barguilla I, Marcos R, Hernández A (2025b) Exploring the impact of nanoplastics on human hepatic cells: dynamics of internalization and harmful effects in HuH-7 cells. Environ Sci Nano https://doi.org/10.1039/d5en00434A.

Morris EJ, Geller HM (1996) Induction of neuronal apoptosis by camptothecin, an inhibitor of DNA topoisomerase-I: evidence for cell cycle-independent toxicity. J Cell Biol 134(3):757–770. https://doi.org/10.1083/JCB.134.3.757

Nayanathara Thathsarani Pilapitiya PGC, Ratnayake AS (2024) The world of plastic waste: a review. Clean Mater 11:100220. https://doi.org/10.1016/j.clema.2024.100220

Ncube LK, Ude AU, Ogunmuyiwa EN, Zulkifli R, Beas IN (2021) An overview of plastic waste generation and management in food packaging industries. Recycling 6(1):1–25. https://doi.org/10.3390/recycling6010012

Omoigui S (2007) The Interleukin-6 inflammation pathway from cholesterol to aging - Role of statins, bisphosphonates and plant polyphenols in aging and age-related diseases. Immun Ageing 4:1. https://doi.org/10.1186/1742-4933-4-1

Płuciennik K, Sicińska P, Misztal W, Bukowska B (2024) Important factors affecting induction of cell death, oxidative stress and DNA damage by nano- and microplastic particles *in vitro*. Cells 13(9):768. https://doi.org/10.3390/cells13090768

Prattichizzo F, Ceriello A, Pellegrini V, la Grotta R, Graciotti L, Olivieri F, Paolisso P, D'Agostino B, Iovino P, Balestrieri ML, Rajagopalan S, Landrigan PJ, Marfella R, Paolisso G (2024) Micro-nanoplastics and cardiovascular diseases: evidence and perspectives. Eur Heart J 45(38):4099–4110. https://doi.org/10.1093/eurheartj/ehae552

Rajendran D, Chandrasekaran N (2023) Journey of micronanoplastics with blood components. RSC Adv 13(45):31435–31459. https://doi.org/10.1039/d3ra05620A

Rubio L, Barguilla I, Domenech J, Marcos R, Hernández A (2020) Biological effects, including oxidative stress and genotoxic damage, of polystyrene nanoparticles in different human hematopoietic cell lines. J Hazard Mater 398:122900. https://doi.org/10.1016/j.jhazmat.2020.122900

Sabourian P, Yazdani G, Ashraf SS, Frounchi M, Mashayekhan S, Kiani S, Kakkar A (2020) Effect of physico-chemical properties of nanoparticles on their intracellular uptake. Int J Mol Sci 21(21):8019. https://doi.org/10.3390/IJMS21218019

Sawyer LC, Grubb DT, Meyers GF (2008) Polymer microscopy, 3d edn, pp 1–540. https://doi.org/10.1007/978-0-387-72628-1

Schindelin J, Arganda-Carreras I, Frise E, Kaynig V, Longair M, Pietzsch T, Preibisch S, Rueden C, Saalfeld S, Schmid B, Tinevez JY, White DJ, Hartenstein V, Eliceiri K, Tomancak P, Cardona A (2012) Fiji: An open-source platform for biological-image analysis. Nat Methods 9(7):676–682. https://doi.org/10.1038/nmeth.2019

Suarez-Arnedo A, Figueroa FT, Clavijo C, Arbeláez P, Cruz JC, Muñoz-Camargo C (2020) An image J plugin for the high throughput image analysis of *in vitro* scratch wound healing assays. PLoS ONE 15(7):e0232565. https://doi.org/10.1371/journal.pone.0232565

Suzuki M, Hashizume M, Yoshida H, Mihara M (2010) Anti-inflammatory mechanism of tocilizumab, a humanized anti-IL-6R antibody: effect on the expression of chemokine and adhesion molecule. Rheumatol Int 30(3):309–315. https://doi.org/10.1007/S00296-009-0953-0

Tavakolpournegari A, Annangi B, Villacorta A, Banaei G, Martin J, Pastor S, Marcos R, Hernández A (2023) Hazard assessment of different-sized polystyrene nanoplastics in hematopoietic human cell lines. Chemosphere 325:138360. https://doi.org/10.1016/j.chemosphere.2023.138360

Villacorta A, Rubio L, Alaraby M, López-Mesas M, Fuentes-Cebrian V, Moriones OH, Marcos R, Hernández A (2022) A new source of representative secondary PET nanoplastics. Obtention, characterization, and hazard evaluation. J Hazard Mater 439:129593. https://doi.org/10.1016/j.jhazmat.2022.129593

Villacorta A, Cazorla-Ares C, Fuentes-Cebrian V, Valido IH, Vela L, Carrillo-Navarrete F, Morataya-Reyes M, Mejia-Carmona K, Pastor S, Velázquez A, Arribas Arranz J, Marcos R, López-Mesas M, Hernández A (2024) Fluorescent labeling of micro/nanoplastics for biological applications with a focus on true-to-life tracking. J Hazard Mater 476:135134. https://doi.org/10.1016/j.jhazmat.2024.135134

Voigt J, Christensen J, Shastri VP (2014) Differential uptake of nanoparticles by endothelial cells through polyelectrolytes with affinity for caveolae. Proc Nat Acad Sci USA 111(8):2942–2947. https://doi.org/10.1073/pnas.1322356111

Wan S, Wang X, Chen W, Xu Z, Zhao J, Huang W, Wang M, Zhang H (2024) Polystyrene nanoplastics activate autophagy and suppress trophoblast cell migration/invasion and migrasome formation to induce miscarriage. ACS Nano 18(4):3733–3751. https://doi.org/10.1021/acsnano.3C11734

Weber A, Schwiebs A, Solhaug H, Stenvik J, Nilsen AM, Wagner M, Relja B, Radeke HH (2022) Nanoplastics affect the inflammatory cytokine release by primary human monocytes and dendritic cells. Environ Int 163:107173. https://doi.org/10.1016/j.envint.2022.107173

Wilson BK, Prud'homme RK (2021) Nanoparticle size distribution quantification from transmission electron microscopy (TEM) of ruthenium tetroxide stained polymeric nanoparticles. J Colloid Interface Sci 604:208–220. https://doi.org/10.1016/j.jcis.2021.04.081

Xue J, Zhang Z, Sun Y, Jin D, Guo L, Li X, Zhao D, Feng X, Qi W, Zhu H (2023) Research progress and molecular mechanisms of endothelial cells inflammation in vascular-related diseases. J Inflamm Res 16:3593–3617. https://doi.org/10.2147/jir.S418166

Zegeye MM, Matic L, Lengquist M, Hayderi A, Grenegård M, Hedin U, Sirsjö A, Ljungberg LU, Kumawat AK (2023) Interleukin-6 trans-signaling induced laminin switch contributes to reduced trans-endothelial migration of granulocytic cells. Atherosclerosis 371:41–53. https://doi.org/10.1016/j.atherosclerosis.2023.03.010

Zhang S, Zhu X, Li G (2020) E2F1/SNHG7/miR-186-5p/MMP2 axis modulates the proliferation and migration of vascular endothelial cells in atherosclerosis. Life Sci 257:118013. https://doi.org/10.1016/J.LFS.2020.118013

Zhang T, Liao Y, Ling J, Zhang J, Zhang D, Yin X, Yu P, Liu X (2025) Tiny trouble: microplastics, nanoplastics, and their heartfelt impact on cardiovascular health. Cardiovasc Res 121(7):992–1010. https://doi.org/10.1093/CVR/CVAF068

Zhao X, Chang S, Long J, Li J, Li X, Cao Y (2019) The toxicity of multi-walled carbon nanotubes (MWCNTs) to human endothelial cells: The influence of diameters of MWCNTs. Food Chem Toxicol 126:169–177. https://doi.org/10.1016/J.FCT.2019.02.026

Ziegler DV, Czarnecka-Herok J, Vernier M, Scholtes C, Camprubi C, Huna A, Massemin A, Griveau A, Machon C, Guitton J, Rieusset J, Vigneron AM, Giguère V, Martin N, Bernard D (2024) Cholesterol biosynthetic pathway induces cellular senescence through

ERRα. Npj Aging 10(1):5. https://doi.org/10.1038/S41514-023-00128-Y

Publisher's note Springer Nature remains neutral with regard to jurisdictional claims in published maps and institutional affiliations.

4

Discussion

4.1. Overview of Key Findings and Thesis Logic

Given the evidence that MNPLs can reach the vascular compartment, this Thesis examines NPL-induced endothelial dysfunction in a primary HUVEC model. We first established a coherent mechanistic-to-functional picture of endothelial injury induced by NPL exposure under standardized conditions. We then tested whether this response was largely generic or instead governed by particle physicochemical properties. To do so, we implemented a progressive material strategy, starting with controlled PS reference particles to isolate the roles of surface functionalization and nanoscale size, and then extending to materials with increasing environmental realism, including real-life PET fragments obtained from post-consumer water bottles. Together, this approach showed that endothelial responses to NPLs were not uniform but strongly shaped by NPL physicochemical properties.

Across our studies, NPLs primarily induced a sublethal endothelial dysfunction phenotype. The response was initiated by substantial cellular uptake and intracellular accumulation, followed by molecular changes, including transcriptomic alterations and oxidative and genotoxic stress. These changes were associated with functional impairment, notably disruption of lipid homeostasis and reduced endothelial repair capacity (migration and angiogenesis). This phenotype is consistent with endothelial dysfunction as an early event in the development of cardiovascular disease.

Specifically, each study dissected a distinct physicochemical driver. In Paper 1, surface functionalization altered uptake dynamics and produced distinct patterns of viability, ROS generation, and genotoxicity, with PS-A-NPLs uniquely reducing viability under our conditions. In Paper 2, nanoscale size (30–100 nm) revealed a shared core transcriptomic response, but also distinct size-specific programs, with 30 nm PS-C-NPLs showing the most divergent signature. Targeted functional and mechanistic assays were consistent with these RNA-seq patterns, including size-dependent differences in genotoxicity, cholesterol homeostasis, migration/angiogenesis, and IL-6 modulation. In Paper 3, environmental realism of NPLs shifted the dominant sublethal outcomes: under standardized exposure conditions, 200 nm PS, PLA, PTFE,

and PET NPLs did not induce acute cytotoxicity or DNA damage, yet irregular PTFE-NPLs and real-life PET-NPLs impaired migration, and PET-NPLs were the only ones associated with increased IL-6 secretion and intracellular cholesterol accumulation.

4.2. Methodological Framework and Study Design

This Thesis was designed to characterize the effects of NPLs on the vascular endothelium and to determine how physicochemical properties shape these responses. Defining these property–effect relationships is essential for better understanding potential impacts on human health and for guiding mitigation strategies, including the protection of occupationally exposed groups and the use of safe-by-design approaches for safer materials. To address this question, we established a framework combining a standardized primary endothelial model, an acute exposure window, and a progressive material strategy. This approach enabled us to capture early functional and mechanistic events and to map how particle properties systematically modulate these outcomes. The following subsections justify the selection of primary HUVECs, the rationale for acute exposure, and the strategy for selecting test materials.

4.2.1. PRIMARY HUVECS AS A PHYSIOLOGICALLY RELEVANT ENDOTHELIAL MODEL

HUVECs were selected as the experimental platform because they are among the most widely used primary human endothelial models for studying endothelial dysfunction. Since their initial isolation, HUVECs have been extensively characterized, providing a robust and well-documented framework to interrogate endothelial processes central to this Thesis, including inflammatory signaling and angiogenic competence (Medina-Leyte et al., 2020). Importantly, they have also been widely applied in vascular nanotoxicology. Cao et al. (2017) synthesized evidence demonstrating that HUVECs exhibit key nanoparticle-induced effects, including cytotoxicity, oxidative stress, and inflammatory activation, supporting their suitability as a reference system for endothelial hazard assessment. A further rationale for this

choice is the use of a primary endothelial model rather than an immortalized line (e.g., EA.hy926). Transformed endothelial lines can exhibit phenotypic drift and metabolic alterations due to transformation and long-term culture, which may confound mechanistic interpretation (Uruski et al., 2021). In contrast, primary HUVECs better preserve native endothelial features required for the complex endpoints assessed in this Thesis (Uruski et al., 2021), thereby supporting the physiological relevance of the interpretation of NPL-induced effects.

To ensure rigorous cross-study comparability, a standardized experimental protocol was maintained across all chapters. Cells were consistently used at low passage (P5–P6) to support phenotypic stability and minimize alterations associated with replicative senescence (Yi et al., 2020). Experiments followed a uniform protocol comprising a 48-h growth phase and a 24-h exposure window. This design ensured reproducible monolayer conditions and facilitated the capture of early mode-of-action events under standardized culture settings. Given that endothelial metabolism contributes to cellular plasticity and responsiveness (Eelen et al., 2015), maintaining consistent culture timing and passage number was also important for interpreting energy-dependent processes, including particle uptake and downstream cellular responses.

4.2.2. THE RATIONALE FOR ACUTE EXPOSURE

In this Thesis, we used a 24-h acute exposure window to capture early mode-of-action signals before longer incubations could engage compensatory programs or progress toward culture deterioration (Visalli et al., 2021). This rationale is supported by the rapid uptake kinetics observed in HUVECs. Consistent with previous reports (Blechinger et al., 2013), our own data show that intracellular burden is established quickly after exposure to PS-NPLs across surface functionalizations and nanoscale sizes: a near-complete fraction of cells became particle-positive within 20 min (Paper 1, Fig. 3A; Paper 2, Fig. 3B), with uptake approaching a plateau by 2 h (Paper 1, Fig. 3B; Paper 2, Fig. 3C). This rapid internalization supports 24 h as an appropriate window to interrogate immediate consequences of intracellular handling, including early oxidative stress and downstream signaling, before primary responses are

obscured by secondary adaptation. Importantly, this efficient uptake is facilitated by the nanoscale size range examined here (≤200 nm). In contrast, larger particles can remain predominantly surface-associated in HUVECs and show reduced intracellular accumulation (Lu et al., 2022). Accordingly, the 24-h window was sufficient in our studies to capture transcriptomic changes and early inflammatory signaling, as well as sublethal functional alterations in endothelial repair capacity, including impaired migration and angiogenesis.

Besides the biological rationale, dosimetry is a key technical consideration when working with nanoparticles. In static *in vitro* systems, chronic exposures typically require repeated medium changes and re-administration of particles, which complicates the estimation of the effective dose delivered to cells over time (Teeguarden et al., 2007). In contrast, a 24-h exposure enables a single administration under standardized conditions, improving reproducibility and facilitating cross-condition comparisons. Moreover, limiting the exposure duration reduces proliferation-related dilution effects, since cell division can redistribute internalized particles between daughter cells and lower the intracellular burden per cell (Bourquin et al., 2019). Taken together, this acute design provides a practical balance between mechanistic interpretability and experimental control for comparing NPL physicochemical properties and materials.

4.2.3. PROGRESSIVE COMPLEXITY APPROACH FOR NPL MATERIAL SELECTION

Literature on MNPL toxicity in *in vitro* systems remains difficult to compare across studies due to substantial methodological variability, particularly in effective particle size, surface charge, dosimetry, and culture conditions (Viana et al., 2025). As a result, inter-study comparisons are often limited, and it remains challenging to extract general rules linking MNPL physicochemical properties to biological outcomes. To address this, we implemented a stepwise material strategy grounded in two rationales. First, we used controlled PS-NPLs spheres as a reference system, as their high uniformity enables head-to-head comparisons in which a single variable (surface functionalization or nanoscale size) can be modified while minimizing confounding effects from morphology

or size dispersion. Second, we extended the work to a standardized 200 nm panel that included PS-NPLs alongside polymers spanning increasing environmental realism. By moving from idealized spherical particles to more heterogeneous and real-life materials under comparable exposure conditions, this approach allowed us to evaluate how increasing environmental realism modulates the endothelial response profile.

PS was selected as the reference platform because it dominates the *in vitro* NPLs literature, accounting for approximately 90% of published studies (Viana et al., 2025), and has also been reported among the polymers detected in human blood samples (Leslie et al., 2022). Importantly, PS is readily available from commercial sources, including fluorescently labeled formats that support quantitative uptake measurements across complementary techniques (Paget et al., 2015). Within this controlled PS framework, Paper 1 compared pristine, carboxylated, and aminated particles to span distinct surface chemistries and charge states and test how these properties shape uptake dynamics and downstream toxicity endpoints. In Paper 2, we focused on 30, 50, and 100 nm PS-NPLs to resolve size effects across the nanoscale range defined by the European Union (More et al., 2021), addressing whether response heterogeneity exists within the nanoscale domain itself beyond the commonly studied contrasts between nanoscale and microscale plastics (e.g., 100 nm vs 10 µm) (Cheng et al., 2025). We used carboxylated particles as a mechanistically informative reference, given their lower cytotoxicity and higher uptake efficiency relative to pristine PS. Finally, the 200 nm panel used in Paper 3 introduced environmental complexity in a graded manner. PS served as the most uniform spherical reference; PLA retained a spherical morphology but with greater size heterogeneity; PTFE introduced irregularity and higher polydispersity; and post-consumer real-life PET represented the highest level of realism, with broad size dispersion and aggregation in biological media. This increase in complexity enabled direct comparisons of how deviations from idealized spheres shift endothelial response patterns under comparable exposure conditions.

Together, this design established a controlled reference framework and then introduced increasing environmental complexity. This structure underpins the

following sections, which first synthesize the functional impairments observed across materials and then integrate the mechanistic sequence and physicochemical determinants underlying these outcomes.

4.3. NPL-Induced Functional Impairment in Endothelial Cells

Across our three studies, NPL exposure predominantly elicited endothelial dysfunction under subcytotoxic conditions. This section first summarizes cytotoxicity outcomes and then synthesizes NPL-induced functional impairments in lipid homeostasis and metabolism, as well as endothelial repair capacity (migration and angiogenic remodeling), which were consistently affected across the experimental framework.

4.3.1. VIABILITY AND CYTOTOXICITY

In our dataset, acute NPL exposure generally preserved endothelial viability, thereby defining a predominantly subcytotoxic working window. This provides a robust context in which downstream changes reflect endothelial dysfunction rather than widespread cell death. Methodologically, viability was assessed using complementary readouts, combining Coulter-based viable cell counting (time-course and dose–response designs) with flow-cytometric Annexin V/PI profiling. Across these approaches, the overall conclusion was that most tested conditions retained high viability after exposure. Notably, 50 nm PS-A-NPLs were the only condition that met the ISO 10993-5 cytotoxicity criterion (>30% reduction) (ISO, 2009), specifically at 100 µg/mL after 12 h and 24 h, whereas the remaining exposures produced low or no cytotoxicity under the tested settings (Paper 1, Fig. 2; Paper 2, Supplementary Fig. S2; Paper 3, Fig.3A).

Overall, this predominantly subcytotoxic profile is consistent with current *in vitro* evidence for PS-NPLs (Viana et al., 2025) and extends beyond PS to other polymers tested under environmentally relevant exposure conditions. For instance, PLA-, PTFE-, and PET-NPLs have been reported to produce negligible acute cytotoxicity in different human epithelial barrier models (nasal and intestinal) at 10–100 µg/mL, while still inducing sublethal hazards such as

genotoxicity (Annangi et al., 2023b; Banaei et al., 2023; Abass et al., 2025). Importantly, cationic surfaces constitute a clear exception to this sublethal profile. PS-A-NPLs have been associated with marked toxicity in HUVECs (Fu et al., 2022), with comparable observations in other human epithelial cell models (Banerjee et al., 2021).

Establishing this predominantly sublethal exposure context is essential, as it indicates that the phenotypes discussed next—altered lipid homeostasis/metabolism, and impaired endothelial repair (migration and angiogenic remodeling)—reflect functional endothelial dysfunction rather than merely consequences of overt cytotoxicity.

4.3.2. LIPID HOMEOSTASIS AND METABOLISM

Across Papers 2 and 3, disruption of intracellular cholesterol homeostasis emerged as a prominent sublethal phenotype in HUVECs. Direct data on endothelial cholesterol homeostasis under MNPL exposure remain scarce, despite *in vivo* evidence that NPLs can disrupt lipid and cholesterol metabolism (Chen et al., 2025). In this context, our work provides direct evidence of intracellular cholesterol dysregulation in endothelial cells under predominantly subcytotoxic conditions. Using Filipin III staining to quantify intracellular free cholesterol, Paper 2 showed that exposure to PS-C-NPL at 100 µg/mL for 24 h increased this signal across the tested nanosize range (30–100 nm), with increases ranging from 9% to 28% relative to control (Paper 2, Fig. 5A–B). This functional readout was supported by transcriptomic evidence, as enrichment analyses (ORA and GSEA) consistently highlighted cholesterol homeostasis among the most dysregulated pathways (Paper 2, Fig. 2C–D), with upregulation of SREBP2-linked targets, consistent with engagement of cholesterol-regulatory transcriptional programs (Fisher et al., 2021). In Paper 3, within the polymer panel (25 µg/mL, 24 h), cholesterol accumulation was not a universal outcome. Only real-life PET-NPLs induced a significant increase (22%), whereas the remaining materials did not show significant changes under the tested conditions (Paper 3, Fig. 5).

Beyond changes in abundance, both studies suggested alterations in cholesterol compartmentalization. In control cells, the Filipin signal was

predominantly perinuclear, consistent with endoplasmic reticulum–associated cholesterol processing and sensing (Hassan et al., 2006; Lyu et al., 2017). In contrast, conditions with cholesterol accumulation exhibited a more dispersed, punctate vesicular pattern, indicative of redistribution among intracellular compartments. In this context, intracellular processing of NPL-containing vesicles may contribute to endolysosomal cholesterol retention. Supporting this interpretation, in Paper 2, the treatments showing the strongest Filipin signal also displayed enrichment of lysosome-related Gene Ontology cellular component terms (Paper 2, Fig. 2E). In line with this, vesicular Filipin-positive phenotypes have been reported in HUVECs under experimental perturbations of cholesterol transport, leading to intracellular sequestration within late endolysosomal compartments (Lyu et al., 2017). Overall, our imaging data support that the accumulation phenotype is consistent with altered cholesterol trafficking and compartmentalization.

From a vascular perspective, intracellular cholesterol accumulation and its vesicular redistribution are not merely biochemical changes but are also linked to processes associated with endothelial dysfunction and early atherogenesis. Endothelial cholesterol imbalance has been associated with impaired nitric oxide signaling, pro-inflammatory activation, and oxidative stress, all of which contribute to a pro-atherogenic endothelial phenotype (Hassan et al., 2006). In hyperlipidemic settings, endothelial cholesterol loading can also precede cholesterol crystal formation and barrier/repair alterations, reinforcing its relevance to early lesion development (Baumer et al., 2017). More broadly, disturbed cholesterol handling can modify membrane organization and signaling platforms that support specialized endothelial behaviors, with downstream implications for migration and angiogenic remodeling (Fielding & Fielding, 2001; Hassan et al., 2006; Lyu et al., 2017). Establishing cholesterol dysregulation as a recurring sublethal phenotype in our framework, therefore, provides a strong rationale for examining whether these metabolic alterations co-occur with functional impairments in endothelial repair capacity, which is addressed next.

4.3.3. ENDOTHELIAL REPAIR CAPACITY: MIGRATION AND ANGIOGENESIS

Endothelial repair capacity relies on coordinated endothelial migration to restore monolayer integrity, and on angiogenic remodeling to support vascular regeneration and tissue revascularization (Jerka et al., 2024; Johnson & Wilgus, 2014). Disruption of these processes is a hallmark of endothelial dysfunction and can contribute to defective repair programs with relevance to early atherogenesis (Li et al., 2020b; Zhang et al., 2020). Within our experimental framework, NPL exposure modulated endothelial repair functions in a context-dependent manner. Migration responses ranged from stimulatory to inhibitory, while angiogenic outcomes followed a non-linear pattern that did not necessarily mirror migration.

Across Papers 2 and 3, migration emerged as a sensitive functional endpoint. In the PS-C-NPL nanosize series (Paper 2; 100 µg/mL), migration showed a bidirectional response within the nanoscale range. 30 nm PS-C-NPLs significantly accelerated wound closure, 100 nm PS-C-NPLs impaired closure, and 50 nm PS-C-NPLs remained broadly comparable to control (Paper 2, Fig. 5.C-D). In the polymer panel (Paper 3; 25 µg/mL), effects were selective and predominantly inhibitory. PS-NPLs and PLA-NPLs did not significantly affect closure kinetics. In contrast, PTFE-NPLs and especially real-life PET-NPLs slowed repair, with the strongest inhibition observed for PET-NPLs (Paper 3, Fig. 6). Overall, NPL exposure could either enhance or compromise endothelial migration, yet inhibition emerged as the dominant outcome in our datasets and in prior reports (Lee et al., 2021; Hu et al., 2022; Lv et al., 2024; Wan et al., 2024). By contrast, enhanced migration is less commonly reported (Traversa et al., 2024) and was likewise restricted in our dataset to a single condition.

Angiogenesis outcomes in Paper 2 further showed that endothelial repair-related functions can be either enhanced or impaired under NPL exposure. 50 and 100 nm PS-C-NPLs increased tube formation parameters, whereas 30 nm PS-C-NPLs reduced the covered area (Paper 2, Fig. 5.E-F). Although migration and angiogenesis are often coupled during endothelial repair, this response did not mirror the migration results, indicating that migration and angiogenic remodeling can be dissociated under the same exposure conditions. Such

dissociation is biologically plausible given that angiogenesis integrates additional processes beyond motility, including proliferation, differentiation, extracellular matrix remodeling, and coordinated signaling (Flournoy et al., 2022). Functionally, both reduced and increased angiogenic responses can be considered pathological deviations. While insufficient angiogenesis may impair necessary vascular repair, excessive or persistent signaling often leads to dysregulated, maladaptive vessel formation rather than restoring tissue homeostasis (Dudley & Griffioen, 2023).

Transcriptomic results in Paper 2 supported the functional repair alterations observed in wound healing and tube formation assays (Paper 2, Fig. 2). At the pathway level, ORA and GSEA consistently identified epithelial–mesenchymal transition (EMT) as significantly dysregulated across exposures to PS-C-NPLs, a program associated with adhesion and motility remodeling with clear relevance to migration potential (Chen et al., 2017). In parallel, angiogenesis-related gene-expression patterns aligned with the tube formation readouts, with treatments showing similar functional directionality also exhibiting more similar transcriptional profiles (Paper 2, Supplementary Fig. S5B). Together, these concordant functional and transcriptomic readouts support an integrated endothelial dysfunction profile in which sublethal perturbations are expressed at both phenotypic and transcriptional levels.

Overall, these data establish that NPL exposure can perturb endothelial repair capacity under largely viable conditions, with migration showing scenario-dependent bidirectionality and angiogenesis exhibiting non-linear modulation that can be uncoupled from motility. Notably, the strongest migration-inhibitory conditions co-occurred with the metabolic phenotype described in Section 4.3.2, consistent with evidence that abnormal intracellular cholesterol accumulation can reduce HUVEC migratory capacity (Lyu et al., 2017). Together, these findings position impaired repair capacity as a functionally relevant layer of endothelial dysfunction in our framework. However, the phenotypic alterations described in this section, including cholesterol accumulation, migration inhibition, and modulation of angiogenesis, are endpoints rather than starting points. Understanding how NPL internalization initiates and sustains these functional defects requires examining upstream

molecular events, including intracellular trafficking, transcriptomic reprogramming, inflammatory signaling, and genome-integrity stress, which are addressed in the following section.

4.4. Mechanisms Driving Endothelial Dysfunction

Across the three studies, functional impairment was accompanied by a coherent set of mechanistic changes that help explain how NPL internalization translates into endothelial dysfunction. This section synthesizes evidence for intracellular burden and trafficking stress, early transcriptomic alterations, and downstream activation-related signaling, including inflammatory modulation, oxidative stress, and disruption of genome integrity, which together provide a mechanistic framework for the functional outcomes described above.

4.4.1. CELLULAR UPTAKE AND INTRACELLULAR TRAFFICKING BURDEN

Internalization was demonstrated using a multi-parameter approach combining flow cytometry, confocal microscopy, and transmission electron microscopy (TEM). Flow cytometry provided population-level quantitative uptake readouts and enabled kinetic analyses. Confocal Z-stack imaging verified that the fluorescent signal corresponded to intracellular particles rather than membrane-associated material. Finally, TEM confirmed vesicular sequestration and provided ultrastructural evidence of the organization of internalized particles within intracellular compartments. This workflow was applied to commercial fluorescent PS reference particles in Papers 1 and 2, and to the polymer panel fluorescently labelled in-house with iDye Poly Pink in Paper 3.

Flow cytometry showed that across the tested PS-NPLs (Papers 1 and 2; 100 µg/mL), uptake in HUVECs was rapid and broadly distributed at the population level, a behavior observed across surface functionalizations and the nanosize range (Paper 1, Fig. 3A; Paper 2, Fig. 3B). This rapid uptake is consistent with the strong endocytic competence previously reported for HUVECs exposed to other nanomaterials (Blechinger et al., 2013). As a minor exception, 50 nm PS-P-NPLs internalized more slowly than the other PS-NPLs, yet still approached full-population positivity over time. Kinetic profiling further indicated a fast

initial uptake phase followed by a marked slowdown from 2 to 24 h, consistent with a tendency toward uptake saturation. Notably, 30 nm PS-C-NPLs showed the clearest early plateau, with no significant increase in particle burden between 2 and 24 h (Paper 2, Fig. 3C; Supplementary Fig. S3). Given this tendency toward saturation under the acute exposure conditions used in Papers 1 and 2, Paper 3 adopted a more environmentally oriented, non-saturating exposure design to enable cross-material comparisons while retaining variability in internalization efficiency. Accordingly, uptake was assessed at a fixed 24 h endpoint across concentrations (12.5–50 µg/mL). Under this design, PS-NPLs and PLA-NPLs reached near-complete positivity across concentrations, and PTFE-NPLs did so at 25–50 µg/mL. In contrast, real-life PET-NPLs did not reach full-population positivity even at the highest concentration tested (Paper 3, Fig. 2A.1).

Confocal microscopy Z-stack imaging localized fluorescent NPL signal within the cytoplasm, supporting that population-level positivity measured by flow cytometry corresponded to internalized material rather than surface adhesion (Paper 1, Fig. 4; Paper 2, Fig. 3A; Paper 3, Fig. 2B). Importantly, in Paper 3 this approach also corroborated the incomplete uptake of real-life PET-NPLs at 25 µg/mL (Paper 3, Fig. 2A.1; Fig. 2B.4). Depending on the tested material, intracellular fluorescence appeared either more diffuse or more punctate, suggestive of differences in intracellular handling and trafficking load; TEM further examined this distinction.

TEM ultrastructural imaging showed that internalized NPLs were confined to membrane-bound vesicular compartments, consistent with endolysosomal routing, as also reported for PS-NPL exposure in endothelial models (Lu et al., 2022). Across conditions, the observed ultrastructure could be summarized into three recurring organization patterns. First, some treatments displayed prominent large vesicular compartments (up to 4–5 µm) occupying substantial cytoplasmic volume and displacing organelles as observed for 50 nm PS-P-NPLs and 50 nm PS-C-NPLs, and for real-life PET-NPLs (Paper 1, Fig. 5; Paper 3, Fig. 4). Second, other treatments displayed numerous submicron vesicles, reflecting a dense vesicular load, as observed for 100 nm PS-C-NPLs, 200 nm PS-NPLs, PTFE-NPLs, and PLA-NPLs (with PLA-NPLs also showing occasional

larger vesicles in some cells, reminiscent of the first pattern) (Paper 2, Fig. 3A; Paper 3, Fig. 4). Third, a subset of exposures showed a more limited vesicular burden, with scarce smaller vesicles and comparatively reduced compartment expansion as observed for 50 nm PS-A-NPLs and 30 nm PS-C-NPLs (Paper 1, Fig. 5; Paper 2, Fig. 3A). Importantly, the presence of particles outside vesicular compartments cannot be excluded, as the low atomic number of polymeric nanoplastics results in weak electron scattering and therefore poor TEM contrast for resolving individual nanoparticles (Sawyer et al., 2008). At a mechanistic level, these distinct vesicular organizations are compatible with differential engagement of endocytic routes that ultimately converge in endolysosomal processing (Foroozandeh & Aziz, 2018; Ho et al., 2018).

Beyond imaging, flow cytometry scatter provided an independent proxy consistent with an increased intracellular burden. Side scatter (SSC), a readout of internal granularity/complexity (Jaroszeski & Radcliff, 1999), showed the largest increases for 50 nm PS-P and 50 nm PS-C-NPLs, 100 nm PS-C-NPLs, and 200 nm PS-NPLs (Paper 1, Fig. 6B; Paper 2, Supplementary Fig. S4B; Paper 3, Supplementary Fig. S1). Likewise, forward scatter (FSC) increased in the tested PS-NPLs (Papers 1–2), broadly tracking the SSC trend (Paper 1, Fig. 6A; Paper 2, Supplementary Fig. S4A). Notably, in Paper 2, the conditions exhibiting the largest SSC increases (50 nm PS-C-NPLs and 100 nm PS-C-NPLs) also showed a more pronounced enrichment of vesicle-/lysosome-associated GO cellular component terms in GSEA (Paper 2, Fig. 2E), consistent with an increased intracellular processing burden.

Taken together, and acknowledging limitations in direct cross-particle comparisons driven by differences in size range and particle source, the combined readouts support an approximate 24 h intracellular-burden ordering for each panel. Within the PS reference set (Papers 1–2), 50 nm PS-C-NPLs and 100 nm PS-C-NPLs showed the largest overall intracellular burden, followed by 50 nm PS-P-NPLs, then 30 nm PS-C-NPLs, while 50 nm PS-A-NPLs consistently displayed the most limited vesicular burden. In the polymer panel in Paper 3, PS-NPLs showed the highest overall intracellular burden, PLA-NPLs and PTFE-NPLs displayed intermediate and closely similar uptake, and real-life PET-NPLs were consistently the least internalized. This provides a clear context

for interpreting the downstream molecular and functional effects, which are discussed next.

4.4.2. TRANSCRIPTOMIC ALTERATIONS

To obtain an overview of early molecular alterations following the internalization of NPLs, transcriptomic profiling was performed in Paper 2 using the nanosize series of PS-C-NPLs. Under our standardized acute exposure conditions (24 h; 100 µg/mL), RNA-seq revealed extensive transcriptional alterations across all treatments (Paper 2, Fig. 2A). Importantly, despite condition-dependent differences, a substantial shared overlap (955 DEGs) was recovered across exposures (Paper 2, Fig. 2B), supporting a core transcriptional response to exposure to PS-C-NPLs. At the functional level, ORA and GSEA revealed both shared and condition-dependent enrichment patterns, providing a mechanistic context for the downstream functional and molecular endpoints assessed throughout this Thesis.

Two recurrent programs dominated the transcriptomic landscape across PS-C-NPL exposures: “Cholesterol homeostasis” and “Epithelial–mesenchymal transition” (EMT) (Paper 2, Fig. 2C–D). Notably, the consistent enrichment of “Cholesterol homeostasis” supported the prioritization of cholesterol-related endpoints, as developed in Section 4.3.2. In parallel, EMT enrichment indicated coordinated changes in adhesion- and motility-related programs, providing pathway-level context for the impaired endothelial repair capacity discussed in Section 4.3.3. Beyond these dominant axes, enrichment analyses also identified molecular changes consistent with endothelial activation and genome-integrity stress. In particular, inflammation-related programs (e.g., TNFα/NF-κB–linked signaling) emerged across conditions (Paper 2, Fig. 2C–D), motivating the analysis of inflammatory output in our model (Section 4.4.3). Moreover, the enrichment of UV response–related programs (“UV_RESPONSE_UP” and “UV_RESPONSE_DN”), commonly linked to DNA damage signaling and repair, provided a transcriptomic rationale to assess genome integrity and supported the genotoxicity analysis discussed in Section 4.4.4 (Nieto Moreno et al., 2023). Consistently, GO cellular component enrichment also highlighted vesicle-/lysosome-associated signatures in a subset of conditions (Paper 2,

Fig. 2E), in line with the intracellular trafficking burden discussed in Section 4.4.1.

Overall, RNA-seq in Paper 2 provided pathway-level context linking exposure to PS-C-NPLs to the cholesterol-related endpoints and the impaired endothelial repair capacity described in Sections 4.3.2 and 4.3.3. In addition, the enrichment of inflammation- and UV response–related programs supported the focused analysis of inflammatory output and genome integrity in Sections 4.4.3 and 4.4.4. While size-dependent transcriptional differences were observed in the RNA-seq dataset, their interpretation in terms of physicochemical determinants is addressed specifically in Section 4.4.

4.4.3. INFLAMMATORY SIGNALING

Building on transcriptomic evidence pointing to deregulation of inflammatory signaling (Section 4.4.2), IL-6 secretion was quantified by ELISA in culture supernatants collected after 24 h of exposure to NPLs. IL-6 was selected as a functional readout of endothelial inflammatory output given its established role in endothelial activation and vascular inflammation (Villar-Fincheira et al., 2021).

Across Papers 2 and 3, IL-6 responses were not uniform and varied with the tested material and exposure setting. In the nanosize series of PS-C-NPLs in Paper 2 (100 µg/mL, 24 h), IL-6 secretion was significantly reduced across all conditions relative to control, with decreases ranging from 17% to 41% depending on the treatment (Paper 2, Fig. 6). Thus, exposure to PS-C-NPLs modulated IL-6 output despite not eliciting a classical pro-inflammatory induction profile. In the polymer panel in Paper 3 (25 µg/mL, 24 h), only real-life PET-NPLs, the most environmentally relevant material within this set, significantly increased IL-6 secretion, inducing a 93% increase (Paper 3, Fig. 4). All other polymers in the panel did not significantly alter IL-6. Notably, this response occurred in the opposite direction to the suppression observed in the nanosize series of PS-C-NPLs.

Consistent with current evidence, our IL-6 findings align with the heterogeneous inflammatory responses reported in MNPL-exposed individuals (Mahmud et al., 2024). This variability is also reflected in experimental studies.

In primary human immune cells, reference 50, 100 and 310 nm PS nanospheres showed limited IL-6 changes, ranging from no significant effect to decreases depending on the condition. In contrast, irregular and polydisperse NPLs were associated with increased IL-6 release and a stronger pro-inflammatory cytokine profile (Weber et al., 2022). Consistently, studies using environmentally sourced or laboratory-prepared mixtures of commercially sourced reference MNPLs report robust IL-6 secretion that varies with plastic composition, with PET-rich samples among the strongest inducers (Bishop et al., 2025). Together, these reports support the view that IL-6 induction is not a default outcome of acute exposure to MNPLs but rather emerges under specific exposure contexts, consistent with our polymer panel, in which only real-life PET-NPLs increased IL-6.

From a functional standpoint, altered IL-6 secretion has direct implications in endothelial biology. IL-6 signaling contributes to endothelial activation by modulating chemokines, such as MCP-1 and IL-8, and adhesion molecules, such as ICAM-1, thereby promoting inflammatory cell adhesion and monocyte recruitment, an early step in atherogenesis (Suzuki et al., 2009; Ohta et al., 2020). IL-6 has also been linked to endothelial barrier disruption and increased permeability, as well as pro-thrombotic shifts that contribute to vascular pathology (Kang et al., 2020). In addition, IL-6 can influence endothelial repair-related processes by modulating pro-angiogenic mediators such as angiopoietins and VEGF (Kayakabe et al., 2012). In this context, both the suppression observed for PS-C-NPLs and the induction triggered by real-life PET-NPLs indicated dysregulated IL-6 output that may contribute to the impaired repair capacity discussed in Section 4.3.3.

Overall, IL-6 responses across Papers 2 and 3 were context-dependent, ranging from reduced secretion in the PS-C-NPL nanosize series to increased release under real-life PET exposure. This supports the role of inflammation as a relevant contributor to NPL-induced endothelial dysfunction and is further examined alongside oxidative stress and genome integrity endpoints in Section 4.4.4.

4.4.4. OXIDATIVE STRESS AND GENOTOXICITY

To further capture sublethal alterations that can accompany endothelial dysfunction, we evaluated oxidative stress and genotoxicity. Intracellular ROS production was quantified only in the surface-functionalization series of PS-NPLs (Paper 1) using a DHE-based assay from 20 min to 24 h. Genome integrity was assessed by alkaline comet assay in all three studies to quantify DNA strand breaks, measured at 2 h and 24 h in Papers 1–2 and only at 24 h in Paper 3, where total DNA damage was also evaluated using the formamidopyrimidine DNA glycosylase (FPG)-modified comet assay (Collins et al., 2023).

Across the surface-functionalization series of PS-NPLs (Paper 1, 100 µg/mL), intracellular ROS increased for all tested PS-NPLs across the full time window, supporting an early and sustained redox imbalance, with only minor time-dependent variation (Paper 1, Fig. 7). In parallel, alkaline comet assays showed that exposures to PS-NPLs in Papers 1–2 (100 µg/mL) can induce basal DNA strand breaks, but with a non-uniform temporal pattern across conditions (Paper 1, Fig. 8A–B; Paper 2, Fig. 4A–B). At 2 h, the most pronounced increases were observed for 50 nm PS-P-NPLs (+57% vs control), 100 nm PS-C-NPLs (+40%), and 50 nm PS-A-NPLs (+39%), whereas 50 nm PS-C-NPLs showed a weaker response that was not consistently significant across analyses. At 24 h, the pattern shifted, with 30 nm PS-C-NPLs emerging as the strongest responder (+55%) together with 50 nm PS-A-NPLs (+39%) and 50 nm PS-P-NPLs (+28%). These profiles indicated distinct temporal behaviors, including conditions in which damage attenuates by 24 h (e.g., 50 nm PS-P-NPLs, 50 nm PS-C-NPLs, and 100 nm PS-C-NPLs), delayed onset with stronger responses at 24 h (30 nm PS-C-NPLs), and sustained damage across time points (50 nm PS-A-NPLs). Mechanistically, these divergent comet profiles were consistent with transcriptomic signatures within the dataset for PS-C-NPLs (Paper 2), with UV response/DNA repair enrichment in conditions showing transient damage and prominent cell-cycle/checkpoint alterations (e.g., E2F targets, G2M checkpoint) in the condition displaying the strongest 24 h damage (Paper 2, Fig. 2C–D). By contrast, in the polymer panel (Paper 3, 25 µg/mL, 24 h), no increase in DNA damage was detected for any material, either in the standard comet assay or in the FPG-modified comet assay (total damage including

oxidized bases), while positive controls responded as expected (Paper 3, Fig. 3B; Supplementary Fig. S4).

Notably, the ROS increase observed in HUVECs after exposure to PS-NPLs is consistent with prior endothelial reports showing intracellular ROS induction across different formulations of PS-NPLs (Wei et al., 2022; Fu et al., 2022). In the literature, genotoxicity outcomes in MNPL studies are highly context-dependent, with both positive and negative findings reported depending on the tested material and exposure conditions (Ballesteros et al., 2020; Domenech et al., 2020; Shi et al., 2022). Consistent with this variability, our comet dataset indicated that NPL-associated DNA damage is not a uniform consequence of acute exposure but rather an exposure-specific outcome that varies across treatments and time points and should therefore be interpreted cautiously when extrapolating across scenarios.

Oxidative stress and genome integrity are complementary endpoints for characterizing sublethal endothelial injury. Increased intracellular ROS levels are mechanistically relevant in endothelial biology because they can compromise vasoprotective signaling (e.g., NO bioavailability) and promote a pro-inflammatory activation state. They also represent a plausible upstream contributor to DNA lesions (Yan et al., 2025). Consistently, the sustained intracellular ROS increase observed in the surface-functionalization series of PS-NPLs occurred alongside comet-detected DNA strand breaks across exposures to PS-NPLs. In turn, DNA strand breaks reflect genome integrity stress that can drive inflammatory reprogramming and reduce endothelial repair capacity, providing a mechanistic layer that converges with IL-6 modulation (Section 4.4.3) and impaired migration and angiogenic remodeling (Section 4.3.3) (Ding et al., 2024b).

Overall, these data indicated that acute NPL exposure can elicit oxidative and genome integrity stress in endothelial cells in a material-dependent manner. The extent to which these responses vary with particle physicochemical properties is addressed in Section 4.4.

4.5. Physicochemical Determinants of Endothelial Responses

As discussed in Sections 4.2 and 4.3, the exposure of HUVECs to NPLs produced a reproducible pattern of endothelial stress and dysfunction. Section 4.5 examines the physicochemical determinants underlying this phenotype by focusing on three properties of NPLs that differ across our test systems: surface functionalization (Paper 1), nanoscale size (Paper 2), and environmental realism (Paper 3). The aim is to identify which properties best explain the differences in endothelial responses observed across conditions.

4.5.1. SURFACE FUNCTIONALIZATION

In Paper 1, the three functionalizations of PS-NPLs showed that greater intracellular accumulation did not necessarily translate into stronger biological impact. PS-C-NPLs showed the most pronounced accumulation, with extensive vesicular sequestration and marked increases in cell size and internal complexity (FSC/SSC). However, they did not trigger the most adverse outcomes. In contrast, PS-A-NPLs yielded the lowest intracellular load across the panel, as supported by TEM and scatter-based metrics, but they elicited the most adverse response profile, including ISO-defined cytotoxicity and the most persistent genotoxicity over time. Taken together, these observations support a point-of-departure perspective, in which surface-dependent interactions and intracellular handling are more informative predictors of endothelial damage than the amount internalized alone.

Several non-mutually exclusive mechanisms may account for the aminated profile without invoking higher accumulation. First, although protein corona formation in biological media tends to reduce the apparent differences in surface charge across the functionalizations of PS-NPLs, corona identity remains surface-dependent (Lundqvist et al., 2008), and PS-A-NPLs still present a less negative interface than PS-P-NPLs and PS-C-NPLs in complete medium. Because mammalian cell surfaces are globally negatively charged, a less negative (or partially cationic) presentation can strengthen electrostatic interactions with the plasma membrane and has been proposed to promote

membrane perturbation and pore-like damage, which could contribute to the higher cytotoxicity observed for aminated materials (Ruenraroengsak et al., 2012; Fu et al., 2022). Second, once particles enter the endo/lysosomal pathway, evidence from PS-A-NPLs indicates that the corona can be progressively degraded, allowing the native surface chemistry—and associated positive charge—to re-emerge intracellularly (Wang et al., 2013). Under acidic lysosomal conditions, cationic surfaces can also drive proton-sponge–like behavior, promoting proton accumulation followed by compensatory influx of chloride and water, osmotic swelling, and lysosomal membrane rupture (Lee et al., 2019). Lysosomal permeabilization would release hydrolytic enzymes into the cytosol, thereby providing a plausible mechanism for cytotoxicity (Wang et al., 2013). Additionally, lysosomal leakage may release nucleases that could contribute to persistent DNA damage at later time points (Boya & Kroemer, 2008), providing a mechanistic rationale for the sustained genotoxic profile observed under aminated exposure.

Overall, Paper 1 supports surface functionalization as a key determinant of endothelial hazard. In HUVECs, the contrast between PS-C-NPLs and PS-A-NPLs indicates that uptake or burden proxies alone are insufficient for hazard ranking, underscoring the importance of damage persistence and intracellular handling for understanding risk and comparing studies.

4.5.2. SIZE AT THE NANOSCALE

In Paper 2, the nanosize series of PS–C-NPLs demonstrated that size differences within the nanoscale range (30–100 nm) were sufficient to modulate endothelial responses. Transcriptomics revealed a core response shared across all sizes, dominated by “Cholesterol homeostasis” and “Epithelial–mesenchymal transition”, together with inflammatory and genome integrity–linked programs. Beyond this shared core, transcriptomic analyses showed a consistent size-specific separation, with 30 nm PS-C-NPLs diverging from the 50/100 nm PS-C-NPLs cluster. 30 nm PS-C-NPLs were preferentially associated with membrane-related terms and chromosome/kinetochore components, alongside a stronger contribution of cell-cycle programs, whereas 50/100 nm PS-C-NPLs showed a predominant association with

lysosomal/vacuolar pathways and DNA damage–related signatures. Notably, pathway-level heatmaps for cholesterol homeostasis, angiogenesis, and EMT further supported this size structuring, with 50 and 100 nm PS-C-NPLs clustering more closely, whereas 30 nm PS-C-NPLs displayed a more distinct pattern. Importantly, targeted functional assays were consistent with both layers of this framework. They supported shared alterations in cholesterol handling and inflammatory output across sizes, as reflected by reduced IL-6 release, while also reinforcing the size-specific split, with 30 nm PS-C-NPLs differing from 50/100 nm PS-C-NPLs in endothelial repair-related functions and in the temporal profile of DNA damage.

A coherent interpretation of the 30 nm versus 50/100 nm clustering is that size differences can shape internalization kinetics and the dominant uptake and handling routes (Zhang et al., 2009; Sahay et al., 2010), thereby influencing downstream molecular and functional endpoints. First, 30 nm PS-C-NPLs showed rapid uptake followed by an early plateau, indicating that most accumulation occurred at early time points rather than progressively over time. This rapid early uptake may be facilitated by the higher particle number delivered at the same mass concentration for smaller particles, thereby increasing early particle–cell interactions (Zhang et al., 2009). In contrast, 50 and 100 nm PS-C-NPLs continued to accumulate over time, consistent with a more sustained uptake and processing load. This temporal contrast in internalization kinetics may contribute to the clustering of 30 nm versus 50/100 nm and help shape downstream responses. Second, our data further suggested size-dependent differences in entry routes and subsequent intracellular trafficking. 30 nm PS-C-NPLs showed a profile with a more diffuse intracellular signal by confocal microscopy, less prominent vesicular accumulation by TEM, and a stronger contribution of membrane-related terms in the transcriptomic analysis. This pattern is compatible with a relatively greater contribution of non-vesicular or less classically endocytic entry mechanisms at 30 nm, potentially including membrane translocation reported for nanomaterials in the lower nanoscale range (Sousa de Almeida et al., 2021). In contrast, 50/100 nm PS-C-NPLs showed more pronounced vesicular accumulation by TEM and stronger lysosomal/vacuolar enrichment in the

transcriptomic analysis. Together with their size range, this pattern is consistent with predominantly vesicular uptake via classical endocytic routes (e.g., clathrin- or caveolae-mediated) (Rejman et al., 2004). Overall, size-dependent differences in entry routes, together with the resulting degree of vesicular sequestration and endolysosomal trafficking, provide a plausible basis for the 30 nm versus 50/100 nm dichotomy on top of a shared core response, and are expected to have functional consequences given the central role of vesicular trafficking in cellular homeostasis (Lyu et al., 2017).

Taken together, Paper 2 highlights nanoscale size as a key determinant of endothelial response patterns within the nanometric range. This supports the integration of size into mechanistic interpretation and hazard assessment studies.

4.5.3. ENVIRONMENTAL REALISM

In Paper 3, a controlled panel of NPLs spanning increasing environmental realism was used to examine endothelial outcomes under matched exposure conditions. In contrast to Papers 1–2, exposures were performed at a lower, more environmentally relevant concentration (25 µg/mL) to preserve polymer-dependent differences in uptake and evaluate how these differences relate to biological impact. By keeping the nominal particle size comparable (200 nm) while shifting from spherical model materials (PS-NPLs) towards more realistic NPLs (PLA, irregular PTFE, and real-life PET), the study showed that increased realism shifted responses towards inflammatory and metabolic alterations even when uptake was reduced. Under subcytotoxic, non-genotoxic acute conditions, the more idealized materials (PS-NPLs and PLA-NPLs) showed minimal functional disruption. In contrast, the more realistic NPLs—particularly PET-NPLs—elicited inflammatory and cholesterol-related alterations and impaired endothelial repair-related function (migration), consistent with a lower point of departure for adverse effects in realistic NPLs.

These results suggested that environmental realism—captured by irregular morphology, broader size dispersion, and aggregation-prone colloidal behaviour in biological media—reshaped NPL–endothelium interactions and thereby modulated downstream outcomes. Several mechanisms may account

for the decoupling between internalization and functional impact observed for realistic NPLs. Real-life PET-NPLs formed large agglomerates in complete medium, frequently exceeding the size range most efficiently internalized via clathrin- or caveolae-mediated pathways in HUVEC. Such agglomeration is consistent with a shift toward internalization via macropinocytosis or phagocytosis-like routes, yielding fewer but larger particle-containing compartments (Sousa De Almeida et al., 2021), as particle size is a key determinant in the selection of endocytic pathways (Rejman et al., 2004). The formation of larger vesicular structures may, in turn, alter endo-lysosomal trafficking, with downstream consequences for cellular dynamics, including metabolic homeostasis (Lyu et al., 2017). Beyond colloidal behaviour, irregular morphology can enhance biological reactivity even when overall internalization is reduced (Hadji & Bouchemal, 2022). Irregular fragments, such as real-life PET-NPLs, can have a larger available surface area per unit mass than smooth spheres (Pradel et al., 2023), thereby increasing the reactive interface and supporting stronger cellular stress responses (Martin et al., 2022). Moreover, sharp edges of irregular NPLs can promote direct mechanical interactions with the plasma membrane, thereby enabling damage-associated signaling and inflammatory activation without requiring high intracellular particle burdens (Bishop et al., 2025). Consistent with stronger effects observed for irregular particles, Weber et al. (2022) reported a higher inflammatory cytokine response following exposure to irregular NPLs compared with spherical reference NPLs in primary immune cells. Finally, surface roughness and chemical heterogeneity are expected to influence the composition and dynamics of the protein corona, which provides particles with a biological identity and can shape both colloidal stability and cellular recognition (Mayordomo et al., 2025). These corona-dependent differences at the plasma membrane can modulate receptor engagement and early signaling, thereby biasing downstream inflammatory and metabolic outcomes (Fleischer & Payne, 2014; Francia et al., 2019), offering an additional route to functional effects that do not scale with net uptake.

Overall, Paper 3 reinforced that internalization data alone are not sufficient predictors of endothelial hazard, as realism-associated properties can elicit

functional responses under low intracellular burdens. Considered alongside Papers 1–2, these findings support a multidimensional framework in which surface functionalization, size, and environmental realism jointly shape NPL–endothelium interactions and the resulting endothelial dysfunction profile. Accordingly, both mechanistic interpretation in cellular models and safer-by-design material development should integrate these physicochemical determinants under biologically relevant dispersion conditions and prioritize functional endothelial endpoints over uptake as a standalone proxy (Tavernaro et al., 2021).

4.6. Limitations and Future Perspectives

The findings presented in this Thesis should be considered within the experimental framework in which they were generated. The use of primary HUVECs under static culture conditions and acute exposure windows (24 h) was strategically chosen to enable controlled mechanistic dissection of NPL–endothelium interactions and to compare physicochemical determinants systematically. However, these design choices inherently limit the physiological complexity captured. To advance translational relevance and bridge mechanistic insights to human risk assessment, future research should prioritize exposure scenarios and vascular models that more accurately reflect the chronic, low-dose nature of environmental MNPL exposure and the vessel wall's structural and hemodynamic features. The following subsections outline key limitations of the current approach and corresponding opportunities to strengthen physiological realism in future studies.

4.6.1. ADVANCING TOWARD REALISTIC EXPOSURE SCENARIOS

In this work, acute 24 h exposures were employed to resolve early mode-of-action events under standardized conditions, enabling controlled mechanistic dissection and systematic comparison of physicochemical properties. This design, however, did not capture the chronic and cumulative nature of human MNPL exposure. Real-world exposure is expected to occur continuously at low doses over years or decades (Domenech & Marcos, 2021), potentially engaging

adaptive responses, cumulative damage, or long-term metabolic reprogramming that remain undetectable in acute settings. Additionally, single-material exposures were used to isolate physicochemical determinants. However, environmental MNPLs occur as heterogeneous mixtures spanning polymer types, sizes, and morphologies, often alongside polymer additives and external contaminants (Yang et al., 2023b; Okoye et al., 2022). Such mixture exposures may produce combined effects (additive, synergistic, or antagonistic) that are not captured by single-material testing. To address these gaps, future work should prioritize chronic low-dose exposure models with time-resolved functional readouts to determine whether responses persist, adapt, or accumulate over time. Moreover, systematic mixture designs, ranging from defined combinations of representative particles to more complex environmental extracts, will be required to quantify interaction effects and identify the main drivers of endothelial responses under realistic exposure scenarios.

4.6.2. ADVANCING TOWARD PHYSIOLOGICALLY RELEVANT VASCULAR MODELS

The experimental strategy of this Thesis relied on primary HUVECs cultured as 2D monolayers under static conditions. This platform is widely validated for endothelial toxicology (Cao et al., 2017) and enables reproducible mechanistic interrogation. However, it lacks key physiological features of the vessel wall and therefore constrains translational relevance. Our design assessed multiple endothelial functions but did not directly quantify barrier integrity. Recent work has reported MNPL-induced endothelial leakiness associated with junctional disruption (Wei et al., 2022), highlighting barrier integrity as a relevant endpoint for future assessment. Additionally, static culture conditions do not reproduce hemodynamic shear stress, which influences endothelial phenotype and particle uptake kinetics (Chen et al., 2020b), and may overrepresent particle delivery through settling. To address these limitations, future studies should incorporate models that explicitly capture endothelial barrier integrity and flow-dependent phenotypes. Transwell-based barrier systems would enable direct quantification of macromolecular permeability and electrical resistance (TEER), allowing integrated assessment of MNPL-induced barrier dysfunction (Wei et

al., 2022; Banaei et al., 2023). In parallel, microfluidic vessel-on-chip platforms and tissue-engineered blood vessels (TEBVs) would introduce controlled perfusion through endothelium-lined channels, enabling evaluation of how physiological flow reshapes particle transport, barrier integrity, and endothelial responses under hemodynamically relevant conditions (Chen et al., 2020b; Dávila et al., 2021). Together, these advances would strengthen physiological relevance and support more predictive assessment of MNPL-driven vascular dysfunction.

5

Conclusions

The work presented in this Thesis provides a comprehensive characterization of NPL-induced endothelial dysfunction in primary HUVECs and establishes that physicochemical properties are key determinants of biological outcomes. The following specific conclusions can be drawn:

Regarding Objective 1 (NPL–endothelium interactions, adverse effects, and mechanisms of action):

1.1. All tested NPLs were rapidly internalized by HUVECs, with uptake detectable within 20 minutes across all conditions. However, internalization efficiency and intracellular burden varied substantially depending on NPL properties.

1.2. Acute NPL exposure induced a sublethal endothelial dysfunction phenotype characterized by intracellular cholesterol accumulation, impaired migration capacity, and altered angiogenic remodeling, with minimal or no cytotoxicity.

1.3. NPL exposure activated multiple mechanistic pathways, including intracellular ROS generation, DNA strand breaks, transcriptomic alterations, and modulation of IL-6 secretion. Collectively, these findings define a coordinated endothelial stress program triggered under subcytotoxic conditions.

Regarding Objective 2 (Physicochemical determinants):

2.1. Surface functionalization emerged as a primary determinant of endothelial hazard. PS-A-NPLs exhibited the highest toxicity, including reduced viability and sustained genotoxicity, despite presenting the lowest intracellular burden.

2.2. Nanoscale size modulated the endothelial response within the 30 to 100 nm range. All sizes activated a shared transcriptomic and functional program, with size influencing the magnitude and profile of this response, particularly between 30 nm PS-C-NPLs and the 50/100 nm PS-C-NPLs cluster.

2.3. Environmental realism of NPLs shifted the endothelial response profile at low, realistic concentrations. Spherical reference particles produced

minimal functional effects, irregular PTFE-NPLs impaired migration, and real-life PET-NPLs induced the strongest response, including IL-6 secretion, cholesterol accumulation, and migration inhibition, despite being the least internalized.

Overall, this Thesis demonstrates that NPL-induced endothelial dysfunction occurs under generally subcytotoxic conditions and is strongly shaped by surface chemistry, nanoscale size, and environmental realism. Importantly, higher internalization did not predict greater biological impact, challenging the use of uptake as a proxy for hazard. Given the critical role of physicochemical properties in determining biological outcomes, the use of environmentally realistic materials is essential to capture relevant hazard profiles. To effectively evaluate these highly heterogeneous materials, the field must prioritize methodological harmonization to ensure cross-study comparability and build a robust understanding of MNPL toxicity relevant to human health.

6

References

Abass, D., Alaraby, M., Elkady, E. F., Morataya-Reyes, M., Banaei, G., Martín-Pérez, J., Rubio, L., Barguilla, I., Marcos, R., Hernández, A., & García-Rodríguez, A. (2025). Polytetrafluoroethylene (PTFE, Teflon) microplastics and nanoplastics induce oxidative stress, mitochondrial damage, and genotoxicity in human intestinal cells. *Journal of Hazardous Materials*, 499, 140255. https://doi.org/10.1016/j.jhazmat.2025.140255

Abbasi, S., Keshavarzi, B., Moore, F., Turner, A., Kelly, F. J., Dominguez, A. O., & Jaafarzadeh, N. (2019). Distribution and potential health impacts of microplastics and microrubbers in air and street dusts from Asaluyeh County, Iran. *Environmental Pollution*, 244, 153–164. https://doi.org/10.1016/j.envpol.2018.10.039

Abdullayeva, M. Y., & Alizadeh, S. N. (2023). Biodegradation of wasted bioplastics. *World Science*, 3(81). https://doi.org/10.31435/rsglobal_ws/30092023/8044

Alaraby, M., Abass, D., Domenech, J., Hernández, A., & Marcos, R. (2022). Hazard assessment of ingested polystyrene nanoplastics in Drosophila larvae. *Environmental Science: Nano*, 9(5), 1845–1858. https://doi.org/10.1039/d1en01199e

Alaraby, M., Abass, D., Farre, M., Hernández, A., & Marcos, R. (2024a). Are bioplastics safe? Hazardous effects of polylactic acid (PLA) nanoplastics in Drosophila. *Science of The Total Environment*, 919, 170592. https://doi.org/10.1016/j.scitotenv.2024.170592

Alaraby, M., Abass, D., Velázquez, A., Hernández, A., & Marcos, R. (2025a). Polytetrafluoroethylene microplastic properties, pollution, toxicity and analysis: a review. *Environmental Chemistry Letters*. https://doi.org/10.1007/s10311-025-01885-w

Alaraby, M., Abass, D., Velázquez, A., Hernández, A., & Marcos, R. (2025b). New insights into the reproductive hazards posed by polystyrene nanoplastics. *Journal of Hazardous Materials*, 492, 138210. https://doi.org/10.1016/j.jhazmat.2025.138210

Alaraby, M., Villacorta, A., Abass, D., Hernández, A., & Marcos, R. (2023). The hazardous impact of true-to-life PET nanoplastics in Drosophila. *Science of The Total Environment*, 863, 160954. https://doi.org/10.1016/j.scitotenv.2022.160954

Alaraby, M., Villacorta, A., Abass, D., Hernández, A., & Marcos, R. (2024b). Titanium-doped PET nanoplastics, from opaque milk bottle degradation, as a model of environmental true-to-life nanoplastics. Hazardous effects on Drosophila. *Environmental Pollution*, 341, 122968. https://doi.org/10.1016/j.envpol.2023.122968

Ali, N., Katsouli, J., Marczylo, E. L., Gant, T. W., Wright, S., & Bernardino de la Serna, J. (2024). The potential impacts of micro-and-nano plastics on various organ systems in humans. *EBioMedicine*, 99, 104901. https://doi.org/10.1016/j.ebiom.2023.104901

Alimba, C., Adesida, S., Owonikoko, W., & Oteyola, A. (2025). Micro (Nano)plastics Vitiation of Genetic Material: Systematic Review of Genotoxic Biomarkers and Model Bioindicators. *Journal of Applied Toxicology*, 46(1), 110-140. https://doi.org/10.1002/jat.4928

Allen, S., Allen, D., Phoenix, V. R., Le Roux, G., Durántez Jiménez, P., Simonneau, A., Binet, S., & Galop, D. (2019). Atmospheric transport and deposition of microplastics in a remote mountain catchment. *Nature Geoscience*, 12(5), 339-344. https://doi.org/10.1038/s41561-019-0335-5

Alqahtani, S., Alqahtani, S., Saquib, Q., & Mohiddin, F. (2023). Toxicological impact of microplastics and nanoplastics on humans: understanding the mechanistic aspect of the interaction. *Frontiers in Toxicology*, 5. https://doi.org/10.3389/ftox.2023.1193386

Alzaben, M., Burve, R., Loeschner, K., Møller, P., & Roursgaard, M. (2023). Nanoplastics from ground polyethylene terephthalate food containers: Genotoxicity in human lung epithelial A549 cells. *Mutation Research Genetic Toxicology and Environmental Mutagenesis*, 892, 503705. https://doi.org/10.1016/j.mrgentox.2023.503705

Amato-Lourenço, L. F., Carvalho-Oliveira, R., Júnior, G. R., dos Santos Galvão, L., Ando, R. A., & Mauad, T. (2021). Presence of airborne microplastics in human lung tissue. *Journal of Hazardous Materials*, 416, 126124. https://doi.org/10.1016/j.jhazmat.2021.126124

Amereh, F., Babaei, M., Eslami, A., Fazelipour, S., & Rafiee, M. (2020). The emerging risk of exposure to nano(micro)plastics on endocrine disturbance and reproductive toxicity: From a hypothetical scenario to a global public health challenge. *Environmental Pollution*, 261, 114158. https://doi.org/10.1016/j.envpol.2020.114158

Annangi, B., Villacorta, A., López-Mesas, M., Fuentes-Cebrian, V., Marcos, R., & Hernández, A. (2023a). Hazard assessment of polystyrene nanoplastics in primary human nasal epithelial cells, focusing on the autophagic effects. *Biomolecules*, 13(2), 220. https://doi.org/10.3390/biom13020220

Annangi, B., Villacorta, A., Vela, L., Tavakolpournegari, A., Marcos, R., & Hernández, A. (2023b). Effects of true-to-life PET nanoplastics using primary human nasal epithelial cells. *Environmental Toxicology and Pharmacology*, 100, 104140. https://doi.org/10.1016/j.etap.2023.104140

Arribas Arranz, J., Villacorta, A., Rubio, L., García-Rodríguez, A., Sánchez, G., Llorca, M., Farré, M., Ferrer, J. F., Marcos, R., & Hernández, A. (2024). Kinetics and toxicity of nanoplastics in *ex vivo* exposed human whole blood as a model to understand their impact on human health. *Science of The Total Environment*, 948, 174725. https://doi.org/10.1016/j.scitotenv.2024.174725

Bahrani, F., Mohammadi, A., Dobaradaran, S., De-la-Torre, G. E., Arfaeinia, H., Ramavandi, B., Saeedi, R., & Tekle-Röttering, A. (2024). Occurrence of microplastics in edible tissues of livestock (cow and sheep). *Environmental Science and Pollution Research*, 31(14), 22145-22157. https://doi.org/10.1007/s11356-024-32424-9

Bai, C.-L., Wang, D., Luan, Y.-L., Huang, S.-N., Liu, L.-Y., & Guo, Y. (2024). A review on micro- and nanoplastics in humans: Implication for their translocation of barriers and potential health effects. *Chemosphere*, 361, 142424. https://doi.org/10.1016/j.chemosphere.2024.142424

Bajt, O. (2021). From plastics to microplastics and organisms. *FEBS Open Bio*, 11(4), 954–966. https://doi.org/10.1002/2211-5463.13120

Ballesteros, S., Domenech, J., Barguilla, I., Cortés, C., Marcos, R., & Hernández, A. (2020). Genotoxic and immunomodulatory effects in human white blood cells after *ex vivo* exposure to polystyrene nanoplastics. *Environmental Science: Nano*, 7(11), 3431-3446. https://doi.org/10.1039/d0en00748j

Banaei, G., Abass, D., Tavakolpournegari, A., Martín-Pérez, J., Gutiérrez, J., Peng, G., Reemtsma, T., Marcos, R., Hernández, A., & García-Rodríguez, A. (2024). Teabag-derived micro/nanoplastics (true-to-life MNPLs) as a surrogate for real-life exposure scenarios. *Chemosphere*, 368, 143736. https://doi.org/10.1016/j.chemosphere.2024.143736

Banaei, G., García-Rodríguez, A., Tavakolpournegari, A., Martín-Pérez, J., Villacorta, A., Marcos, R., & Hernández, A. (2023). The release of polylactic acid nanoplastics (PLA-NPLs) from commercial teabags. Obtention, characterization, and hazard effects of true-to-life PLA-NPLs. *Journal of Hazardous Materials*, 458, 131899. https://doi.org/10.1016/j.jhazmat.2023.131899

Banerjee, A., & Shelver, W. L. (2021). Micro- and nanoplastic induced cellular toxicity in mammals: A review. *Science of The Total Environment*, 755, 142518. https://doi.org/10.1016/j.scitotenv.2020.142518

Banerjee, A., Billey, L. O., & Shelver, W. L. (2021). Uptake and toxicity of polystyrene micro/nanoplastics in gastric cells: Effects of particle size and surface functionalization. *PLOS ONE*, 16(12), e0260803. https://doi.org/10.1371/journal.pone.0260803

Baumer, Y., McCurdy, S., Weatherby, T. M., Mehta, N. N., Halbherr, S., Halbherr, P., Yamazaki, N., & Boisvert, W. A. (2017). Hyperlipidemia-induced cholesterol crystal production by endothelial cells promotes atherogenesis. *Nature Communications*, 8(1). https://doi.org/10.1038/s41467-017-01186-z

Besseling, E., Redondo-Hasselerharm, P., Foekema, E. M., & Koelmans, A. A. (2019). Quantifying ecological risks of aquatic micro- and nanoplastic.

Critical Reviews in Environmental Science and Technology, 49(1), 32–80. https://doi.org/10.1080/10643389.2018.1531688

Bishop, B., Webber, W. S., Atif, S. M., Ley, A., Pankratz, K. A., Kostelecky, R., Colgan, S. P., Dinarello, C. A., Zhang, W., & Li, S. (2025). Micro- and nano-plastics induce inflammation and cell death in human cells. *Frontiers in Immunology*, 16. https://doi.org/10.3389/fimmu.2025.1528502

Blechinger, J., Bauer, A. T., Torrano, A. A., Gorzelanny, C., Bräuchle, C., & Schneider, S. W. (2013). Uptake Kinetics and Nanotoxicity of Silica Nanoparticles Are Cell Type Dependent. *Small*, 9(23), 3970-3980. https://doi.org/10.1002/smll.201301004

Bourquin, J., Septiadi, D., Vanhecke, D., Balog, S., Steinmetz, L., Spuch-Calvar, M., Taladriz-Blanco, P., Petri-Fink, A., & Rothen-Rutishauser, B. (2019). Reduction of Nanoparticle Load in Cells by Mitosis but Not Exocytosis. *ACS Nano*, 13(7), 7759-7770. https://doi.org/10.1021/acsnano.9b01604

Boya, P., & Kroemer, G. (2008). Lysosomal membrane permeabilization in cell death. *Oncogene*, 27(50), 6434-6451. https://doi.org/10.1038/onc.2008.310

Bråte, I. L. N., Hurley, R., Iversen, K., Beyer, J., Thomas, K. V., Steindal, C. C., Green, N. W., Olsen, M., & Lusher, A. (2018). Mytilus spp. as sentinels for monitoring microplastic pollution in Norwegian coastal waters: A qualitative and quantitative study. *Environmental Pollution*, 243, 383-393. https://doi.org/10.1016/j.envpol.2018.08.077

Brouwer, H., Busch, M., Yang, S., Venus, T., Aalderink, G., Ferrer Crespo, J. F., Villacorta, A., Hernández, A., Estrela-Lopis, I., Boeren, S., & Bouwmeester, H. (2025). Toxicity of true-to-life microplastics to human iPSC-derived intestinal epithelia correlates to their protein corona composition. *Journal of Hazardous Materials*, 495, 138908. https://doi.org/10.1016/j.jhazmat.2025.138908

Büks, F., & Kaupenjohann, M. (2020). Global concentrations of microplastics in soils – A review. *SOIL*, 6, 649–662. https://doi.org/10.5194/soil-6-649-2020

Cai, L., Wang, J., Peng, J., Tan, Z., Zhan, Z., Tan, X., & Chen, Q. (2017). Characteristic of microplastics in the atmospheric fallout from Dongguan city, China: preliminary research and first evidence. *Environmental Science and Pollution Research*, 24(32), 24928–24935. https://doi.org/10.1007/s11356-017-0116-x

Cao, Y., Gong, Y., Liu, L., Zhou, Y., Fang, X., Zhang, C., Li, Y., & Li, J. (2017). The use of human umbilical vein endothelial cells (HUVECs) as an *in vitro* model to assess the toxicity of nanoparticles to endothelium: a review. *Journal of Applied Toxicology*, 37(12), 1359–1369. https://doi.org/10.1002/jat.3470

Carbery, M., O'Connor, W., & Palanisami, T. (2018). Trophic transfer of microplastics and mixed contaminants in the marine food web and implications for human health. *Environment International*, 115, 400-409. https://doi.org/10.1016/j.envint.2018.03.007

Chen, L., Sui, G., Wu, J., Li, N., Zhang, Z., Du, Y., Lü, M., Yan, X., Pan, G., & Jia, L. (2025). Untargeted metabolomics and transcriptomics joint analysis of the effects of polystyrene nanoplastics on lipid metabolism in the mouse liver. *Lipids in Health and Disease*, 24(1). https://doi.org/10.1186/s12944-025-02613-7

Chen, T., You, Y., Jiang, H., & Wang, Z. Z. (2017). Epithelial–mesenchymal transition (EMT): A biological process in the development, stem cell differentiation, and tumorigenesis. *Journal of Cellular Physiology*, 232(12), 3261-3272. https://doi.org/10.1002/jcp.25797

Chen, Y., Leng, Y., Liu, X., & Wang, J. (2020a). Microplastic pollution in vegetable farmlands of suburb Wuhan, central China. *Environmental Pollution*, 257, 113449. https://doi.org/10.1016/j.envpol.2019.113449

Chen, Y. Y., Syed, A. M., MacMillan, P., Rocheleau, J. V., & Chan, W. C. W. (2020b). Flow Rate Affects Nanoparticle Uptake into Endothelial Cells. *Advanced Materials*, 32(24). https://doi.org/10.1002/adma.201906274

Cheng, Y., Chen, J., Fu, R., Zhang, P., Chen, H., Cao, H., Jiang, Z., Hong, Y., Li, Y., He, C., Tao, F., Li, T., Zhang, J., Chen, B., & Cao, G. (2025). Molecular

mechanism differences between nanoplastics and microplastics in colon toxicity: nanoplastics induce ferroptosis-mediated immunogenic cell death, while microplastics cause cell metabolic reprogramming. *Journal of Nanobiotechnology*, 23(1). https://doi.org/10.1186/s12951-025-03545-1

Choi, D., Hwang, J., Bang, J., Han, S., Kim, T., Oh, Y., Hwang, Y., Choi, J., & Hong, J. (2021). In vitro toxicity from a physical perspective of polyethylene microplastics based on statistical curvature change analysis. *Science of The Total Environment*, 752, 142242. https://doi.org/10.1016/j.scitotenv.2020.142242

Cole, M., Gomiero, A., Jaén-Gil, A., Haave, M., & Lusher, A. (2024). Microplastic and PTFE contamination of food from cookware. *Science of The Total Environment*, 929, 172577. https://doi.org/10.1016/j.scitotenv.2024.172577

Collin-Faure, V., Villacorta, A., Vitipon, M., Diemer, H., Cianférani, S., Marcos, R., Darrouzet, E., Hernández, A., & Rabilloud, T. (2025). About the effects of true-to-life polyethylene terephthalate nanoparticles on macrophages. *Environmental Science: Nano*, 12, 2799–2813. https://doi.org/10.1039/D4EN01063A

Collins, A., Møller, P., Gajski, G., Vodenková, S., Abdulwahed, A., Anderson, D., Bankoglu, E. E., Bonassi, S., Boutet-Robinet, E., Brunborg, G., Chao, C., Cooke, M. S., Costa, C., Costa, S., Dhawan, A., de Lapuente, J., Bo′, C. D., Dubus, J., Dusinska, M., … Azqueta, A. (2023). Measuring DNA modifications with the comet assay: a compendium of protocols. *Nature Protocols*, 18(3), 929-989. https://doi.org/10.1038/s41596-022-00754-y

Cormier, B., Cachot, J., Blanc, M., Cabar, M., Clérandeau, C., Dubocq, F., Le Bihanic, F., Morin, B., Zapata, S., Bégout, M.-L., & Cousin, X. (2022). Environmental microplastics disrupt swimming activity in acute exposure in Danio rerio larvae and reduce growth and reproduction success in chronic exposure in D. rerio and Oryzias melastigma. *Environmental Pollution*, 308, 119721. https://doi.org/10.1016/j.envpol.2022.119721

Crosset-Perrotin, G., Moraz, A., Portela, R., Alcolea-Rodriguez, V., Burrueco-Subirà, D., Smith, C., Bañares, M. A., Foroutan, H., & Fairbrother, D. H. (2025).

Production, labeling, and applications of micro- and nanoplastic reference and test materials. *Environmental Science: Nano*, 12(6), 2911-2964. https://doi.org/10.1039/d4en00767k

Da Costa Filho, P. A., Andrey, D., Eriksen, B., Peixoto, R. P., Carreres, B. M., Ambühl, M. E., Descarrega, J. B., Dubascoux, S., Zbinden, P., Panchaud, A., & Poitevin, E. (2021). Detection and characterization of small-sized microplastics (≥ 5 µm) in milk products. *Scientific Reports*, 11(1). https://doi.org/10.1038/s41598-021-03458-7

Dávila, S., Cacheux, J., & Rodríguez, I. (2021). Microvessel-on-Chip Fabrication for the *In Vitro* Modeling of Nanomedicine Transport. *ACS Omega*, 6(39), 25109-25115. https://doi.org/10.1021/acsomega.1c00735

Dhakal, B., Shiwakoti, S., Park, E.-Y., Kang, K.-W., Schini-Kerth, V. B., Park, S.-H., Ji, H.-Y., Park, J. S., Ko, J.-Y., & Oak, M.-H. (2023). SGLT2 inhibition ameliorates nano plastics-induced premature endothelial senescence and dysfunction. *Scientific Reports*, 13(1). https://doi.org/10.1038/s41598-023-33086-2

Din, K. S., Khokhar, M. F., Parvez, S., & Niazi, M. B. K. (2024). Emerging environmental challenge: A critical review of airborne microplastics. *Environmental Research Communications*, *6*(9), 092003. https://doi.org/10.1088/2515-7620/ad75eb

Ding, R., Chen, Y., Shi, X., Li, Y., Yu, Y., Sun, Z., & Duan, J. (2024a). Size-dependent toxicity of polystyrene microplastics on the gastrointestinal tract: Oxidative stress related-DNA damage and potential carcinogenicity. *Science of The Total Environment*, 912, 169514. https://doi.org/10.1016/j.scitotenv.2023.169514

Ding, W., Chen, J., Zhao, L., Wu, S., Chen, X., & Chen, H. (2024b). Mitochondrial DNA leakage triggers inflammation in age-related cardiovascular diseases. *Frontiers in Cell and Developmental Biology*, 12. https://doi.org/10.3389/fcell.2024.1287447

Domenech, J., & Marcos, R. (2021). Pathways of human exposure to microplastics, and estimation of the total burden. *Current Opinion in Food Science*, 39, 144-151. https://doi.org/10.1016/j.cofs.2021.01.004

Domenech, J., Hernández, A., Rubio, L., Marcos, R., & Cortés, C. (2020). Interactions of polystyrene nanoplastics with in vitro models of the human intestinal barrier. *Archives of Toxicology*, 94(9), 2997-3012. https://doi.org/10.1007/s00204-020-02805-3

Domenech, J., Villacorta, A., Ferrer, J. F., Llorens-Chiralt, R., Marcos, R., Hernández, A., & Catalán, J. (2024). In vitro cell-transforming potential of secondary polyethylene terephthalate and polylactic acid nanoplastics. *Journal of Hazardous Materials*, 469, 134030. https://doi.org/10.1016/j.jhazmat.2024.134030

Dris, R., Gasperi, J., Saad, M., Mirande, C., & Tassin, B. (2016). Synthetic fibers in atmospheric fallout: a source of microplastics in the environment? *Marine Pollution Bulletin*, 104(1–2), 290–293. https://doi.org/10.1016/j.marpolbul.2016.01.006

Du, F., Cai, H., Zhang, Q., Chen, Q., & Shi, H. (2020). Microplastics in take-out food containers. *Journal of Hazardous Materials*, 399, 122969. https://doi.org/10.1016/j.jhazmat.2020.122969

Dudley, A. C., & Griffioen, A. W. (2023). Pathological angiogenesis: mechanisms and therapeutic strategies. *Angiogenesis*, 26(3), 313-347. https://doi.org/10.1007/s10456-023-09876-7

Dusza, H. M., van Boxel, J., van Duursen, M. B., Forsberg, M. M., Legler, J., & Vähäkangas, K. H. (2023). Experimental human placental models for studying uptake, transport and toxicity of micro- and nanoplastics. *Science of The Total Environment*, 860, 160403. https://doi.org/10.1016/j.scitotenv.2022.160403

Edo, C., González-Pleiter, M., Leganés, F., Fernández-Piñas, F., & Rosal, R. (2020). Fate of microplastics in wastewater treatment plants and their

environmental dispersion with effluent and sludge. *Environmental Pollution*, 259, 113837. https://doi.org/10.1016/j.envpol.2019.113837

Eelen, G., de Zeeuw, P., Simons, M., & Carmeliet, P. (2015). Endothelial Cell Metabolism in Normal and Diseased Vasculature. *Circulation Research*, 116(7), 1231-1244. https://doi.org/10.1161/circresaha.116.302855

EFSA Panel on Contaminants in the Food Chain (CONTAM). (2016). Statement on the presence of microplastics and nanoplastics in food, with particular focus on seafood. *EFSA Journal*, 14(6), 4501. https://doi.org/10.2903/j.efsa.2016.4501

El Hadri, H., Gigault, J., Maxit, B., Grassl, B., & Reynaud, S. (2020). Nanoplastic from mechanically degraded primary and secondary microplastics for environmental assessments. *NanoImpact*, 17, 100206. https://doi.org/10.1016/j.impact.2019.100206

Enyoh, C. E., Devi, A., Kadono, H., Wang, Q., & Rabin, M. H. (2023). The Plastic Within: Microplastics Invading Human Organs and Bodily Fluids Systems. *Environments*, 10(11), 194. https://doi.org/10.3390/environments10110194

Facciolà, A., Visalli, G., Ciarello, M. P., & di Pietro, A. (2021). Newly emerging airborne pollutants: Current knowledge of health impact of micro and nanoplastics. *International Journal of Environmental Research and Public Health*, 18(6), 2997. https://doi.org/10.3390/ijerph18062997

Fan, X., Wei, X., Hu, H., Zhang, B., Yang, D., Du, H., Zhu, R., Sun, X., Oh, Y., & Gu, N. (2022). Effects of oral administration of polystyrene nanoplastics on plasma glucose metabolism in mice. *Chemosphere*, 288, 132607. https://doi.org/10.1016/j.chemosphere.2021.132607

Fazlollahi, F., Angelow, S., Yacobi, N. R., Marchelletta, R., Yu, A. S., Hamm-Alvarez, S. F., Borok, Z., Kim, K.-J., & Crandall, E. D. (2011). Polystyrene nanoparticle trafficking across MDCK-II. *Nanomedicine: Nanotechnology, Biology and Medicine*, 7(5), 588-594. https://doi.org/10.1016/j.nano.2011.01.008

Fielding, C. J., & Fielding, P. E. (2001). Caveolae and intracellular trafficking of cholesterol. *Advanced Drug Delivery Reviews*, 49(3), 251-264. https://doi.org/10.1016/s0169-409x(01)00140-5

Fisher, A. L., Srole, D. N., Palaskas, N. J., Meriwether, D., Reddy, S. T., Ganz, T., & Nemeth, E. (2021). Iron loading induces cholesterol synthesis and sensitizes endothelial cells to TNFα-mediated apoptosis. *Journal of Biological Chemistry*, 297(4), 101156. https://doi.org/10.1016/j.jbc.2021.101156

Fleischer, C. C., & Payne, C. K. (2014). Nanoparticle–Cell Interactions: Molecular Structure of the Protein Corona and Cellular Outcomes. *Accounts of Chemical Research*, 47(8), 2651-2659. https://doi.org/10.1021/ar500190q

Flournoy, J., Ashkanani, S., & Chen, Y. (2022). Mechanical regulation of signal transduction in angiogenesis. *Frontiers in Cell and Developmental Biology*, 10. https://doi.org/10.3389/fcell.2022.933474

Foroozandeh, P., & Aziz, A. A. (2018). Insight into Cellular Uptake and Intracellular Trafficking of Nanoparticles. *Nanoscale Research Letters*, 13(1). https://doi.org/10.1186/s11671-018-2728-6

Fournier, S. B., D'Errico, J. N., Adler, D. S., Kollontzi, S., Goedken, M. J., Fabris, L., Yurkow, E. J., & Stapleton, P. A. (2020). Nanopolystyrene translocation and fetal deposition after acute lung exposure during late-stage pregnancy. *Particle and Fibre Toxicology*, 17(1). https://doi.org/10.1186/s12989-020-00385-9

Francia, V., Yang, K., Deville, S., Reker-Smit, C., Nelissen, I., & Salvati, A. (2019). Corona Composition Can Affect the Mechanisms Cells Use to Internalize Nanoparticles. *ACS Nano*, 13(10), 11107-11121. https://doi.org/10.1021/acsnano.9b03824

Fu, Y., Fan, M., Xu, L., Wang, H., Hu, Q., & Jin, Y. (2022). Amino-Functionalized Polystyrene Nano-Plastics Induce Mitochondria Damage in Human Umbilical Vein Endothelial Cells. *Toxics*, 10(5), 215. https://doi.org/10.3390/toxics10050215

Gao, L., Sun, M., Wang, X., Sun, Z., & Duan, J. (2021). Impact and molecular mechanism of microplastics on zebrafish in the presence and absence of copper nanoparticles. *Frontiers in Marine Science*, 8, 762530. https://doi.org/10.3389/fmars.2021.762530

García-Rodríguez, A., Gutiérrez, J., Villacorta, A., Arribas Arranz, J., Romero-Andrada, I., Lacoma, A., Marcos, R., Hernández, A., & Rubio, L. (2024). Polylactic acid nanoplastics (PLA-NPLs) induce adverse effects on an in vitro model of the human lung epithelium: The Calu-3 air-liquid interface (ALI) barrier. *Journal of Hazardous Materials*, 475, 134900. https://doi.org/10.1016/j.jhazmat.2024.134900

Geyer, R., Jambeck, J. R., & Law, K. L. (2017). Production, use, and fate of all plastics ever made. *Science Advances*, 3(7). https://doi.org/10.1126/sciadv.1700782

Gigault, J., El Hadri, H., Nguyen, B., Grassl, B., Rowenczyk, L., Tufenkji, N., Feng, S., & Wiesner, M. R. (2021). Nanoplastics are neither microplastics nor engineered nanoparticles. *Nature Nanotechnology*, *16*(5), 501–507. https://doi.org/10.1038/s41565-021-00886-4

Grafmueller, S., Manser, P., Diener, L., Diener, P.-A., Maeder-Althaus, X., Maurizi, L., Jochum, W., Krug, H. F., Buerki-Thurnherr, T., von Mandach, U., & Wick, P. (2015). Bidirectional Transfer Study of Polystyrene Nanoparticles across the Placental Barrier in an ex Vivo Human Placental Perfusion Model. *Environmental Health Perspectives*, 123(12), 1280-1286. https://doi.org/10.1289/ehp.1409271

Grand View Research. (2024). *Global plastic market size & outlook, 2023-2030*. Retrieved December 1, 2025, from https://www.grandviewresearch.com/industry-analysis/global-plastics-market

Gutiérrez-García, J., Egea, R., Barguilla, I., Nymark, P., García-Rodríguez, A., Guyot, B., Maguer-Satta, V., Marcos, R., Rubio, L., & Hernández, A. (2025). Long-term exposure to real-life polyethylene terephthalate nanoplastics

induces carcinogenesis *in vitro*. *Environmental Science & Technology*, 59(22), 10891-10904. https://doi.org/10.1021/acs.est.5c01628

Haave, M., Gomiero, A., Schönheit, J., Nilsen, H., & Olsen, A. B. (2021). Documentation of microplastics in tissues of wild coastal animals. *Frontiers in Environmental Science*, 9. https://doi.org/10.3389/fenvs.2021.575058

Hadji, H., & Bouchemal, K. (2022). Effect of micro- and nanoparticle shape on biological processes. *Journal of Controlled Release*, 342, 93-110. https://doi.org/10.1016/j.jconrel.2021.12.032

Halfar, J., Čabanová, K., Vávra, K., Delongová, P., Motyka, O., Špaček, R., Kukutschová, J., Šimetka, O., & Heviánková, S. (2023). Microplastics and additives in patients with preterm birth: The first evidence of their presence in both human amniotic fluid and placenta. *Chemosphere*, 343, 140301. https://doi.org/10.1016/j.chemosphere.2023.140301

Hartmann, N. B., Hüffer, T., Thompson, R. C., Hassellöv, M., Verschoor, A., Daugaard, A. E., Rist, S., Karlsson, T., Brennholt, N., Cole, M., Herrling, M. P., Hess, M. C., Ivleva, N. P., Lusher, A. L., & Wagner, M. (2019). Are we speaking the same language? Recommendations for a definition and categorization framework for plastic debris. *Environmental Science & Technology*, *53*(3), 1039–1047. https://doi.org/10.1021/ACS.EST.8B05297

Hassan, H. H., Denis, M., Krimbou, L., Marcil, M., & Genest, J. (2006). Cellular cholesterol homeostasis in vascular endothelial cells. *Canadian Journal of Cardiology*, 22, 35B-40B. https://doi.org/10.1016/s0828-282x(06)70985-0

He, P., Wang, F., Xi, G., Li, Y., Wang, F., Wang, H., Li, L., Ma, X., Han, Y., & Shi, Y. (2025). Association of microplastics in human cerebrospinal fluid with Alzheimer's disease-related changes. *Journal of Hazardous Materials*, 494, 138748. https://doi.org/10.1016/j.jhazmat.2025.138748

He, Y., Li, J., Chen, J., Miao, X., Li, G., He, Q., Xu, H., Li, H., & Wei, Y. (2020). Cytotoxic effects of polystyrene nanoplastics with different surface functionalization on human HepG2 cells. *Science of The Total Environment*, 723, 138180. https://doi.org/10.1016/j.scitotenv.2020.138180

Hernandez, L. M., Yousefi, N., & Tufenkji, N. (2017). Are there nanoplastics in your personal care products? *Environmental Science & Technology Letters*, 4(7), 280-285. https://doi.org/10.1021/acs.estlett.7b00187

Ho, Y. T., Kamm, R. D., & Kah, J. C. Y. (2018). Influence of protein corona and caveolae-mediated endocytosis on nanoparticle uptake and transcytosis. *Nanoscale*, 10(26), 12386-12397. https://doi.org/10.1039/c8nr02393j

Hong, Y. (2023). Study on the maximum level of disposable plastic product waste. *Sustainability*, 15(12), 9360. https://doi.org/10.3390/su15129360

Houssini, K., Li, J., & Tan, Q. (2025). Complexities of the global plastics supply chain revealed in a trade-linked material flow analysis. *Communications Earth and Environment*, *6*(1), 1–11. https://doi.org/10.1038/S43247-025-02169-5

Hu, J., Zhu, Y., Zhang, J., Xu, Y., Wu, J., Zeng, W., Lin, Y., & Liu, X. (2022). The potential toxicity of polystyrene nanoplastics to human trophoblasts *in vitro*. *Environmental Pollution*, 311, 119924. https://doi.org/10.1016/j.envpol.2022.119924

Huo, C., Zhu, Y., Fang, X., Cui, J., Ye, H., Zhao, H., Ye, L., & Zhou, L. (2024). Polystyrene microplastics induce injury to the vascular endothelial through NLRP3-mediated pyroptosis. *Environmental Toxicology*, 39(11), 5086–5098. https://doi.org/10.1002/tox.24387

International Organization for Standardization. (2009). ISO 10993-5:2009. Biological evaluation of medical devices – Part 5: Tests for in vitro cytotoxicity. International Organization for Standardization. Retrieved December 17, 2025, from https://www.iso.org/standard/36406.html

Irion, U., & Nüsslein-Volhard, C. (2022). Developmental genetics with model organisms. *Proceedings of the National Academy of Sciences*, 119(30). https://doi.org/10.1073/pnas.2122148119

Ishfaq, M., Shakoor, N., Rillig, M. C., & Geilfus, C.-M. (2025). Airborne microplastics in leaves and food safety risks. *Trends in Plant Science*, 30(10), 1063–1065. https://doi.org/10.1016/j.tplants.2025.05.012

IUPAC. (1996). Glossary of basic terms in polymer science (IUPAC Recommendations 1996). *Pure and Applied Chemistry*, *68*(12), 2287–2311. https://doi.org/10.1351/pac199668122287

IUPAC. (2012). Terminology for biorelated polymers and applications (IUPAC Recommendations 2012). *Pure and Applied Chemistry*, 84(2), 377–410. https://doi.org/10.1351/PAC-REC-10-12-04

Ivleva, N. P. (2021). Chemical analysis of microplastics and nanoplastics: Challenges, advanced methods, and perspectives. *Chemical Reviews*, *121*(19), 11886–11936. https://doi.org/10.1021/acs.chemrev.1c00178

Jahedi, F., & Jaafarzadeh Haghighi Fard, N. (2025). Micro- and nanoplastic toxicity in humans: Exposure pathways, cellular effects, and mitigation strategies. *Toxicology Reports*, 14, 102043. https://doi.org/10.1016/j.toxrep.2025.102043

Jaroszeski, M. J., & Radcliff, G. (1999). Fundamentals of flow cytometry. *Molecular Biotechnology*, 11(1), 37-53. https://doi.org/10.1007/bf02789175

Jerka, D., Bonowicz, K., Piekarska, K., Gokyer, S., Derici, U. S., Hindy, O. A., Altunay, B. B., Yazgan, I., Steinbrink, K., Kleszczyński, K., Yilgor, P., & Gagat, M. (2024). Unraveling Endothelial Cell Migration: Insights into Fundamental Forces, Inflammation, Biomaterial Applications, and Tissue Regeneration Strategies. *ACS Applied Bio Materials*, 7(4), 2054-2069. https://doi.org/10.1021/acsabm.3c01227

Jeong, J., Im, J., & Choi, J. (2024). Integrating aggregate exposure pathway and adverse outcome pathway for micro/nanoplastics: a review on exposure, toxicokinetics, and toxicity studies. *Ecotoxicology and Environmental Safety*, 272, 116022. https://doi.org/10.1016/j.ecoenv.2024.116022

Jin, H., Ma, T., Sha, X., Liu, Z., Zhou, Y., Meng, X., Chen, Y., Han, X., & Ding, J. (2021). Polystyrene microplastics induced male reproductive toxicity in mice. *Journal of Hazardous Materials*, 401, 123430. https://doi.org/10.1016/j.jhazmat.2020.123430

Johnson, K. E., & Wilgus, T. A. (2014). Vascular Endothelial Growth Factor and Angiogenesis in the Regulation of Cutaneous Wound Repair. *Advances in Wound Care*, 3(10), 647-661. https://doi.org/10.1089/wound.2013.0517

Kang, H. J., Park, H. J., Kwon, O. K., Lee, W. S., Jeong, D. H., Ju, B. K., & Kwon, J. H. (2018). Occurrence of microplastics in municipal sewage treatment plants: A review. *Environmental Health and Toxicology*, 33(3), e2018013. https://doi.org/10.5620/eht.e2018013

Kang, S., Tanaka, T., Inoue, H., Ono, C., Hashimoto, S., Kioi, Y., Matsumoto, H., Matsuura, H., Matsubara, T., Shimizu, K., Ogura, H., Matsuura, Y., & Kishimoto, T. (2020). IL-6 trans-signaling induces plasminogen activator inhibitor-1 from vascular endothelial cells in cytokine release syndrome. *Proceedings of the National Academy of Sciences*, 117(36), 22351-22356. https://doi.org/10.1073/pnas.2010229117

Kayakabe, K., Kuroiwa, T., Sakurai, N., Ikeuchi, H., Kadiombo, A. T., Sakairi, T., Matsumoto, T., Maeshima, A., Hiromura, K., & Nojima, Y. (2012). Interleukin-6 promotes destabilized angiogenesis by modulating angiopoietin expression in rheumatoid arthritis. *Rheumatology*, 51(9), 1571-1579. https://doi.org/10.1093/rheumatology/kes093

Khan, A., & Jia, Z. (2023). Recent insights into uptake, toxicity, and molecular targets of microplastics and nanoplastics relevant to human health impacts. *iScience*, 26(2), 105995. https://doi.org/10.1016/j.isci.2023.105995

Kihara, S., Ashenden, A., Kaur, M., Glasson, J., Ghosh, S., van der Heijden, N., Brooks, A. E. S., Mata, J. P., Holt, S., Domigan, L. J., Köper, I., & McGillivray, D. J. (2021). Cellular interactions with polystyrene nanoplastics—The role of particle size and protein corona. *Biointerphases*, 16(4), 041001. https://doi.org/10.1116/6.0001124

Kik, K., Bukowska, B., & Sicińska, P. (2020). Polystyrene nanoparticles: sources, occurrence in the environment, distribution in tissues, accumulation, and toxicity to various organisms. *Environmental Pollution*, 262, 114297. https://doi.org/10.1016/j.envpol.2020.114297

Kim, D., Lee, S., Lee, J., Jeong, J., & Bae, O.-N. (2022). Amine-modified nanoplastics promote the procoagulant activation of isolated human red blood cells and thrombus formation in rats. *Particle and Fibre Toxicology*, 19(1), 60. https://doi.org/10.1186/s12989-022-00500-y

Kim, Y., Kim, H., Jeong, M., Kim, D., Kim, J., Jung, J., Seo, H., Han, H., Lee, W., & Choi, C. (2023). Microplastics in gastrointestinal tracts of gentoo penguin (Pygoscelis papua) chicks on King George Island, Antarctica. *Scientific Reports*, 13. https://doi.org/10.1038/s41598-023-39844-6

Lampitt, R. S., Fletcher, S., Cole, M., Kloker, A., Krause, S., O'Hara, F., Ryde, P., Saha, M., Voronkova, A., & Whyle, A. (2023). Stakeholder alliances are essential to reduce the scourge of plastic pollution. *Nature Communications*, 14(1), 2849. https://doi.org/10.1038/s41467-023-38613-3

Landrigan, P. J., Dunlop, S., Treskova, M., Raps, H., Symeonides, C., Muncke, J., Spring, M., Stegeman, J., Almroth, B. C., Chiles, T. C., Cropper, M., Deeney, M., Fuller, L., Geyer, R., Karasik, R., Mafira, T., Mangwiro, A., Matias, D. M., Mulders, Y., … Rocklöv, J. (2025). The Lancet Countdown on health and plastics. *The Lancet*, *406*(10507), 1044–1062. https://doi.org/10.1016/S0140-6736(25)01447-3

Lee, D. U., Park, J.-Y., Kwon, S., Park, J. Y., Kim, Y. H., Khang, D., & Hong, J. H. (2019). Apoptotic lysosomal proton sponge effect in tumor tissue by cationic gold nanorods. *Nanoscale*, 11(42), 19980-19993. https://doi.org/10.1039/c9nr04323c

Lee, H. S., Amarakoon, D., Wei, C.-I., Choi, K.-Y., Smolensky, D., & Lee, S.-H. (2021). Adverse effect of polystyrene microplastics (PS-MPs) on tube formation and viability of human umbilical vein endothelial cells. Food and *Chemical Toxicology*, 154, 112356. https://doi.org/10.1016/j.fct.2021.112356

Lehner, R., Weder, C., Petri-Fink, A., & Rothen-Rutishauser, B. (2019). Emergence of nanoplastic in the environment and possible impact on human health. *Environmental Science & Technology*, 53(4), 1748–1765. https://doi.org/10.1021/acs.est.8b05512

Lei, L., Wu, S., Lu, S., Liu, M., Song, Y., Fu, Z., Shi, H., Raley-Susman, K. M., & He, D. (2018). Microplastic particles cause intestinal damage and other adverse effects in zebrafish Danio rerio and nematode Caenorhabditis elegans. *Science of The Total Environment*, 619, 1-8. https://doi.org/10.1016/j.scitotenv.2017.11.103

Leslie, H. A., van Velzen, M. J., Brandsma, S. H., Vethaak, A. D., Garcia-Vallejo, J. J., & Lamoree, M. H. (2022). Discovery and quantification of plastic particle pollution in human blood. *Environment International*, 163, 107199. https://doi.org/10.1016/j.envint.2022.107199

Li, D., Shi, Y., Yang, L., Xiao, L., Kehoe, D. K., Gun'ko, Y. K., Boland, J. J., & Wang, J. J. (2020a). Microplastic release from the degradation of polypropylene feeding bottles during infant formula preparation. *Nature Food*, 1(11), 746–754. https://doi.org/10.1038/s43016-020-00171-y

Li, H., Liu, S., Hu, Y., Zhao, B., Sun, Y., & Xu, D. (2020b). Endosulfan promotes cell migration via PTP4A3-mediated signaling pathways in HUVECs. *Ecotoxicology and Environmental Safety*, 192, 110267. https://doi.org/10.1016/j.ecoenv.2020.110267

Li, Q., Wu, J., Zhao, X., Gu, X., & Ji, R. (2019). Separation and identification of microplastics from soil and sewage sludge. *Environmental Pollution*, 254(Pt B), 113076. https://doi.org/10.1016/j.envpol.2019.113076

Li, Q., Lai, Y., Li, P., Liu, X., Yao, Z., Liu, J., & Yu, S. (2022). Evaluating the occurrence of polystyrene nanoparticles in environmental waters by agglomeration with alkylated ferroferric oxide followed by micropore membrane filtration collection and Py-GC/MS analysis. *Environmental Science & Technology*, 56(12), 8255–8265. https://doi.org/10.1021/acs.est.2c02033

Li, S., & Malmstadt, N. (2013). Deformation and poration of lipid bilayer membranes by cationic nanoparticles. *Soft Matter*, 9(20), 4969. p. https://doi.org/10.1039/c3sm27578g

Li, Y. W., Shao, L. Y., Wang, W. H., Zhang, M. Y., Feng, X. L., Li, W. J., Zhang, R. J., Liu, Y. M., Zhang, Y. L., Wang, W., Wang, G. H., Zhang, W. X., Sun, W. F., Wang, Z. F., & Wang, Y. Q. (2020c). Airborne fiber particles: Types, size and concentration observed in Beijing. *Science of The Total Environment*, *705*, 135967. https://doi.org/10.1016/j.scitotenv.2019.135967

Li, Z., Zhu, S., Liu, Q., Wei, J., Jin, Y., Wang, X., & Zhang, L. (2020d). Polystyrene microplastics cause cardiac fibrosis by activating Wnt/β-catenin signaling pathway and promoting cardiomyocyte apoptosis in rats. *Environmental Pollution*, 265, 115025. https://doi.org/10.1016/j.envpol.2020.115025

Liu, K., Wang, X., Fang, T., Xu, P., Zhu, L., & Li, D. (2019a). Source and potential risk assessment of suspended atmospheric microplastics in Shanghai. *Science of The total environment*, 675, 462–471. https://doi.org/10.1016/j.scitotenv.2019.04.110

Liu, L., Xu, K., Zhang, B., Ye, Y., Zhang, Q., & Jiang, W. (2021). Cellular internalization and release of polystyrene microplastics and nanoplastics. *Science of The Total Environment*, 779, 146523. https://doi.org/10.1016/j.scitotenv.2021.146523

Liu, M., Song, Y., Lu, S., Qiu, R., Hu, J., Li, X., Bigalke, M., Shi, H., & He, D. (2019b). A method for extracting soil microplastics through circulation of sodium bromide solutions. *Science of The Total Environment*, 691, 341–347. https://doi.org/10.1016/j.scitotenv.2019.07.144

Liu, S., Guo, J., Liu, X., Yang, R., Wang, H., Sun, Y., Chen, B., & Dong, R. (2023). Detection of various microplastics in placentas, meconium, infant feces, breastmilk and infant formula: a pilot prospective study. *Science of The Total Environment*, 854, 158699. https://doi.org/10.1016/j.scitotenv.2022.158699

Liu, S., Yang, Y., Du, Z., Wang, C., Li, L., Zhang, M., Ni, S., Yue, Z., Yang, K., Gao, H., Zeng, Y., Qin, Y., Li, J., Yin, C., & Zhang, M. (2024). Percutaneous coronary intervention leads to microplastics entering the blood: Interventional devices are a major source. *Journal of Hazardous Materials*, 476, 135054. https://doi.org/10.1016/j.jhazmat.2024.135054

Lu, Y., Cao, M., Tian, M., & Huang, Q. (2023). Internalization and cytotoxicity of polystyrene microplastics in human umbilical vein endothelial cells. *Journal of Applied Toxicology*, 43(2), 262-271. https://doi.org/10.1002/jat.4378

Lu, Y.-Y., Li, H., Ren, H., Zhang, X., Huang, F., Zhang, D., Huang, Q., & Zhang, X. (2022). Size-dependent effects of polystyrene nanoplastics on autophagy response in human umbilical vein endothelial cells. *Journal of Hazardous Materials*, 421, 126770. https://doi.org/10.1016/j.jhazmat.2021.126770

Lundqvist, M., Stigler, J., Elia, G., Lynch, I., Cedervall, T., & Dawson, K. A. (2008). Nanoparticle size and surface properties determine the protein corona with possible implications for biological impacts. *Proceedings of the National Academy of Sciences*, 105(38), 14265–14270. https://doi.org/10.1073/pnas.0805135105

Lunov, O., Syrovets, T., Loos, C., Nienhaus, G. U., Mailänder, V., Landfester, K., Rouis, M., & Simmet, T. (2011). Amino-Functionalized Polystyrene Nanoparticles Activate the NLRP3 Inflammasome in Human Macrophages. *ACS Nano*, 5(12), 9648-9657. pp. https://doi.org/10.1021/nn203596e

Lv, J., He, Q., Yan, Z., Xie, Y., Wu, Y., Li, A., Zhang, Y., Li, J., & Huang, Z. (2024). Inhibitory Impact of Prenatal Exposure to Nano-Polystyrene Particles on the MAP2K6/p38 MAPK Axis Inducing Embryonic Developmental Abnormalities in Mice. *Toxics*, 12(5), 370. https://doi.org/10.3390/toxics12050370

Lv, X., Tan, Z., An, Z., Xu, R., Zhang, L., & Li, Z. (2025). Co-exposure to polystyrene nanoplastics and F-53B induces vascular endothelial cell pyroptosis through the NF-κB/NLRP3 pathway. *Journal of Hazardous Materials*, 481, 137114. https://doi.org/10.1016/j.jhazmat.2025.137114

Lyu, J., Yang, E. J., Head, S. A., Ai, N., Zhang, B., Wu, C., Li, R.-J., Liu, Y., Yang, C., Dang, Y., Kwon, H. J., Ge, W., Liu, J. O., & Shim, J. S. (2017). Pharmacological blockade of cholesterol trafficking by cepharanthine in endothelial cells suppresses angiogenesis and tumor growth. *Cancer Letters*, 409, 91-103. https://doi.org/10.1016/j.canlet.2017.09.009

Mahmud, F., Sarker, D. B., Jocelyn, J. A., & Sang, Q.-X. A. (2024). Molecular and cellular effects of microplastics and nanoplastics: focus on inflammation and senescence. *Cells*, 13(21), 1788. https://doi.org/10.3390/cells13211788

Malinowska, K., Bukowska, B., Piwoński, I., Foksiński, M., Kisielewska, A., Zarakowska, E., Gackowski, D., & Sicińska, P. (2022). Polystyrene nanoparticles: the mechanism of their genotoxicity in human peripheral blood mononuclear cells. *Nanotoxicology*, 16(6-8), 791-811. https://doi.org/10.1080/17435390.2022.2149360

Marfella, R., Prattichizzo, F., Sardu, C., Fulgenzi, G., Graciotti, L., Spadoni, T., D'Onofrio, N., Scisciola, L., La Grotta, R., Frigé, C., Pellegrini, V., Municinò, M., Siniscalchi, M., Spinetti, F., Vigliotti, G., Vecchione, C., Carrizzo, A., Accarino, G., Squillante, A., … Paolisso, G. (2024). Microplastics and nanoplastics in atheromas and cardiovascular events. *The New England Journal of Medicine*, *390*(10), 900–910. https://doi.org/10.1056/NEJMoa2309822

Martin, L. M. A., Gan, N., Wang, E., Merrill, M., & Xu, W. (2022). Materials, surfaces, and interfacial phenomena in nanoplastics toxicology research. *Environmental Pollution*, 292(Pt B), 118442. https://doi.org/10.1016/j.envpol.2021.118442

Mason, S. A., Welch, V. G., & Neratko, J. (2018). Synthetic Polymer Contamination in Bottled Water. *Frontiers in Chemistry*, 6. https://doi.org/10.3389/fchem.2018.00407

Materić, D., Ludewig, E., Brunner, D., Röckmann, T., & Holzinger, R. (2021). Nanoplastics transport to the remote, high-altitude Alps. *Environmental Pollution*, 288, 117697. https://doi.org/10.1016/j.envpol.2021.117697

Materić, D., Holzinger, R., & Niemann, H. (2022a). Nanoplastics and ultrafine microplastic in the Dutch Wadden Sea – The hidden plastics debris? *Science of The Total Environment*, 846, 157371. https://doi.org/10.1016/j.scitotenv.2022.157371

Materić, D., Kjær, H. A., Vallelonga, P., Tison, J.-L., Röckmann, T., & Holzinger, R. (2022b). Nanoplastics measurements in Northern and Southern polar ice. *Environmental Research*, 208, 112741. https://doi.org/10.1016/j.envres.2022.112741

Matthews, C., Moran, F., & Jaiswal, A. K. (2021). A review on European Union's strategy for plastics in a circular economy and its impact on food safety. *Journal of Cleaner Production*, 283, 125263. https://doi.org/10.1016/j.jclepro.2020.125263

Mayordomo, N. M., Zatarain-Beraza, A., Valerio, F., Álvarez-Méndez, V., Turegano, P., Herranz-García, L., López de Aguileta, A., Cattani, N., Álvarez-Alonso, A., & Fanarraga, M. L. (2025). The Protein Corona Paradox: Challenges in Achieving True Biomimetics in Nanomedicines. *Biomimetics*, 10(5), 276. https://doi.org/10.3390/biomimetics10050276

Medina-Leyte, D. J., Domínguez-Pérez, M., Mercado, I., Villarreal-Molina, M. T., & Jacobo-Albavera, L. (2020). Use of Human Umbilical Vein Endothelial Cells (HUVEC) as a Model to Study Cardiovascular Disease: A Review. *Applied Sciences*, 10(3), 938. https://doi.org/10.3390/app10030938

Moore, C. J., Lattin, G. L., & Zellers, A. (2005). Density of plastic particles found in zooplankton trawls from coastal waters of California to the North pacific central gyre. In *Proceedings of the Plastic Debris Rivers to Sea Conference* (pp. 1–16). Algalita Marine Research Foundation.

Morataya-Reyes, M., Villacorta, A., Arribas Arranz, J., Martín-Pérez, J., Ferrer, J. F., Pastor, S., Egea, R., Barguilla, I., Marcos, R., & Hernández, A. (2025a). Exploring the impact of nanoplastics on human hepatic cells: dynamics of internalization and harmful effects in HuH-7 cells. *Environmental Science: Nano*, 12(11), 4920-4934. https://doi.org/10.1039/d5en00434a

Morataya-Reyes, M., Villacorta, A., Gutiérrez-García, J., Egea, R., Martín-Pérez, J., Barguilla, I., Marcos, R., & Hernández, A. (2025b). The long-term in vitro co-exposure of polyethylene terephthalate (PET) nanoplastics and cigarette smoke condensate exacerbates the induction of carcinogenic traits. *Journal*

of Hazardous Materials, 493, 138359. https://doi.org/10.1016/j.jhazmat.2025.138359

More, S., Bampidis, V., Benford, D., Bragard, C., Halldorsson, T., Hernandez-Jerez, A., Bennekou, S., Koutsoumanis, K., Lambré, C., Machera, K., Naegeli, H., Nielsen, S., Schlatter, J., Schrenk, D., Silano, V., Turck, D., Younes, M., Castenmiller, J., Chaudhry, Q., Cubadda, F., Franz, R., Gott, D., Mast, J., Mortensen, A., Oomen, A., Weigel, S., Barthélemy, E., Rincón, A., Tarazona, J., & Schoonjans, R. (2021). Guidance on technical requirements for regulated food and feed product applications to establish the presence of small particles including nanoparticles. *EFSA Journal*, 19(8), e06769. https://doi.org/10.2903/j.efsa.2021.6769

Nan, B., Su, L., Kellar, C., Craig, N. J., Keough, M. J., & Pettigrove, V. (2020). Identification of microplastics in surface water and Australian freshwater shrimp *Paratya australiensis* in Victoria, Australia. *Environmental Pollution*, 259, 113865. https://doi.org/10.1016/j.envpol.2019.113865

Nieto Moreno, N., Olthof, A. M., & Svejstrup, J. Q. (2023). Transcription-Coupled Nucleotide Excision Repair and the Transcriptional Response to UV-Induced DNA Damage. *Annual Review of Biochemistry*, 92(1), 81-113. https://doi.org/10.1146/annurev-biochem-052621-091205

Nik Mut, N. N., Na, J., & Jung, J. (2024). A review on fate and ecotoxicity of biodegradable microplastics in aquatic system: Are biodegradable plastics truly safe for the environment? *Environmental Pollution*, 344, 123399. https://doi.org/10.1016/j.envpol.2024.123399

Nihart, A. J., Garcia, M. A., El Hayek, E., Liu, R., Olewine, M., Kingston, J. D., Castillo, E. F., Gullapalli, R. R., Howard, T., Bleske, B., Scott, J., Gonzalez-Estrella, J., Gross, J. M., Spilde, M., Adolphi, N. L., Gallego, D. F., Jarrell, H. S., Dvorscak, G., Zuluaga-Ruiz, M. E., … Campen, M. J. (2025). Bioaccumulation of microplastics in decedent human brains. *Nature Medicine*, 31(4), 1114-1119. https://doi.org/10.1038/s41591-024-03453-1

O'Neill, S. M., & Lawler, J. (2021). Knowledge gaps on micro and nanoplastics and human health: A critical review. *Case Studies in Chemical and*

Environmental Engineering, 3, 100091. https://doi.org/10.1016/j.cscee.2021.100091

Ohta, M., Kihara, T., Toriuchi, K., Aoki, H., Iwaki, S., Kakita, H., Yamada, Y., & Aoyama, M. (2020). IL-6 promotes cell adhesion in human endothelial cells via microRNA-126–3p suppression. *Experimental Cell Research*, 393(2), 112094. https://doi.org/10.1016/j.yexcr.2020.112094

Okoye, C. O., Addey, C. I., Oderinde, O., Okoro, J. O., Uwamungu, J. Y., Ikechukwu, C. K., Okeke, E. S., Ejeromedoghene, O., & Odii, E. C. (2022). Toxic Chemicals and Persistent Organic Pollutants Associated with Micro- and Nanoplastics Pollution. *Chemical Engineering Journal Advances*, 11, 100310. https://doi.org/10.1016/j.ceja.2022.100310

Oliveira, J., Belchior, A., da Silva, V. D., Rotter, A., Petrovski, Ž., Almeida, P. L., Lourenço, N. D., & Gaudêncio, S. P. (2020). Marine environmental plastic pollution: Mitigation by microorganism degradation and recycling valorization. *Frontiers in Marine Science*, 7, 567126. https://doi.org/10.3389/fmars.2020.567126

Oliveri Conti, G., Ferrante, M., Banni, M., Favara, C., Nicolosi, I., Cristaldi, A., Fiore, M., & Zuccarello, P. (2020). Micro- and nano-plastics in edible fruit and vegetables. The first diet risks assessment for the general population. *Environmental Research*, 187, 109677. https://doi.org/10.1016/j.envres.2020.109677

Paget, V., Dekali, S., Kortulewski, T., Grall, R., Gamez, C., Blazy, K., Aguerre-Chariol, O., Chevillard, S., Braun, A., Rat, P., & Lacroix, G. (2015). Specific uptake and genotoxicity induced by polystyrene nanobeads with distinct surface chemistry on human lung epithelial cells and macrophages. *PLOS ONE*, 10(4), e0123297. https://doi.org/10.1371/journal.pone.0123297

Pan, Z., Guo, H., Chen, H., Wang, S., Sun, X., Zou, Q., Zhang, Y., Lin, H., Cai, S., & Huang, J. (2019). Microplastics in the Northwestern Pacific: abundance, distribution, and characteristics. *Science of The Total Environment*, 650, 1913–1922. https://doi.org/10.1016/j.scitotenv.2018.09.244

Paul, M. B., Schlief, M., Daher, H., Braeuning, A., Sieg, H., & Böhmert, L. (2023). A human Caco-2-based co-culture model of the inflamed intestinal mucosa for particle toxicity studies. *In Vitro Models*, 2, 141–153. https://doi.org/10.1007/s44164-023-00047-y

Pechcińska, A., Malejczyk, J., Tulewicz-Marti, E. M., & Małkiewicz, K. (2025). Multiple effects of microplastic particles on human internal organs – narrative review. *Annals of Agricultural and Environmental Medicine*. https://doi.org/10.26444/aaem/210744

Pellini, G., Gomiero, A., Fortibuoni, T., Ferrà, C., Grati, F., Tassetti, A., Polidori, P., Fabi, G., & Scarcella, G. (2018). Characterization of microplastic litter in the gastrointestinal tract of *Solea solea* from the Adriatic Sea. *Environmental Pollution*, 234, 943-952. https://doi.org/10.1016/j.envpol.2017.12.038

Petersen, F., & Hubbart, J. A. (2021). The occurrence and transport of microplastics: The state of the science. *Science of The Total Environment*, 758, 143936. https://doi.org/10.1016/j.scitotenv.2020.143936

Piehl, S., Leibner, A., Löder, M. G. J., & Schulbert, C. (2018). Identification and quantification of macro- and microplastics on an agricultural farmland. *Scientific Reports*, 8, 17950. https://doi.org/10.1038/s41598-018-36172-y

Pilapitiya, P. G. C. N. T., & Ratnayake, A. S. (2024). The world of plastic waste: A review. *Cleaner Materials*, 11, 100220. https://doi.org/10.1016/j.clema.2024.100220

Pivokonsky, M., Cermakova, L., Novotna, K., Peer, P., Cajthaml, T., & Janda, V. (2018). Occurrence of microplastics in raw and treated drinking water. *Science of The Total Environment*, 643, 1644-1651. https://doi.org/10.1016/j.scitotenv.2018.08.102

Plastics Europe. (2025). Plastics – the fast facts 2025. Retrieved November 15, 2025, from https://plasticseurope.org/knowledge-hub/plastics-the-fast-facts-2025/

Płuciennik, K., Sicińska, P., Misztal, W., & Bukowska, B. (2024). Important factors affecting induction of cell death, oxidative stress and DNA damage

by nano- and microplastic particles *in vitro*. *Cells*, 13(9), 768. https://doi.org/10.3390/cells13090768

Pradel, A., Catrouillet, C., & Gigault, J. (2023). The environmental fate of nanoplastics: What we know and what we need to know about aggregation. *NanoImpact*, 29, 100453. https://doi.org/10.1016/j.impact.2023.100453

Prattichizzo, F., Ceriello, A., Pellegrini, V., La Grotta, R., Graciotti, L., Olivieri, F., Paolisso, P., D'Agostino, B., Iovino, P., Balestrieri, M. L., Rajagopalan, S., Landrigan, P. J., Marfella, R., & Paolisso, G. (2024). Micro-nanoplastics and cardiovascular diseases: evidence and perspectives. *European Heart Journal*, 45(38), 4099-4110. https://doi.org/10.1093/eurheartj/ehae552

Prietl, B., Meindl, C., Roblegg, E., Pieber, T. R., Lanzer, G., & Fröhlich, E. (2014). Nano-sized and micro-sized polystyrene particles affect phagocyte function. *Cell Biology and Toxicology*, 30(1), 1–16. https://doi.org/10.1007/s10565-013-9265-y

Rampado, R., Crotti, S., Caliceti, P., Pucciarelli, S., & Agostini, M. (2020). Recent advances in understanding the protein corona of nanoparticles and in the formulation of "stealthy" nanomaterials. *Frontiers in Bioengineering and Biotechnology*, 8, 166. https://doi.org/10.3389/fbioe.2020.00166

Rejman, J., Oberle, V., Zuhorn, I. S., & Hoekstra, D. (2004). Size-dependent internalization of particles via the pathways of clathrin- and caveolae-mediated endocytosis. *Biochemical Journal*, 377(1), 159–169. https://doi.org/10.1042/bj20031253

Revel, M., Châtel, A., & Mouneyrac, C. (2018). Micro(nano)plastics: A threat to human health? *Current Opinion in Environmental Science & Health*, 1, 17-23. https://doi.org/10.1016/j.coesh.2017.10.003

Reynaud, S., Aynard, A., & Grassl, B. (2021). Nanoplastics: From model materials to colloidal fate. *Current Opinion in Colloid & Interface Science*, 57, 101528. https://doi.org/10.1016/j.cocis.2021.101528

Rocabert, A., Martín-Pérez, J., Pareras, L., Egea, R., Alaraby, M., Cabrera-Gumbau, J. M., Sarmiento, I., Martínez-Urtaza, J., Rubio, L., Barguilla, I.,

Marcos, R., García-Rodríguez, A., & Hernández, A. (2025). Nanoplastic exposure affects the intestinal microbiota of adult Drosophila flies. *Science of The Total Environment*, 980, 179545. https://doi.org/10.1016/j.scitotenv.2025.179545

Rodrigues, A., de Jesus, G., Waked, D., Gomes, G., Silva, T., Yariwake, V., da Silva, M., Magaldi, A., & Veras, M. (2022). Scientific evidence about the risks of micro and nanoplastics (MNPLs) to human health and their exposure routes through the environment. *Toxics*, 10(6), 308. https://doi.org/10.3390/toxics10060308

Roursgaard, M., Hezareh Rothmann, M., Schulte, J., Karadimou, I., Marinelli, E., & Møller, P. (2022). Genotoxicity of Particles From Grinded Plastic Items in Caco-2 and HepG2 Cells. *Frontiers in public health*, 10, 906430. https://doi.org/10.3389/fpubh.2022.906430

Rubio, L., Marcos, R., & Hernández, A. (2019). Potential adverse health effects of ingested micro- and nanoplastics on humans. Lessons learned from in vivo and in vitro mammalian models. *Journal of Toxicology and Environmental Health*, Part B, 23(2), 51–68. https://doi.org/10.1080/10937404.2019.1700598

Ruenraroengsak, P., Novak, P., Berhanu, D., Thorley, A. J., Valsami-Jones, E., Gorelik, J., Korchev, Y. E., & Tetley, T. D. (2012). Respiratory epithelial cytotoxicity and membrane damage (holes) caused by amine-modified nanoparticles. *Nanotoxicology*, 6(1), 94–108. https://doi.org/10.3109/17435390.2011.558643

Sabourian, P., Yazdani, G., Ashraf, S. S., Frounchi, M., Mashayekhan, S., Kiani, S., & Kakkar, A. (2020). Effect of physico-chemical properties of nanoparticles on their intracellular uptake. *International Journal of Molecular Sciences*, 21(21), 8019. https://doi.org/10.3390/ijms21218019

Sahay, G., Alakhova, D. Y., & Kabanov, A. V. (2010). Endocytosis of nanomedicines. *Journal of Controlled Release*, 145(3), 182-195. https://doi.org/10.1016/j.jconrel.2010.01.036

Sarasamma, S., Audira, G., Siregar, P., Malhotra, N., Lai, Y.-H., Liang, S.-T., Chen, J.-R., Chen, K. H.-C., & Hsiao, C.-D. (2020). Nanoplastics cause neurobehavioral impairments, reproductive and oxidative damages, and biomarker responses in zebrafish: throwing up alarms of wide spread health risk of exposure. *International Journal of Molecular Sciences*, 21(4), 1410. https://doi.org/10.3390/ijms21041410

Sarma, D. K., Dubey, R., Samarth, R. M., Shubham, S., Chowdhury, P., Kumawat, M., Verma, V., Tiwari, R. R., & Kumar, M. (2022). The Biological Effects of Polystyrene Nanoplastics on Human Peripheral Blood Lymphocytes. *Nanomaterials*, 12(10), 1632. https://doi.org/10.3390/nano12101632

Sawyer, L. C., Grubb, D. T., & Meyers, G. F. (2008). *Polymer microscopy* (3rd ed.). Springer. https://doi.org/10.1007/978-0-387-72628-1

Schiano, M. E., D'Auria, L. J., D'Auria, R., Seccia, S., Rofrano, G., Signorelli, D., Sansone, D., Caprio, E., Albrizio, S., & Cocca, M. (2024). Microplastic contamination in the agri-food chain: The case of honeybees and beehive products. *Science of The Total Environment*, 948, 174698. https://doi.org/10.1016/j.scitotenv.2024.174698

Setyawati, M. I., Tay, C. Y., Bay, B. H., & Leong, D. T. (2017). Gold Nanoparticles Induced Endothelial Leakiness Depends on Particle Size and Endothelial Cell Origin. *ACS Nano*, 11(5), 5020-5030. https://doi.org/10.1021/acsnano.7b01744

Shi, Q., Tang, J., Liu, X., & Liu, R. (2021). Ultraviolet-induced photodegradation elevated the toxicity of polystyrene nanoplastics on human lung epithelial A549 cells. *Environmental Science: Nano*, 8(9), 2660–2675. https://doi.org/10.1039/D1EN00465D

Shi, X., Wang, X., Huang, R., Tang, C., Hu, C., Ning, P., & Wang, F. (2022). Cytotoxicity and genotoxicity of polystyrene micro- and nanoplastics with different size and surface modification in A549 cells. International *Journal of Nanomedicine*, 17, 4509–4523. https://doi.org/10.2147/IJN.S381776

Siemiątkowska, B., & Szczepanowska, J. (2025). Mitochondrial stress response in lung cells triggered by the inhaled nanoplastics. *Archives of Toxicology*. https://doi.org/10.1007/s00204-025-04194-x

Smyth, E., Solomon, A., Visser, M., Wisser, D., & Oberle, V. (2015). Induction and enhancement of platelet aggregation in vitro and in vivo by model polystyrene nanoparticles. *Nanotoxicology*, 9(3), 356–364. https://doi.org/10.3109/17435390.2014.933902

Sökmen, T. Ö., Sulukan, E., Türkoğlu, M., Baran, A., Özkaraca, M., & Ceyhun, S. B. (2020). Polystyrene nanoplastics (20 nm) are able to bioaccumulate and cause oxidative DNA damages in the brain tissue of zebrafish embryo (*Danio rerio*). *NeuroToxicology*, 77, 51-59. https://doi.org/10.1016/j.neuro.2019.12.010

Sørensen, L., Gerace, M. H., & Booth, A. M. (2024). Small micro- and nanoplastic test and reference materials for research: current status and future needs. *Cambridge Prisms: Plastics*, 2, e13. https://doi.org/10.1017/plc.2024.13

Sousa de Almeida, M., Susnik, E., Drasler, B., Taladriz-Blanco, P., Petri-Fink, A., & Rothen-Rutishauser, B. (2021). Understanding nanoparticle endocytosis to improve targeting strategies in nanomedicine. *Chemical Society Reviews*, 50(9), 5397-5434. https://doi.org/10.1039/d0cs01127d

Su, L., Deng, H., Li, B., Chen, Q., Pettigrove, V., Wu, C., & Shi, H. (2019). The occurrence of microplastic in specific organs in commercially caught fishes from coast and estuary area of east China. *Journal of Hazardous Materials*, 365, 716-724. https://doi.org/10.1016/j.jhazmat.2018.11.024

Sun, M., Ding, R., Ma, Y., Sun, Q., Ren, X., Sun, Z., & Duan, J. (2021). Cardiovascular toxicity assessment of polyethylene nanoplastics on developing zebrafish embryos. *Chemosphere*, 282, 131124. https://doi.org/10.1016/j.chemosphere.2021.131124

Suzuki, M., Hashizume, M., Yoshida, H., & Mihara, M. (2009). Anti-inflammatory mechanism of tocilizumab, a humanized anti-IL-6R antibody: effect on the

expression of chemokine and adhesion molecule. *Rheumatology International*, 30(3), 309-315. https://doi.org/10.1007/s00296-009-0953-0

Tang, K. H. D. (2025). Genotoxicity of Microplastics on Living Organisms: Effects on Chromosomes, DNA and Gene Expression. *Environments*, 12(1), 10. https://doi.org/10.3390/environments12010010

Tavakolpournegari, A., Annangi, B., Villacorta, A., Banaei, G., Martín, J., Pastor, S., Marcos, R., & Hernández, A. (2023). Hazard assessment of different-sized polystyrene nanoplastics in hematopoietic human cell lines. *Chemosphere*, 325, 138360. https://doi.org/10.1016/j.chemosphere.2023.138360

Tavakolpournegari, A., Villacorta, A., Morataya-Reyes, M., Arribas Arranz, J., Banaei, G., Pastor, S., Velázquez, A., Marcos, R., Hernández, A., & Annangi, B. (2024). Harmful effects of true-to-life nanoplastics derived from PET water bottles in human alveolar macrophages. *Environmental Pollution*, 348, 123823. https://doi.org/10.1016/j.envpol.2024.123823

Tavernaro, I., Dekkers, S., Soeteman-Hernández, L. G., Herbeck-Engel, P., Noorlander, C., & Kraegeloh, A. (2021). Safe-by-Design part II: A strategy for balancing safety and functionality in the different stages of the innovation process. *NanoImpact*, 24, 100354. https://doi.org/10.1016/j.impact.2021.100354

Teeguarden, J. G., Hinderliter, P. M., Orr, G., Thrall, B. D., & Pounds, J. G. (2007). Particokinetics in vitro: dosimetry considerations for in vitro nanoparticle toxicity assessments. *Toxicological sciences : an official journal of the Society of Toxicology*, 95(2), 300–312. https://doi.org/10.1093/toxsci/kfl165

Thrift, E., Galloway, T., & Mathews, F. (2025). Microplastic contamination is widespread across invertebrate taxa frequently consumed by terrestrial vertebrates. *Environmental Toxicology and Chemistry*, 44(7), 1835-1846. https://doi.org/10.1093/etojnl/vgaf103

Traversa, A., Mari, E., Pontecorvi, P., Gerini, G., Romano, E., Megiorni, F., Amedei, A., Marchese, C., Ranieri, D., & Ceccarelli, S. (2024). Polyethylene

Micro/Nanoplastics Exposure Induces Epithelial–Mesenchymal Transition in Human Bronchial and Alveolar Epithelial Cells. *International Journal of Molecular Sciences*, 25(18), 10168. https://doi.org/10.3390/ijms251810168

Uruski, P., Mikuła-Pietrasik, J., Drzewiecki, M., Budkiewicz, S., Gładki, M., Kurmanalina, G., Tykarski, A., & Książek, K. (2021). Diverse functional responses to high glucose by primary and permanent hybrid endothelial cells in vitro. *Journal of Molecular and Cellular Cardiology*, 156, 1-6. https://doi.org/10.1016/j.yjmcc.2021.03.004

van Boxel, J., Nijmeijer, S. M., Heinzelmann, M. T., Rupp, S., & van Duursen, M. B. (2025). Limited passage and functional effects of polystyrene micro- and nanoplastics in a physiologically-relevant *in vitro* human placental co-culture model. *Reproductive Toxicology*, 136, 108956. https://doi.org/10.1016/j.reprotox.2025.108956

Van Cauwenberghe, L., & Janssen, C. R. (2014). Microplastics in bivalves cultured for human consumption. *Environmental Pollution*, 193, 65-70. https://doi.org/10.1016/j.envpol.2014.06.010

Vela, L., Villacorta, A., Venus, T., Estrela-Lopis, I., Pastor, S., García-Rodriguez, A., Rubio, L., Marcos, R., & Hernández, A. (2023). The potential effects of in vitro digestion on the physicochemical and biological characteristics of polystyrene nanoplastics. *Environmental Pollution*, 329, 121656. https://doi.org/10.1016/j.envpol.2023.121656

Vethaak, A. D., & Legler, J. (2021). Microplastics and human health. *Science*, 371(6530), 672-674. https://doi.org/10.1126/science.abe5041

Viana, M., Tonin, F. S., & Ladeira, C. (2025). Assessing the Impact of Nanoplastics in Biological Systems: Systematic Review of In Vitro Animal Studies. *Journal of Xenobiotics*, 15(3), 75. https://doi.org/10.3390/jox15030075

Villacorta, A., Rubio, L., Alaraby, M., López-Mesas, M., Fuentes-Cebrian, V., Moriones, O. H., Marcos, R., & Hernández, A. (2022). A new source of representative secondary PET nanoplastics. Obtention, characterization,

and hazard evaluation. *Journal of Hazardous Materials*, 439, 129593. https://doi.org/10.1016/j.jhazmat.2022.129593

Villar-Fincheira, P., Sanhueza-Olivares, F., Norambuena-Soto, I., Cancino-Arenas, N., Hernandez-Vargas, F., Troncoso, R., Gabrielli, L., & Chiong, M. (2021). Role of Interleukin-6 in Vascular Health and Disease. *Frontiers in Molecular Biosciences*, 8. https://doi.org/10.3389/fmolb.2021.641734

Visalli, G., Facciolà, A., Pruiti Ciarello, M., De Marco, G., Maisano, M., & Di Pietro, A. (2021). Acute and Sub-Chronic Effects of Microplastics (3 and 10 µm) on the Human Intestinal Cells HT-29. *International Journal of Environmental Research and Public Health*, 18(11), 5833. https://doi.org/10.3390/ijerph18115833

Vlacil, A.-K., Bänfer, S., Jacob, R., Trippel, N., Kuzu, I., Schieffer, B., & Grote, K. (2021). Polystyrene microplastic particles induce endothelial activation. *PLOS ONE*, 16(11), e0260181. https://doi.org/10.1371/journal.pone.0260181

Wakkaf, T., El Zrelli, R., Kedzierski, M., Balti, R., Shaiek, M., Mansour, L., Tlig-Zouari, S., Bruzaud, S., & Rabaoui, L. (2020). Microplastics in edible mussels from a southern Mediterranean lagoon: Preliminary results on seawater-mussel transfer and implications for environmental protection and seafood safety. *Marine Pollution Bulletin*, 158, 111355. https://doi.org/10.1016/j.marpolbul.2020.111355

Wan, S., Wang, X., Chen, W., Xu, Z., Zhao, J., Huang, W., Wang, M., & Zhang, H. (2024). Polystyrene Nanoplastics Activate Autophagy and Suppress Trophoblast Cell Migration/Invasion and Migrasome Formation to Induce Miscarriage. *ACS Nano*, 18(5), 3733–3751. https://doi.org/10.1021/acsnano.3c11734

Wang, F., Yu, L., Monopoli, M. P., Sandin, P., Mahon, E., Salvati, A., & Dawson, K. A. (2013). The biomolecular corona is retained during nanoparticle uptake and protects the cells from the damage induced by cationic nanoparticles until degraded in the lysosomes. *Nanomedicine: Nanotechnology, Biology and Medicine*, 9(8), 1159-1168. https://doi.org/10.1016/j.nano.2013.04.010

Wang, J., Chen, Z.-L., Liang, C.-G., Yang, H.-Y., Wu, X.-F., & Sun, H.-M. (2025). Toxicological impacts of polypropylene nanoparticles similar in size to nanoplastics in plastic-bottle injections on human umbilical vein endothelial cells. *Toxics*, 13(9), 802. https://doi.org/10.3390/toxics13090802

Wang, K., Du, Y., Li, P., Guan, C., Zhou, M., Wu, L., Liu, Z., & Huang, Z. (2024). Nanoplastics causes heart aging/myocardial cell senescence through the Ca2+/mtDNA/cGAS-STING signaling cascade. *Journal of Nanobiotechnology*, 22(1), 96. https://doi.org/10.1186/s12951-024-02375-x

Wang, X., Jia, Z., Zhou, X., Su, L., Wang, M., Wang, T., & Zhang, H. (2023a). Nanoplastic-induced vascular endothelial injury and coagulation dysfunction in mice. *Science of The Total Environment*, 865, 161271. https://doi.org/10.1016/j.scitotenv.2022.161271

Wang, X., Ren, X. M., He, H., Li, F., Liu, K., Zhao, F., Hu, H., Zhang, P., Huang, B., & Pan, X. (2023b). Cytotoxicity and pro-inflammatory effect of polystyrene nano-plastic and micro-plastic on RAW264.7 cells. *Toxicology*, *484*, 153391. https://doi.org/10.1016/j.tox.2022.153391

Washihira, N., Murakami, M., Nakamura, M., Fujii, S., Matsushima, T., Asahara, H., Kishida, A., Tanabe, T., Kimura, T., Kobayashi, M., & Yamamoto, M. (2024). Application of a genetically engineered macrophage cell line for evaluating cellular effects of UV/US-treated poly(ethylene terephthalate) microplastics. *Colloids and Surfaces B: Biointerfaces*, 234, 113735. https://doi.org/10.1016/j.colsurfb.2023.113735

Weber, A., Schwiebs, A., Solhaug, H., Stenvik, J., Nilsen, A. M., Wagner, M., Relja, B., & Radeke, H. H. (2022). Nanoplastics affect the inflammatory cytokine release by primary human monocytes and dendritic cells. *Environment International*, 163, 107173. https://doi.org/10.1016/j.envint.2022.107173

Wei, J., Wang, X., Liu, Q., Zhou, N., Zhu, S., Li, Z., Li, X., Yao, J., & Zhang, L. (2021). The impact of polystyrene microplastics on cardiomyocytes pyroptosis through NLRP3/Caspase-1 signaling pathway and oxidative

stress in Wistar rats. *Environmental Toxicology*, 36(6), 989–999. https://doi.org/10.1002/tox.23125

Wei, W., Li, Y., Lee, M., Andrikopoulos, N., Lin, S., Chen, C., Leong, D. T., Ding, F., Song, Y., & Ke, P. C. (2022). Anionic nanoplastic exposure induces endothelial leakiness. *Nature Communications*, 13(1), 4757. https://doi.org/10.1038/s41467-022-32532-5

Wright, S., Ulke, J., Font, A., Chan, K., & Kelly, F. (2020). Atmospheric microplastic deposition in an urban environment and an evaluation of transport. *Environment International*, 136, 105411. https://doi.org/10.1016/j.envint.2019.105411

Wu, D., Feng, Y., Wang, R., Jiang, J., Guan, Q., Yang, X., Wei, H., Xia, Y., & Luo, Y. (2023). Pigment microparticles and microplastics found in human thrombi based on Raman spectral evidence. *Journal of Advanced Research*, 49, 141-150. https://doi.org/10.1016/j.jare.2022.09.004

Xie, X., Deng, T., Duan, J., Xie, J., Yuan, J., & Chen, M. (2020). Exposure to polystyrene microplastics causes reproductive toxicity through oxidative stress and activation of the p38 MAPK signaling pathway. Ecotoxicology and *Environmental Safety*, 190, 110133. https://doi.org/10.1016/j.ecoenv.2019.110133

Xu, M., Halimu, G., Zhang, Q., Song, Y., Fu, X., Li, Y., Li, Y., & Zhang, H. (2019). Internalization and toxicity: A preliminary study of effects of nanoplastic particles on human lung epithelial cell. *Science of The Total Environment*, 694, 133794. https://doi.org/10.1016/j.scitotenv.2019.133794

Yacobi, N. R., Malmstadt, N., Fazlollahi, F., DeMaio, L., Marchelletta, R., Hamm-Alvarez, S. F., Borok, Z., Kim, K.-J., & Crandall, E. D. (2010). Mechanisms of Alveolar Epithelial Translocation of a Defined Population of Nanoparticles. *American Journal of Respiratory Cell and Molecular Biology*, 42(5), 604-614. https://doi.org/10.1165/rcmb.2009-0138oc

Yagublu, V., Karimova, A., Hajibabazadeh, J., Reissfelder, C., Muradov, M., Bellucci, S., & Allahverdiyev, A. (2022). Overview of Physicochemical

Properties of Nanoparticles as Drug Carriers for Targeted Cancer Therapy. *Journal of Functional Biomaterials*, 13(4), 196. https://doi.org/10.3390/jfb13040196

Yan, J., Pan, Y., He, J., Pang, X., Shao, W., Wang, C., Wang, R., He, Y., Zhang, M., Ye, J., Lin, C., Lin, F., Wang, Y., Li, T., Lan, Y., Guo, Y., Wang, M., Sun, M., Gong, Y., … Dong, S. (2023). Toxic vascular effects of polystyrene microplastic exposure. *Science of The Total Environment*, 905, 167215. https://doi.org/10.1016/j.scitotenv.2023.167215

Yan, R., Zhang, X., Xu, W., Li, J., Sun, Y., Cui, S., Xu, R., Li, W., Jiao, L., & Wang, T. (2025). ROS-induced endothelial dysfunction in the pathogenesis of atherosclerosis. *Aging and Disease*, 16(1), 250–268. https://doi.org/10.14336/AD.2024.0309

Yang, Y., Xie, E., Du, Z., Peng, Z., Han, Z., Li, L., Zhao, R., Qin, Y., Xue, M., Li, F., Hua, K., & Yang, X. (2023a). Detection of various microplastics in patients undergoing cardiac surgery. *Environmental Science & Technology*, 57(29), 10911–10918. https://doi.org/10.1021/acs.est.2c07179

Yang, Z., DeLoid, G. M., Zarbl, H., Baw, J., & Demokritou, P. (2023b). Micro- and nanoplastics (MNPs) and their potential toxicological outcomes: State of science, knowledge gaps and research needs. *NanoImpact*, 32, 100481. https://doi.org/10.1016/j.impact.2023.100481

Yee, M. S., Hii, L. W., Looi, C. K., Lim, W. M., Wong, S. F., Kok, Y. Y., Tan, B. K., Wong, C. Y., & Leong, C. O. (2021). Impact of microplastics and nanoplastics on human health. *Nanomaterials*, *11*(2), 496. https://doi.org/10.3390/nano11020496

Yi, S., Lin, K., Jiang, T., Shao, W., Huang, C., Jiang, B., Li, Q., & Lin, D. (2020). NMR-based metabonomic analysis of HUVEC cells during replicative senescence. *Aging*, 12(4), 3626-3646. https://doi.org/10.18632/aging.102834

Yu, Y., & Flury, M. (2021). Current understanding of subsurface transport of micro-and nanoplastics in soil. *Vadose Zone Journal*, 20(4), e20108. https://doi.org/10.1002/vzj2.20108

Yu, Z., Li, Q., Wang, J., Yu, Y., Wang, Y., Zhou, Q., & Li, P. (2020). Reactive oxygen species-related nanoparticle toxicity in the biomedical field. *Nanoscale Research Letters*, 15(1), 115. https://doi.org/10.1186/s11671-020-03344-7

Yu, Z., Fan, X., Zhao, X., He, T., Li, X., Du, H., Zhao, M., Zhu, R., Li, M., Zhang, Z., & Han, F. (2024). Polystyrene nanoplastics induce lipid metabolism disorder by activating the PERK-ATF4 signaling pathway in mice. *ACS Applied Materials & Interfaces*, 16(27), 34524–34537. https://doi.org/10.1021/acsami.4c04416

Zhang, J., Peng, M., Lian, E., Xia, L., Asimakopoulos, A. G., Luo, S., & Wang, L. (2023a). Identification of poly(ethylene terephthalate) nanoplastics in commercially bottled drinking water using surface-enhanced raman spectroscopy. *Environmental Science & Technology*, 57(22), 8365-8372. https://doi.org/10.1021/acs.est.3c00842

Zhang, S., Li, J., Lykotrafitis, G., Bao, G., & Suresh, S. (2009). Size-Dependent Endocytosis of Nanoparticles. *Advanced Materials*, 21(4), 419-424. https://doi.org/10.1002/adma.200801393

Zhang, S., Zhu, X., & Li, G. (2020). E2F1/SNHG7/miR-186-5p/MMP2 axis modulates the proliferation and migration of vascular endothelial cell in atherosclerosis. *Life Sciences*, 257, 118013. https://doi.org/10.1016/j.lfs.2020.118013

Zhang, T., Yang, S., Ge, Y., Wan, X., Zhu, Y., Yang, F., Li, J., Gong, S., Cheng, Y., Hu, C., & Liang, G. (2023b). Multi-dimensional evaluation of cardiotoxicity in mice following respiratory exposure to polystyrene nanoplastics. *Particle and Fibre Toxicology*, 20(1), 7. https://doi.org/10.1186/s12989-023-00557-3

Zhang, T., Liao, Y., Ling, J., Zhang, J., Zhang, D., Yin, X., Yu, P., & Liu, X. (2025). Tiny trouble: microplastics, nanoplastics, and their heartfelt impact on

cardiovascular health. *Cardiovascular Research*, 121(7), 992-1010. https://doi.org/10.1093/cvr/cvaf068

Zhang, Y., Yin, K., Wang, D., Wang, Y., Lu, H., Zhao, H., & Xing, M. (2022). Polystyrene microplastics-induced cardiotoxicity in chickens via the ROS-driven NF-κB-NLRP3-GSDMD and AMPK-PGC-1α axes. *Science of The Total Environment*, 840, 156727. https://doi.org/10.1016/j.scitotenv.2022.156727

Zhu, J., & Wang, C. (2020). Recent advances in the analysis methodologies for microplastics in aquatic organisms: current knowledge and research challenges. *Analytical Methods*, 12(23), 2944-2957. https://doi.org/10.1039/d0ay00143k

Zhu, X., Wang, C., Duan, X., Liang, B., Genbo, X. E., & Huang, Z. (2023). Micro- and nanoplastics: a new cardiovascular risk factor? *Environment International*, 171, 107662. https://doi.org/10.1016/j.envint.2022.107662